

**The Biomechanical Interaction between Sports Players and
Artificial Turf for the Development of a Validated Artificial Turf
Testing Rig**

By

Steven Blackburn

The Bioengineering Unit

University of Strathclyde

Glasgow, Scotland UK

Doctor of Philosophy in Bioengineering

2012

DECLARATION OF AUTHENTICITY AND AUTHOR'S RIGHTS

This thesis is the result of the author's original research. It has been composed by the author and has not been previously submitted for examination which has led to the award of a degree.

The copyright of this thesis belongs to the author under the terms of the United Kingdom Copyright Acts, as qualified by University of Strathclyde Regulation 3.50. Due acknowledgement must always be made of the use of any material contained in, or derived from, this thesis.

Signed:

A handwritten signature in black ink, appearing to be 'M. J. Kelly', written on a light-colored background.

Date: 15th February 2013

ACKNOWLEDGEMENT

Firstly, I would like to thank the EPSRC for funding this PhD programme and the people who gave up their valuable time to participate as subjects in this study.

Secondly, I'd like to thank my supervisor, Sandy Nicol, for his guidance, support and long-standing patience throughout my time at the University of Strathclyde and since.

Thirdly, I'd like to thank all of the technical staff at the Bioengineering Unit, particularly John McLean and David Robb, for their craftsmanship, enthusiasm and time to help me construct what became affectionately known as 'The Beast'.

Most of all, I'd like to thank my partner, Sarah, for helping me find the inspiration and belief to finally complete this thesis. Without her amazing and unremitting kindness, love, motivation, understanding and patience it would not have been possible.

PUBLICATIONS RESULTING FROM THIS PHD PROGRAMME

1. Blackburn S, Nicol AC, Walker C, Brachet P. Knee joint moments during sports activities on artificial turf. *XXth Congress of the International Society of Biomechanics*.
2. Blackburn S, Nicol AC, Walker C. Development of a biomechanically validated turf testing device. *XXth Congress of the International Society of Biomechanics*.
3. Blackburn S, Brachet P, Nicol AC, Walker C. Player/ground interactions on artificial turf. *XIXth Congress of the International Society of Biomechanics*.
4. Blackburn S, Brachet P, Nicol AC, Walker C. Inertial errors of forceplate analysis of artificial turf. *XIXth Congress of the International Society of Biomechanics*.
5. Brachet P, Blackburn S, Nicol AC, Walker C. Body and limb accelerations during football activities on artificial turf. *XIXth Congress of the International Society of Biomechanics*.

CONTENTS PAGE

DECLARATION OF AUTHENTICITY AND AUTHOR'S RIGHTS.....	ii
ACKNOWLEDGEMENT	iii
PUBLICATIONS RESULTING FROM THIS PHD PROGRAMME	iv
CONTENTS PAGE	v
LIST OF TABLES	ix
LIST OF FIGURES.....	xi
ABSTRACT	xvi
CHAPTER 1. INTRODUCTION	1
1.1 History and Development of Artificial Turf	1
1.2 Biomechanical Testing of Artificial Turf	5
1.3 Aim of the PhD Programme	6
1.4 Structure of the Thesis	7
CHAPTER 2. LITERATURE REVIEW	9
2.1 Injuries.....	9
2.1.1 Injury Incidence in Sports	9
2.1.2 Lower Extremity Sports Injuries	10
2.1.3 Injury Risk Factors on Artificial Turf	13
2.1.4 Impact of Artificial Turf on Injury Incidence.....	15
2.2 The Testing of Artificial Turf.....	18
2.2.1 Definitions of Measurement Variables.....	18
2.2.2 Mechanical Turf Testing	21
2.2.3 Artificial Turf Assessment Procedures for Specific Sports	36
2.3 Biomechanical Analysis of Player/Surface Interaction	38
2.3.1 Ground Loadings (Ground Reaction Forces and Moments).....	38
2.3.2 The Effect of Artificial Turf on Ground Loadings	43
2.3.3 Ground Loadings of Complex Movements Performed on Artificial Turf	44
2.3.4 Kinematic Adaptations to Artificial Turf	47
2.3.5 Kinematic and Kinetic Analysis of Complex Movements	51
2.3.6 Biomechanical Shoe Testing	54
2.4 Summary of Literature Review and Rationale of the Current Study	55
CHAPTER 3. METHODOLOGY	58
3.1 Subjects.....	58
3.2 Laboratory tests	59
3.2.1 Artificial Turf	60
3.2.2 Motion Analysis System	64
3.2.3 Subject Instrumentation.....	67
3.2.4 Subject Calibration.....	73
3.2.5 Anatomical Reference Frames	73

3.2.6	Joint Centres of Rotation.....	82
3.2.7	Joint Coordinate Systems (JCS).....	85
3.2.8	Sport Movements.....	86
3.2.9	Testing Procedure.....	90
3.3	Outdoor Field Testing.....	90
3.4	Data Processing & Analysis.....	91
3.4.1	Vicon System.....	91
3.4.2	Biomechanical Analysis.....	95
3.4.3	Data Logger.....	99
3.4.4	Statistical Analysis.....	100
CHAPTER 4.	BIOMECHANICAL RESULTS.....	101
4.1	Subject Participation.....	101
4.2	Approach Velocities.....	102
4.3	Stance Times.....	103
4.4	Ground Loading Profiles.....	105
4.4.1	Movement: RUN.....	105
4.4.2	Movement: STOP.....	107
4.4.3	Movement: 45-degree turns.....	109
4.4.4	Movement: 90-degree turns.....	113
4.4.5	Movement: 180T.....	116
4.5	Peak Ground Loadings.....	117
4.5.1	Phases of peak loadings.....	117
4.5.2	Vertical GRF.....	118
4.5.3	Horizontal GRF.....	121
4.5.4	Free Moment.....	124
4.6	Vertical Loading Rates.....	127
4.7	Linear and Rotational Traction.....	128
4.8	Knee Angles.....	129
4.8.1	Knee Angle Profiles.....	130
4.8.2	Knee Angles at Initial Contact.....	133
4.8.3	Peak Knee Angles.....	134
4.9	Internal Knee Moments.....	136
4.9.1	Knee Moment Profiles.....	136
4.9.2	Peak Knee Moments.....	142
4.10	Validation of Biomechanical Data.....	148
4.10.1	Knee angles.....	148
4.10.2	Shank and pelvic acceleration.....	150
CHAPTER 5.	DISCUSSION.....	152
5.1	Summary of Main Results.....	152
5.2	Comparability of Results with Other Studies.....	153
5.3	The Impact of Artificial Turf on Ground Loadings.....	154

5.3.1	Influence of the Surface Mechanical Properties on Ground Loadings	156
5.3.2	Influence of the Shoe-Surface Interface	158
5.4	The Impact of Artificial Turf on Knee Biomechanics.	159
5.4.1	Knee kinematics	159
5.4.2	Knee kinetics	161
5.4.3	Methods of biomechanical analysis.....	162
5.4.4	Summary of biomechanical response to artificial turf.....	162
5.5	The Impact of Movement Type on Ground Loadings	163
5.5.1	Vertical GRF and Loading Rates	163
5.5.2	Horizontal GRF.....	164
5.5.3	Free moment of rotation	165
5.5.4	Linear and rotational traction	166
5.6	The Impact of Movement Type of Knee Biomechanics	168
5.6.1	Kinematics.....	168
5.6.2	Kinetics	170
5.7	Study Originality and Importance	173
5.8	Limitations of the Testing Procedure.....	174
5.9	Implications for Artificial Turf Design.....	176
5.10	Implications for the Future of the Mechanical Testing of Artificial Turf.....	177
5.11	Implications for Future Research.....	178
CHAPTER 6.	DEVELOPMENT AND INITIAL TESTING OF A PROTOTYPE ARTIFICIAL TURF TEST RIG.....	181
6.1	Introduction	181
6.1.1	Design Specifications	182
6.2	Design Concepts Considered	184
6.2.1	Concept A: Drop weight and ‘tilting wedges’	184
6.2.2	Concept B: Two drop weights with pulleys and rotating disc	184
6.2.3	Concept C: Weighted pendulum and flywheel.....	185
6.2.4	Concept D: Drop weight with hydraulic rams.....	186
6.2.5	Concept E: Multiple drop weights with cable system	188
6.2.6	Concept F: Multiple drop-weights and lever system.....	189
6.3	Strathclyde Sports Turf Testing Rig	190
6.3.1	Basic concept	190
6.3.2	Strathclyde Sports Turf Testing Testing Rig Components	192
6.3.3	Weighted Pendulums.....	194
6.3.4	Pendulum release mechanism	202
6.3.5	Centre Block.....	204
6.3.6	Vertical shaft system	206
6.3.7	Test Foot.....	210
6.3.8	L-crank lever system	212
6.3.9	Rig Support Feet	213
6.3.10	Wheels	214

6.3.11	Safety features.....	215
6.3.12	Transportation.....	216
6.3.13	Data Collection System.....	216
6.3.14	Data filtering.....	219
6.3.15	Pylon Transducer and Calibration.....	221
6.4	In Situ Pitch Testing.....	223
6.4.1	Pitch Areas.....	223
6.4.2	Types of Test.....	224
6.4.3	Rig Testing Procedure.....	226
6.4.4	Data analysis.....	227
6.5	Results and Discussion.....	231
6.5.1	Linear Traction (Under Static Vertical Loading).....	231
6.5.2	Linear Traction (Under Dynamic Vertical Loading) Test.....	238
6.5.3	Combined Linear & Rotational Traction Test.....	242
6.5.4	Vertical Impact Test.....	250
6.5.5	3D Low Impact Test.....	256
6.5.6	3D High Impact Test.....	256
6.5.7	Comparison of the Multidirectional Test to the Unidirectional Tests.....	259
6.6	Summary of the Design and Initial Testing of the Strathclyde Sports Turf Testing Rig.....	262
6.6.1	Design.....	262
6.6.2	Biomechanical validity.....	265
CHAPTER 7.	CONCLUSIONS.....	270
Bibliography	274	
APPENDIX A:	Force Platform Pilot Studies.....	287
APPENDIX B:	Ground Loadings of Individual Subjects.....	288
APPENDIX C:	Knee Angles of Individual Subjects.....	289
APPENDIX D:	Knee Moments of Individual Subjects.....	290
APPENDIX E:	SSTTR Initial Testing Results.....	291

LIST OF TABLES

Table 2.1 Recommended specifications for human/surface interaction tests on artificial turf.....	37
Table 3.1 Subject details ('f' denotes female subjects).....	58
Table 3.2 Footwear worn by subject during testing. [Sole type: c=cleated; P=pimples; nc=not cleated]. Mass of shoe in brackets.	59
Table 3.3 Default anthropometric data (* the mass of the shoe was added to the Dempster's value for the foot segment mass. The relative shoe mass as a ratio of total mass was estimated to be 0.005).....	95
Table 4.1 Subject participation in the 3 laboratory testing sessions (Y=Participated, N=Did not participate).....	101
Table 4.2 Times of the impact and propulsion phases for each movement.....	118
Table 4.3 Mean (sd) magnitude and times of peak vertical GRFs during the impact and propulsion phases of 7 movements performed on 3 different artificial turfs.....	119
Table 4.4 Mean (sd) magnitude and times of peak horizontal GRFs during the impact and propulsion phases of 7 movements performed on 3 different artificial turfs.....	122
Table 4.5 Mean (sd) magnitude and times of peak free moments during the impact and propulsion phases of 7 movements performed on 3 different artificial turfs.....	125
Table 4.6 Mean (sd) peak vertical loading rates for the movements on each artificial turf for all subjects.....	128
Table 4.7 Peak linear and rotation traction coefficients. The values display the mean (\pm sd) measurements for all the subjects on each artificial turf.....	129
Table 4.8 Consistency of the direction of initial contact and peak frontal plane knee angle for each movement in the 3 turf conditions.....	133
Table 4.9 Mean difference in knee angles in outdoors (T4, T6) conditions from laboratory conditions (T2). Shown is the aggregated data is from 5 subjects performing <i>RUN</i> , <i>STOP</i> , <i>45R</i> , <i>90L</i> and <i>180T</i> movements.....	149
Table 5.1 Ground loading data from the present compared with other studies.....	154
Table 5.2. Knee kinematic and kinetic data from the present study compared with other studies.....	154
Table 6.1 Approximate load criteria for test rig, based on upper quartile Ground Reaction Force results obtained during the biomechanical testing of artificial turf.....	183
Table 6.2 Approximate loads to be applied by the turf testing rig.....	199
Table 6.3 Pendulum mechanics.....	202
Table 6.4 Total amplifier gain and bridge excitation voltages used for the instrumented pylon transducer during testing and calibration sessions.....	218
Table 6.5 Standardised test areas.....	224
Table 6.6 Parameters calculated for each of the six tests.....	227
Table 6.7 Description of the test parameters calculations.....	227
Table 6.8 Peak forces and traction coefficients for the linear traction (under static vertical loading) test.....	232

Table 6.9 Linear Traction (Under Static Vertical Loading) Test: Mean peak horizontal displacement.....	236
Table 6.10 Peak forces (N) and traction coefficients for the linear traction (under dynamic vertical loading) test	241
Table 6.11 Linear Traction (Under Dynamic Vertical Loading) Test: Peak horizontal acceleration and displacement	241
Table 6.12 Combined linear & rotational traction test: results.....	246
Table 6.13 Combined linear & rotational traction test (pimpled foot): Peak horizontal displacement and rotational displacement.....	250
Table 6.14 Vertical impact test: Results.....	255
Table 6.15 3D High Impact Test: results	258
Table 6.16 Test results of the multidirectional 3d high impact test relative to unidirectional vertical impact test values (approximate values). NC= No consistent difference	260
Table 6.17 Approximate multidirectional test horizontal values relative to Combined Linear & Rotational Traction Test horizontal values. NC= No consistent difference.....	261
Table 6.18 Approximate multidirectional test rotational values relative to Combined Linear & Rotational Traction Test rotational values. NC = no consistent difference.....	262

LIST OF FIGURES

Figure 2.1 Artificial Athlete Stuttgart	22
Figure 2.2 Berlin Artificial Athlete	23
Figure 2.3 Prototype vertical impact test rig (Nunome et al, 2008)	25
Figure 2.4 BS7044 Sliding distance test	29
Figure 2.5 Modified Le Roux Pendulum.....	30
Figure 2.6 Securisport Sports Surface Tester	31
Figure 2.7 Verhelst et al (2007) friction testing device	31
Figure 2.8 IBV friction test device.....	32
Figure 2.9 SERG sports surface traction rig.....	32
Figure 2.10 BS EN 15301-1:2007 Rotational resistance test	33
Figure 2.11 TrakTester device	34
Figure 2.12 S2T2 friction tester	35
Figure 2.13 Examples of different vertical GRF profiles during running (Nigg, 1983).....	40
Figure 3.1 Turf 1 (T1), with rubber underlay and sand infill	61
Figure 3.2 Turf 2 (T2), with rubber underlay and sand infill	61
Figure 3.3 Turf (T3), with rubber and sand infill	62
Figure 3.4 Artificial turf installed in Biomechanics laboratory.....	63
Figure 3.5 Plan view of the layout of the laboratory with location of the cameras (Cam)	64
Figure 3.6 L-frame calibration reference object.....	65
Figure 3.7 Cross section of elevated L-frame reference object located on the turf covered force platform.....	66
Figure 3.8 Sign convention used in this study.....	67
Figure 3.9 Data collection systems.....	68
Figure 3.10 Foot/shoe segment marker set.....	69
Figure 3.11 Shank marker set.....	70
Figure 3.12 Single axis accelerometer	71
Figure 3.13 Flexible electrogoniometer	72
Figure 3.14 Portable data logger with 'event marker' system	72
Figure 3.15 Foot/shoe complex anatomical reference frame.....	74
Figure 3.16 Illustration of two anatomical reference systems for the shank. X,Y,Z has a flexion axis (Z-axis) suitable for an ankle JCS. x,y,z has a longitudinal axis (y-axis) suitable for a knee JCS. Adapted from International Society of Biomechanics (2002).....	76
Figure 3.17 Shank-KJCS anatomical reference frame (from Cappozzo et al. (1995)	78

Figure 3.18 Shank-ACJS anatomical reference frame (Adapted from International Society of Biomechanics (2002))	79
Figure 3.19 Thigh anatomical reference frame	80
Figure 3.20 Pelvic anatomical reference frame (Adapted from International Society of Biomechanics (2002)).....	81
Figure 3.21 HAT anatomical reference frame.....	82
Figure 3.22 45-degree turn (cutting turn technique).....	88
Figure 3.23 90-degree turn (cross turn technique)	89
Figure 3.24 180-degree turn (<i>180T</i>)	89
Figure 3.25 Movement cycle for running and turning activities (except 180° turn): IC, initial contact; TO, toe off.....	94
Figure 3.26 Sign convention used in this study.....	98
Figure 4.1 Mean (sd) approach velocities to the force platform.....	102
Figure 4.2 Correlation of approach velocities between the three turfs.....	103
Figure 4.3 Mean (sd) duration of stance phase for each movement all the three turfs	103
Figure 4.4 Correlation of stance times between the three turfs	104
Figure 4.5 Mean normalised ground loadings on each surface during the <i>RUN</i> movement: a) vertical and horizontal GRF; b) free moment. Error bars show \pm sd for Turf 1.....	107
Figure 4.6 Mean normalised ground loadings on each surface during the <i>STOP</i> movement: a) vertical and horizontal GRF; b) free moment. Error bars show \pm sd for Turf 1.....	108
Figure 4.7 Mean normalised ground loadings on each surface during the <i>45L</i> movement: a) vertical and horizontal GRF; b) free moment. Error bars show \pm sd for Turf 1.....	111
Figure 4.8 Mean normalised ground loadings on each surface during the <i>45R</i> movement: a) vertical and horizontal GRF; b) free moment. Error bars show \pm sd for Turf 1.....	112
Figure 4.9 Mean normalised ground loadings on each surface during the <i>90L</i> movement: a) vertical and horizontal GRF; b) free moment. Error bars show \pm sd for Turf 1.....	114
Figure 4.10 Mean normalised ground loadings on each surface during the <i>90R</i> movement: a) vertical and horizontal GRF; b) free moment. Error bars show \pm sd for Turf 1.....	115
Figure 4.11 Mean normalised ground loadings on each surface during the <i>180T</i> movement: a) vertical and horizontal GRF; b) free moment. Error bars show \pm sd for Turf 1.....	116
Figure 4.12 Vertical impact GRFs for 7 movements performed on 3 artificial turfs (values are normalised to subjects' bodyweight (BW)).....	120
Figure 4.13 Vertical propulsion GRFs for 7 movements performed on 3 artificial turfs (values are normalised to subject's bodyweight (BW))	121
Figure 4.14 Horizontal impact GRFs for 7 movements performed on 3 artificial turfs (values are normalised to subjects' bodyweight (BW))	123
Figure 4.15 Horizontal propulsion GRFs for 7 movements performed on 3 artificial turfs (values are normalised to subjects' bodyweight (BW))	124

Figure 4.16 Impact Free Moments for 7 movements performed on 3 artificial turfs (values are normalised to subjects' bodyweight and height (Nm/BW.h))	126
Figure 4.17 Propulsion Free Moments for 7 movements performed on 3 artificial turfs (values are normalised to subjects' bodyweight and height (Nm/BW.h)).....	126
Figure 4.18 Knee angles for the <i>RUN</i> , <i>STOP</i> , <i>45L</i> and <i>45R</i> movements in the a) frontal plane; b) sagittal plane. Error bars show \pm sd for Turf 1	131
Figure 4.19 Knee angles for the <i>90L</i> , <i>90R</i> and <i>180T</i> movements in the a) frontal plane; b) sagittal plane. Error bars show \pm sd for Turf 1	132
Figure 4.20 Frontal knee angle at initial contact (mean absolute values).....	134
Figure 4.21 Sagittal knee angle at initial foot contact (mean values).....	134
Figure 4.22 Peak frontal knee angle during stance phase (absolute values).....	135
Figure 4.23 Peak sagittal knee angle during stance phase (mean values)	136
Figure 4.24 Knee moments during movements performed on 3 artificial turf surfaces: a) <i>RUN</i> movement, b) <i>STOP</i> movement. Moments displayed are internal moments (X= frontal plane: +ve= abductor moment, -ve= adductor moment; Y=transverse plane: +ve= external rotator moment, -ve= internal rotator moment; Z=sagittal plane: +ve= extensor moment, -ve=flexor moment)	139
Figure 4.25 Knee moments during movements performed on 3 artificial turf surfaces: a) <i>45L</i> movement, b) <i>45R</i> movement. Moments displayed are internal moments (X= frontal plane: +ve= abductor moment, -ve= adductor moment; Y=transverse plane: +ve= external rotator moment, -ve= internal rotator moment; Z=sagittal plane: +ve= extensor moment, -ve=flexor moment)	140
Figure 4.26 Knee moments during movements performed on 3 artificial turf surfaces: a) <i>90L</i> movement, b) <i>90R</i> movement. Moments displayed are internal moments (X= frontal plane: +ve= abductor moment, -ve= adductor moment; Y=transverse plane: +ve= external rotator moment, -ve= internal rotator moment; Z=sagittal plane: +ve= extensor moment, -ve=flexor moment)	141
Figure 4.27 Knee moments during <i>180T</i> movement performed on 3 artificial turf surfaces. Moments displayed are internal moments (X= frontal plane: +ve= abductor moment, -ve= adductor moment; Y=transverse plane: +ve= external rotator moment, -ve= internal rotator moment; Z=sagittal plane: +ve= extensor moment, -ve=flexor moment).....	142
Figure 4.28 Normalised knee moments at initial contact for movements performed on the three artificial turfs	145
Figure 4.29 Peak, normalised knee movements during the impact phase of stance (1-20%) for movements performed on the three artificial turfs.....	146
Figure 4.30 Peak, normalised knee moments during the propulsion phase of stance (20-100%) for movements performed on the three artificial turfs.....	147
Figure 4.31 Comparison of peak knee angles during movements performed by 5 subjects in laboratory conditions (T2) and on outdoors surfaces (T4, T6).....	149
Figure 4.32 Typical knee angles before and after foot strike on the laboratory based and outdoor surfaces (Subject F5)	150
Figure 6.1 'Tilting wedges' concept.....	184

Figure 6.2 Two drop weight pulley concept.....	185
Figure 6.3 Weighted pendulum and flywheel	186
Figure 6.4 Drop weight with hydraulic rams.....	187
Figure 6.5 Multiple drop-weights with cable system	188
Figure 6.6 Multiple drop-weights with L-crank levers.....	189
Figure 6.7 Double weighted pendulums with L-crank lever/cable system.....	191
Figure 6.8 3D schematic of SSTTR, from above and below	192
Figure 6.9 Mind map of the SSTTR components.....	193
Figure 6.10 Aluminium chassis.....	194
Figure 6.11 Weighted Pendulums	195
Figure 6.12 Pendulum winch	196
Figure 6.13 Pendulum heads	197
Figure 6.14 Displacement (spring deflection) versus time in simple harmonic motion	199
Figure 6.15 Electromagnet	203
Figure 6.16 Instron test results examining the effect of the air gap on magnetic holding force.....	204
Figure 6.17 Schematic of centre block.....	205
Figure 6.18 Rotary Spline Bearing.....	205
Figure 6.19 Linear bush bearings for the horizontal shafts	206
Figure 6.20 Vertical shaft system.....	207
Figure 6.21 Horizontal cable attachment block.....	208
Figure 6.22 Instrumented transducer	209
Figure 6.23 Instrumented pylon transducer with positive loading conventions shown. These are positive as applied by the transducer to the test foot. Three accelerometers are also shown in place	210
Figure 6.24 Test feet: pimped (left) and studded (right)	211
Figure 6.25 L-crank lever (left) and steel cable attachment to the vertical shaft (right)	212
Figure 6.26 Rig support feet.....	214
Figure 6.27 Strathclyde Sports Turf Testing Rig (SSTTR).....	216
Figure 6.28 Data collection system.....	218
Figure 6.29 Screenshot from LabView data collection programme.....	219
Figure 6.30 Standardised pitch areas for football (left), rugby (middle) and hockey (right) pitches	224
Figure 6.31 Plan view of accelerations acting on the test foot	228
Figure 6.32 Linear Traction (Under Static Vertical Loading) Test: Force profiles on surfaces tested with pimped test foot.....	231
Figure 6.33 Static linear traction test: force profiles on surfaces tested with studded test foot.....	232

Figure 6.34 Static linear traction test: time to peak shear force	234
Figure 6.35 Static linear traction test: shear force loading rates.....	235
Figure 6.36 Linear Traction (Under Static Vertical Loading) Test: Mean peak horizontal acceleration	235
Figure 6.37 Linear Traction (Under Dynamic Vertical Loading) Test: force profiles on surfaces tested with pimples test foot ...	238
Figure 6.38 Linear Traction (Under Dynamic Vertical Loading) Test: force profiles on surfaces tested with studded test foot....	239
Figure 6.39 Combined Linear & Rotational Traction Test: force profiles on surfaces tested with pimples test foot	243
Figure 6.40 Combined linear and rotational traction test: force profiles on surfaces tested with studded test foot	244
Figure 6.41 Combined linear & rotational traction test: time to peak shear and peak torque	247
Figure 6.42 Combined linear & rotational traction test: shear force loading rate	248
Figure 6.43 Combined linear & rotational traction test: torque loading rate	248
Figure 6.44 Combined linear & rotational traction test: peak horizontal acceleration of the test foot	249
Figure 6.45 Combined linear & rotational traction test: peak angular acceleration of the test.....	250
Figure 6.46 Vertical impact test: vertical force profile on concrete	251
Figure 6.47 Vertical impact test: vertical force profiles (pimples test foot)	253
Figure 6.48 Vertical impact test: vertical force profiles (studded test foot)	254
Figure 6.49 3D High Impact Test: Loading profiles on surfaces tested with pimples (top) and studded (bottom) test feet	257
Figure 6.50 Comparison of the 3-dimensional loading profiles obtained during the biomechanical analysis of upper quartile ground reaction forces of five types of sports movements and from the SSTTR on similar 3G artificial turfs	268

ABSTRACT

Artificial turf is increasingly becoming prevalent in field sports traditionally played on natural grass surfaces. However, current artificial turf test methods are not biomechanically representative. This study investigated the interaction between players and sports surfaces in order to develop a new biomechanically valid testing rig for the mechanical characterisation of artificial turf.

A biomechanical analysis of thirteen sports players performing five running and turning movements on three types of artificial turf was conducted. Three-dimensional ground loadings (ground reaction forces (GRFs), free moment) and knee biomechanics (angles, moments) were measured. A subset of eight subjects who completed trials on all three types of surfaces were included in statistical analyses.

There were no significant differences in ground loadings or knee biomechanics between the turfs. However, ground loadings and knee biomechanics varied significantly between movements, according to movement velocity and the degree of turn. Larger vertical GRFs, peak knee flexion, and sagittal knee moments were measured in faster movements. Larger horizontal GRFs, free moment, traction coefficient, peak frontal knee angle, frontal and transverse knee moment were measured in turning movements.

Using two weighted pendulums, the Strathclyde Sports Turf Testing Rig (SSTTR) can apply simultaneous vertical, horizontal and rotational loads. Initial testing of the rig was conducted *in situ* on nine outdoor artificial turfs. Linear and rotational traction, and vertical, shear and torque loading was measured on each surface and compared with the biomechanical results. The SSTTR produced loads typical of a range of sports movement that are performed on artificial turf, indicating that the biomechanical validity of the SSTTR was broadly demonstrated in that it applies realistic biomechanical loads in a timely fashion.

In summary, this study has generated new knowledge and further understanding regarding the three-dimensional biomechanical interaction of players and artificial turf. The biomechanically validated SSTTR is unique in terms of its ability to combine three load actions of different magnitudes which are truly representative of the loading that occur in a number of typical sporting movements.

CHAPTER 1. INTRODUCTION

Artificial turf is becoming increasingly prevalent in field sports, such as football (soccer), rugby and hockey, which have traditionally been played on natural grass surfaces. The industry now produces 700,000 tonnes of artificial turf product per year, with a market value estimated at €1.3 billion and is expected to exceed €2 billion in 2013 (AMI, 2010).

While the industry has grown considerably in the last ten years, artificial turf has been used at the professional level for sports like American Football and baseball for many decades. Though it is unlikely to ever completely replace natural grass as a sports surface, the introduction of artificial turf may provide a suitable alternative for field sports, such as football (soccer), field hockey and rugby.

Typically installed when grass cultivation and management is environmentally, logistically or economically unviable, the wider use of artificial turf may increase access to and participation of sports, and facilitate the health and economic benefits provided by sports to its participants and society.

1.1 History and Development of Artificial Turf

Artificial (or synthetic) turf can be described as any surface made of a variety of synthetic materials manufactured to resemble natural grass (European Synthetic Turf Organisation, 2010). Typically, there are four components which comprise an artificial turf system: the fibres that collectively make the surface of an artificial turf; the type of infill (if present); underlying shock-pad (if present); and the solid base (typically concrete or asphalt).

The design and manufacturing of artificial turf has changed considerably over the years since it was first installed (in a professional sport) at the Houston Astrodome in 1966. Built as a baseball stadium, the enclosed dome design of the Astrodome stadium caused the original grass surface to die as a result of insufficient sunlight. In response, a medium-pile artificial turf, made from nylon ribbons on a polyester nylon mat bonded onto a rubber and polyvinyl chloride (PVC) underlay pad, was installed. This type of

surface where the carpet-like material was the playing surface became what we now refer to as a *first generation artificial turf (1G)*.

During the late 1960s and throughout the 1970s, several American football and baseball teams installed first generation turfs. It was not until the 1980's when the next milestone in artificial turf design took place. Perhaps due to the economic reasons, the material pile density of the so-called *2nd generation (2G) artificial turfs* was reduced and replaced by a cheaper silica sand infill. These turfs became widely popular and led to their first use in professional association football with the installation of the so-called “plastic pitch” at Loftus Road, the former home of Queens Park Rangers, in 1981. Several other English clubs followed suit, including Luton Town's Kenilworth Road, Oldham Athletic's Boundary Park and Preston's Deepdale until the English FA banned them in 1988 following the reports of a high and irregular ball bounce, player injuries, and the general negative attitude to the surfaces by players, coaches and the public.

The next major milestone in the history of artificial turf was the development of the *next generation or third generation (3G)* surfaces during the late 1990s. These longer pile surfaces (35-65mm) have softer polyethylene fibres with a sand and/or rubber granule infill. Whilst providing a softer surface than previous generations, these 3G surfaces are reported to reflect the playing conditions of natural turf, allow players to wear normal studded (cleated) footwear and players can fall or slide on the surface with less likelihood of receiving the dreaded “carpet burn” abrasion injuries often associated with 1G and 2G pitches. As the potential benefits of 3G turfs became realised, the Fédération Internationale de Football Association (FIFA) (association football's governing body) published *Quality Concept for Artificial Turf* in 2001 (updated in 2009), which set out performance standards for the artificial pitches used in football (Fédération Internationale de Football Association, 2009a). Governing bodies of other sports soon followed suit by publishing their own quality standards.

In football, FIFA and UEFA (Europe's football governing body) started a series of trials of 3G

turfs in competitive games, including the Under 17 World Championship in Helsinki, Finland in 2003. However, due to the chequered history of artificial turf in football, it was not until 2004 that 3G turfs were taken seriously by the football world. The International Football Association Board changed the *Laws of the Game* (International Football Associations Board, 2012) that govern how football is played at all levels, to include rules that all competitive games could be played on artificial turfs, as well as natural grass pitches.

Since then, the use and acceptance of 3G turf in professional football has slowly increased, although it still creates very serious debate and resistance with players, coaches and supporters whenever a high profile game is played on (or there are plans to play on) artificial turf. Most noticeable was the Euro 2008 qualifier between England and Russia at the Luzhniki Olympic stadium in Moscow and the 2008 Champions League final at the same stadium. The latter the artificial turf pitch was eventually replaced with natural grass pitch prior to the game after a UEFA ruling.

The use of artificial turf in field hockey has thrived since the development of 1G and 2G surfaces, and most competitive games are now played on them. The shorter turf length and more even surface proffered by artificial turf led to significant improvements in the speed of the game and subsequently players' skill levels. The sport's governing body, the International Hockey Federation, now requires that all international hockey matches are played on artificial surfaces. The widespread use of artificial turf in competition drove the development of water-based artificial surfaces, designed specifically for hockey. Instead of sand-infilled surfaces, the pitch is fully irrigated with a layer of water which results in an extremely fast and smooth motion of the hockey ball. Irrigation is achieved by pop up sprinklers or water cannons located around the pitch but this equipment is often too expensive for more local, amateur clubs. Also, the environmental consideration of heavy pitch watering has led to a push to the development of a dry elite playing surface for hockey.

In rugby, The International Rugby Board (IRB) provided guidelines to clubs and industry outlining the specific needs of surfaces for rugby (IRB Performance Specification for Artificial Surfaces for Rugby -

Regulation 22) and approved the use of artificial turfs in 2002 (International Rugby Board, 2010). However, the uptake of artificial turf in rugby has been less, perhaps to the specific nature of the sport and high demands placed on the surface. Following lengthy reviews and injury surveillance studies, the IRB launched the *One Turf Programme* in 2011 to regulate and standardise the development, performance and maintenance of artificial turf in rugby. With the English Premier League team Saracens announcing that their home games will be played on artificial turf from the 2011/2012 season, it is expected that artificial turfs will become more commonplace in rugby.

Fourth generation turfs have recently been developed which are in the main variations of the *third generation* predecessors. For football and rugby, these prototype surfaces are utilising a mix of monofilament, textured fibres of variable lengths which eliminate the need for infill. For hockey, dry pitches have been developed for elite level. These are a variation on 1G pitches (high-density of low-pile height fibres), but now using polyethylene fibre so that these pitches can be used dry at times when field watering is not possible or desired.

A further development in the history of artificial turf is the hybrid turf. These are surfaces consisting of natural grass reinforced with synthetic turf fibres injected into the ground. The natural grass roots entwine with the synthetic fibres, reportedly providing a stable and even surface and improved drainage. A typical hybrid turf playing surfaces comprises approximately 97% natural turf and 3% artificial turf. While perhaps not receiving as much public attention, hybrid turfs have tended to be more widely accepted than their fully artificial counterparts. There are many hybrid turf playing surfaces worldwide. One hybrid turf manufacturer, Desso, has installations in 450 stadia and training centres worldwide, including ten English Premier League football clubs, two NFL teams and several Rugby Union clubs. In fact, two of the stadia built for 2010 FIFA World Cup Finals in South Africa and four matches at the 2011 IRB Rugby World Cup Finals in New Zealand used hybrid turf pitches.

1.2 Biomechanical Testing of Artificial Turf

As the use of artificial turfs in sport increases, the question of how do we test surfaces to ensure safety requirements and performance expectations are met is vital. Over recent years, several test procedures have been developed to test for a range of surface properties and characteristics. These can be broadly categorised into three main areas: 1) tests of the ball-surface interaction, 2) tests of the player-surface interaction and 3) test of surface durability.

The ball-surface interaction properties include how a ball rebounds and rolls on a surface. Tests for ball-surface interaction includes the vertical ball rebound test; angled ball rebound test; and ball roll tests. Player-surface interaction properties are the mechanical characteristics of a surface with respect to the loads placed on it by players. These include shock absorption (also referred to as force reduction), deformation, hardness, stiffness, friction (or traction) and abrasiveness. The properties tested to characterise the durability of a surface include joint strength, resistance to abrasion, and resistance to water, heat and UV radiation.

The focus of this study is the testing of the player-surface interaction. There are international and national standards for quality and safety. In Europe, artificial turf quality is governed by the European Standards Committee CEN/TC217 standard EN 15330-1 “*Surfaces for sports areas - Synthetic turf and needle-punched surfaces primarily designed for outdoor use - Part 1: Specification for synthetic turf*” (British Standards Institute, 2007b). Many of the quality standards developed by individual sporting governing bodies are aligned with the EN 15330-1. In the US, the ASTM *F-355* standard sets out the shock absorption requirements of artificial surfaces.

However, as will be discussed in this thesis, it has been argued that many of the tests advocated in the above standards are not biomechanically valid, in that they often do not fully simulate the loading response of artificial turf in actual sporting situations. For example, earlier studies have shown that the loads applied by the Berlin Athlete test, outlined in FIFA’s Artificial Turf Quality Concept as the standard measure of the surfaces shock absorption, is uncorrelated with loads applied by real-life athletes (Nigg and Yeadon, 1987;

Nunome *et al.*, 2007; Nunome *et al.*, 2008).

Furthermore, conventional testing procedures tend to consider the loads in only one direction. For example, impact tests apply vertical loads to the turf surface, friction tests apply horizontal loads. However, sports movements by nature are highly complex activities involving player-surface interactions in multiple directions and planes within a small time frame. Therefore, in order to fully characterise the player-surface interaction of artificial turfs, the test procedure itself ought to replicate three-dimensional loading of actual sporting movements. Therefore, a better understanding of the player-artificial turf interaction is required in order to develop biomechanically validated test procedures. This should lead to a better characterisation of the properties of artificial turf used in sports to improve its quality of playing conditions and the safety of players.

1.3 Aim of the PhD Programme

The principal aim of this PhD programme was to investigate the interaction between elite players and sports surface and to derive the critical biomechanical characteristics of this interaction. This information would allow the production of test methods and apparatus which could be biomechanically validated for testing the dynamic mechanical characteristics of natural and artificial turf used for football, rugby and hockey.

In order to achieve this aim, the primary research question was:

- *“What are the 3-dimensional ground contact loadings and knee joint biomechanics of elite players performing a series of activities commonly occurring during competitive games and training on different types of artificial turf?”*

In order to validate the biomechanical data collected in the artificial environment of a biomechanics laboratory, outdoor field tests on both artificial and natural pitches were conducted, following the same experimental protocol. The biomechanical analysis of the player-artificial turf interaction forms the main focus of this study.

A secondary research question was:

- *“Is it possible to design and construct a biomechanically valid artificial turf testing rig which replicates the biomechanical interactions observed in real-life sporting movements?”*

To answer this question, the study set out to incorporate the biomechanical data into the design and construction of a prototype test rig. The test rig was to measure the 3-dimensional compliance of artificial and natural turfs and generated characteristics of these turfs in relation to a specifically selected range of sports movements. Initial testing of the prototype rig on natural and artificial turf on external pitches would be conducted to measure the mechanical characteristics of the surfaces under various environmental conditions and provide recommendations for the future testing of sports surfaces.

This work is presented in the second half of this thesis.

1.4 Structure of the Thesis

This thesis is structured into 5 main parts:

Chapter 1: Introduction to the study

Provides the background to and the aims of the study

Chapter 2: Literature review

This chapter provides a detailed review of the literature relating to the subject area. The literature review covers the prevalence, types and aetiologies of injuries in field sports, and how the introduction of artificial turf has impacted injury rates. It also provides an overview of the current testing methods for characterising artificial turf, including both mechanical testing procedures and the biomechanical analysis of the player-artificial turf interaction.

Chapter 3: Methodology

Here, a thorough description of the methods employed to conduct the biomechanical analysis of the player-artificial interaction is provided (section 2). It includes details of the subjects who participated in the study,

the artificial turfs tested, and the running and turning movements performed by the subjects. It also provides an account of the motion analysis system, player-worn equipment and data processing methods used to conduct the biomechanical analysis.

Chapter 4: Results

In Chapter 4, the results obtained from the laboratory based biomechanical assessment of the three types of artificial turf are presented, including ground loadings, knee moments and knee angles. A comparison of the data collected inside and outside of the laboratory on different surfaces is provided in order to validate the laboratory based biomechanical analysis.

Chapter 5: Discussion

This chapter discusses the main findings and advances of the study in light of published data and theories. It also discusses the limitations of the study, the implications for the development of artificial turf testing and new opportunities offered by these findings for future research.

Chapter 6: Development and Initial Testing of a Prototype Test Rig

This chapter describes the development and initial testing of a new prototype test rig that mimics the 3-dimensional loading actions of a sports player for the assessment of sport turfs, in terms of its design, manufacture and application.

Chapter 7: Overall Conclusion

This chapter provides a summary of the study outcomes, highlights its original contribution to this field of research and provides recommendations for future research.

CHAPTER 2. LITERATURE REVIEW

2.1 Injuries

2.1.1 Injury Incidence in Sports

Team games, such as football, field hockey and rugby, create an environment in which injuries can occur. Epidemiological studies of injury have shown these sports have high but variables rates of injuries. In UEFA Champions League football, injury incidence of 30.5 injuries per 1000 match hours has been reported (Walden *et al.*, 2005). In contrast, Werner et al (2009) found the total injury incidence was 1.1 per 1000 hours (3.5 per 1000 match hours versus 0.6 per 1000 training hours) during a 7 year study of 23 European teams.

The majority of the injuries sustained by football players are soft tissue and joint injuries, with three quarters occurring in the lower extremities, particularly in the knee and ankle (Ekstrand and Nigg, 1989; Fried and Lloyd, 1992).

The overall incidence of injury in English Premier League rugby is reported between 52 and 91 injuries per 1000 match hours (Brooks *et al.*, 2005; Schneiders *et al.*, 2009). In a prospective study of 156 semi-professional rugby league players over two seasons, injuries were more frequently sustained during competition than in training and injury rates were higher for forwards than for backs, due to the more physical contact experienced per game during forward play (Stephenson *et al.*, 1996). Muscular and joint injuries accounted for 48.5% of injuries. Over 20% of all injuries were experienced in the lower extremity, with 13% occurring at the knee. Although the majority of injuries were sustained during a tackling situation, non-contact injuries, such as falling/stumbling, overexertion/overuse and twisting to pass/accelerate accounted for 40, 20 and 10 injuries per 1000 hours play, respectively (Stephenson *et al.*, 1996).

In a review by Murtaugh (2009), male hockey players experienced a greater number and more severe injuries than females players. The most severe injuries were caused by contact with the ball or stick and

include trauma to the head face and upper limb. Rishiraj's (2009) study of elite female hockey players found that most injuries were, however, non-contact. These were mostly muscle strains and tendonitis. The lower back and ankle/foot were the most vulnerable to injury, followed by the knee. Dick et al (2007) reported an injury incidence of 7.9 per 1000 match hours, with ankle ligament sprains the most common at 14% of injuries. They were also frequent cause of severe injuries, resulting in time off playing.

2.1.2 Lower Extremity Sports Injuries

Sports injuries result from a single or a few traumatic tissue overloading episodes (acute injuries) or repeated loading leading to tissue damage (chronic injuries) (Zernicke and Whiting, 2000). Sports injuries can affect bones or soft tissue (ligaments, muscles, tendons). When discussing team sports, injuries can also be classified according to how they were sustained. Contact injuries occur when a player collides with another player or equipment, such as goalposts, sticks or ball. These situations usually cause acute injuries such as fractures, contusions and haematomas.

In contrast, non-contact injuries occur as a result of the player's own body motions and/or contact with the ground which generate forces greater than those which can be tolerated by biological structures (Lees and Nolan, 1998). These types of injuries can be either acute or chronic and can result in stress fractures, muscle sprains or ligament strains.

As this study is primarily concerned with the assessment of joint motions and loading during running and turning activities, the following discussion on injuries will focus on non-contact, lower extremity injuries.

2.1.2.1 *Thigh and Hip Injuries*

The highly dynamic nature of team sports such football, rugby and hockey, in which the players perform fast acceleration/deceleration and twisting/turning manoeuvres, give rise to a variety of injuries in the lower extremities. In the thigh region, hamstring strains are commonly reported in soccer players (Petersen and

Holmich, 2005; Reilly and Howe, 1996) and rugby players (Brooks *et al.*, 2006). These usually occur during a forceful extension of the knee during late forward swing of the leg, decelerating the lower limb during acceleration at push-off of the stance leg, or overexertion (Norris, 1998; Reilly & Howe, 1996; Woods *et al.*, 2004).

An adductor strain or ‘groin strain’ occurs as a result of damage to the musculotendinous junction when the hip adductors are used for propulsion during a rapid change of direction (Norris, 1998). Iliotibial band syndrome is a common chronic injury sustained during running, caused by friction on the iliotibial band moving over the lateral femoral condyle as the knee flexes/extends (Reilly & Howe, 1996).

2.1.2.2 *Knee Injuries*

Injuries to the knee can have a devastating effect on a player’s future participation in a sport. In American football, 39% of significant injuries and 58% of major injuries were sustained at the knee (Nicholas *et al.*, 1988). The knee joint is especially susceptible to injury in a sport such as football, due to the long levers attached to the knee and the potentially large moments that could be generated around the knee joint (Reilly & Howe, 1996).

Injury to the anterior cruciate ligament (ACL) is a significant injury to any sports person and can lead to intense rehabilitation or ACL reconstruction in severe cases. It has been reported that approximately one ACL tear is sustained for every 1500 player-hours for those participating in American football, skiing, basketball and football (Elmqvist and Johnson, 1994). The ACL ligament passes laterally and posteriorly from the anterior surface of the intercondylar area of the tibia to the medial surface of the posterior aspect of the femoral condyle. It provides resistance to anterior and medial displacement of the knee joint (Palastanga *et al.*, 1994).

ACL damage generally occurs as a result of a non-contact movement such as rapid deceleration which involves sudden changes in direction, landing from a jump in or near full extension, and during a cutting movements involving pivoting with near full knee extension over a planted foot (Alentorn-Geli *et al.*,

2009; Besier *et al.*, 2001b).

Common playing situations precluding a non-contact ACL injury include a change of direction or cutting manoeuvres combined with deceleration. 70% of ACL injuries occur in non-contact situations (Griffin *et al.*, 2000). The combination of large external loads during knee extension, abduction and external rotation is typical of ACL injuries (Norris, 1998). Senter and Hame (2006) identified a greater risk for ACL injury associated with a combination of anterior tibial force, internal tibial torque, and near full knee extension.

The posterior cruciate ligament (PCL) originates from the posterior intercondylar area of the tibia and travels anteriorly, medially, crossing the ACL and is inserted on the lateral surface of the medial femoral condyle. The PCL is taught in knee flexion and its function is to resist forces that cause posterior and lateral knee joint displacement (Palastanga *et al.*, 1994). It is damaged during forced hyperextension that may occur as a result of landing heavily on an extended knee or during a direct blow to the front of the leg (Senter and Hame, 2006).

The medial and lateral collateral ligament (MCL, LCL) function to protect the knee from valgus (abduction) and varus (adduction) subluxation, respectively (Reilly & Howe, 1996). The MCL travels from the medial epicondyle of the femur to the medial condyle and upper medial shaft of the tibia. The PCL travels from the lateral epicondyle of the femur to the lateral surface of the head of the tibia (Palastanga *et al.*, 1994). The MCL and PCL are commonly damaged as a result of blows during tackles to the outside and inside of the knee, respectively (Reilly & Howe, 1996). Injury to the MCL can also occur as a result of excessive knee abduction coupled with external rotation; while LCL damage can be sustained through excessive knee abduction coupled with internal rotation.

The menisci (medial and lateral) are fibrocartilage structures that are positioned on the superior aspect of the tibial condyles. They function to distribute the loads across the knee. Menisci injury is usually associated during weight bearing stances during a movement which combines twisting on a flexed knee with

the foot fixed on the ground (Norris, 1998; Reilly & Howe, 1996). A devastating injury that can occur involves simultaneous damage to the medial meniscus, medial collateral ligament and anterior cruciate, which is referred to as O'Donoghue's triad (Reilly & Howe, 1996).

Jumper's knee (quadricep tendonitis), anterior compartment syndrome and stress fractures to the tibia and fibula are chronic injuries associated with frequent running or jumping on hard surfaces or wearing faulty footwear that fail to attenuate shock adequately (Norris, 1998).

2.1.2.3 *Ankle and Foot Injuries*

In a systematic review of injury patterns of more than 200,000 participants in 70 sports worldwide over 18 years, the ankle was the second most common injured body site after the knee, and ankle sprain was the most common type of ankle injury (Fong *et al.*, 2007). Injuries to the ankle account for 25% of all lost time injuries in high-risk sports, such as football and rugby (Reid, 1992). Eighty-five percent of ankle injuries are sprains, and of those sprains, 85% are lateral inversion sprains (Young, 2009).

The most common injury of the ankle occurs as a result of damage to the anterior talofibular ligament by a combination of excessive inversion, plantarflexion and adduction loading. Damage to the calcaneocuboid ligament occurs as result of a combination of supination and adduction. Excessive inversion while the foot is in a neutrally flexed position can injure the calcaneofibular ligament. A combination of plantarflexion, eversion and abduction can lead to tears in the medial collateral ligament (Norris, 1998).

'Turf-toe' is an acute injury of the first metarsophalangeal joint caused by forceful dorsiflexion of the toe as a result of increased friction between the shoe and surface. This injury has been observed in American football players and can occur when the player is accelerating away from a crouching stance or when a player's body weight falls onto their foot while being tackled (Rodeo *et al.*, 1990).

2.1.3 **Injury Risk Factors on Artificial Turf**

The aetiologies of sports injuries are numerous. A detailed discussion on the causes of all injuries sustained

in sport is beyond the scope of this thesis. However, for a review of the risk factors associated with lower extremity injury, the reader is referred to Murphy *et al* (2003).

Generally, sports injuries can be attributed to intrinsic and extrinsic risk factors (Inkelaar, 1994). Intrinsic factors are related to the player's physical composition, such as age, gender, body size, fitness, joint laxity, muscle tightness, anatomical alignment and medical/injury history. Extrinsic risk factors include the level of competition, equipment (such as footwear and protective accessories), rules and foul play, climatic conditions, training errors (lack of warm up) and playing surface (grass, artificial surface) (Ekstrand & Nigg, 1989; Inkelaar, 1994; Murphy *et al.*, 2003; Nigg, 1985; Reilly *et al.*, 1988; Renstrom *et al.*, 1977).

Surface related injury risk factors include an uneven playing surface, high stiffness, too high or too low friction, and alteration in training surfaces. (Ekstrand and Gillquist, 1983; Murphy *et al.*, 2003). Knee and ligament damage are common in injuries collectively known as 'foot-fixation' injuries. These occur when a player's foot remains locked on the surface while the rest of the body rotates/twists over the ankle and knee. This may result in high translational and/or rotational forces, which can stress the ankle and knee joint systems significantly. The surface stiffness and its frictional properties are important for the aetiology of sport injuries, particularly non-contact chronic injuries (Naunheim, 2008; Nigg & Yeadon, 1987). However, it has been reported that the stiffness of the surfaces is not related to acute soccer injuries, but may account for some chronic injuries. Ekstrand and Nigg (1989) found that 24% of injuries sustained while playing association football have been attributed to the playing surface.

The introduction of artificial pitches into major sports such as American football, hockey and football changed styles of play (Andersson *et al.*, 2008; Bharti *et al.*, 2006), which may influence the biomechanical interactions between players and the surface and impact on injury risk. For example, artificial turf use in hockey has had a major effect on how the sport is played. Artificial surfaces presented a smooth playing surface and promoted fast paced, continuous play (Murtaugh, 2001). However, little recent research is evident regarding the effect of artificial surfaces on injury rates in hockey.

2.1.4 Impact of Artificial Turf on Injury Incidence

There are conflicting reports in the literature regarding the effect of playing on artificial surfaces on injury rates. Many of the studies relating to injuries on different surfaces are difficult to compare due to methodological deficiencies and inconsistencies. In particular, studies have not used a not standard definition of what an injury is or been consistent in how injury rates are calculated. It is not always clear whether acute or chronic injuries (or both) are being reported, nor the location of the injury. Also, some studies include injuries that have occurred in competitive play only, while others include both competitive play and training. Furthermore, case studies or injury surveys that are retrospective in nature are prone to bias, as they cannot accurately characterize the multiple variables that must be evaluated, such as injury type or cause. In addition, there is generally no baseline information regarding the athletes before the injury occurred (Murphy *et al.*, 2003).

Surface-related injury research is further complicated by the large number of variables involved (Dragoo and Braun, 2010; Williams *et al.*, 2011). For a comprehensive comparison of injury rates between different types of artificial turfs and natural turf, the following factors need to be considered: the level of competition, training or match play, contact or non-contact injuries, the type of footwear each player wears; the players' individual intrinsic injury risk factors (muscle imbalance, injury status and history); the surface properties (type and age of surface); the climate effect; the exact injury mechanism (whether the injury is attributable to the surface or not, the movement performed when the injury occurred and whether it was contact or non contact injury) (Dragoo & Braun, 2010; Powell and Schootman, 1992).

There can be variation in the properties of different brands of artificial turfs evaluated. Also, use of 'natural turf' as a catch-all categorization in injury studies masks the spatial and temporal variation within and among such surfaces (Stiles *et al.*, 2009). Consequently, it may be impossible to provide a generalised statement testifying that injury rates are higher on artificial turf compared to natural turf.

2.1.4.1 *Studies Reporting a Higher Incidence of Injuries on Artificial Turf.*

Much of the early research which reports a higher injury incidence on artificial turf tends to be earlier and focused on American football and 1G surfaces, such as *Astroturf*. The introduction of artificial turf has been the suspected cause for an increase in ‘foot-fixation’ injuries, such as anterior cruciate ligament (ACL) damage, and ‘turf-toe’ (Pine, 1991). In a review of the epidemiological studies on injury rates Skovron *et al* (1990) concluded that playing and practicing on artificial turf was associated with a 30-50% increase in the risk of time loss injuries to the lower extremities. In practical terms, this may be equated to one excess injury per team per season. More recently, Williams *et al* (Williams *et al.*, 2011) reported that while there was no overall difference in injury rates, playing on third and fourth generation turf may lead to a higher risk of ankle injury compared to natural turf.

A survey of intercollegiate American football during a seven-year period in the 1980s, showed that natural turf and artificial turf accounted for 12% and 7% of all surface related injuries, respectively (Pine, 1991). In a similar survey of intercollegiate soccer, injury rates for natural surfaces were 7.51 per 1000 player exposures and 10.68 per 1000 exposures for artificial turf. During a ten year study of professional American football, Powell *et al.* (1992) reported higher rates of ACL injuries for special team players (punting and kick-off) competing on *Astroturf* artificial turf compared to natural turf. In a study of American football players, 83% of those players where it could be determined on which surface an injury occurred, reported initial turf-toe injury on an artificial surface (Rodeo *et al.*, 1990).

2.1.4.2 *Studies Reporting No Differences in Injury Incidence Between Natural and Artificial Turf*

Since the introduction of 3G turf, the injury incidence research has tended to report no differences in amount or type of injuries between artificial and natural turf. Recent systematic literature review concluded that despite differences in injury type, the rate of injury on third-generation and natural grass surfaces appears to be comparable (Dragoo & Braun, 2010; Williams *et al.*, 2011). The following is a summary of the relevant studies.

Differences in the injury incidences of 292 professional football players were examined by Ekstrand *et al* (2006). One group consisted of players from 10 elite European clubs playing their home games on 3G artificial turf and away games on natural turf. The control group consisted of 202 footballers playing their home games on natural turf in the Swedish Premier League. The authors concluded that no evidence of a greater risk of injury was found when football was played on artificial turf compared with natural grass. Significantly more ankle sprains were observed on artificial turf but the initial incidence of ankle sprains was low.

The studies by Fuller *et al* (2007) collected injury data from over 100 male and female university football teams over a 2-year period. Details of the playing surface and the location, diagnosis, severity and cause of all training and match play injuries were recorded. The authors reported no major differences between the incidence, severity, nature or cause of injuries sustained on new generation artificial turf and on grass by either men or women. This result was the same for both training and during matches.

In a case-controlled, prospective study of over 300 youth football players during one season, Aoki *et al* (2010) found no significant differences in acute injuries during training and competition. However, there was a significantly higher incidence of low back pain in the group training on the artificial turf. Similarly, Steffen *et al* (2007) reported no differences in injury incidences in 2020 young female football players on artificial and natural turf.

While an earlier study of 1G artificial turf by Renstrom *et al.* (1977) found no differences in injury frequencies between playing on an artificial football surface and natural grass, it was observed playing on artificial turf with studded footwear increased the injury rate. In addition, more injuries occurred during sliding and tackling on artificial pitches. These injuries tended to be abrasion injuries, reflecting the difference between the frictional properties of the early synthetic turf and natural turf (Ekstrand & Nigg, 1989).

In a 26-year retrospective study of injuries in players of an American football team, Nicholas *et al.*

(1988) also found no significant differences in rates of major injuries per game on either natural or artificial surfaces. However, contact and non-contact injuries were not differentiated in this study. Interestingly, Scranton (1999) reported that an American football player is five times more likely to injure their ACL on natural grass than on artificial turf in a game situation. Of 78 ACL injuries that were sustained in game and practice situations over 5 years in the National Football League (NFL), 65% occurred on natural grass and 35% occurred on artificial turf. While injury rates per team session were higher for natural than artificial turf during game situations, the opposite was true for practice situations. This study also highlighted the importance of considering the shoe worn when conducting injury studies, as some shoes are not suitable for certain surfaces.

2.1.4.3 Studies Reporting Lower Incidence of Injuries on Artificial Turf

A study by Meyers (Meyers, 2010) examined injury rates sustained in 465 collegiate American Football games played on either FieldTurf artificial turf or natural grass during 3 seasons. They reported a significantly lower total injury incidence, including both minor and severe injuries on the artificial turf compared to the natural grass surface. Although the standard of collegiate football is high, these results cannot be generalised to the professional levels of competition.

An earlier report by Winterbottom (1985) for the English Football Association on use of 1G surfaces in English First Division football during the 1980s stated that injury rates were lower on artificial turf compared to natural turf.

2.2 The Testing of Artificial Turf

2.2.1 Definitions of Measurement Variables

Sports surfaces can be characterised by a number of variables. The cushioning ability of a material can be described as its potential to reduce impact force peaks (Nigg, 1990). Harder (or stiffer) surfaces are generally assumed to have a detrimental effect on an athlete. The variables measured to produce a description of the

cushioning are peak impact force, peak acceleration/deceleration of a falling mass, and deformation of the surface.

The measured forces and deformation will enable a calculation of the surface stiffness, which is defined as the ratio between the force applied directly perpendicular onto a surface and the elastic (or recoverable) deformation in the direction of the applied force (Nigg, 1990). The hardness is a measure of the yield stress of a surface and is related to the plastic (or permanent) deformation. It has been suggested that the recoverable properties of a sports surface are of most relevance, indicating the importance of measuring surface stiffness (Dixon *et al.*, 1999).

The property of a surface to resist horizontal loading and allow an athlete to make movements without excessive slipping or falling is referred to either friction or traction. Friction is necessary for athletes to make sharp changes in direction or increases in speed. Therefore, a certain amount of surface friction is necessary and beneficial for sports performance but excessive friction prevents a player's foot from moving freely during turns, cuts and twists and may increase the risk of foot fixation injuries (Shorten *et al.*, 2003).

Frictional forces occur whenever there are two contacting bodies and one body is forced to move relative to the other body. If no relative movement occurs between the two bodies, it is static friction. If relative movement does occur, it is kinetic friction, which opposes the direction of the movement. For ideal surfaces (uniform and rigid bodies), a coefficient of friction (μ) can be determined through the application of Coulomb's law of friction:

$$\mathbf{F}_f = \mu_f \mathbf{F}_n \quad \text{(Eq. 2.1)}$$

Where F_f = frictional force

F_n = normal force

μ_f = coefficient of friction

If there is no relative movement between two surfaces, a coefficient of static friction (μ_s) is calculated. If

there is relative movement between two surfaces, a coefficient of kinetic friction (μ_k) is calculated. Coulomb's law is relevant for both linear and rotational movement, resulting in linear or translational resistance and rotational resistance. In terms of rotational movements about an arbitrary axis, a coefficient of rotational friction can be calculated in a similar fashion, utilising the free moment of rotation about an axis perpendicular to the surface plane through the point of application (Stucke *et al.*, 1984):

$$\mathbf{M}_r = \mu_r \mathbf{F}_n \quad (\text{Eq. 2.2})$$

Where M_r = free moment of rotation

F_n = normal force

μ_r = coefficient of rotational friction

However, it has been argued that this coefficient of rotational friction is not a true coefficient as it has units of length. With consideration to a human/surface interaction, this coefficient does not take into account any changes in contact area which can occur (Nigg, 1990). It has been reported that the moment of rotation depends on the pressure distribution in the contact area and the size of the contact area (Nigg & Yeadon, 1987). Therefore, it has been suggested that the moment of rotation should suffice to describe the resistance to rotational motion of the shoe-surface interaction (Nigg, 1990).

The classical law of friction described above assumes that the coefficient of friction is dependent on the materials of the two surfaces and the relative constant velocity between them but independent of the normal force and the contact area.

However, the surfaces and shoe materials that are present during sporting environments are not ideal surfaces so the classical laws of friction do not adequately describe the complex interaction between these compliant and non-uniform surfaces (Shorten *et al.*, 2003; Shorten and Himmelsbach, 2002; Van Gheluwe *et al.*, 1983). It has been reported that the friction coefficient can be influenced by changes in the normal force, contact area and sliding velocity (Schlaepfer *et al.*, 1983; Valiant, 1987; Van Gheluwe *et al.*, 1983).

As a result, the term ‘traction’ has been adopted to describe the shoe-surface interactions that do not comply with the classical laws of friction (Shorten *et al.*, 2003). The symbol ‘ τ ’ is used to describe a coefficient of traction as the ratio of traction force to the normal force, which is defined in the same manner as for the coefficient of friction (see Eq. 2.1). The use of the term traction implies that a) the interaction between the surfaces is non-linear and does not comply to Coulomb’s Laws and b) the measurements of resistance to motion are applicable to only the loading conditions similar to those under which the measurements are being made (Shorten & Himmelsbach, 2002). The resistance of a surface to horizontal loading will be described as traction in the remainder of this thesis.

2.2.2 Mechanical Turf Testing

Artificial surfaces can be tested by a number of methods. They range from laboratory-based procedures on a small samples to tests conducted *in situ* on surfaces that are to be used or being used for sports competition or training. The methods can also be categorised according to the type of loading that apply to the surface: vertical impact tests, linear traction tests, rotational traction tests or tests incorporating a combination of loadings.

The following is a description of the methods that have been devised to mechanically assess artificial turf, specifically in relation to the human-surface interaction. Some of tests methods are currently widely used and form part of internationally recognised testing standards or sporting governing body assessment procedures. Tests for evaluating the ball-surface interaction and other characteristics such as weathering, ageing, pile strength, etc are not included in this review. The CEN Technical Committees CEN/TC 217 and PRI/57 “Surfaces for sports areas” have developed a number of standards for sports surfaces in Europe which cover a range of characteristics (British Standards Institute, 2007b).

2.2.2.1 Impact Tests

Impact tests involve a mass that is falling under gravity, or mechanically propelled, impacting with the test surface. The force of the impact or deceleration of the mass during impact is used as a measure of the shock absorption of a surface. Following is a summary of impact tests for artificial turf.

Artificial Athlete Stuttgart

The Artificial Athlete Stuttgart is a portable impact-testing device originally devised for assessing point-elastic surfaces, such as gymnasium floors. It consists of a 20kg mass falling on to a 69mm diameter spiral spring with a stiffness of 40N/mm from a height of 120mm. Beneath the spring is a force transducer and a displacement cell which measures the loads transferred by a 70mm diameter, 3.5kg test foot to the surface under assessment. The Artificial Athlete Stuttgart is also used to determine the standard vertical deformation of the surface (British Standards Institute, 2005b).

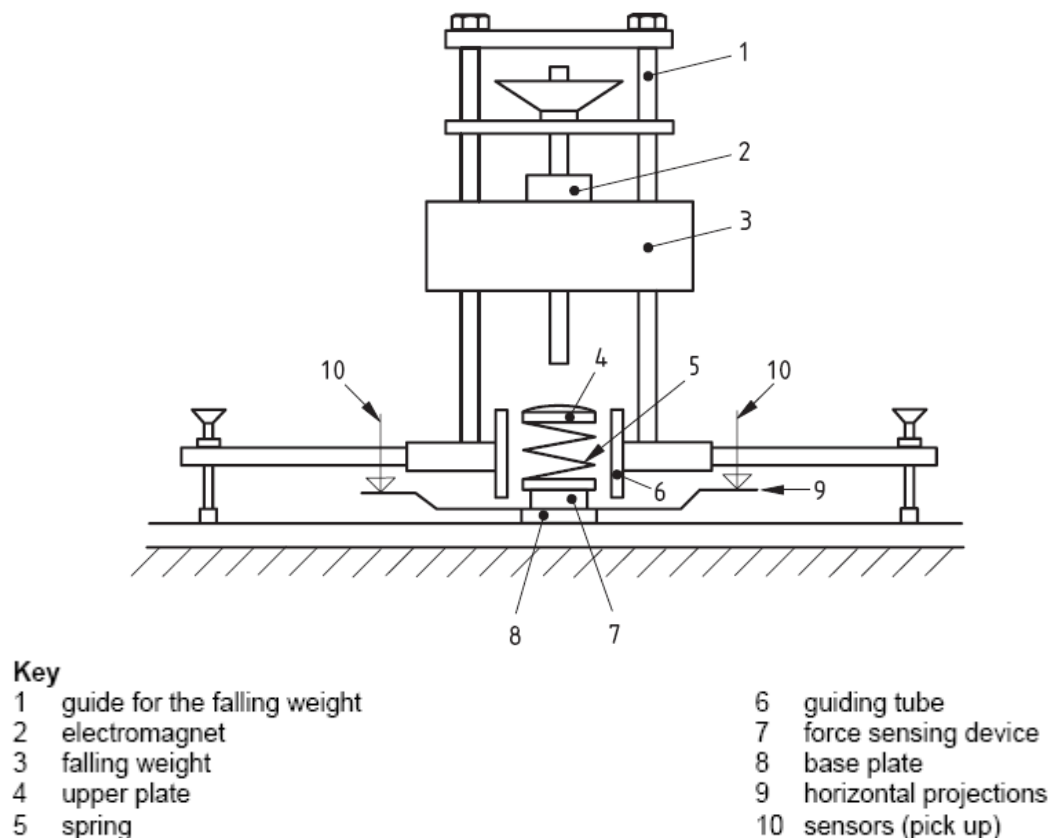


Figure 2.1 Artificial Athlete Stuttgart

Berlin Artificial Athlete

The Berlin Artificial Athlete (Figure 2.2) is a development of the Artificial Athlete Stuttgart, which allows the assessment of higher frequency loads with a shorter contact time, which are similar to those observed during a human foot contact during a sporting movement (Nigg & Yeadon, 1987). The rig is intended to simulate lower extremity impact. The Berlin Artificial Athlete (DIN 18035) has been the most commonly used test for determining the shock absorbency properties of a surface and is currently the test for the British/European Standard for determining shock absorbency (British Standards Institute, 2005a) and FIFA's recommended testing procedure (Fédération Internationale de Football Association, 2009b). It consists of a rig containing a 20kg mass dropped 55mm onto a linear spring (spring stiffness: 2000Nmm^{-1}) that is located above a test foot (70mm diameter, 3kg) through which the force is applied to the surface.

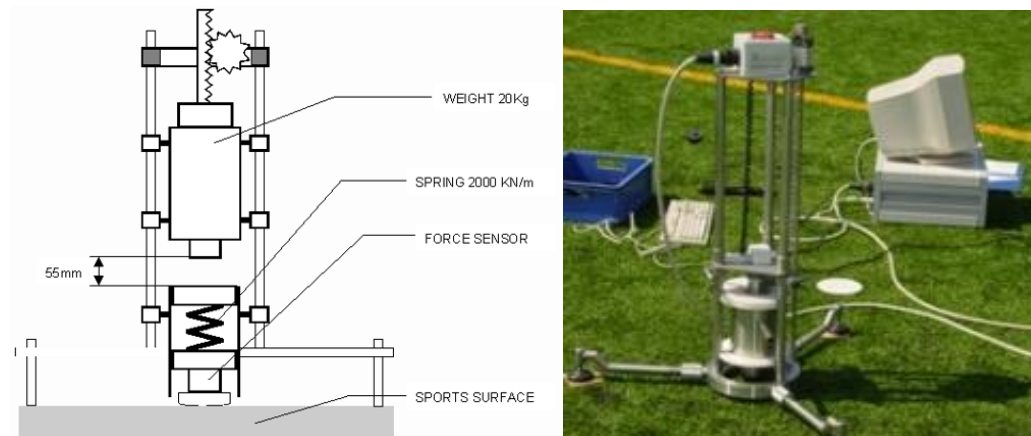


Figure 2.2 Berlin Artificial Athlete

A force transducer, with a capacity of 10kN measures the impact force of the test foot with the surface. The amount by which the peak value of the force is lower than the peak value measured when the test is performed on a reference concrete substrate is reported as the *Force Reduction %*. Based on Harrison (1999) calculations, this device can produce a maximum force of 6740N in a time of approximately 10 ms on concrete.

When the Berlin Athlete is tested on a reference concrete sample, it acts as a one mass – one spring system. In practice, during artificial surface testing, the Berlin athlete acts as a two mass-two spring

mechanical system. The effect of the test foot combined with the sample of artificial surface being impacted produces a second mass-spring system.

The recorded signal from the force transducer includes a relatively high degree of mechanical noise that arises from the metallic nature of the apparatus, which incorporates little damping, the oscillation of the spring coils and other random noise. In the Berlin Athlete, the oscillations of the spring have been reported to have frequency components of approximately 2kHz and 4kHz (Harrison and Harting, 2000). Also, the stiffness of the test sample and the properties of the test foot will affect the frequency of the oscillation of the lower mass-spring system. The frequency has been reported to be as low as 130 Hz during test on a soft sample using a test foot with a mass of 3kg (Harrison & Harting, 2000).

Harrison (1999) compared the peak value of a recorded signal produced during Berlin Athlete tests on a concrete floor using different springs with different filtering techniques. It was suggested that a 9th order Butterworth filter with a 220Hz cut-off would be appropriate to remove all the unwanted components from the signal. BS EN 14808 states a 2nd order Butterworth characteristic with a -3 dB frequency of 120Hz (British Standards Institute, 2005a).

It is important to have a reference standard in order to base the results of test samples on. Traditionally, the reference norm for artificial athletes has been concrete. Now, entirely metallic reference devices have been produced, comprising of conical steel spring washers in a housing (Harrison & Harting, 2000). These reference norms have the advantage that it can be reliably reproduced to within defined tolerances. Ideally, a 'standard' artificial surface should be used as a reference norm. However, there are inherent problems with the use of a polymeric reference such as reproducibility, uniformity, linearity and ageing of the surface.

Impact Severity Test

The Impact Severity Test (The Sports Council, 1984) determines the peak deceleration during impact which gives a measure of the ability of the surface to absorb the energy of a player falling onto it. This test

employs an *impact severity rig* (BS 7188:1989, *now withdrawn as a standard*), which consists of a spherical mass ($4.6\pm 0.05\text{kg}$, diameter: $160\pm 5\text{mm}$) instrumented with an accelerometer, released from different drop heights. The peak deceleration of the mass upon impact gives rise to a Severity Index related to the drop height.

Nunome et al (2007; 2008) Vertical Load Test Rig

The prototype vertical loading test rig developed by Nunome *et al* (2007; 2008) consists of a drop mass system using a length adjustable pendulum (Figure 2.3). The rig can apply vertical loads of between 7000N and 11000N to represent the loading conditions measured in human landing on 3G turfs (Nunome *et al.*, 2007).



Figure 2.3 Prototype vertical impact test rig (Nunome et al, 2008)

Portable Biomechanical Artificial Surface Tester

The University of Strathclyde has developed a prototype Portable Biomechanical Artificial Surface Tester that is reported to simulate a human footfall in terms of applied force, loading time and spring ('leg') stiffness (O'Hara, 2003). It consists of a 15kg mass that is dropped from an adjustable height, guided inside an aluminium pipe. The mass has a spring-dampening system attached to it, with a spring stiffness of 97kNm^{-1} . The dampening aspect of this device is stated to minimise the need for rigorous data filtering.

The mass impacts a piezo-electric load cell that is attached to the test foot. With a drop height of 150mm, a maximum load of 14.74kN with a loading time to peak force of approximately 10ms has been

achieved on a reference sample of concrete.

Other Instrumented Impact Tests

Other traditional forms of mechanical turf testing are laboratory based and come in the form of instrumented impact tests. There are two general types of machines which perform instrumented impact test: 1) pendulum or drop-weight machines, in which a swinging or falling weight strikes the specimen and 2) servo-hydraulic or pneumatic machines that force an impactor onto the sample at different velocities. Both methods produce information on force, displacement, velocity and the energy absorbed by the sample.

2.2.2.2 Standards for the Impact Testing of Artificial Turf

British and European

The European Standards Committee CEN/TC217 (2007b) has produced the standard EN 15330-1 “Surfaces for sports areas - Synthetic turf and needle-punched surfaces primarily designed for outdoor use - Part 1: Specification for synthetic turf” to supersede the previous British Standard BS 7044:1990. It specifies the properties required from synthetic turf surfaces intended for the sports of football, hockey, rugby, tennis or multi-sports use.

The standard has a comprehensive range of ball/surface requirements including ball rebound, ball roll and angle ball rebound. The standard also specifies requirement for the player/surface interaction shock absorption, vertical deformation and rotational resistance. Requirements for the effects of resistance to artificial weathering, joint strength and simulated use are specified too.

In terms of impact testing, the BS EN 14808 ‘Surfaces for sports areas. Determination of shock absorption’ (British Standards Institute, 2005a) describes the use of the Berlin Athlete device as a test of a surface’s resistance to vertical loading. Standard BS EN 14809 ‘Surfaces for sports areas. Determination of vertical deformation’ (British Standards Institute, 2005b) describes the use of the Artificial Athlete (Stuttgart) to measure the vertical deformation of sports surfaces.

The *Head Injury Criterion & Critical Fall Height* are test methods specified by the common European Standard BS EN 1177 ‘Impact attenuating playground surfacing: Determination of critical fall height’ (British Standards Institute, 2008). This standard describes the use of an instrumented headform, representing the head of a falling person, dropped from various standard heights onto the test sample. The headform, instrumented with an accelerometer, consists of an aluminium ball or a hemispherical ended missile with a diameter of 160 ± 5 mm and a mass of 4.6 ± 0.05 kg. The deceleration of the headform as it is brought to rest is monitored and the crucial maximum rate of deceleration is calculated. The kinetic energy of the headform is used to express a Head Injury Criterion (HIC). From the series of tests, the maximum acceptable drop height of the headform to yield a HIC of 1000 is calculated. This is the rated Critical Fall Height for the surface.

United States

The *ASTM F-355 falling missile test* determines the shock absorbing properties of playing surfaces (American Society for Testing and Materials, 1994). It measures acceleration values during impact to approximate a relatively severe blow to the head during falling. A flat-faced missile (9.8kg), equipped with an accelerometer is dropped from a height of 60cm and the deceleration during impact is measured.

2.2.2.3 Limitations of Impact Testing Procedures

There are several reported limitations with the application of the current tests, which have been thoroughly documented by Nigg (1990) and Dixon *et al.* (1999). With respect to vertical impact/cushioning tests, mechanical drop tests results are specific to the chosen experimental set-up. Varying the drop height, the mass of the object and the contact area of the test foot can have a considerable effect on the rating of a surface’s cushioning ability (Nigg, 1990). Although, it has been suggested that, in terms of the Berlin Artificial Athlete test, any constant variable error would affect both the reference and test sample results (Harrison & Harting, 2000).

In tests where only peak impact forces, peak accelerations or peak deformations are reported during

cushioning tests, the possible inertial effects of the test foot and/or the part of sample under movement are not accounted for. For the Berlin Athlete tests, Nigg (1990) calculated these inertial effects to be up to 40N, which are considerably large enough not to be neglected.

The impact forces produced in tests currently used to measure the cushioning of a surface have been shown to be not correlated with the impact forces produced by athletes during sporting movements and could therefore be biomechanically invalid (Nigg & Yeadon, 1987). This study compared the results from the analysis of heel-toe running with a series of drop tests and reported a correlation coefficient of less than 0.5. Numone *et al* (2007; 2008) reported that the Berlin Athlete test significantly produced lower loads than the experienced when landing for a jump from 50cm and, therefore, may be inappropriate to evaluate artificial turf for high impact sports actions.

Furthermore, higher impact forces are observed on stiffer surfaces during Berlin Athlete test. In contrast, athletic impact forces have been shown not to be correlated with surface stiffness (Feehery, 1986; Nigg & Yeadon, 1987). As a result of these limitations, careful consideration should be taken before test methods, such as the Berlin Athlete, are used to predict the external loadings placed on an athlete during sporting movements or used to predict the potential of a surface to reduce surface-related injuries (Nigg, 1990).

The Berlin Athlete was initially designed for use on area-elastic surfaces, such as gymnasium floors, which have a linear loading response. The visco-elastic nature of artificial turf demonstrates a non-linear loading response, resulting in an increase in stiffness with surface deformation. This visco-elasticity is also time dependent. It has been suggested that the loading timing of the Berlin Athlete is too short compared to a human footfall (Dunlop, 2002; Shorten, 2001). It could also be argued that the current tests do not replicate the time history or impulse of the force applied by sports performers. Therefore, any testing should approximate the magnitude and timescale of a human footfall during sporting movements (Walker, 2003).

2.2.2.4 Linear Resistance Tests

The following is a summary of the mechanical tests to evaluate the linear resistance (or traction) of a surface.

ASTM Sports Shoe Traction Test

The Sports Shoe Traction Test (ASTM F-1551-94-AT 030) (American Society for Testing and Materials, 1997) determines the traction coefficient between shoes and playing surfaces. A barbell weight is placed on top of a regular sports shoe or modified sports shoe with the uppers cut off. A nylon belt is placed around the shoe and is attached to a push-pull gauge, which is pulled in a horizontal direction. The minimum force required to either initiate sliding (static friction) or maintain movement (kinetic friction) is recorded. Traction is defined as the horizontal force divided by the vertical force applied by the weight and the shoe (ASTM,1997).

British Standard (BS 7044 2.2:1990)

This now withdrawn standard provided methods for assessing sliding distance and slip resistance (Winterbottom, 1985). Sliding distance gives a measure of the resistance to the player's foot sliding on the surface. To determine sliding distance, a weighted trolley ($45\pm 2\text{kg}$) with a sliding foot, bonded with some sports shoe sole material, placed in a trailing position is used (Figure 2.4) The trolley travels down an inclined plane under gravity onto the surface and the distance it travels is measured (British Standards Institute, 1990).



Figure 2.4 BS7044 Sliding distance test

Modified Le Roux Pendulum

Slip resistance is currently measured with a Portable Skid Resistance Tester (commonly known as Modified Le Roux pendulum) (British Standards Institute, 2006), which uses a rubber foot attached to the end of a pendulum (Figure 2.5). After release, the foot is allowed to slide over the surface. A friction coefficient is determined using the maximum height attained by the foot following sliding on the surface. This test is now used as the European Standard (BS EN 14837:2006) for determining the linear resistance of a sports surface (British Standards Institute, 2006). It is also FIFA's (2009b) and the IRB's (2010) recommended test procedure for linear resistance of the shoe-surface interaction. A sports shoe sole or studded test foot can be used in this device.



Figure 2.5 Modified Le Roux Pendulum

Securisport Sports Surface Tester

As FIFA's recommended procedure for determining skin/surface friction, the Securisport Sports Surface Tester (Wassing GmbH, 2006) comprises a test foot lined with silicon which is moved in a circular motion across a test surface (Figure 2.6). A vertical force of 100N is applied to the test foot before it is allowed to rotate. The test foot then makes 5 revolutions at a speed of 40 revs/min. A coefficient of friction is calculated. However, Verlhest (2007) identifies the limitations of the device: it does not measure friction at the start of movement; the speed and pressure applied to the test foot is low; the use a rotational movement for determine linear traction, and the lack of any temperature measurement.



Figure 2.6 Securisport Sports Surface Tester

Verhelst et al Friction Sledge

Verhelst *et al* (2007) have developed a friction evaluation device (Figure 2.7). It comprises a ramp from which a sledge is launched down onto the test surface. The sledge mass ranges between 15-31kg and is travels down the ramp at a speed up to 22kmh^{-1} . The test foot at the bottom of the sledge is lined with artificial skin. The sliding distance, coefficient of friction and the temperature at the contact surface is measured.

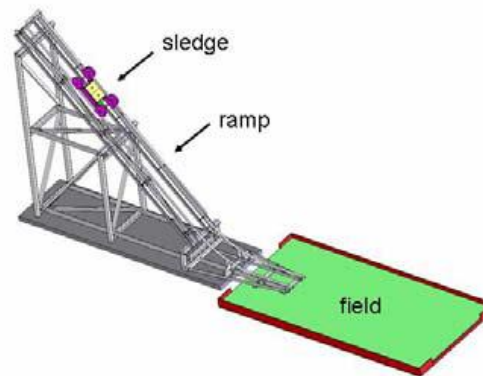


Figure 2.7 Verhelst et al (2007) friction testing device

Instituto de Biomecanica de Valencia (IBV) Friction Test Device

IBV have developed a test device to represent the sliding tackle in football (Sanchis *et al.*, 2008) (Figure 2.8). A test foot coated with a silicone skin is slid along a surface by a machine at a constant velocity of

0.4ms^{-1} . A constant 150N vertical force is applied to the test foot as it is moved across the test surface. The device measures both coefficients of static and dynamic friction.

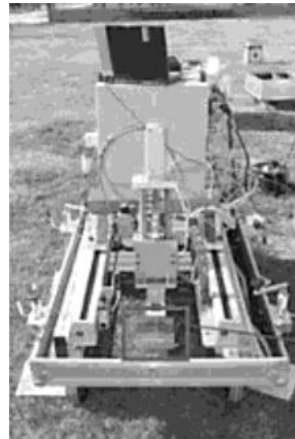


Figure 2.8 IBV friction test device

Schlaepfer et al. Friction Sled

Schlaepfer *et al.* (1983) developed a rig consisting of a sled, incorporating a variable weighted sports shoe, which is pulled across a force platform. It was used to determine the friction coefficients of sports shoes that were tested on different surfaces.

University of Sheffield SERG Sports Surface Traction Test Rig

The Sports Engineering Research Group at the University of Sheffield have developed a force controlled traction rig to measure the initial resistance of a surface to motion (Figure 2.9) (Clarke *et al.*, 2008). Commercial and bespoke studs can be attached to the loaded test plate in a variety of orientations.



Figure 2.9 SERG sports surface traction rig

University of South Wales Hydraulic Friction Tester

A hydraulically powered device developed by the University of New South Wales measures the dynamic friction of the shoe/surface interaction (Lloyd and Stevenson, 1990). A sports shoe is attached to the end of a pendulum arm. The arm is driven across the surface by a hydraulic cylinder. A vertical/normal force is applied by another hydraulic cylinder on the pendulum arm itself. This device allows the use of variable vertical loadings and shoe contact angles.

2.2.2.5 Rotational Resistance Tests

Following is a summary of the mechanical tests to evaluate the rotational resistance of a surface.

British Standards Institute (BS EN 15301-1:2007)

The BS EN 15301-1:2007 describes a test method to determine the rotational resistance of sports surfaces (British Standards Institute, 2007a). A weighted, circular test foot (mass: 46 ± 2 kg, diameter: 150 ± 2 mm) attached with a piece of sports shoe sole material is manually rotated from a stationary position against a surface and the torque required to cause movement is measured using a torque wrench (Figure 2.10).

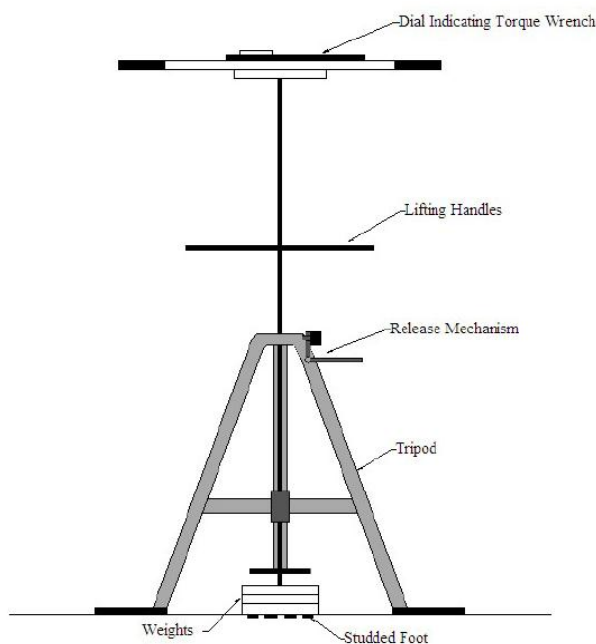


Figure 2.10 BS EN 15301-1:2007 Rotational resistance test

This is similar to the German standard for traction testing. The Stuttgart Sliding device, as described in DIN standard 18032, measures the rotational friction of a playing surface from the application of a specified

constant torque. A standard leather sole is adhered to the base of the test foot, which is in contrast to the similar British test, which uses a sports shoe sole.

2.2.2.6 Combined Loading Tests

The following is a summary of the mechanical tests which incorporate the combined application of two or more loads in different directions or planes to evaluate different surface properties.

TrakTester

The TrakTester was developed from a systematic analysis of ACL injuries and computer simulation of injury situations (Grund *et al.*, 2007; Grund and Senner, 2010). The device consists of a frame housing an artificial lower leg, a load application unit and a pneumatic control unit (Figure 2.11). The artificial leg can be tilted in the sagittal and frontal planes, and incorporates a pin-jointed foot and shank to simulate plantar/dorsi-flexion and supination/pronation. The pneumatic cylinder can impart a maximum 4700N along the axis of the shaft. Torque is produced around the longitudinal axis of the shaft by a ‘pneumatic muscle’, which can produce torques up to 219Nm. The TrakTester is similar to the earlier PENNFOOT (McNitt *et al.*, 1997) which consisted of a framework that supports a leg and foot assembly to measure both rotational and linear traction using different footwear under various loading weights.

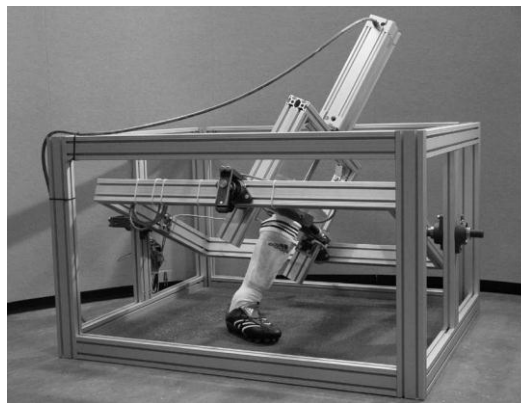


Figure 2.11 TrakTester device

Exeter Research ST2T

The Exeter Research ST2T (Exeter Research, 2010) is a semi-portable tester for measuring translational and rotational friction between shoes and surfaces (Figure 2.12). The device consists of a test foot, on which a shoe can be mounted, attached to a vertical shaft that is loaded with free weights. The shaft assembly is pulled along the test surface by a cable driven by a variable speed electric motor. The tension in the cable is measured using a force transducer, giving a measure of traction force generated. In a separate test, an instrumented torque wrench rotates the shaft and gives a measure of the moment of force resisting rotation (Shorten & Himmelsbach, 2002).

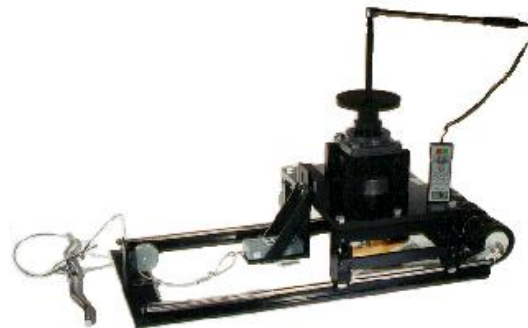


Figure 2.12 S2T2 friction tester

Other Lab-based Devices

Andreasson *et al.* (1986) developed a method for the simultaneous measurement of torque and frictional force of a sliding shoe. An artificial foot, on which different shoes could be applied, is positioned onto the sample of test surface and is attached to a rotating circular disc that is driven by an electric motor. The speed of rotation can be varied to simulate the range of speeds from walking to running. The artificial foot is attached to an aluminium pipe that is instrumented with strain gauges, to which a vertical load is applied via a pneumatic cylinder.

Heidt *et al.* (1996) developed a testing apparatus that employed rotary pneumatic actuators to rotate a test surface and linear pneumatic actuators to provide translation to a weighted sports shoe. A six-channel load cell is placed on the shaft positioning the sports shoe. The combined effects of the actuators simulated

the loadings that occur during a plant and cut motion.

2.2.2.7 *Limitations of Traction Testing Devices*

The current tests used to assess the frictional or tractional properties of the artificial playing surface have some limitations. As is the case with the impact test, several procedures apply forces and use test shoe materials which are not the same as those observed in a real athletic situation. It has been suggested that new test procedures be developed that use the appropriate shoe materials for the sports movements likely to be performed on the surface (Dixon *et al.*, 1999).

Moreover, some of the current tests either test for linear or rotational traction. There is no well-defined correlation between the resistance to translational movement and rotational movement. It is therefore recommended that the assessment of the frictional properties of a surface must include tests using both movements (Dixon *et al.*, 1999; Nigg, 1990).

Many of the traction testing methods use lower vertical forces than what would be evident in actual sporting movements. These tests utilise the coefficient of friction, while assuming Coulomb's Law, as a measure of traction. However, there is a significant influence of the normal force in friction test results. It has been shown that an increasing normal force can either increase or decrease the friction coefficient (Nigg, 1990; Schlaepfer, 1983; Valiant *et al.*, 1985). Furthermore, Severn *et al.* (2010) reported that the greatest effect on peak rotational traction resulted from changing the static normal force applied (i.e. static weight applied to the test device during a test). More recent devices, such as the *TrakTester* and *S2T2* seem to overcome some of these limitations, although detailed information of their design and operation is limited.

2.2.3 *Artificial Turf Assessment Procedures for Specific Sports*

In 2001 the Fédération Internationale de Football Association (FIFA), the world football governing body, produced the "*FIFA: Guide to artificial surfaces*" (FIFA, 2001), as part of FIFA's Quality Concept programme, in order to standardise artificial turf quality and to ensure the safety of footballers alongside

developments in the industry. Subsequently, the Union of European Football Associations (UEFA) produced its “*Artificial turf manual*” in 2002. These were superseded by FIFA’s “*Quality Concept for artificial turf*” (Fédération Internationale de Football Association, 2009b). These documents described comprehensive laboratory and field tests in order to assess an artificial turf’s performance in terms of certain criteria, including durability, climatic resistance, player/surface interaction and ball/surface interaction.

The tests adopted by FIFA and UEFA to assess the player/surface interaction are the Berlin Athlete to measure shock absorbency and vertical deformation (using 40N/mm spring), the Modified Le Roux Pendulum Tester to determine slip resistance, the BS EN 15301-1:2007 Torque Wrench Test to measure rotational traction and the BS EN 14837:2006 Sliding Distance Test.

The International Rugby Board (IRB) and the Federation Internationale de Hockey (FIH) have also produced guidelines regarding the testing of synthetic surfaces to be used in their respective sports (Federation Internationale de Hockey, 2008; International Rugby Board, 2010).

Table 2.1 details the recommended specifications for each test. Both sets of guidelines use the same test procedures as the FIFA/UEFA guidelines, except that IRB includes the ASTM F-355 for the maximum deceleration of an object during an impact, quoting a maximum acceleration requirement of 125g.

Characteristic	FIFA (2009)	IRB (2010)	FIH (2008)
Shock Absorbency (FR%)	55-70%	60-75%	40-65%
Vertical Deformation (mm)	4-9 (Low Impact) 7-15 (High Impact)	4-10 (Low Impact) 7-16 (High Impact)	N/A N/A
Rotational Traction (Nm)	25-50	30-50	N/A
Slip Resistance (μ)	0.6-1.0	0.6-1.0	0.6-1.0
Sliding Distance (m)	0.25-0.55	N/A	N/A

Table 2.1 Recommended specifications for human/surface interaction tests on artificial turf

2.2.3.1 Tests to assess playing quality of surface

There are other tests conducted to describe the playing quality and performance standards of artificial surfaces used in sport, in terms of ball-surface interaction, ageing, climatic resistance, and durability resilience. These are beyond the scope of this thesis and the reader is referred to European Standards Committee CEN/TC217 which has produced the standard EN 15330-1 “*Surfaces for sports areas - Synthetic*

turf and needle-punched surfaces primarily designed for outdoor use - Part 1: Specification for synthetic turf” (British Standards Institute, 2007b) to supersede the previous British Standard BS 7044:1990.

This standard specifies the properties required from synthetic turf surfaces intended for the sports of football, hockey, rugby, tennis or multi-sports use. The standard has a comprehensive range of ball/surface requirements including amount of ball roll and the angle of the ball rebound. The standard also provides requirements for the player/surface interaction shock absorption, vertical deformation and rotational resistance. Requirements for the effects of resistance to artificial weathering, joint strength and simulated use are detailed too.

The reader is referred to FIFA (2009), IRB (2010) and FIH (2008) for further information on sports specific surface requirements.

2.3 Biomechanical Analysis of Player/Surface Interaction

2.3.1 Ground Loadings (Ground Reaction Forces and Moments)

An understanding of the loading response of artificial surfaces may lead to the reduction of non-contact injuries (Nigg, 1990). Nigg and Yeadon (1987) described the ‘hardness’ of the surface and its frictional properties as important aspects to the aetiology of surface related injuries. Nigg (1990) and Dixon (1999) recommended that the mechanical testing of playing surfaces should be performed using the actual forces applied by an athlete during standard test movements.

The loadings applied by an athlete to the ground, or alternatively the ground reaction forces (GRFs) and moments, can be measured using force plates or platform. GRF magnitudes are reported in Newtons (N) or as a multiple of bodyweight (BW). The resultant GRFs can be separated into its three components, one vertical (F_y) and two horizontal (F_x , F_z) to produce the following measurement variables: peak forces, times to peak forces, loading rates, and the duration of contact.

Furthermore, force platforms can be used to measure the free moment of rotation (My'), defined as a

force couple about a vertical axis (*Y*-axis) which results from horizontal shear forces *F_x* and *F_z* (along the *X*-axis and *Z*-axis, respectively) between the foot and ground (Holden and Cavanagh, 1991). It represents the resistance to rotation of the foot on the ground. Force platforms measure the moments applied about the three orthogonal axes through the centre of the platform. The magnitude of moments is reported as Newton metres (Nm). The moment around the vertical axis (*M_y*) is the sum of two moments. The first moment is provided by the resultant shear force (*F_s*) acting through the foot's centre of pressure (COP) at a distance (*r*) from the centre of the platform. The second moment is provided by the free moment, *M_y'*.

Therefore, the free moment is calculated by subtracting the resultant shear moment from the moment around the vertical axis at the force platform origin:

$$M_{y'} = M_y - (F_s \times r) \quad (\text{Eq. 2.3})$$

The ground reaction forces observed during running display distinctive patterns, depending on the style of initial foot contact with the ground (Cavanagh and LaFortune, 1980), the stiffness in the shoe sole (Nigg, 1983), and the effects of the low frequency motions of the body on the GRF signal (Shorten, 2002). Examples of the different patterns of the vertical ground reaction force that are observed during running are illustrated in Figure 2.13.

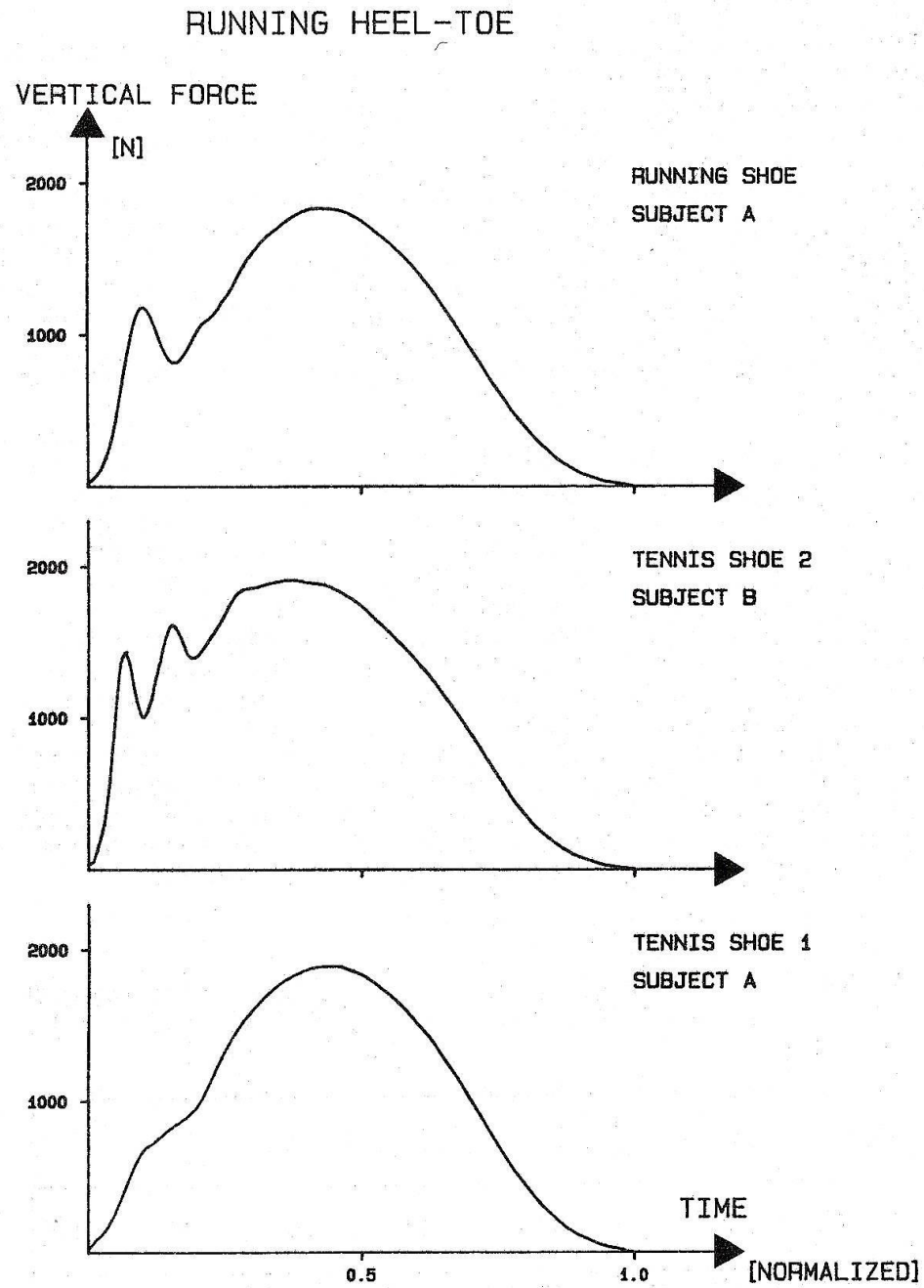


Figure 2.13 Examples of different vertical GRF profiles during running (Nigg, 1983)

The top graph displays two distinctive peaks. The first peak, which occurs in the first 50ms of contact and corresponds to the high deceleration of the foot and leg following initial ground contact (Dixon *et al.*, 1999), has been termed the impact peak (Frederick *et al.*, 1981), passive forces (Nigg, 1983) and initial forces

(Cavanagh & LaFortune, 1980). Due to the evidence of muscle preactivation prior to foot contact (Nigg and Wakeling, 2001) and the concept of two bodies colliding with each other, the use of the *impact force* term has been recommended (Nigg, 1983).

The variables that affect the magnitude of the impact force were described by Nigg (1983) as the velocity of contact, the effective mass at contact, the area of contact and the material properties of the damping elements (soft tissue, shoe, surface). Although, Bobbert *et al.* (1992a) and Shorten (2011) reported that the impact peak's magnitude is mostly determined by low frequency accelerations of the rest of the body.

The second peak has been termed the active force peak (Creaby and Dixon, 2008; Nigg, 1983) or the propulsive force peak (Clarke *et al.*, 1983; Keenan *et al.*, 2011). This peak generally occurs after the first 50ms of initial contact and is characterised by a lower loading rate than impact forces. The active force peak corresponds with full weight acceptance of the body on the foot and the push-off stage (Dixon *et al.*, 1999). Its magnitude is generally greater than the impact peak during running (Shorten and Winslow, 1992).

The top graph characterises a typical heel-toe runner or rear-foot striker (Cavanagh & LaFortune, 1980), where the initial contact is made by the runner's heel, followed by the rolling of the foot during the propulsion stage onto the toes at the end of contact. The middle graph shows two impact peaks that may be present in a heel-toe runner. The second impact could be a result of the forefoot slapping on to the ground (Nigg, 1983).

Finally, the bottom graphs displays a vertical GRF with an absent impact peak. This is characteristic of a mid-foot or forefoot striker (Cavanagh & LaFortune, 1980; Novacheck, 1998), who makes initial ground contact with their midfoot or toes. Runners can be classified as rear-foot strikers or mid-foot strikers as a result of their natural style of running or by their running speed. It was found that foot strike patterns change from being predominantly rear-foot to predominantly midfoot strikers at running speeds greater than 6 ms^{-1} (Keller *et al.*, 1996). This corresponded with a change in the vertical GRF-time histories from a double peak

to a single peak.

Due to higher forces that are observed in the vertical aspect of GRFs, the vast majority of research into ground loadings during running has tended to focus on this direction. Anteroposterior GRFs during running display a braking force period followed by an opposite propulsive force period. Midfoot strikers are shown to produce a double peaked braking phase (Cavanagh & LaFortune, 1980). In the mediolateral direction, there is variability amongst individual runners (Cavanagh & LaFortune, 1980). This may be due to the degree of pronation or supination an individual naturally demonstrates during walking and running, or the stabilising role of the shoes worn.

The magnitude of forces applied to the surface by subjects performing simple movements such as straight line running have been well documented (Bobbert *et al.*, 1992b; Cavanagh, 1990; Cavanagh & LaFortune, 1980; Clarke *et al.*, 1983; Creaby & Dixon, 2008; De Wit *et al.*, 2000; Dixon *et al.*, 2000; Garcilazo, 2007; Guisasola, 2008; Korhonen *et al.*, 2010; McGhie and Ettema, 2012; Meijer *et al.*, 2006; Milner *et al.*, 2006; Novacheck, 1998; Pohl *et al.*, 2008; Reenalda *et al.*, 2011; Stiles *et al.*, 2007; Stiles and Dixon, 2006; Vaughan, 1984). Typical peak ground reaction forces (active forces) during running are approximately 2-3 times bodyweight (BW) (1400-2100N) vertically; 0.4BW (175N) anteroposteriorly and 0.1BW (70N) mediolaterally. Typical peak vertical impact forces during running are approximately 1.5-2BW.

The maximal loading rate (G_{\max}) has been shown to be well correlated with the impact peak and may serve as a useful outcome measure when the impact force peak is not present in the GRF-time history (Nigg, 1983). However, published data on loading rates vary among studies due to methods employed. Typical loading rates during impact for running at 3.5ms^{-1} are approximately $47\text{BW}\text{s}^{-1}$ on 3G turf (Dixon *et al.*, 2000), while Keller (1996) reported slightly loading rates of $18\text{-}30\text{BW}\text{s}^{-1}$ for running at speeds of $3.5\text{-}6.0\text{ms}^{-1}$ on an instrumented uncovered running platform. In contrast, Zifchock *et al.* (Zifchock *et al.*, 2006) reported a loading rate of $77.5\text{BW}\text{s}^{-1}$ in female runners.

There has been little published data regarding the free moment resisting rotations of the foot during running activities. It has been observed that free moments seem to remain below 25Nm (Nigg, 1990). Holden and Cavanagh (1991) reported typical maximum free moments of 12Nm during running at 4.5ms⁻¹.

However, higher free moments up to 20Nm have been reported during various manoeuvres on artificial turf (Stefanyshyn *et al.*, 2010). These maximum free moments acted in a positive direction (tending to resist foot abduction) during the first 70% of contact, followed by a period of negative free moment (tending to resist foot adduction) of decreased magnitude. The maximum positive free moments were observed to increase with increased foot pronation, tending to abduct the foot. Moreover, Milner *et al.* (2006) found that higher levels of free moments are significantly related to increased incidence of tibial stress fractures.

2.3.2 The Effect of Artificial Turf on Ground Loadings

It is argued that changes to surface properties produces no significant changes in the peak impact loads during *in vivo* testing (Dixon *et al.*, 2005; Dixon *et al.*, 2000; Feehery, 1986; Ferris *et al.*, 1998; Ferris *et al.*, 1999; Kaelin *et al.*, 1985; McGhie & Ettema, 2012; Nigg, 2001; Nigg & Wakeling, 2001; Nigg & Yeadon, 1987). For example McGhie and Ettema (McGhie & Ettema, 2012) reported traction coefficients remained almost identical across turf systems and shoes, indicating that players adjusted for undesirable traction conditions.

However, some studies have shown that performing on different types of artificial surfaces result in differences in ground loadings (Dixon *et al.*, 2000; Guisasola, 2008; Lafortune *et al.*, 1996a; 2007; 2007). For example, stiffer surfaces have been observed to cause an increase in the maximum loading rate, i.e. the time to peak impact force is shorter. Using a portable measurement system to investigate the interaction of human with natural playing surfaces, Guisasola (2008) identified significantly greater peak vertical loading rates and peak pressure loading rates for the sand compared to the clay-based natural grass surface during running and cutting activities. Similarly, others have reported a decrease in the loading rate for a softer

artificial surface (Dixon *et al.*, 2000) and a significant correlation between loading rate and surface cushioning (Stiles and Dixon, 2007). In contrast, a study using a pendulum device used to apply a load to the bottom of a subject's foot that simulated the impact conditions during running found that harder surfaces increased both the magnitude and rate of the peak impact force (Lafortune *et al.*, 1996a).

Experimental and simulation studies have also shown that the hardness of the surface and/or shoe-sole does have an effect on the maximum loading rate (Clarke *et al.*, 1983; Feehery, 1986; Nigg and Liu, 1999).

2.3.3 Ground Loadings of Complex Movements Performed on Artificial Turf

While most research regarding subject biomechanical loadings of artificial turf has generally been focussed on straight line running, more recent publications have examined different types of running and turning movements (Low, 2010; Stiles, 2006; Meijer, 2006; Guisasola, 2008; Morag, 2001; Stefanyshyn, 2010; Garcilazo, 2007).

In sports such as football, rugby and hockey, players execute a range of high frequency stopping and turning movements. Rand and Ohtsuke (2000) described the techniques used by the athletes performing turns or cuts, as they are sometimes referred to, during running. An 'open' technique or 'sidestep cut' involves the athlete using the foot on the opposite side to the direction he/she wants to turn. A 'crossover' technique involves the use of the foot on the same side as the direction he/she wants to turn. The contralateral leg then crosses the plane in which the run up occurred and continues in the new direction. The former technique is recognised to be more efficient when a rapid change of direction is required. The open technique causes less speed reduction and fewer steps to complete the turn. In contrast, the greater speed reduction involved in the crossover technique may allow a tighter turn to be achieved. The ability to turn quickly is an important asset to any sports performer. Turning allows a player to change direction, in order to get beyond opponents, move towards or catch the ball, to avoid tackles or run into space (Bencke *et al.*, 2000).

In early studies of more complex movements, Stucke *et al.* (1984) and Kaelin *et al.* (1985) analysed the player-surface interaction with subjects performing typical sports movement, such as stopping while running and turning. An artificial playing surface was mounted on to a force platform and the time histories of the GRFs were recorded while the subject performed the movements in appropriate shoes. Typical ground reaction forces for stopping a running movement were approximately 2000N (vertical) and 1500N (horizontal). For a standing 90° turn, a free moment of approximately 15-20Nm resisting rotation was observed (Stucke, *et al.*, 1984). Similarly, Stefanyshyn *et al* (Stefanyshyn *et al.*, 2010) and Wannop *et al* (Wannop *et al.*, 2010) reported free moments 16-24Nm for two types of running and turning movements performed on 3G artificial turf.

Bencke *et al* (2000) analysed GRFs and the leg muscle activity (EMG) of handball players performing sidestep cutting. It was reported that a peak vertical GRF of 2.88BW and 2.63BW occurred during stance for the braking phase and propulsive phase, respectively.

Durà *et al.* (Durá and Martinez, 1999) examined a 180° turning movement performed from a standing start on five different surfaces, each with different coefficients of friction (mechanically measured). It was found that the surface friction influenced the duration of the phases of the movement examined and higher rotational moments (or free moments) were observed on surfaces that had a higher friction coefficient.

Garcilazo (2007) compared the forces on the lower extremity while landing and side cutting (rapid direction change at approximately 45 degrees) on artificial football turf with different styles of football cleats. Peak vertical ground reaction forces for running and cutting techniques were approximately 2500N and 3500N, respectively. The choice of footwear did not affect the peak vertical ground reaction force measured. Bencke *et al* (2000) analysed GRFs and the leg muscle activity (EMG) of handball players performing sidestep cutting. It was reported that a peak vertical GRF of 2.88BW and 2.63BW occurred during stance for the braking phase and propulsive phase, respectively.

Stiles and Dixon (2003) conducted a biomechanical assessment of a tennis 'running forehand plant'

movement and reported greater peak impact forces on tennis playing surfaces compared to a baseline concrete surface. This could not be readily explained by the measured kinematic variables but the heel impact velocity and peak loading rate were also lower on the concrete surface.

Valiant (1987) examined the ground reaction forces and moments produced during different sporting movements on Astroturf performed by eight athletes. The movements analysed were straight-line running, a 90° cut turn and a 180° pivot. Mean peak vertical GRF, expressed in multiples of bodyweight (BW) were 2.46BW, 3.45BW and 3.02BW for the run, 90° cut and pivot, respectively. Peak shear forces during the running movement were -0.06BW anteroposterior (A-P) and 0.66BW mediolateral (M-L). For the 90° cut: -1.55BW (A-P) and 1.85BW (M-L). For the 180° pivot: -1.46BW (A-P), 1.60BW (M-L). The mean free moment (the torque developed to resist rotation during turning) was 17.2Nm for the 180° pivot movement.

Morag and Johnson (Morag & Johnson, 2001) studied the ground reaction forces of football players of three different age groups performing two types of movement on Astroturf. For cutting movements peak M-L braking forces ranged from 0.97-1.17 BW with corresponding traction ratios ranging from 0.46-0.51. For an acceleration type movement, peak A-P propulsion forces ranged from 0.46-0.73 BW and the traction ratios ranging from 0.52-0.69. It was reported that significant lower traction requirements were observed for children compared to adults for these movements.

Shorten *et al.* (2003) compared the traction properties of natural turf, conventional synthetic turf and 3G in-filled synthetic turf with the measured traction requirements of American football players performing cutting movements. From the analysis of ground reaction forces, a 95th percentile peak traction coefficients of 1.19, 1.23 and 1.25 for 45°, 90° and 180° cutting movements, respectively, were reported. It was found that the average traction made available by the in-filled surfaces, exceeded these player traction requirements, suggesting that the players would be less likely to slip during the execution of these turning movements. In addition, the in-fill turfs displayed similar translational and rotational tractions to that of natural turf.

2.3.4 Kinematic Adaptations to Artificial Turf

The analysis of ground reaction forces and moments is only a measurement of the external forces and shocks applied to the body. Results from such tests do not reflect the potential kinematic changes experienced by players on artificial surfaces, which have been reported by previous research (Dixon *et al.*, 2005; Dixon *et al.*, 1999; Dixon *et al.*, 2000; Frederick, 1986; Gerritsen *et al.*, 1995; Hardin *et al.*, 2004; Nigg, 1990).

To use ground reaction forces to assess injury risk, this data must be used conjunction with other biomechanical methods, such as motion cameras or tracking systems, that can measure the position of body segments in relation to the application of the external forces, in order to quantify the internal moments and forces around joints.

Increases in external loading are likely to increase the moments around the joints of the lower segment of the body. This will cause muscles to generate more force to counteract these external loadings, thus increasing the loading of the joint. Theoretically, kinematic adjustments are seen to reduce or minimise these joint loadings (Dixon *et al.*, 2005), with reductions achieved mainly by changing the geometry of the acting forces (Nigg, 1985).

The loadings applied to the lower segments of the human body during physical activity on different surfaces can be influenced by changing the foot and leg kinematics, ankle and knee joint stiffness, and/or the coupling between the soft and rigid structures of the leg (Nigg, 2001). A reason for the relative consistency of ground reaction forces across different surfaces reported by some authors has been associated to the kinematic adaptations by the athlete (Clarke *et al.*, 1983; Dixon *et al.*, 2000; Dixon, 2008; Lafortune *et al.*, 1996a; Nigg & Yeadon, 1987). Consistent peak impact forces across surfaces could be explained by changes in heel impact velocity, with significantly reduced initial heel velocities observed on stiffer surfaces (Dixon *et al.*, 1999). Although in a later study, Dixon *et al.* (2000) found that initial heel velocities were unchanged by changes in the surface. A significant correlation ($r=0.72$) was observed between relative decreases in vertical heel velocity and force loading rate by Patritti *et al.* (2003).

Hardin *et al* (2004) and Ferris *et al* (1998) reported changes in a runner's leg stiffness on different surface stiffness in order to maintain similar running mechanics, in terms of ground reaction force, centre of mass movement and ground contact time. Runners increase leg stiffness on elastic surfaces and decrease leg stiffness on stiff surfaces (Hardin *et al.*, 2004). A decrease in leg stiffness on hard non-compliant surfaces is shown by an increase in joint flexion, thus increasing joint moments and joint forces (Ferris *et al.*, 1998). It was later reported that this alteration in leg stiffness and kinematics in accommodation to changes in surface stiffness can occur after for their first step on a new surface after the transition (Ferris *et al.*, 1999). In a study modelling leg stiffness during a hopping action on surfaces of different stiffness, Farley *et al* (1998) reported that an increase in ankle stiffness is also an important factor to increasing leg stiffness.

Dixon *et al.* (2000), in a study of shod heel-toe running on 3 different surfaces, supported the view of greater initial knee flexion as a compensatory adjustment to allow the lower extremity to cushion the impact experienced on less compliant surfaces. In addition, a trend for increased peak ankle flexion, peak knee flexion and peak ankle flexion velocity was reported for some individual subjects for surfaces providing increased mechanical cushioning, concluding that subject kinematics following impact is influenced by factors more than just initial joint angles and the mechanisms of adaptation varies among individual, recommending the need to perform individual subject analyses. In a later study, Dixon *et al* (Dixon *et al.*, 2005) also found individual variations in general knee kinematics on different surfaces but they reported individual increases in knee flexion on stiffer surfaces.

Lafortune *et al.* (Lafortune *et al.*, 1996a) concluded that although an increased initial knee angle at impact can substantially decrease the effective axial leg stiffness (Lafortune *et al.*, 1996b), its effect may not be as important as the foot/shoe/surface interface. It was stated that “*the foot-interface compression accounted for more than 90% of the leg during initial impact*” and “*leg stiffness during the initial phase of impact loading was found to be almost exclusively dependent on the heel fat pad and impacting interfaces*”. Although this study simulated impact conditions using a horizontal human pendulum device, the effect of

muscle-preactivation prior to impact that occurs during normal running on different surfaces (Nigg, 2001) on lower extremity joint stiffness was not accounted for.

It has been further demonstrated that an increase in initial knee flexion from 0 to 40° during contact with the ground during running decreases the effective axial stiffness of the body and reduces the transmission of high frequency shock (5-60Hz) through the body to the head but adversely exposes the lower leg to 57% more severe shock (Lafortune *et al.*, 1996a; Lafortune *et al.*, 1996b), leading to a substantial increase in the rate of energy utilisation (McMahon *et al.*, 1987).

Other studies have demonstrated increases in knee flexion angle and angular velocity (Dixon *et al.*, 2005; Durá & Martinez, 1999; Hardin *et al.*, 2004; Herzog, 1978), and changes in rear foot pronation (Stergiou and Bates, 1997) throughout the stance phase of a movement in response to increases in surface stiffness. Hardin *et al.* (2004) also reported increased ankle and hip flexion velocities on harder surfaces, as a result of an uncontrollable response to the impact forces. Stucke *et al.* (1984) reported that higher knee flexion angles were present during a stopping movement on a surface of a higher static friction, which prevented any sliding of the foot on the surface.

Dowling *et al.* (2010) found that performing on a high friction surface resulted in a lower knee flexion angle, lower external knee flexion moment and higher external knee valgus moment compared to a low friction surface. However, other than this study, there appears to be general lack of literature on the impact of artificial turfs on the frontal plane kinematics of the lower extremities.

Nigg and Liu (1999) described a new concept for the effect of impact forces on the musculoskeletal system. In a review of the literature, it was reported that much of the evidence did not support the traditional concept of impact forces as one prime reason for the onset of running injuries. Nigg (1997) proposed a concept of muscle tuning or muscle preactivation in order to minimise the soft tissue vibrations caused by the high frequency impact loadings. This hypothesis has since been investigated in a number of studies by Boyer and Nigg (2007; 2004; 2006) and other authors (Friesenbichler *et al.*, 2011; Wakeling *et al.*, 2001;

Zadpoor and Nikooyan, 2010).

In summary the muscle tuning theory states that repetitive impact forces during physical activities cause changes in myoelectric activity (muscle tuning) to minimize soft tissue vibrations (Nigg & Wakeling, 2001). The natural frequency of soft tissues in the lower segments is in the range of 10-50Hz, and impact peaks during running have a major frequency content which is typically 10-20Hz. Therefore, impact forces may cause the resonance of soft tissues (Wakeling and Nigg, 2001).

Soft tissue vibrations during physical activity are seen to have an adverse effect on comfort and performance and contribute to increased work and fatigue (Nigg, 2001). It is proposed that the muscle preactivation prior to impact creates a damped vibrating system, as it has been shown that both the natural frequency and damping coefficients of the soft tissues of the lower extremity change with altered muscle activity (Wakeling & Nigg, 2001).

The degree and manner of muscle preactivation in response to different loading rates of impact forces appear to be subject-specific and muscle specific (Nigg & Wakeling, 2001). A human pendulum system was used in order to isolate the muscle activity required for minimising soft tissue vibration during an impact from the muscle activity required to move the leg (Wakeling *et al.*, 2001). Some subjects demonstrated an increased muscle preactivation in response to a harder sole insert while other subjects demonstrated a decreased muscle preactivation response.

A study measured the changes in muscle activity and soft tissue vibrations that occurred during walking with soft and hard shoe conditions (Wakeling *et al.*, 2003). It was reported that significant increases in pre-impact (50ms) EMG intensity of the biceps femoris and the lateral gastrocnemius muscles and a reduction in the vibration frequency in the axial direction of the hamstring, quadriceps and tibialis anterior muscles at impact occurred with the soft shoe condition (Wakeling *et al.*, 2003).

In contrast to the muscle tuning theory to reduce soft tissue vibration during impact, the displacement of soft tissues has been seen to have a positive role during running. It has been reported that the ability of

the wobbling mass of the shank to dissipate energy during impact is significant (Pain and Challis, 2001).

2.3.5 Kinematic and Kinetic Analysis of Complex Movements

It is important to quantify the loadings on the body while performing complex movements as stopping, turning, landing and rotating are considered to present a higher risk of injury (Stacoff *et al.*, 1996). However, the kinematics of complex movements on artificial turf, other than straight-line running, have not been extensively analysed to date. One possible reason for this could be the selection of reliable movements that can be analysed can be difficult.

The most common type of movement which has undergone biomechanical analysis is the cutting turn (as described in section 2.3.3). Stefanyshyn *et al* (2010) quantified the ankle and knee joint moments for a group of 12 recreational soccer players while performing cutting and turning movements at 4.0 ms^{-1} on the same artificial turf. In a similar study, Wannop *et al* (2010) reported peak ankle external rotation moments of 80-90Nm, peak knee external rotation moments of 32-36Nm and peak knee adduction moments of 186-224Nm.

While Kaila (2007) did not examine different types of turf, significantly greater tibial internal rotation and abduction moments were reported for sidestep cutting at 30° and 60° compared with straight-ahead running on 3G artificial turf. It was also show that different types of footwear sole design (studded and bladed cleats) did not impact knee loading during 30° and 60° sidestep cutting movements.

Besier *et al* (Besier *et al.*, 2001b) studied the knee biomechanics of 11 male subjects performing running, sidestep (open technique) cutting at different angles and crossover cutting on artificial turf. It was reported that sidestep and crossover cutting produced significantly greater abduction/adduction and internal/external rotation than during normal running, which could place potentially damaging loads on specific knee ligaments. Flexion moments remained similar. The sidestep cutting turn generally produced a combination of external flexion, valgus (abduction) and internal rotation moments, while the crossover technique produced external flexion, varus (adduction) and external rotation loading. However, different

techniques and individual responses were also observed. Some subjects performed sidestepping cuts with a varus (adduction) moment applied to the knee, while the other six had a valgus (abduction) moment applied. As the subjects performed the movements barefoot in this study, it may be expected that the kinematics of the subject may alter if performed wearing sports shoes or on a sports surface.

McLean *et al* (1999) found no significant differences in knee joint motion between males and females performing sidestep cutting. However, females displayed an increased maximum abduction angle during stance, which was attributed to the larger Q angle than males. It was also concluded that the intrasubject variability in knee joint kinematics observed may be related to the level of experience a subject has performing the manoeuvres.

Many of these studies incorporated sidestepping movements, in which the subjects were aware beforehand where and when they should perform the turn. In a study of unanticipated movements, it was reported that knee abduction/adduction and internal/external rotation moments can double during unanticipated manoeuvres compared to anticipated manoeuvres (Besier *et al.*, 2001b). Pollard *et al* (Pollard *et al.*, 2003) reported that while the magnitude of knee joint moments remained similar between males and females during unanticipated cutting manoeuvres, the female subjects reached a maximum internal rotation during stance earlier than males, when the knee is in greater flexion. It was suggested that this may place a female's ACL ligament under greater load and a higher risk of injury.

Simonsen *et al* (2000) reported that the greatest loading of the knee during a sidestepping movement of handball players occurred in the sagittal plane, with a peak internal knee extensor moment of 239Nm (99-309Nm). This produced a knee shear/ACL loading of approximately 520N (215-673N), indicating that an individual manoeuvre would not cause the rupture of the ACL ligament. However these values may underestimate the loading produced in other sports as the subjects only took a two-step run before executing a preplanned movement.

Cutting movement causes medial side of the foot to touch the ground first, creating a large lever arm

that generates an inversion moment (Stacoff *et al.*, 1996). In a study examining the effects of shoe design on the lateral stability of the ankle joint complex, Stacoff *et al* (1996) reported that wearing shoes increases this lever arm, decreases lateral stability and increases the risk of ankle sprains. It was concluded that shoes that provided lateral stability in their design reduced ankle inversion. It was also observed that subjects performed two types of landing technique while performing a sidestep cut, depending on whether the subject wore shoes. In the barefoot condition, a ‘flat foot’ approach was adopted. In the shod condition, subjects adopted a ‘rolling’ approach, where the foot rolls over the medial border of the shoe.

With regards to other types of movement, a study of 180° turns reported significant differences across five surfaces in knee flexion during the braking phase of the movement (Durá & Martinez, 1999). Greater knee flexion angles were observed on surfaces with a higher friction coefficient. This was attributed to a protective mechanism, with the subject trying to reduce the effect of the increased torques around the knee by increasing the duration of the braking phase with more knee flexion. However, no information was presented with regards to the joint moments that occurred during this movement.

In a study of landing from a jump following a heading movement performed on 3G turf and natural turf, Jones *et al* (2009) reported similar knee flexion/extension and internal/external rotation angles throughout the landing contact phase, whilst differences occurred in knee adduction/abduction angles. Furthermore, greater movement variability was demonstrated in all three knee joint angles in movements performed on 3G turf compared to natural turf.

Sports-specific movements play an important role for individual sports. Examples of sport-specific movements include the sliding tackle, header and kicking in football; mauling, rucking, line-out jumping in rugby; and the drive, penalty stroke, push, lateral turn in field hockey. However, this study was focussed on the biomechanics of generic movements that are observed in many different field sports. For a detailed description and review of the biomechanics of football (soccer) skills, the reader is referred to Lees and Nolan (Lees *et al.*, 2010; Lees & Nolan, 1998). Generally, kicking has been the skill that has been most

thoroughly examined, as it is the most important aspect of the sport. For the biomechanics of specific field hockey movements, the reader is referred to the following studies: Hussain *et al.* (2011) and Lopez *et al.* (2010). For the biomechanics of specific rugby movements, the reader is referred to the following studies: Mellalieu *et al.* (2008), Milburn (1993) and Trewartha *et al.* (2008).

2.3.6 Biomechanical Shoe Testing

It is important to remember that the biomechanical interaction also includes the human/shoe interface. The kinematic and kinetic interactions associated with running in different types of shoes have been well documented (Bentley *et al.*, 2011; Clarke *et al.*, 1983; Hennig, 2011; McNair and Marshall, 1994; Nigg *et al.*, 1984; Queen *et al.*, 2008) and a general discussion of this aspect is beyond the scope of this study.

However, in terms of artificial turf studies, Heidt *et al.* (1996) reported that greater torques were generated on artificial turf in a study of 15 American Football shoes on wet and dry, artificial and natural turf surfaces. Bonstingel *et al.* (1975) also found that rotational moments were higher on artificial turf than natural turf for both flat soled and studded footwear.

More recently, research in this area has been focussed on the cleat (stud) design and configuration. For example, Bentley *et al.* (2011) investigated peak pressures placed on the foot from wearing football boots with conventional round-studded cleats versus blade-shaped cleats during running and cutting on artificial turf. They concluded that the observed increased pressures on the lateral aspect of the foot caused by the blade design could be potentially hazardous. Stefanyshyn *et al.* (2010) reported that cleated shoes caused significantly higher ankle and knee rotation moments in turning movements. A similar finding was also reported by Queen *et al.* (2008). In contrast, McGhie and Etna (2012) reported similar traction coefficients across different shoe configurations and artificial turf systems.

2.4 Summary of Literature Review and Rationale of the Current Study

Research has shown that injuries are highly prevalent in field sports such as football, rugby and hockey, with non-contact muscle strains and joint sprain being most common in the lower extremities. The knee joint is particularly susceptible to these types of injuries and serious injuries can be hugely detrimental to a player's future participation and/or career. With the introduction of artificial turfs, there has been concern to whether players experience more or less injuries as a result of playing on these surfaces. Though the literature remains inconclusive overall, more recent research indicates that injury rates on new generations of artificial turf are similar to natural turf. Nevertheless, understanding injuries and their potential mechanisms is important when considering the safety of current and future artificial sports surfaces and their impact on players' performance.

Previous biomechanical research regarding artificial turf has typically involved the analysis of simple straight line running, often conducted at a much slower velocity than what might be expected in competitive play. While some recent studies have examined the ground loadings and knee biomechanics which occur more complex and high velocity running and turning movements, this is a general lack of research in this field. In particular, there is a lack of evidence regarding horizontal and free moment ground loading for movements performed on artificial turf. Therefore, the current study set out to fill this gap in knowledge by conducting a 3-dimensional biomechanical analysis of ground contact loadings and the knee joint for players performing a series of activities commonly occurring in elite football, rugby and hockey during competitive games and training on three different types of artificial turf. The knee joint was selected because the literature indicates that this is the most common lower extremity joint which is injured during competitive sport. Moreover, serious knee joint injuries can often restrict participation or even bring a halt a player's career. This study focussed on elite levels of these three sports for the following reasons:

1. Elite sports players are highly trained and should therefore perform movements more consistently than amateur players, thus producing more reliable data.

2. Elite players are likely to conduct running and turning movements at a high level of performance than amateur players. Therefore, the biomechanical data used as the input to the artificial turf testing rig would represent the higher end of ground loadings that are achievable by athletes.
3. Football, hockey and rugby are high-profile sports, which have high levels of participation at professional levels (as well as at both amateur level).
4. Artificial turf has been recently introduced into these sports at the elite level and there is great interest in widening its use.
5. As a result, the sporting governing bodies of these sports in Scotland (Scottish Football Association, Scottish Rugby Union, Scottish Hockey Association) provided their support to this study during the EPSRC funding application and throughout the research, providing access to players and coaches.

With regards to the mechanical testing of artificial turf in relation to the human-surface interaction, it is generally accepted within the literature that test procedures should reflect the realistic loading actions which occur in normal playing conditions. There are many different types of test to determine the turfs response to vertical, linear and rotational loading, several of which have been adopted within the quality standards for artificial turf by sporting governing bodies. However, the literature indicates that some of these tests are likely to be biomechanically invalid because the loads applied by the testing apparatus are typically not correlated with the forces produced by athletes during sporting movements and nor do they use appropriate materials for the test foot. Furthermore, many of these testing procedures apply loads dynamically in a single direction; however sports movements are highly dynamic and complex, and normally includes loading in multiple directions. Moreover, research has demonstrated no correlation between these loads, particularly horizontal and rotational loading, suggesting that test procedures acting in a single degree of freedom are

potentially invalid. As a result, the literature suggests that mechanical artificial turf testing procedures should apply forces to the surface in a combination of directions within the same action to be truly reflective of real-life sporting actions.

Therefore, this study will incorporate biomechanical data into the design and construction of a new prototype test rig, which can replicate the three-dimensional biomechanical interactions which occur in running and turning movements on artificial turf.

CHAPTER 3. METHODOLOGY

This chapter details the biomechanical analysis of the player/turf interaction during running and turning activities. It describes the methods employed to measure the motion of the athletes and the ground loadings during different types of movement performed on various artificial and natural turf. These tests were conducted inside and outside of the biomechanics laboratory. This part of the study was primarily concerned with the motions and loading placed on the stance leg used for running and turning activities.

3.1 Subjects

Thirteen participants took part in the study: 5 footballers (all male, ages 26 to 42 years), 4 hockey players (2 male, 2 female, ages 19 to 24 years) and 4 rugby players (all male, ages 22 to 27 years). Table 3.1 presents a description of the subjects used in this study. All participants had performed at the professional level or a high standard of competition in each of their respective sports.

All subjects conformed to the inclusion criteria set for this study. This stated that the subject should not be injured at the commencement of tests; or have been injured within 3 months prior to the start of testing which required more than two weeks inactivity; or have undergone surgery within the last twelve months prior to the start of testing. All subjects were made aware of the testing procedure, including the potential risks involved, and signed a consent form.

Subject	Age	Height (m)	Weight (kg)	Sport	Position	Level
F1	46	1.74	81.7	Football	Defence	Ex-Pro
F2	43	1.78	75.5	Football	Midfield	Ex-Pro
F3	34	1.70	72.0	Football	Midfield	Ex-Pro
F4	25	1.80	78.0	Football	Defence	Semi-Pro
F5	26	1.95	85.0	Football	Defence	Semi-Pro
H1	18	1.79	67.0	Hockey	Defence	Uni 1 st XI
H2	23	1.79	72.5	Hockey	Midfield	Uni 2 nd XI
H3 (f)	20	1.66	62.0	Hockey	Midfield	Uni 1 st XI
H4 (f)	18	1.55	55.5	Hockey	Forward	Nat. League
R1	24	1.75	97.0	Rugby Union	Centre	Internat'l
R2	22	1.81	88.0	Rugby Union	Wing	Internat'l
R3	27	2.02	115.5	Rugby Union	Forward	Pro
R4	26	1.87	99.0	Rugby Union	Centre	Pro

Table 3.1 Subject details ('f' denotes female subjects)


F1: Adidas Copa Mundial [c] (340g)	F2: Adidas Tremor [nc] (280g)	F3: Unisport Mondial [P] (300g)	F4: Unisport Mondial [P] (330g)	F5: Adidas Art [P] (335g)
				
H1: Dita 350 [P] (335g)	H2: Kangaroos X-Turf [P] (385g)	H3: Adidas Response [nc-turf] (268g)	H4: Dita Turf [P]	
				
R1: Asics Gel Kayano 7 [nc] (418g)	R2: Adidas Supernova [nc] (350g)	R3: Mizuno Xao [nc] (505g)	R4: Nike Air X [nc] (415g)	
				

Table 3.2 Footwear worn by subject during testing. [Sole type: c=cleated; P=pimples; nc=not cleated]. Mass of shoe in brackets.

On arrival at the laboratory, the subjects changed into the clothes required for the testing and their heights and weights were recorded. The subjects wore shorts (and a vest top if the subject was female). The subjects were asked to wear their own preferred sports footwear that they would normally use on artificial turf (Table 3.2).

It was decided that the participants might not feel comfortable if the shoe type was standardised, as it may have resulted in an unnatural execution of the movements. In addition, hockey artificial turf shoes have a different design to football artificial turf shoes, and there is currently no artificial turf footwear designed specifically for rugby.

3.2 Laboratory tests

Prior to the commencement of testing, the necessary and required risk assessments were conducted and the

departmental Ethical Committee granted the appropriate ethical approval.

3.2.1 Artificial Turf

The Biomechanics Laboratory at the Bioengineering Unit, University of Strathclyde was laid out with three types of artificial turf on separate occasions. The three turfs were chosen to represent a general range of the types of turfs currently used: from short pile turfs to the new longer pile 3G turfs. The selected turfs were also dictated by what could be sourced from local suppliers. However, all turfs were previously unused, although exact ages were unavailable.

Turf 1 (T1) was an AstroTurf[®] short pile sand infill turf (depth=15mm), with rubber underlay (depth=10mm) (Figure 3.1). This type of turf is commonly used on community 5-a-side football pitches. Turf 2 (T2) was a medium pile, sand dressed turf (depth=25mm), manufactured by Tarkett Sommer[®] (Figure 3.2). This turf is also used with a rubber underlay (depth=10mm) and is commonly employed for synthetic hockey pitches. Turf 3 (T3) was manufactured by FieldTurf[®], a long pile turf (depth=50mm) with sand/rubber infill (Figure.3.3). This type of turf is an example of the new 3G type of turf recently tested by FIFA and UEFA for its suitability for use for competitive professional football matches.

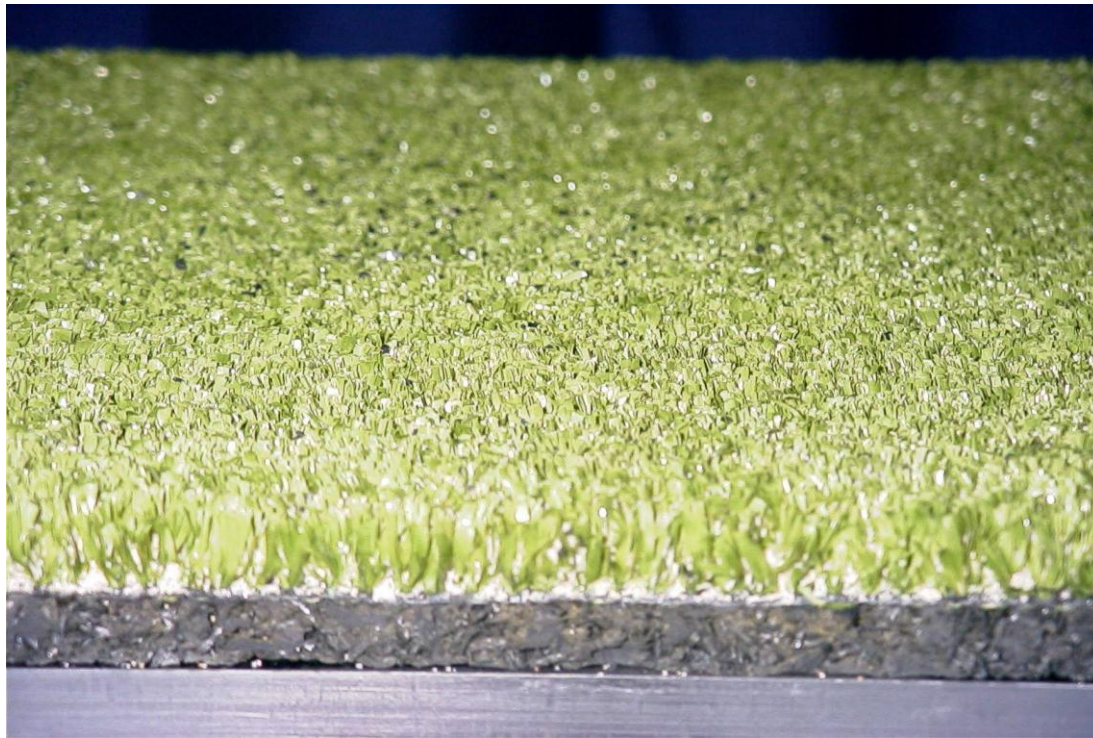


Figure 3.1 Turf 1 (T1), with rubber underlay and sand infill

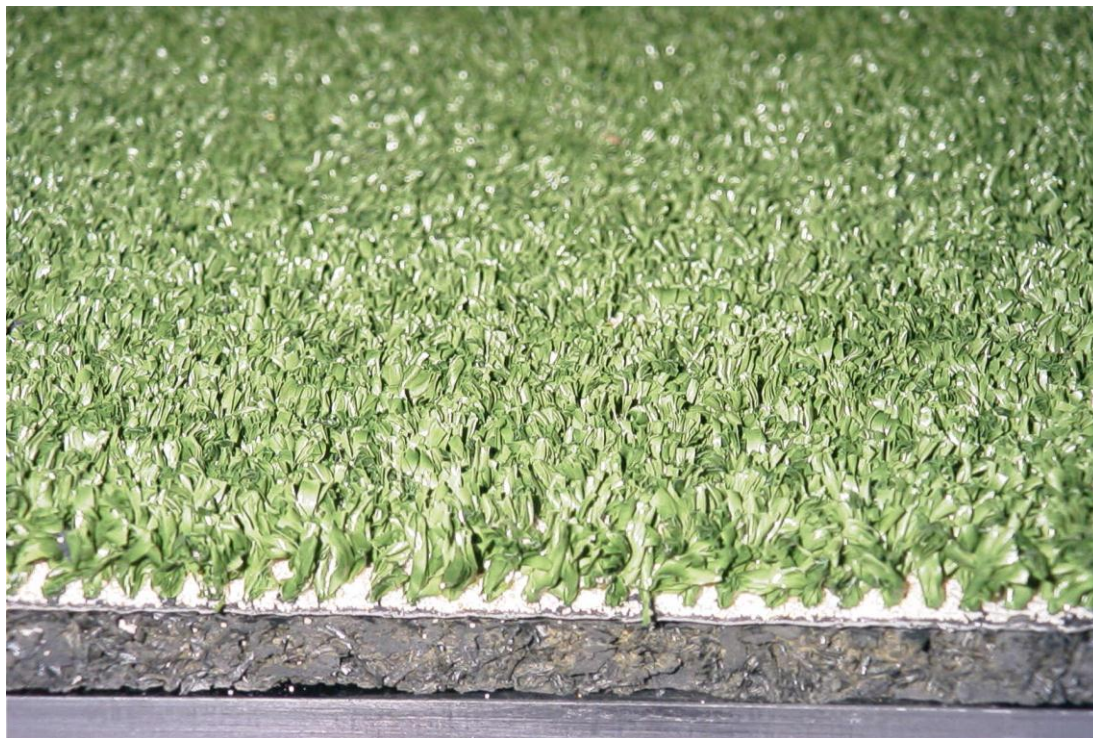


Figure 3.2 Turf 2 (T2), with rubber underlay and sand infill



Figure.3.3 Turf (T3), with rubber and sand infill

The turf covered an area of the laboratory large enough for the selected movements to be performed fully (Figure 3.4). The laboratory was laid out with each turf to allow at least a 7m run-up from each direction to a force-plate and a 7m run-off area to allow sufficient distance for the subject to slow down. For safety reasons during the testing sessions, the subjects were instructed to stay on the artificial turf, which was free from cameras and cables. Also, gymnastic landing mats were secured to the wall at the end of each runway in order to minimise the risk of any potential injuries.



Figure 3.4 Artificial turf installed in Biomechanics laboratory

Each turf was installed and prepared to the manufacturers' specifications. The same 10mm depth rubber underlay, made from reconstituted car tyres was used for both Turf 1 and Turf 2. A rubber underlay was not required for Turf 3. Turf 1 (depth=15mm) was filled with 10mm depth of silica sand so the sand was just below the top of the turf fibres. Type 2 (depth=25mm) was filled with 15mm depth of silica sand so the sand was just over half the depth of the turf fibres. Turf 3 (depth=50mm) was filled with 25mm of silica sand and then 25 mm of rubber granules (manufactured from reconstituted car tyres). The turfs were then raked to ensure uniformity of the sand/rubber infill. All underlay and infill materials were provided by the manufacturers of the artificial turfs.

A cut-out piece of turf (and rubber underlay, if required), equal to the dimensions of the force platform (600 x 400mm) was attached to a force platform with strong double-sided carpet tape. This was done to prevent any force transference along the turf, which could lead to inaccuracies in the measurement of the ground reaction forces (GRFs). Unless the turf was closely inspected, it was difficult to identify the cut-out piece of turf and hence the force platform. Each turf was laid *in situ* for a period of two weeks at a time.

After each testing session with individual subjects, the whole turf surface was raked thoroughly to

eliminate areas which may have been compacted by multiple impacts and to ensure that the surface was consistent between subjects.

3.2.2 Motion Analysis System

An 8-camera 120Hz Vicon 612 motion analysis system (Oxford Metrics, Oxford) measured the trajectories of markers fixed to the subjects and a Kistler force platform (model 9281BII) (Winterthur, Switzerland) measured the reactive forces and moments applied by the ground to the subject. The infrared motion analysis cameras were equally distributed around the force platform, which was positioned approximately in the centre of the runway (Figure 3.5).

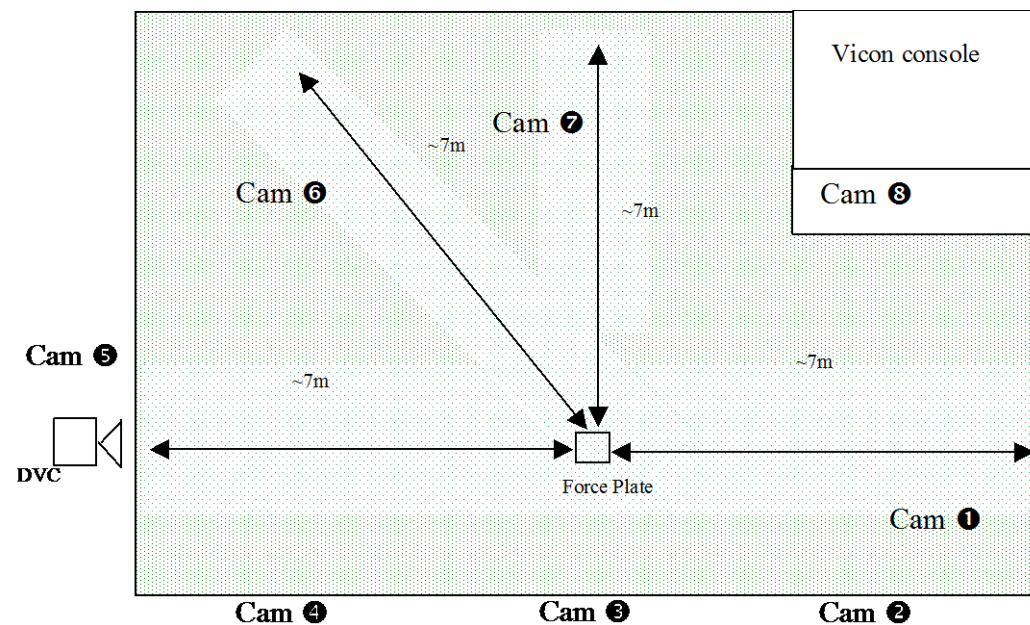


Figure 3.5 Plan view of the layout of the laboratory with location of the cameras (Cam)

The cameras were either positioned on tripods at the side of the artificial turf or rigidly suspended from the laboratory ceiling or wall. This was to ensure that subject safety and reduce the risk of the camera vibration.

In addition to the Vicon system, a Canon XM1 digital video camera (DVC) (25Hz, 1/120 shutter speed) was positioned at one end of the laboratory. This provided a visual reference of the sports movements performed by the participants.

Prior to each testing session, the Vicon motion analysis system was calibrated within the laboratory. This procedure involved two stages: a static and dynamic stage. The static stage fixed the position of each camera relative to each other and to a L-frame reference object. The reference object had four retroreflective markers in known positions and provided an origin to the laboratory and its coordinate system (Figure 3.6). One of the corners of the force platform defined the origin of the laboratory or global coordinate system (GCS) (see section 3.2.2.1).

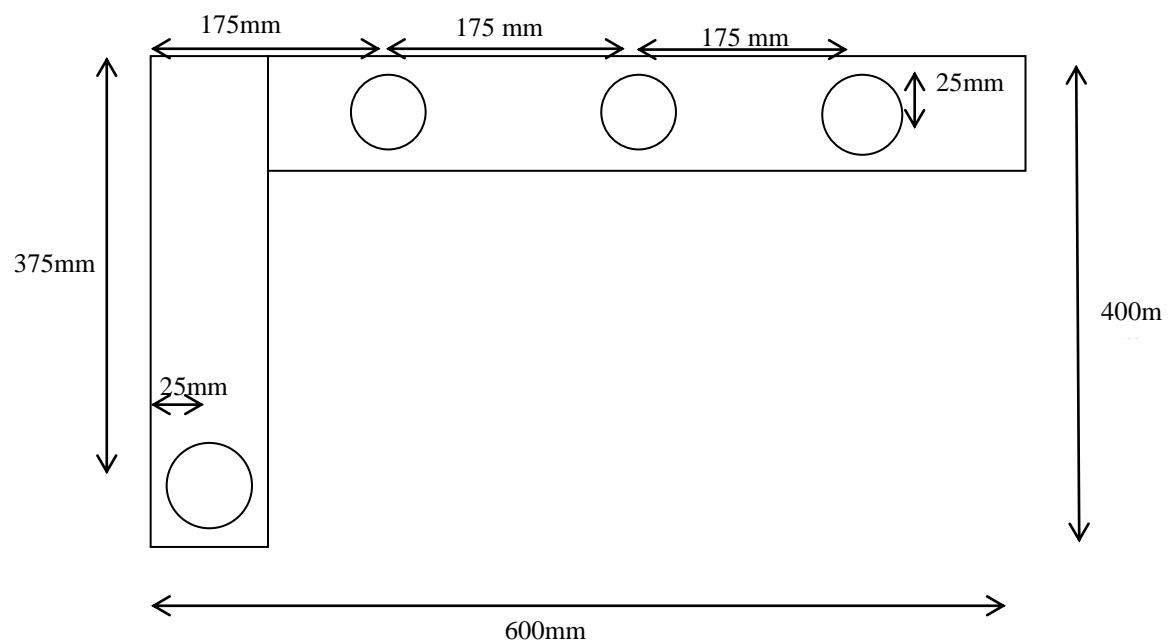


Figure 3.6 L-frame calibration reference object

The reference frame used normally in the lab is positioned over the corner of one force platform with latches keeping it in place to the side of the force platform. However, as artificial turf of different pile lengths was to be placed over the force platform, the original reference object configuration could not be used and a special reference object had to be manufactured for this project.

Therefore, a platform was constructed that could be placed above the artificial turf and located securely onto the force platform (Figure 3.7). The platform was made of polycarbonate and possessed four

short legs on each corner which were inserted into bushes positioned in locating holes at each corner of the force platform. Four small holes were made on the corners of each cut out section of turf (and rubber underlay if required) that was to be laid on the force platform. The length of the legs of the platform was long enough to ensure that the bottom of the platform was clear of the artificial turf. The L-frame reference object was placed over the one of the corners of the platform and the latches kept it on place to the sides of the platform.

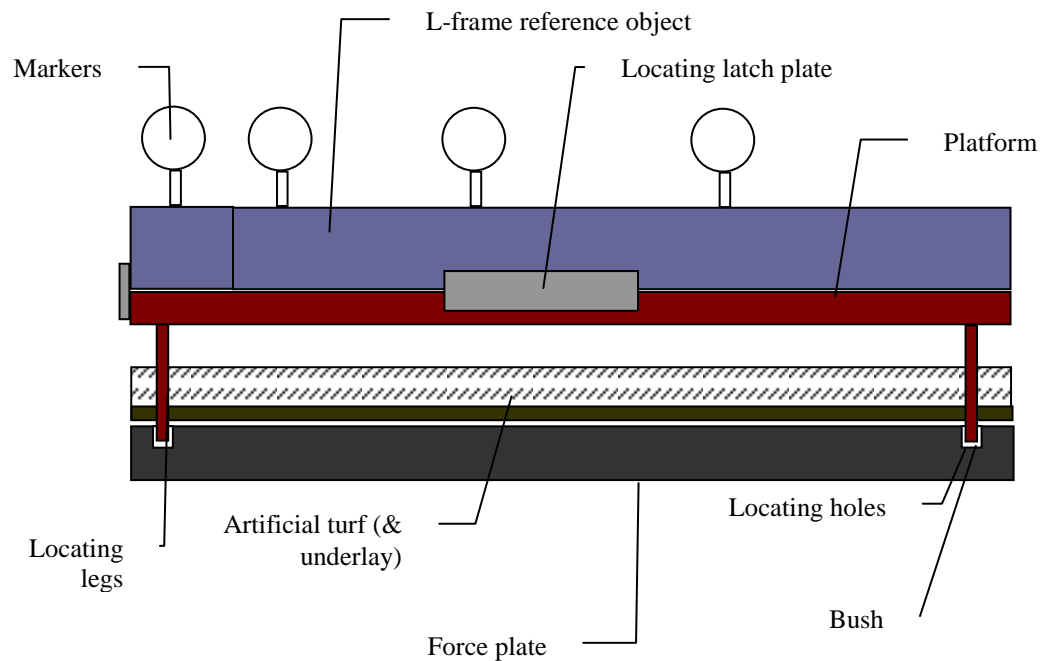


Figure 3.7 Cross section of elevated L-frame reference object located on the turf covered force platform

The three dimensional coordinates of the markers on the reference object relative to the corner of the force platform (origin of lab) were measured and stored as a new .cro file (calibration reference object) in the Vicon software. The position of each camera relative to the new elevated reference object was measured during the static calibration stage.

The dynamic stage of the calibration involved waving a wand, which has two markers on it, around a volume (approximately 3x3x2 metres) surrounding the force platform, while the cameras tracked the position of the markers. The wand was waved for approximately 30-45 seconds. Vicon's integral dynamic

calibration procedures used the known distance between the markers on the wand to establish the scale of the volume. For each testing session, the residual error resulting from the calibration process was less than 1.5mm.

3.2.2.1 *Global Coordinate System (GCS)*

The sign convention for the Global Coordinate System (GCS) used in this study is shown in Figure 3.8. Spatio-temporal parameters and forces were defined by the three orthogonal axes: the *Y*-axis defined the vertical direction (positive upwards); the *X*-axis defined the anterioposterior horizontal direction (positive forwards); and the *Z*-axis defined mediolateral horizontal (positive to the right) directions. Moments are defined as rotations around each of the three axes, with an anticlockwise rotation defining a positive rotation (+).

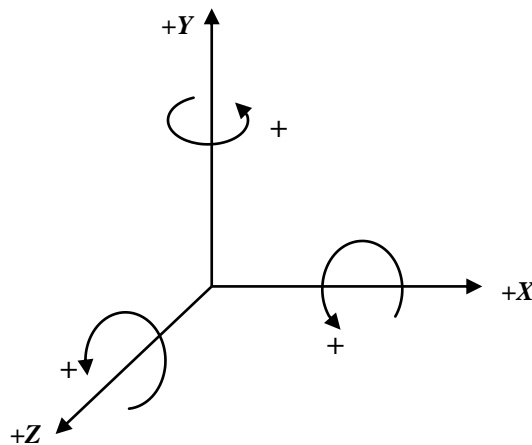


Figure 3.8 Sign convention used in this study

3.2.3 Subject Instrumentation

Several data collection instruments were placed on the subject during the biomechanical tests (Figure 3.9). Also shown are the infra-red motion cameras which were either suspended from the ceiling or on tripods and the location of the force plate underneath the turf. The following section describes each of the subject

instrumentation in further detail.

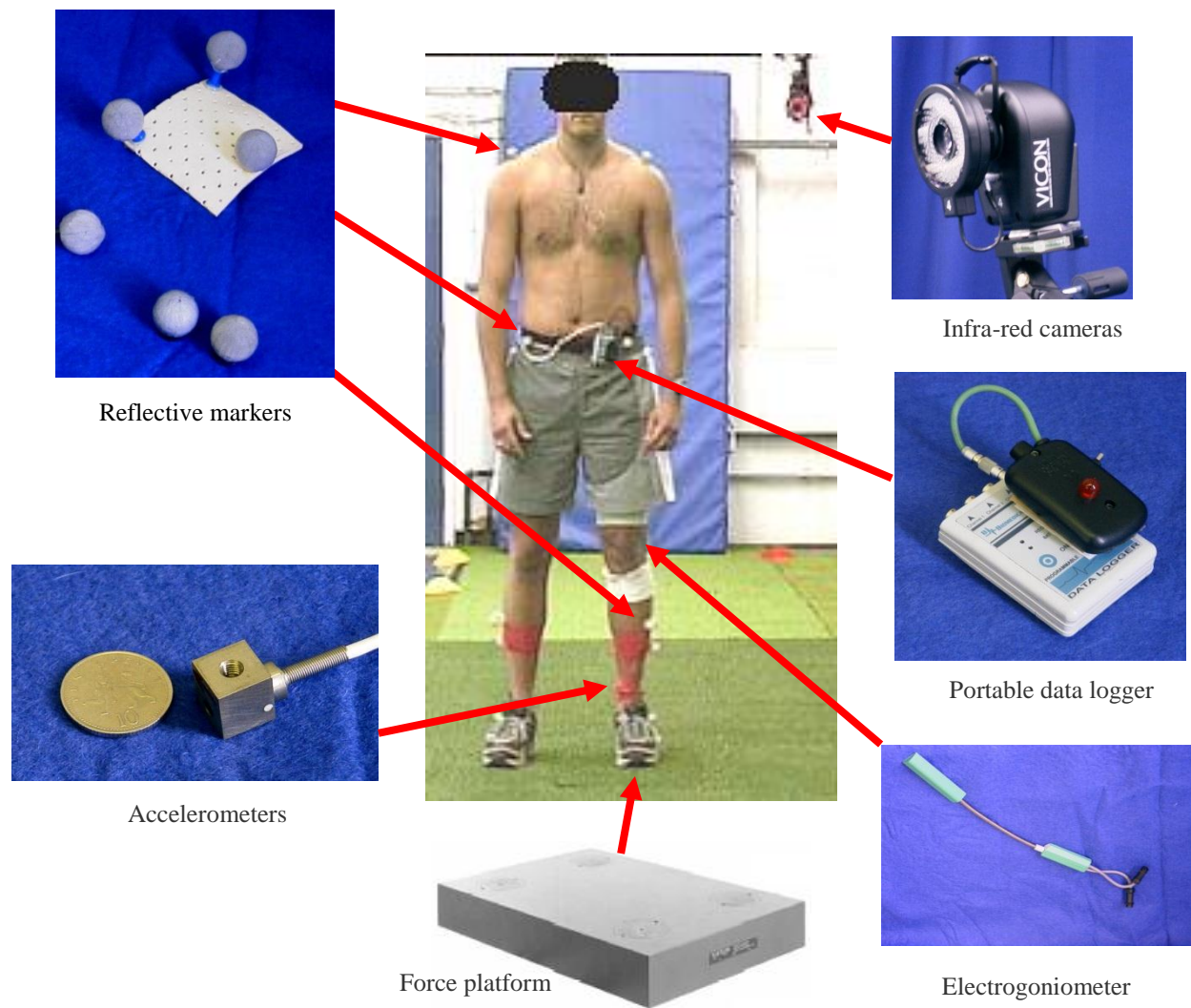


Figure 3.9 Data collection systems

3.2.3.1 *Marker Systems*

The motions of the subjects' segments were measured by defining an 8-segment rigid body model: HAT (head, arms and trunk), pelvis, 2 thighs, 2 shanks, and 2 feet/shoes. The subjects were instrumented with retroreflective markers. The marker trajectories were tracked by the Vicon infra-red cameras and reconstructed into three-dimensional coordinates, relative to the global coordinate system (GCS). The lightweight markers were made from 25mm diameter polystyrene balls, covered in retroreflective tape and

securely attached to a base made from the plastic part of map-pins.

Three markers defined bone embedded frames (BEF), otherwise referred to as a technical coordinate system (TCS), within each segment. The three markers were placed on body segments, except for the thigh segments. Pilot testing determined that excessive skin movement over bony prominences and a large degree of wobbling muscle mass during fast sports movements made it extremely difficult to rigidly attach markers on the thigh segment. It was therefore decided to calculate the orientation of the thigh segment indirectly from the orientation of the pelvic and shank segments. Consequently, it was not possible to calculate the axial rotation of the thigh.

Foot/Shoe Segment

Three markers positioned on the shoe of the participant defined the foot/shoe TCS. It was assumed that the foot and the shoe acted as one rigid system and possessed the same motion. An example of the marker positioning on a subject's shoe is shown in Figure 3.10.



Figure 3.10 Foot/shoe segment marker set

Markers were secured to the shoe with double-sided tape. One marker was near the heel counter, one near the top of the shoelaces and one just above the heel. The locations of the markers were such to minimise marker occlusion, inter marker movement and markers falling off during the high-speed movements performed by the subjects.

Shank Segments

The shank TCS on each leg defined by a cluster of three markers rigidly attached to a section of Orthoplast

(50x50x3mm), which was moulded to the approximate curvature of the lateral aspect of the shank (Figure 3.11). The marker cluster was also attached with toupee tape to the lateral aspect of the shank, approximately midway between the knee and the ankle. 3M Vetrap (Bracknell, UK) self-bonding compression bandage was wrapped around the leg to further secure the marker cluster in place.

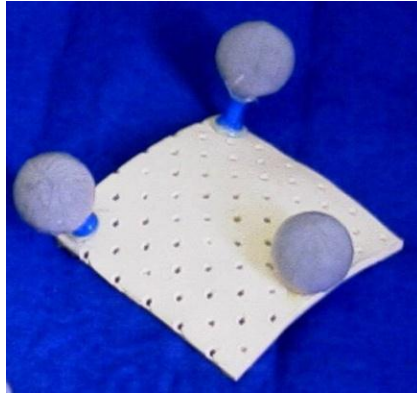


Figure 3.11 Shank marker set

Pelvic Segment

Three markers positioned on appropriate and accessible locations on the subject's pelvis defined the pelvic TCS. One marker was placed either side of the pelvis, close to the anterior superior iliac spines (ASIS), and one placed on a small aluminium plate (25x40x5mm) attached midway between the posterior superior iliac spines (MPSIS) with toupee tape. An elasticated belt around the pelvis was able to pass through the aluminium plate, which further secured the plate in place. It was assumed that any motion at the sacroiliac joint was negligible.

Head, Arms and Trunk (HAT) Segment

The HAT TCS was defined by markers placed on the left and right acromion processes, and a marker located at the MPSIS, shared with the pelvic TCS, completed the pelvic TCS.

3.2.3.2 Electronic instrumentation

Participants were also instrumented with accelerometers and a goniometer. This instrumentation provided a quantifiable link between the laboratory testing and the outdoor field-testing, as it was not possible to use the Vicon motion system or force platforms outside.

Accelerometry

The participants were instrumented with two single axis accelerometers (Entran EGCS-D1SM-50, $\pm 50g$ range, 0-600Hz frequency response, 12g mass (Figure 3.12). The accelerometers measured the acceleration (impact shock) at the lower shank level and at the pelvic region.



Figure 3.12 Single axis accelerometer

One of the accelerometers was attached to the aluminium plate just below the MPSIS marker (described earlier) with double-sided tape. It was further secured with electrical tape wrapped around the accelerometer and aluminium plate. The sensitive axis of the accelerometer was aligned visually to the vertical.

The other accelerometer was affixed to a small piece of lightweight, balsa wood (15x15x2mm) in the same manner and attached to the medial, distal aspect of the participant's left leg: 20% of the distance from the medial malleolus to the tibial tuberosity. It was visually aligned so that the sensitive axis of the accelerometer was parallel with the subject's tibia. The accelerometer/balsa wood complex was secured in place by toupee tape and a compression bandage.

Goniometry

A flexible electrogoniometer (Biometrics XM180, Gwent, UK) (Figure 3.13) measured the sagittal knee angle on the participant's left leg. It was attached to the lateral aspect of the participant's left knee with toupee tape. The electrogoniometers and the connecting cables of the shank accelerometer were further secured in place with an elastic tubular bandage.

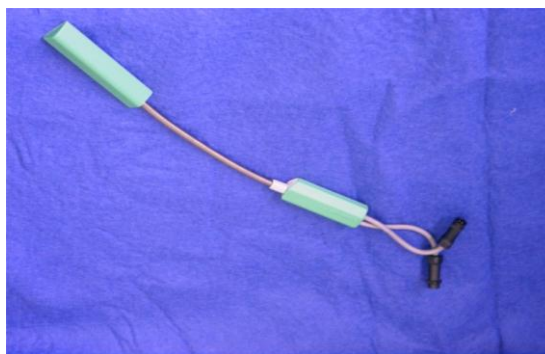


Figure 3.13 Flexible electrogoniometer

Data Logger

A portable data logger (Biomedical Monitoring BM42, 4 channels, $\pm 2.5V$ excitation, 12-bit resolution, Glasgow, UK) sampled the outputs of the accelerometers and electrogoniometer at a 500Hz sampling frequency (Figure 3.14).



Figure 3.14 Portable data logger with 'event marker' system

The data logger was clipped to the pelvic belt worn by the participant. An 'event marker system', consisting of a circuit breaker switch and a light emitting diode (LED), was connected into the fourth channel of the data logger. When the switch was turned on, the illuminated LED was visible to the digital video camera and a square spike was produced in the output of the data logger.

The video recordings were analysed to measure the timings between the LED illumination to the foot strike on the force platform (identified from the video). These timings enabled the selection of the appropriate foot strike data from the data logger.

3.2.4 Subject Calibration

Static subject calibration trials were conducted to define the positions of anatomical landmarks relative to the segment TCS. The anatomical landmarks were then used to define segment anatomical reference frames and joint centres. The subject was asked to stand in the anatomical standing position, with feet apart (shoulder width) and pointing directly forward, parallel to the force platform's X- (anteroposterior) axis. The subject's arms hung straight down by their sides, with their palms facing forwards.

A researcher used a small wand, instrumented with two retroreflective markers that were separated by a known distance from the end of the wand, to determine the location of the following anatomical landmarks, with respect to the global coordinate system: ASISs, MPSIS, tibial tuberosities, fibula heads, lateral and medial malleoli. Also, the following standardised positions on the subject's shoes were calibrated: most posterior and anterior parts of the shoe along the midline of the shoe, and a position on the lateral aspect of the shoe. This created a plane level with the artificial surface.

For each anatomical landmark and shoe position, the 3-dimensional locations of the markers on the wand and the subject were collected with the Vicon system and saved as separate static calibration files. In total, eighteen separate static calibration trials were conducted. This included one reference 'whole body' static trial, in which the wand was not used to capture the relative positions of all the markers on the subject.

3.2.5 Anatomical Reference Frames

The calibrated anatomical landmarks defined the anatomical reference frames for each segment, described below as: 'o', define the origin, 'x', 'y' and 'z' axes for each anatomical reference frame, respectively.

3.2.5.1 *Foot/shoe Complex Anatomical Reference Frame*

The foot and shoe were considered as one rigid system. Any motion of the foot relative to the shoe was ignored. Also, any motion of the foot due to the flattening of the longitudinal arch, talocrural joint motion, subtalar joint motion and flexion of the metatarsals and phalanges was also ignored. Figure 3.15 shows the

foot/shoe complex anatomical reference that was defined by the following landmarks on the shoe:

PSHOE: Most posterior aspect of the shoe at the level of the ground/playing surface, along the midline of the shoe.

ASHOE: Most anterior aspect of the shoe at the level of the ground/playing surface, along the midline of the shoe.

LSHOE: Most lateral aspect of the shoe at the level of the ground/playing surface.

o: The origin is located at the PSHOE landmark

y: The line connecting the PSHOE and ASHOE landmarks, and pointing posteriorly.

x: The PSHOE, ASHOE and LSHOE defines a transverse plane. The *x*-axis lies perpendicular to this transverse plane, and pointing proximally.

z: The line orthogonal to the *x*-and *y*- axis, pointing to the right.

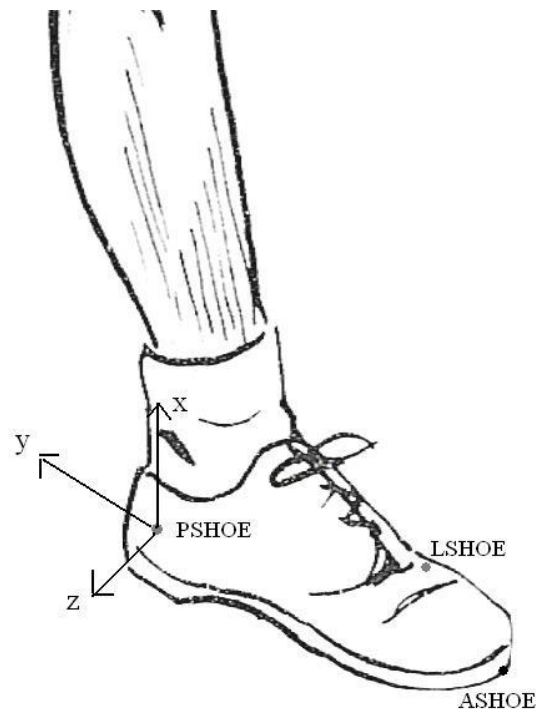


Figure 3.15 Foot/shoe complex anatomical reference frame

3.2.5.2 *Shank Anatomical Reference Frame*

Applying the procedure proposed by Cole *et al.* (1993) to select the fixed axis to describe a JCS presented a difficulty when defining a single anatomical reference frame for the shank. The orientation of a particular axis system may be suitable for an ankle JCS but may not be suitable for a knee JCS. For example, the axis of flexion for an ankle JCS can be defined as the axis fixed to the tibia/fibula, coincident with a line connecting the medial malleolus and lateral malleolus (International Society of Biomechanics, 2002). This axis angles downward and posteriorly, moving from medial to lateral (Nordin and Frankel, 2001). As such, the corresponding y-axis is directed superiorly and laterally away from the mechanical longitudinal axis of the tibia.

In contrast, the axis of internal-external rotation for a knee JCS can be defined as the axis fixed to the tibia/fibula, which passes midway between the two intercondylar prominences proximally and through the centre of the ankle distally (i.e. the longitudinal axis of the shank). (Grood and Suntay, 1983). This difference between the two y-axis orientations is illustrated in Figure 3.16.

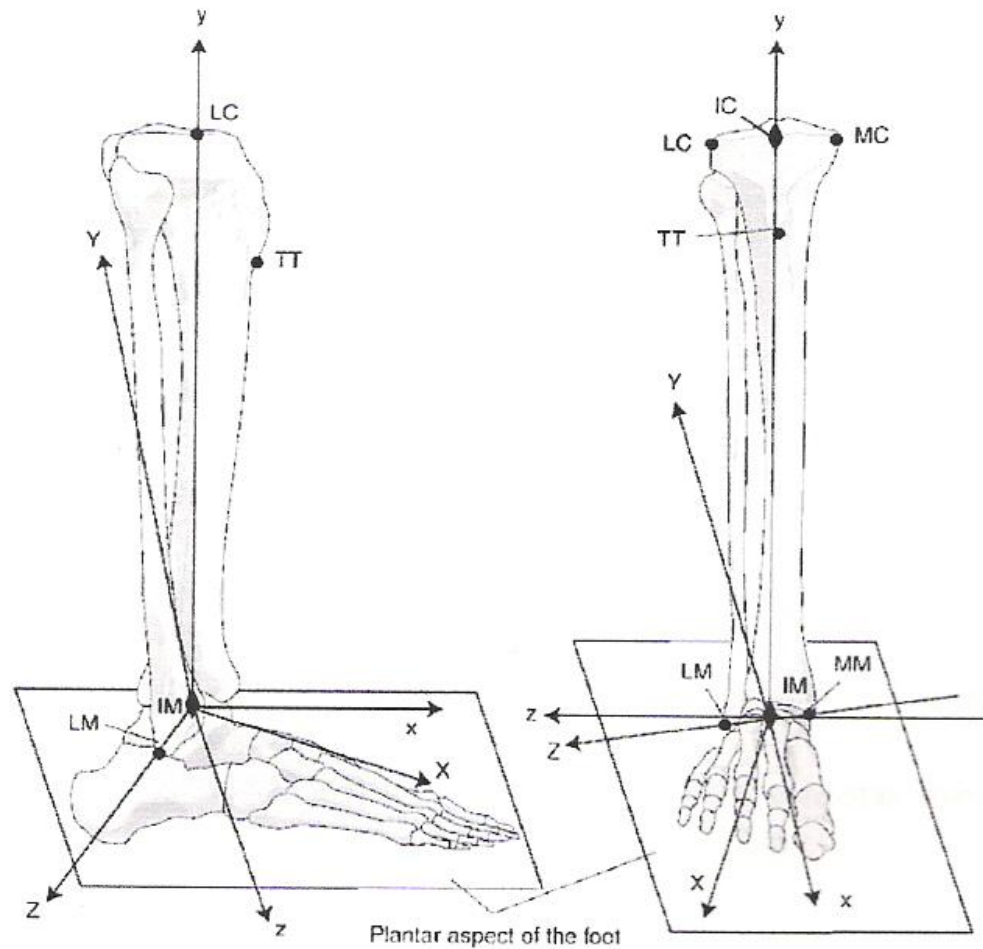


Figure 3.16 Illustration of two anatomical reference systems for the shank. X,Y,Z has a flexion axis (Z-axis) suitable for an ankle JCS. x,y,z has a longitudinal axis (y-axis) suitable for a knee JCS. Adapted from International Society of Biomechanics (2002)

Therefore, with consideration to the methods proposed by other authors, two anatomical reference frames were defined for the shank. One was defined for a knee JCS and one for an ankle JCS. These were named ‘shank-KJCS’ and ‘shank-AKJS’, respectively. This would allow the selection of appropriate fixed axes in the proximal and distal segment, following the proposal by Cole *et al.* (Cole *et al.*, 1993).

3.2.5.3 Shank-KJCS Anatomical Reference Frame

The definitions of the shank-KJCS anatomical reference frames were based on Cappozzo *et al.* (Cappozzo *et al.*, 1995). The International Society of Biomechanics (2002) have proposed recommendations relating to the standard definitions of anatomical coordinate systems of the lower limbs. In these recommendations, the

lateral and medial tibial condyles are used to define the tibial-fibula anatomical planes of the shank segment.

However, it was difficult to palpate these condyles on knees with considerable surrounding musculature, as found on some sports players – particularly rugby players. Therefore, the malleoli and the fibula head landmarks were used to define a quasi-frontal plane (Cappozzo *et al.*, 1995). The anatomical landmarks used to define the anatomical reference frames in this study were easy to palpate and identify on different subjects. The anatomical landmarks/locations used were as follows (Figure 3.17):

- FIBHEAD: Most prominent aspect of the fibula head.
- LATMAL: Most prominent aspect of the lateral malleolus.
- MEDMAL: Most prominent aspect of the medial malleolus.
- KJC: Knee joint centre (w.r.t. GCS)
- o*: The origin was located at the midpoint between the LATMAL and MEDMAL, the ankle joint centre (AJC).
- y*: The line connecting the AJC and the KJC, pointing cranially.
- x*: A line perpendicular to a quasi-frontal plane created by the AJC, KJC and FIBHEAD, pointing anteriorly.
- z*: A line perpendicular to both the *x*- and *y*- axes, pointing to the right.

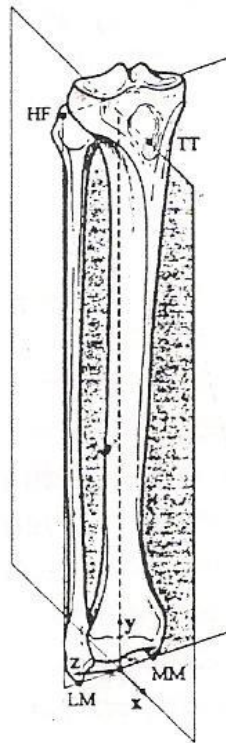


Figure 3.17 Shank-KJCS anatomical reference frame (from Cappozzo et al. (1995))

3.2.5.4 *Shank-AJCS Anatomical Reference Frame*

The Shank-AJCS anatomical reference frame was defined as follows, using the following anatomical landmarks (Figure 3.18):

LATMAL: Most prominent aspect of the lateral malleolus.

MEDMAL: Most prominent aspect of the medial malleolus.

KJC: Knee joint centre (w.r.t. GCS)

o: The origin was located at the midpoint between the LATMAL and MEDMAL, the ankle joint centre (AJC).

z: A line connecting the MEDMAL and LATMAL, and pointing to the right.

x: A line perpendicular the plane created by the MEDMAL, LATMAL and KJC, pointing anteriorly.

y: A line perpendicular to both the x- and z- axes, pointing cranially.

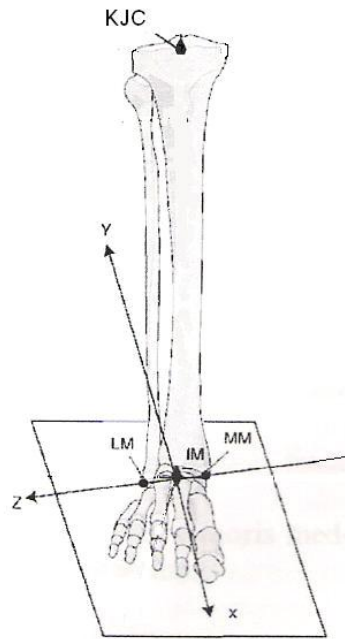


Figure 3.18 Shank-ACJS anatomical reference frame (Adapted from International Society of Biomechanics (2002))

3.2.5.5 *Thigh Anatomical Reference Frame*

As described in Section 3.2.3, no markers were attached to the thigh segments. In order to calculate knee angles, an anatomical thigh segment was reconstructed from the location of the hip joint centre in the pelvic anatomical reference frame and the location of the knee joint centre in the shank anatomical reference frame. As the orientation of the subject's thigh could not be determined due to the lack of external markers, a frontal plane was defined by the frontal plane of the shank-KJCS anatomical reference frame. Therefore, it was assumed that there was no axial rotation of the thigh segment. Consequently, no internal or external rotation of the knee could be calculated. The anatomical landmark/locations used were as follows (Figure 3.19):

HJC: Hip joint centre (w.r.t. GCS) (FH: Fibula head)

KJC: Knee joint centre (w.r.t. GCS)

AJC: Ankle joint centre (w.r.t. GCS)

- o*: The origin was located at the KJC.
- y*: The line connecting the KJC with the HJC, directed proximally.
- x*: The line perpendicular to the plane created by the *y*-axis and the Shank-KJCS *z*-axis, pointing anteriorly.
- z*: The line perpendicular to both the *x*- and *y*-axes, pointing to the right.

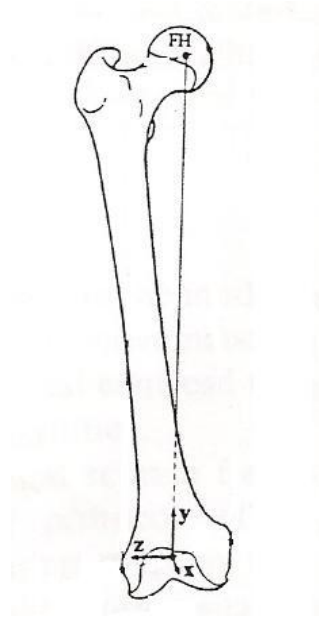


Figure 3.19 Thigh anatomical reference frame

Pelvic anatomical reference frame

The pelvic anatomical reference frame was defined using Cappozzo *et al.* (Cappozzo *et al.*, 1995), using the following anatomical landmarks:

- LASIS: Left anterior superior iliac spine
- RASIS: Right anterior superior iliac spine
- PSIS: Posterior superior iliac spines (left and right)
- MPSIS: Midpoint between the PSISs

- o*: The origin was located at the midpoint between the anterior superior iliac spines (LASIS and RASIS). Please note: the origin pelvic anatomical reference frame was translated to the

left and right HJC, respectively, and the HJCs were calculated with respect to the pelvic anatomical reference frame (International Society of Biomechanics, 2002) as shown in Figure 3.20.

- z: The line parallel to a line connecting the LASIS and RASIS, and pointing to the right.
- x: The line parallel to a line lying in the plane defined by the two ASISs and the MPSIS, orthogonal to the Z-axis and pointing anteriorly.
- y: The line perpendicular to both the X- and Z-axes, pointing cranially.

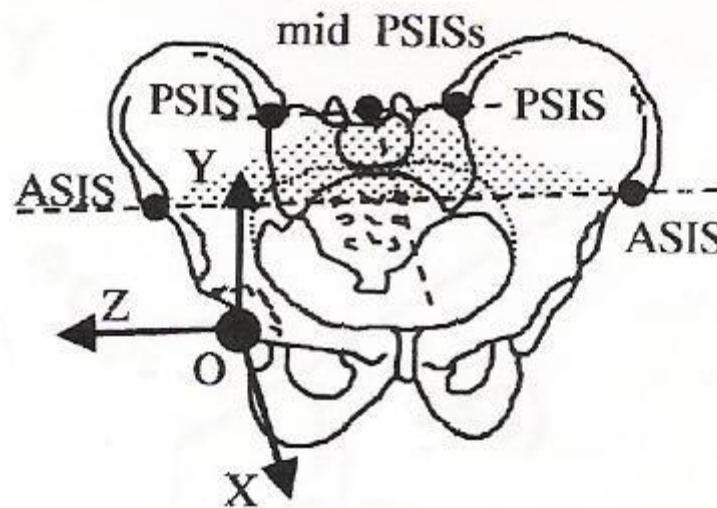


Figure 3.20 Pelvic anatomical reference frame (Adapted from International Society of Biomechanics (2002))

3.2.5.6 Head, Arms and Trunk (HAT) Anatomical Reference Frame

The HAT anatomical reference frame is shown in Figure 3.21. The following anatomical landmarks/locations were used to define the HAT anatomical frame:

- LACR: Left acromion processes
- RACR: Right acromion process
- MPSIS: Midpoint of posterior superior iliac spines (left and right)

- o*: The origin was located at the MPSIS.
- y*: The line parallel to the line connecting the MPSIS and the midpoint of the LACR and RACR, pointing cranially.
- z*: The line parallel to the line connecting the LACR and RACR, pointing to the right.
- x*: The line perpendicular to both the Y- and Z-axes, pointing anteriorly.

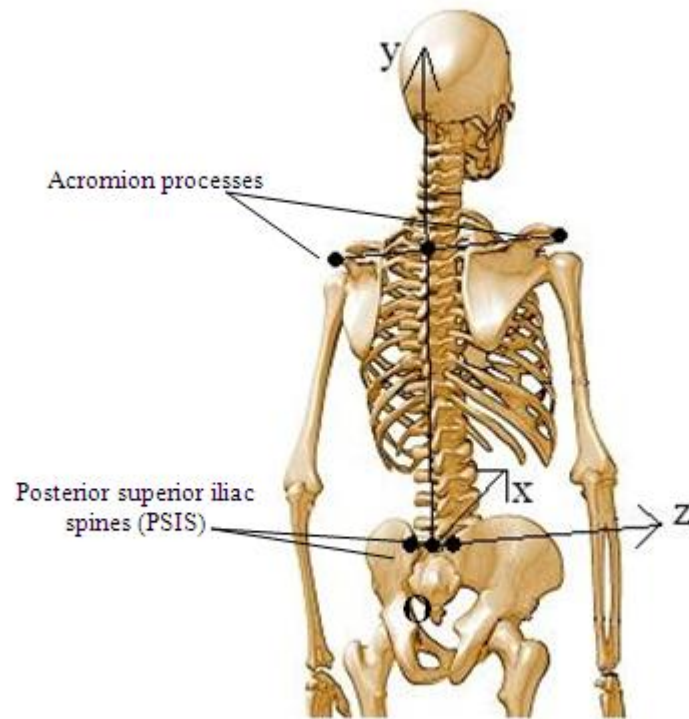


Figure 3.21 HAT anatomical reference frame

3.2.6 Joint Centres of Rotation

The calibrated anatomical landmarks were used to define anatomical joint centres of rotation, defined as single points in space around which the rotations of one anatomical segment relative to another occur (Grood & Suntay, 1983). HAT (Sacral), hip (left and right), knee (left and right) and ankle (left and right) joint centres were defined in this study. The locations of the respective joint centres were calculated relative to specific anatomical landmarks during a static standing trial.

3.2.6.1 HAT (Sacral) Joint Centre

The HAT centre of rotation was defined to originate at the midpoint of the posterior superior iliac spines. This was assumed to be a good approximation of the sacral joint.

3.2.6.2 Hip Joint Centre

The hip centre of rotation or hip joint centre (HJC) was defined as the position from the left and right ASIS (LASIS, RASIS), calculated as a percentage of the distance between the ASISs ($dASIS$). These distances were 19% posterior, 30% distal and 14% medial to the ASIS, measured in the pelvic anatomical (pa) reference frame (Bell *et al.*, 1990).

Therefore:

$$[X, Y, Z]_{LHJC-pa} = [LASIS - (0.19 \times dASIS), LASIS - (0.3 \times dASIS), LASIS + (0.14 \times dASIS)]_{pa} \quad [\text{Eq. 5.1}]$$

$$[X, Y, Z]_{RHJC-pa} = [RASIS - (0.19 \times dASIS), RASIS - (0.3 \times dASIS), LASIS - (0.14 \times dASIS)]_{pa} \quad [\text{Eq. 5.2}]$$

3.2.6.3 Knee Joint Centres

The knee joint centre of rotation (KJC) was defined using a method described by Stansfield (2000) and (Ishai, 1975), which assumed that the KJC lies on the longitudinal axis (Y-axis) of the shank anatomical reference frame. The location of the KJC was calculated using orthogonal distances from anthropometric landmarks, with respect to the global coordinate system (G). These distances were:

D_1 = anteroposterior distance from the tibial tuberosity (TT), directed posteriorly.

D_2 = mediolateral distance from the fibula head (FH) (directed medially for left knee; laterally for right knee)

D_3 = inferosuperior distance from the tibial tuberosity, directed superiorly.

In order to calculate these distances, the following anthropometrical measurements were obtained from each

subject:

S_1 = Mediolateral distance between the tibial condyles

S_2 = Mediolateral distance between the medial tibia condyle and the fibula head

S_3 = Distance between the tibial plateau and the tibial tuberosity.

The coordinates of the joint centre for the left knee ($\{X, Y, Z\}_{LKJC-G}$) and right knee ($\{X, Y, Z\}_{RKJC-G}$) in the global coordinate system were calculated as follows:

$$D_1 = S_2 - S_1 + (S_1 \div 2) \quad [\text{Eq. 5.3}]$$

$$D_2 = 8.2 + (0.5 \times 47.1 \times (S_1 \div 97.95)) \quad [\text{Eq. 5.4}]$$

$$D_3 = S_3 + (25 \times (S_1 \div 97.95)) \quad [\text{Eq. 5.5}]$$

$$\{X, Y, Z\}_{LKJC-G} = \{TT_L - D_1, TT_L + D_3, FH_L + D_2\}_G \quad [\text{Eq. 5.6}]$$

$$\{X, Y, Z\}_{RKJC-G} = \{TT_R - D_1, TT_R + D_3, FH_R - D_2\}_G \quad [\text{Eq. 5.7}]$$

The $(S_1 \div 97.95)$ term used in the calculations of D_2 and D_3 (Equations 5.4 and 5.5) was used as a subject scaling factor (Stansfield, 2000). A value of 97.95mm was the average distance between the tibial condyles for all the subjects in this study.

A static trial of the subject, standing in the anatomical position, was obtained to determine the location of the ‘static’ KJC in the global coordinate system. This position was transformed into the shank technical coordinate system so that location of the KJC could be reconstructed during the dynamic trials.

3.2.6.4 Ankle Joint Centres

The location ankle joint centre (AJC) in the ankle anatomical reference frame (aa) was determined as the midpoint between the medial and lateral malleoli ($MMAL$, $LMAL$, respectively):

$$\{X, Y, Z\}_{AJC-aa} = \frac{\{X, Y, Z\}_{MMAL-aa} + \{X, Y, Z\}_{LMAL-aa}}{2} \quad [\text{Eq. 5.8}]$$

A definition of the respective Joint Coordinate Systems for the ankle, knee, hip and sacral joints follows a

description of how joint centres were defined.

3.2.7 Joint Coordinate Systems (JCS)

The relative motions between segments were calculated using the joint coordinate systems of defining intersegmental angles, as proposed by Grood & Suntay (Grood & Suntay, 1983) and developed by Cole *et al.* (1993). This method defined the fixed axes for the joint coordinate system specified in the present study.

Cole *et al.* (1993) proposed that a JCS consisting of a fixed axis, e_1 , embedded in the proximal segment, should represent the joint flexion-extension axis. The longitudinal axis of the distal segment should be selected to represent the axis of axial rotation, e_3 . The third “floating axis” axis of the JCS, calculated as the cross product of the e_1 and e_3 , should represent the axis of ad-abduction, e_2 .

The joint coordinate systems used in the present study are defined below.

3.2.7.1 Ankle JCS

- $e_1 =$ The axis fixed to the shank and coincident with the z-axis of the shank-AJCS anatomical reference frame. The rotation around this axis was dorsiflexion/plantarflexion.
- $e_2 =$ The axis fixed to the foot/shoe complex and coincident with the y-axis of the foot/shoe complex reference frame. The rotation around this axis was inversion/eversion.
- $e_3 =$ The floating axis, the common axis perpendicular to e_1 and e_2 . The rotation around this axis was internal/ external rotation of the foot.

3.2.7.2 Knee JCS

- $e_1 =$ The axis fixed to the thigh and coincident with the z-axis of the thigh anatomical reference frame. The rotation around this axis was flexion/extension
- $e_2 =$ The axis fixed to the shank and coincident with the y-axis of the shank-KJCS anatomical reference frame. The rotation around this axis was internal/external rotation.
- $e_3 =$ The floating axis, the common axis perpendicular to e_1 and e_2 . The rotation around this axis

was abduction/adduction of the knee.

3.2.7.3 Hip JCS

- $e_1 =$ The axis fixed to the pelvis and coincident with the z-axis of the pelvic anatomical reference frame. The rotation around this axis was flexion/extension of the hip.
- $e_2 =$ The axis fixed to the thigh and coincident with the y-axis of the thigh anatomical reference frame. The rotation around this axis was internal/external rotation.
- $e_3 =$ The floating axis, the common axis perpendicular to e_1 and e_2 . The rotation around this axis was abduction/adduction of the hip.

3.2.7.4 Sacral JCS

- $e_1 =$ The axis fixed to the HAT segment and coincident with the z-axis of the HAT anatomical reference frame. The rotation around this axis was flexion/extension of the HAT segment.
- $e_2 =$ The axis fixed to the pelvis and coincident with the y-axis of the pelvic anatomical reference frame. The rotation around this axis was left/right rotation of the HAT segment.
- $e_3 =$ The floating axis, the common axis perpendicular to e_1 and e_2 . The rotation around this axis was left/right lateral flexion of the HAT segment.

3.2.8 Sport Movements

The participants performed 7 movements that are generic to all three sports. These were chosen through a process of analysing videos and live football, rugby union and hockey matches; and consultation with players and coaches. The movements were:

1. Sprint running (RUN)
2. Stopping (STOP)
3. A running 45° turn to the left (open technique) (45L)
4. A running 45° turn to the right (open technique) (45R)
5. A running 90° turn to the left (cross technique) (90L)
6. A running 90° turn to the right (cross technique) (90R)
7. 180° turn to the right from a static start (180T)

An ‘open technique’ for the 45° turns involved the athlete using the foot on the opposite side to the direction he/she wants to turn. A ‘cross technique’ involved the use of the foot on the same side as the direction he/she wants to turn. The contralateral leg then crosses the plane in which the run up occurred and continues in the new direction.

The subjects were instructed to conduct each movement as fast as possible to complete the manoeuvre safely. The starting position of the subjects for all movements, with the exception of the 180° turn, was from a standing start, approximately 7m from the force platform. The sprinting (*RUN*) movement involved the subject sprinting along the runway, which was approximately 14m long. The subjects were instructed not to slow down until they had passed a designated marker, positioned approximately 4m past the force platform.

The running-stop (*STOP*) movement involved the subject sprinting 7m towards to the force platform. The subject was instructed to stop on their left leg at a position level with a marker that was located adjacent to the force platform. A trial was defined as successful if the subject was able to stop their forward momentum within two steps of the stopping action and if the researcher assessed that the action on the left leg was the main stopping action and that the left foot landed fully on the force platform.

For the turning activities, it was necessary to place markers on the turf in order to designate the

position that the subjects were to perform the respective turns. This allowed the stance foot, on which the turn took place, to impact the force platform. The 45° turns involved running towards the markers and performing the turn using an ‘open’ technique on the left foot and running off 45° to the right (*45R*) (Figure 3.22). The turn was repeated using the right foot to turn and running off 45° to the left (*45L*).



Figure 3.22 45-degree turn (cutting turn technique)

The 90° turn involved the subject running towards the markers and perform the turn using the ‘cross’ technique on the left foot and running off 90° to the left (*90L*) (Figure 3.23). The process was repeated using the right foot to turn and running off 90° to the right (*90R*).



Figure 3.23 90-degree turn (cross turn technique)

The 180° turn (*180T*) involved the subject starting from an upright standing position with their left foot positioned on the force platform (Fig. 5). On command, the subject was asked to turn to their right (medial rotation of the left foot) through 180° and sprint off in a forward direction.



Figure 3.24 180-degree turn (*180T*)

3.2.9 Testing Procedure

Prior to the start of testing, the subjects were allowed a warm-up period to prepare themselves for exercise and also to become accustomed to the equipment they were wearing.

The players wore their own preferred footwear and were instructed to perform each running movement as fast as possible. The subjects were given sufficient attempts to practise so that they were able to execute the movements naturally and comfortably, and to ensure that their foot was placed fully on the force platform without attempting to target the force platform or alter their normal movement pattern significantly.

At the start of each trial, the subject was instructed to face the video camera and press the event marker switch, located on the data logger. This caused the LED on the event marker system to illuminate and the change in current (the event marker) was measured on the data logger. The subject was then asked to start the required movement. Three successful trials of each type of movement were performed on each of the three artificial turfs.

The whole testing session on one artificial turf took less than two hours, including a rest break of fifteen minutes. The three turfs were tested on different days, separated by a period of two weeks.

3.3 Outdoor Field Testing

The field tests were conducted in order to validate the data collected in the laboratory by allowing the participants to perform the above movements in a more realistic playing environment, without the constrictions and distractions of the laboratory. The quantitative link between the indoor and outdoor testing sessions was provided by data from the two accelerometers and the electrogoniometer worn by the subject.

The tests were conducted on various types of artificial turfs and also natural grass turf. An area of the pitches, approximating that in the lab, was marked out with cones. The sites and turf (and their comparison with the turfs used for the laboratory testing) are as follows:

Stepps Playing Fields, Millerston:

- Turf 4: Medium pile, curly top, sand dressed (with underlay) (Same as Turf 2)
- Turf 5: Long ‘rugby’ natural grass turf
- Turf 6: Short ‘football’ natural grass turf

Glasgow Green Football Centre:

- Turf 7: Short pile, sand infill turf (similar to Turf 1)
- Turf 8: Medium pile, runner infill turf (similar to Turf 3)

Ibrox Community Trust Pitch, Ibrox:

- Turf 9: Long pile, rubber infill FieldTurf (same as Turf 3)

Weather permitting, the tests were conducted with the turf in wet and dry conditions. Wet conditions were simulated by sprinkling approximately 20 litres of water over a marked area where the sports movements would occur. The participants performed the same movements performed in the lab tests, with the exception of the 45° turns to the left and the 90° turns to the right. This was due to the fact that all participants wore the shank accelerometer and the electrogoniometer on their left leg, so movements where the stance leg was the right leg were not conducted.

As with the indoor laboratory tests, the trials were videotaped using the digital video camera, as a visual reference to the movements and provide synchronisation with the data logger.

3.4 Data Processing & Analysis

3.4.1 Vicon System

The trajectories of the markers attached to the subject and the loads applied to the force platform were collected using Vicon *Workstation* and processed using *BodyBuilder* software (Oxford Metrics, Oxford).

The data processing was conducted in four stages:

1. Static calibration trials
2. Dynamic trials pipelining
3. Data export and reduction
4. Movement cycle identification

3.4.1.1 *Static Calibration Trials*

A *Bodybuilder* ‘static’ model was written to calculate the individual segments’ TCS from the markers placed on the subject; transform the global coordinates of the anatomical landmarks (including shoe landmarks) into the respective segmental TCS; and calculate the ankle and knee joint centres relative to the shank TCS’s.

The relative positions of the anatomical landmarks, knee joint centres, and ankle joint centres were stored in a subject parameter file. The anthropometric measurements taken at the start of the testing session were also included in the subject parameter file.

After labelling the markers, the static calibration trials were batch processed, applying the *Bodybuilder* ‘static’ model to each trial.

3.4.1.2 *Dynamic Trial Pipelining*

The purpose of the dynamic trial data processing was to label the retroreflective markers, fill in any small gaps in the trajectories of markers, apply an appropriate filter to both the force platform data marker trajectories, and apply a *Bodybuilder* ‘dynamic’ model. A *pipelining* procedure was conducted to apply these functions to all the dynamic trials as a batch process.

The dynamic trials were labelled during an *autolabelling* process using a predefined, standard marker configuration. Any small gaps in the subsequent marker trajectories were ‘filled in’ using the *Vicon Workstation*’s in built marker interpolation function.

The ground reaction force data was filtered using a plug-in 4th Order Butterworth filter, with a cut off frequency of 25Hz. The marker trajectories were filtered using a Woltring GCV spline filter.

A *BodyBuilder* ‘dynamic model’ program (Appendix A) was written to reconstruct the joint centres, anatomical landmarks and frames from the orientations of the technical frames. The positions of anatomical landmarks to the respective segmental TCS obtained from the static calibration trials were stored in a subject specific parameter file. This information was referred to during processing of the dynamic trials. The outputs of the *BodyBuilder* program were joint angles, external joint moments, joint angular velocities, linear velocities of the centre of mass and left and right heels and ground reaction forces (GRFs).

After the dynamic model was applied, each trial was checked to ensure that joint centres and anatomical frames were reconstructed correctly. For trials where erroneous trajectories were identified, the labelling of the markers were inspected and reprocessed, if appropriate.

3.4.1.3 *Data Export and Reduction*

The Vicon data files (.c3d format) were exported into an ASCII format: a more manageable file to conduct further data analysis. A Matlab program (Mathworks, Massachussets) was written to reduce the data into the respective movement cycles, using the event sample numbers and analyse the data.

3.4.1.4 *Movement Cycle Identification*

A movement cycle was identified for each of the trials. The data within each trial was reduced into a movement cycle. In many gait studies, the movement of the body is divided into a gait cycle, commencing from the initial contact of one limb (‘heel strike’ or ‘foot strike’) to the next occurrence of that same event on the ipsilateral limb. In walking, a single limb’s stance phase occupies 60% of the cycle, with a period of double limb support. However, during running activities, where there are no periods of double support, stance phase can account for 30-40% stance phase, with the limb is swing phase for the rest of the cycle (Novacheck, 1998). The length of a running stride can also be very long, up to 2.4 metres for top class sprinting (International Association of Athletics Federations, 2003).

The focus of this study was primarily what happens at stance phase of the running cycle. Therefore,

to ensure that adequate data is captured within the measurement volume, a movement cycle was defined so that the stance phase of the stance limb on the force platform would occur towards the middle section of the cycle. As such, the movement cycle was defined by events of the non-stance limb (Figure 3.25). For all the movements analysed in this study, except for the 180° turn, the movement cycle was defined by the initial contact event of the non-stance limb to the following initial contact event of the same limb.

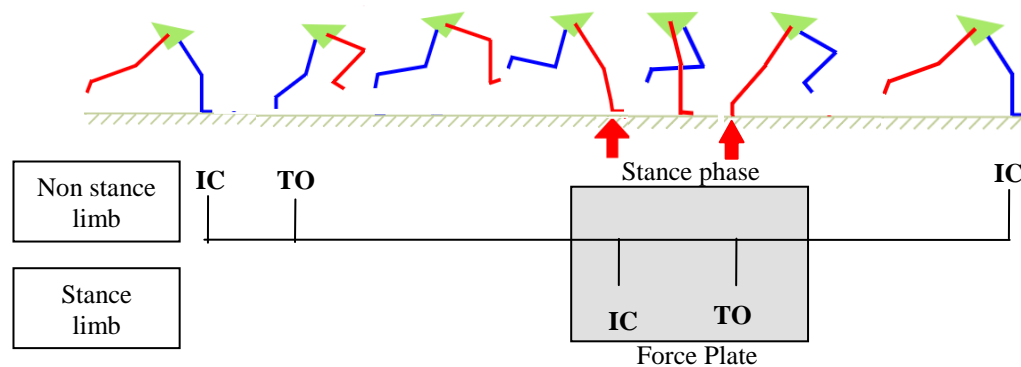


Figure 3.25 Movement cycle for running and turning activities (except 180° turn): IC, initial contact; TO, toe off.

For the 180° turning activity (180T), the subject stood still at the start of the activity. The start of the movement cycle for the 180T, therefore, was defined by the toe off event of the non-stance limb to the toe-off event of the ipsilateral limb following the turn.

The sample numbers for the start and end of the movement cycle were identified and recorded for each trial. The stance phase of the movement cycle was identified from the force platform data. The initial contact of the stance phase was defined as the first vertical GRF data point greater than 30N. The end of the stance phase was defined by the return of the vertical GRF to 0N. The stance phase of each movement cycle was extracted and saved as a separate file.

A cubic spline function was used to interpolate both the movement cycle and the stance phase of each trial to 100 data points. This would enable different events to be described as a percentage of the whole

movement cycle or the stance phase.

3.4.2 Biomechanical Analysis

3.4.2.1 Joint Kinematics and Kinetics

Joint kinematics and kinetics were calculated as part of the *BodyBuilder* ‘dynamic’ model. The rotations of segments about defined embedded axes were calculated using the floating axis Joint Coordinate System (Cole *et al.*, 1993; Grood & Suntay, 1983). The output of this calculation describes rotations about the axes of joint flexion, abduction and rotation, respectively.

External joint moments were calculated by inverse dynamics, using information of the joint centres, accelerations of the segmental centre of masses and the external loads applied to the body by the ground. The segmental centres of masses (Table 3.3) were calculated using Dempster’s segmental anthropometric parameter model (Dempster, 1955; Winter, 1990).

Segment name	Endpoints (proximal to distal)	Seg. Mass/ total mass	Centre of mass/ segment length (distal)	Radius of gyration/ segment length (CG)
HAT	Greater trochanter to glenohumeral joint	0.536	0.374	0.496
Pelvis	L4-L5 to trochanter	0.142	0.865	0.5
Femur	Greater tronchanter to femoral condyles	0.1	0.567	0.323
Tibia	Femoral condyles to medial malleolus	0.0465	0.567	0.302
Foot/Shoe*	Lateral malleolus to anterior aspect of shoe	0.0195	0.5	0.475

Table 3.3 Default anthropometric data (* the mass of the shoe was added to the Dempster’s value for the foot segment mass. The relative shoe mass as a ratio of total mass was estimated to be 0.005)

The *BodyBuilder* model performed the inverse dynamics process using a macro function named REACTION. This function summates all the reactions acting on a given segment, making the assumption that only one reaction (acting at the proximal end) is unknown. All of the components are added to give the compensating reaction that needs to be applied to the segment to keep it in dynamic equilibrium.

The forces due to acceleration (including gravity) and moments of inertia are calculated from the position of the centre of mass of the segment (as given in the anthropometric table) from the current frame, and frames ± 0.25 seconds from the current frame.

In the frontal and transverse planes, the sign of the external joint moments calculation for the right hand side of the body was reversed to allow the direction of the applied moment to equal the same sign to that of the left hand side. For example, before sign correction, a positive applied moment to the knee in the frontal plane would signify an abduction moment around the left knee but an adduction moment around the right knee. The sign correction allowed an appropriate comparison of joint moments between the left and right sides of the body.

3.4.2.2 *Ground Loadings*

The force platform output was analysed for the seven movements conducted on the three different artificial turfs (T1, T2, T3), respectively. The ground loadings were described in terms of a vertical ground reaction force (GRF), a resultant horizontal ground reaction force and a free moment (My') with respect to the normalised percentage of stance phase. In addition, a vertical loading rate was calculated through the differentiation of the vertical GRF.

For all ground loadings, it was assumed that forces and moments acted at the top surface of the artificial turf (i.e. height of the turf pile plus the rubber underlay, if used, (y_T)). Therefore, the calculation of the centre of pressure (COP) and subsequent free moment was adjusted to account for the additional distance of the centre of pressure from the origin of the force plate, as follows:

Free moment calculation:

$$(My') = My - (Fs \times (\sqrt{x^2 + z^2}))$$

where;

My = moment around the vertical axis

Fs = resultant shear force ($(\sqrt{Fx^2 + Fz^2})$)

x = x-coordinate of centre of pressure

z = z-coordinate of centre of pressure

and;

$$x = \frac{Mz - Fx \times (y_O + y_T)}{Fy}$$

$$z = \frac{Mx - Fz \times (y_O + y_T)}{Fy}$$

where;

Mx = moment about the X-axis

Mz = moment about the Z-axis

Fx = anterior-posterior force (along the X-axis)

Fz = medio-lateral force (along the Z-axis)

y_O = vertical distance from the surface of the force plate to the origin of the force plate
(negative value)

y_T = height of the artificial turf (and rubber underlay, if included) (negative value)

Ground reaction forces and free moments are expressed in relation to the sign convention shown in Figure 3.26. Vertical GRF is represented by forces in the Y-direction. Forces in the anteroposterior and mediolateral directions are represented by forces in the X- and Z-directions, respectively. A positive M_y' corresponds with a free moment that resists an internally rotated moment applied to the ground by the subject around the Y-axis (i.e. resists foot adduction). Conversely, a negative M_y' corresponds with a free moment that resists an externally rotated moment applied to the ground by the subject (i.e. resists foot abduction), with respect to the subject's stance leg.

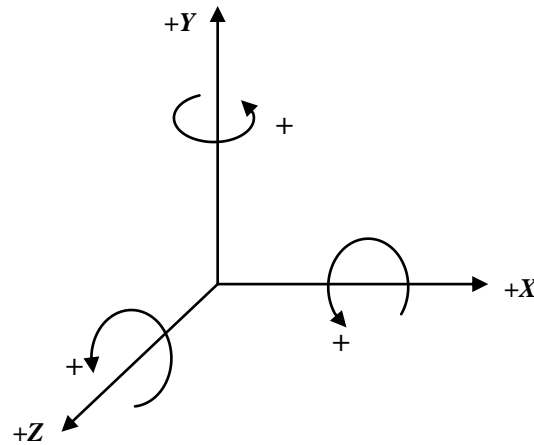


Figure 3.26 Sign convention used in this study

The horizontal GRF is the resultant horizontal ground reaction force, which was calculated from the anteroposterior and mediolateral horizontal ground reaction forces, respectively. The free moment, My' , of ground reaction was defined as a force couple about a vertical axis (assuming a horizontal running surface), which results from the horizontal force between the foot and the ground (Holden & Cavanagh, 1991).

For each trial, the ground reaction forces and vertical loading rate were normalised by dividing by the subjects' bodyweight (BW). All free moment values were normalised by the product of the subject's BW and height.

3.4.2.3 Traction Coefficients

A linear traction coefficient (Equation 5.9) and a rotational traction coefficient (Equation 5.10) were calculated. A linear traction coefficient, τ_s , provided an indication of the resistance to linear movement of the foot on the surface. The equation is essentially the same calculation for a conventional friction coefficient, μ . However, this use of this term was deemed inappropriate as it has been reported that sports surfaces do not follow the classic Coulumb's laws of friction (Shorten *et al.*, 2003; Van Gheluwe *et al.*, 1983).

A rotational traction coefficient, τ_r , was calculated to provide an indication of the resistance to rotation by the turf, while taking into consideration the magnitude of the vertical force. The unit of τ_r is given in millimetres.

$$\tau_s(t) = \frac{Fh(t)}{Fy(t)} \quad [\text{Eq. 5.9}]$$

$$\tau_r(t) = \frac{My'(t)}{Fy(t)} \quad [\text{Eq. 5.10}]$$

Six outcome measures were analysed from the force platform data: the peak vertical GRF, the peak horizontal, the peak moment of rotation, the peak vertical rate, the peak linear traction coefficient and the peak rotational traction coefficient.

3.4.2.4 Approach Velocities

The approach velocity was defined as the velocity of the whole body centre of mass in the X (fore-aft) direction at initial contact with the force platform. The whole body centre of mass (CM) is the weighted sum of the CM of every segment of the body (Eames et al, 1999) (Equation 5.11).

$$CM_i = \frac{\sum_j m_j \cdot p_{i,j}}{\sum_j m_j} \quad [\text{Eq. 5.11}]$$

where m_j is the mass of segment j ($j=1 \dots 8$), and $p_{i,j}$ is the i^{th} component ($i = x, y, z$) of the position vector of its centre of mass. Values for segment mass and position of CM were obtained from anthropometric tables (Table 3.3). The CM velocity was calculated using the linear velocity and acceleration (LINVELACC) function in the *BodyBuilder* programme.

3.4.3 Data Logger

As described in Section 3.2.3, an LED ‘event marker’ on the data logger identified the start of an individual trial. This event marker was used to extract the accelerometer and electrogoniometer data from the data logger. The video files were analysed to approximate the time taken between the event marker and the stance phase of interest during the trial. This time was used to extract a 1 second (i.e. 500 data logger samples) window of data around the stance phase.

A Matlab program was written to extract the 1 second window of data out of each data logger file. The accelerometer channels and electrogoniometer channel was filtered using a 4th order Butterworth filter with cut-off filters of 100Hz and 20Hz, respectively.

The outputs from the accelerometer and electrogoniometer channels were converted into multiples of gravity (g) and degrees, respectively, using the calibration data obtained from the manufacturers of the devices. Each of the individuals trials were subsequently manually analysed to identify the foot strike event of the movement. This was defined by a sharp and rapid rise in the output of the shank accelerometer. The sample number when this event occurred was recorded.

The peak shank accelerations, hip accelerations, peak knee angle during the stance phase and the knee angle at foot strike were calculated.

3.4.4 Statistical Analysis

In order to test for significant differences in parameters between turfs and movements, a two-way (turf x movement) repeated measures ANOVA with Bonferonni adjustment for multiple comparisons was conducted using *SPSS for Windows Version 16.0* statistical software.

CHAPTER 4. BIOMECHANICAL RESULTS

This section describes the results obtained from the laboratory based biomechanical assessment of the three types of artificial turf. Ground loadings, knee moments and knee angles are presented. Also included is a comparison of the data obtained from the data logger when the subject performed the same movements inside and outside of the laboratory on different surfaces.

4.1 Subject Participation

Unfortunately, not all the subjects were able to attend the all of the testing sessions for each of the surfaces. Each of the three artificial turfs (T1, T2, T3) was laid out in the biomechanics laboratory for the duration of rigid two week period. Due to the logistics of removing the previous turf, arranging delivery of the turfs and the infill material, installing the artificial turf and preparing the laboratory, plus the limited available laboratory time in a busy research department, it was difficult to accommodate any changes to the subjects' availability. Table 4.1 outlines the sessions that each subject attended.

Surface	Subject													Total
	F1	F2	F3	F4	F5	H1	H2	H3	H4	R1	R2	R3	R4	
T1	Y	Y	Y	Y	N	Y	Y	Y	Y	Y	Y	Y	Y	12
T2	N	Y	Y	N	Y	Y	Y	Y	Y	Y	N	Y	Y	10
T3	Y	Y	Y	Y	Y	Y	Y	Y	N	Y	Y	Y	Y	11

Table 4.1 Subject participation in the 3 laboratory testing sessions (Y=Participated, N=Did not participate)

Eight subjects completed trials on all three surfaces. Twelve, ten and eleven subjects completed trials on T1, T2 and T3, respectively. In order to test for significant statistical differences between turfs and movements, only the data from a subset of 8 subjects who completed trials on all three turfs were included in any repeated measures ANOVA analyses to test for statistical differences in parameters between surfaces. The data from these 8 subjects are provided in the following sections. Data for all the subjects who participated in the study is presented in Appendix 1.

4.2 Approach Velocities

Figure 4.1 shows the mean approach velocities for all the movements on the three turfs. No approach velocity was calculated for the *180T* movement as the subject started the turn from a standing position.

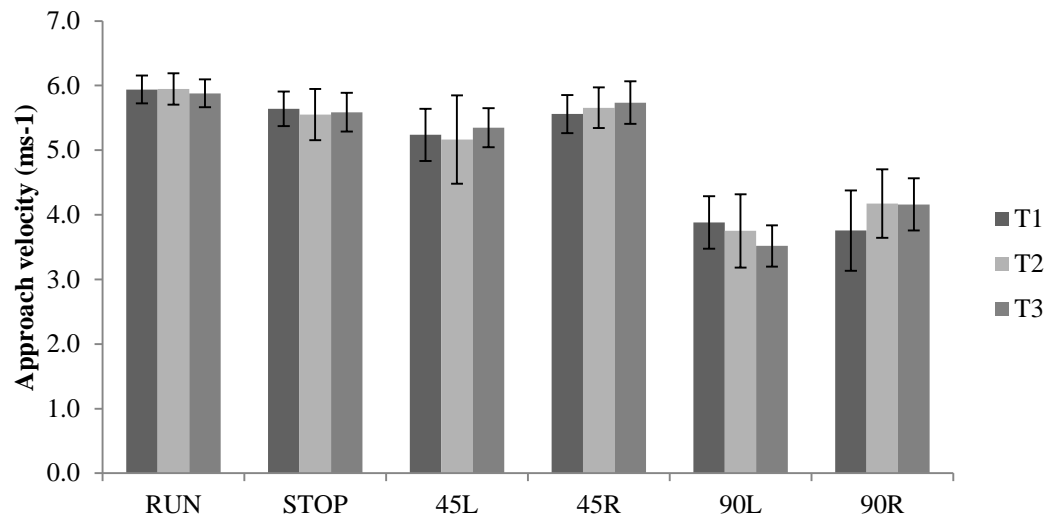


Figure 4.1 Mean (sd) approach velocities to the force platform

The *RUN* movement had the fastest approach velocity of approximately 5.9 ms⁻¹. This was significantly faster than all the other movements ($P<0.001$), except for the *45L* and *45R* movements. Interestingly, *45L* was 0.4 ms⁻¹ faster than *45R*. The *90L* and *90R* movements, which require a sharp change in direction, were significantly slower than all the other movements ($P<0.002$).

There were no statistically significant differences in approach velocities for the three separate testing sessions on the three different surfaces. Figure 4.2 and Pearson correlation calculations show a high correlation of approach velocities between the three turfs (T1-T2: $r=0.903$, $P<0.001$; T2-T3: $r=0.892$, $P<0.001$; T1-T3: $r=0.881$; $P<0.001$).

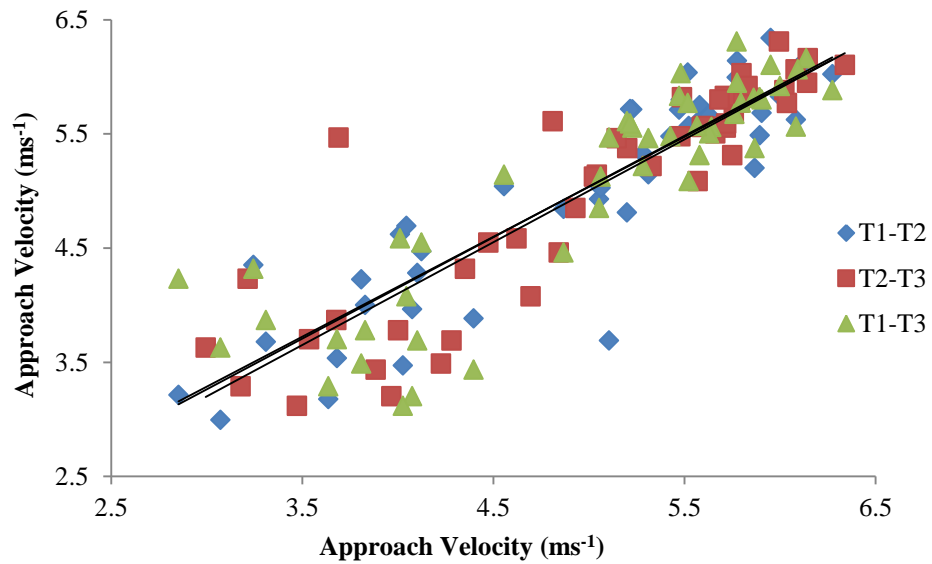


Figure 4.2 Correlation of approach velocities between the three turfs

4.3 Stance Times

The mean stance phase durations are presented in Figure 4.3. The *RUN* movement had significantly shorter stance duration than all the other movements ($P<0.05$), except the *STOP* movement, with a duration of approximately 175ms. There were no significant differences between durations on the three turfs for any of the movements.

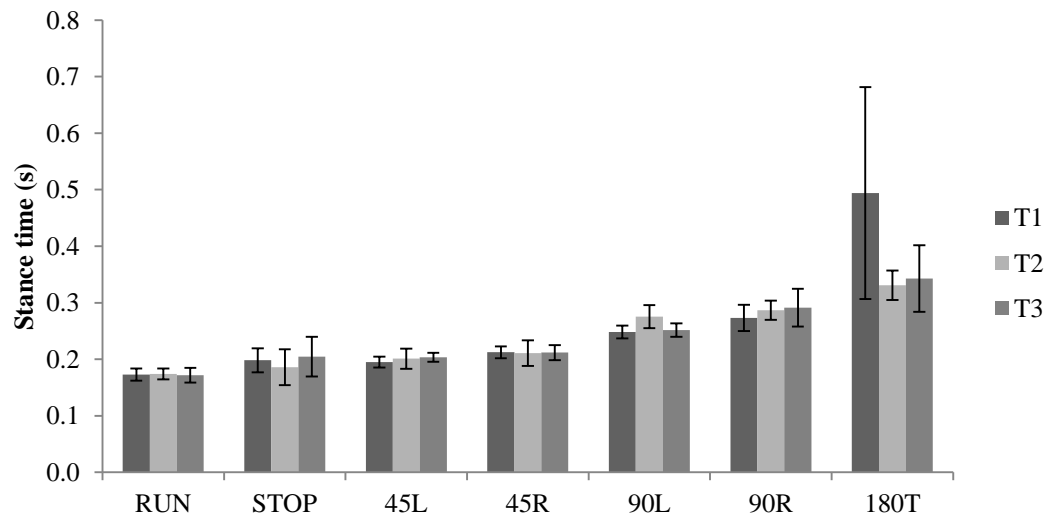


Figure 4.3 Mean (sd) duration of stance phase for each movement all the three turfs

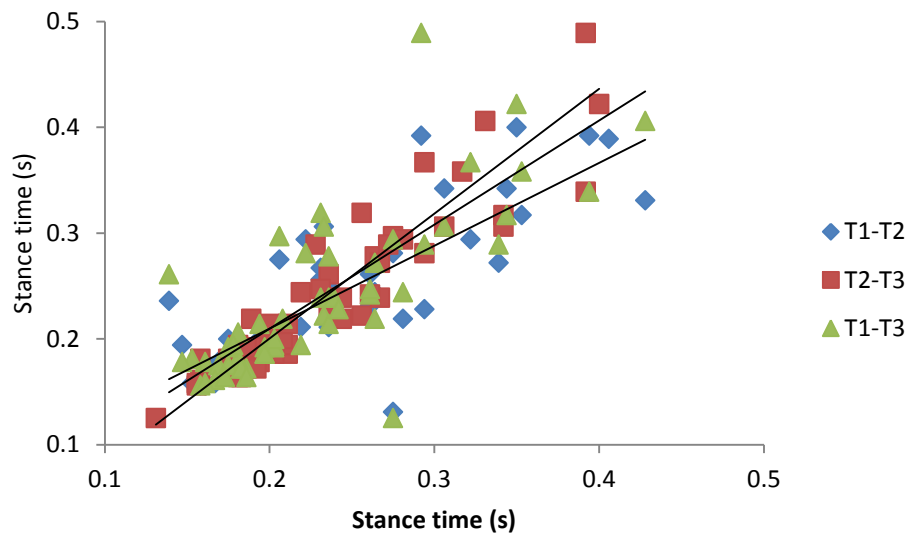


Figure 4.4 Correlation of stance times between the three turfs

Figure 4.4 and Pearson correlation calculations shows high correlations in the approach velocities between the three turfs (T1-T2: $r=0.814$, $P<0.001$; T2-T3: $r=0.924$, $P<0.001$; T1-T3: $r=0.802$; $P<0.001$).

The movements with a greater angle of turn corresponded with an increased stance time. For example, the stance phase durations of the 90° turns ($90L$, $90R$) were approximately 60ms longer than the 45° turns ($45L$, $45R$) ($P<0.05$). Despite large variation between subjects, the duration of the $180T$ movement was significantly larger than all the movements ($P<0.05$), except for the $90R$. The mean duration for the $180T$ movement ranged from 343 ms to 494 ms across the three turfs.

There was a small disparity in the stance phase duration between the different directions of the respective turning movements. The duration of the $45R$ stance phase on each of the three turfs was approximately 12ms longer than the $45L$ movement. However, the difference was only 5ms on Turf 3. Similarly, the $90R$ movement was on average 25 ms longer than the $90L$ movement.

4.4 Ground Loading Profiles

On the following pages, Figure 4.5-4.11 show the mean ground reaction forces (GRF) and the free moment profiles as a percentage of the stance phase duration for the seven movements performed by all subjects (n=13) on the three turfs.

Two charts are provided: vertical and horizontal GRFs are shown on one chart (figure a); and free moments are shown on a separate chart (figure b).

The error bars show the standard deviation for loadings of all subjects on Turf 1. This is displayed to provide an illustration of the variability between subjects. The standard deviation was similar for the other two turfs for each of the ground loading parameters.

As described before, the ground reaction forces were normalised by dividing by the subjects' bodyweight (N/BW); free moment values were normalised by the product of the subject's BW and height (Nm/BW.h).

4.4.1 Movement: RUN

In the *RUN* movement, the vertical GRF rate of loading increased rapidly during the first 15% stance phase (25ms) (Figure 4.5a). This corresponds with the initial foot contact at weight acceptance period of the stance phase. The vertical GRF reached a peak at approximately 45-60% stance phase (75-100ms).

At approximately 10% stance phase (17ms), a small peak occurred in the horizontal GRF. A larger peak is observed at approximately 75% stance phase (130ms), which corresponded to the later stages of the propulsion phase.

The mean free moment loading profiles shown in Figure 4.5b suggest that the *RUN* could be divided into three phases: 0-25% stance phase; 25-75% stance phase; 75-100% stance phase. The largest free moment occurred during the middle of the stance phase. The summarised data indicates that the free moments measured on Turf 3 was slightly lower than Turf 1 and 2. However, this difference between turfs was insignificant.

As can be seen from the error bars, there was variation in the free moment between subjects within each of the three phases. Although, most subjects (n=11) maintained a similar free moment pattern across all the turfs, the variation was evident in its direction. A free moment resisting foot adduction was measured in seven of the subjects; a free moment resisting foot abduction in three subjects, and one subject did not produce any significant free moment during the first 25% stance phase.

During the middle 25-75% period of stance phase, there was more consistency between subjects as a free moment peak resisting foot abduction occurred in eleven of the subjects. Only one subject demonstrated a free moment resisting foot adduction during this period. In the final 25% stance phase, ten of the subjects produced a small free moment resisting foot adduction peak, although this peak was diminished on Turf 3.

Two subjects (F4, H4) experienced a change in direction of the free moment loading profile as they performed the *RUN* movement over the different turfs. On Turf 1, subjects F4 had a change in free moment resisting foot adduction to a free moment resisting foot abduction on Turf 3, in the first 25% stance phase. This subject experienced a peak free moment resisting foot abduction during the middle 25-75% stance phase on all three turfs.

Subject H4 produced a negative free moment peak (resisting foot abduction) on Turf 1 during the first 25% stance phase. However, a free moment resisting foot adduction occurred on Turfs 2 and 3 during this period. This subject also experienced a peak free moment resisting foot abduction during the middle 25-75% stance phase on all three turfs.

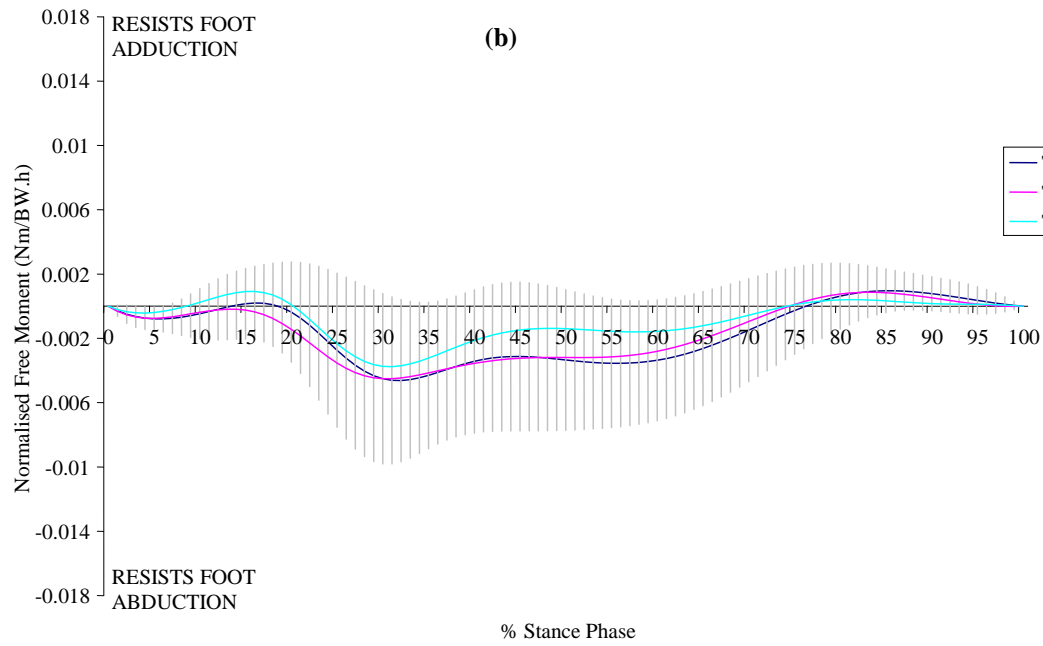
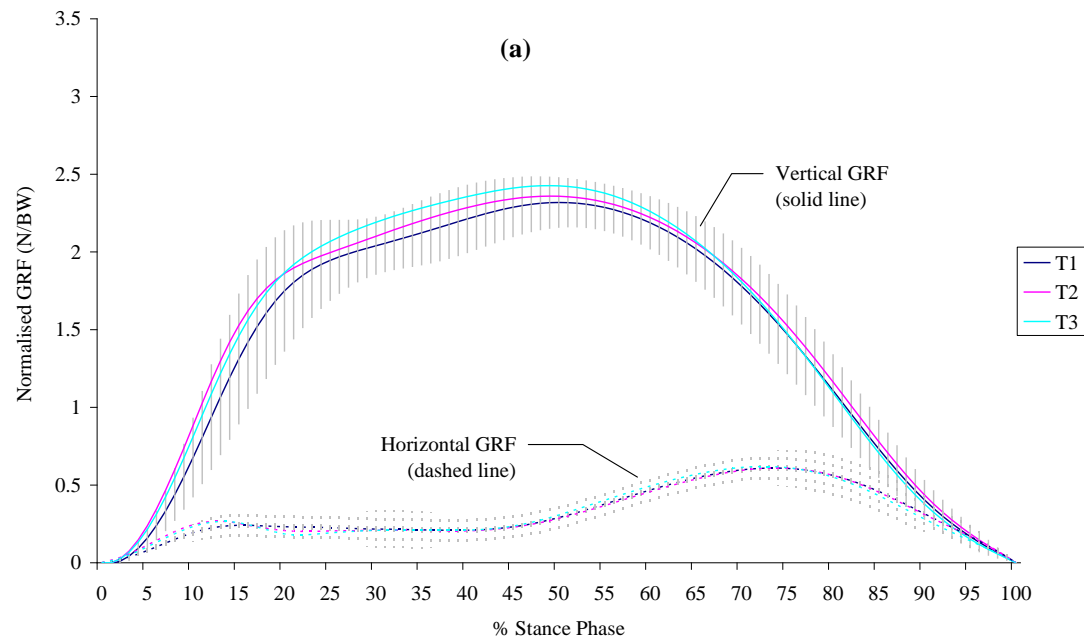


Figure 4.5 Mean normalised ground loadings on each surface during the *RUN* movement: a) vertical and horizontal GRF; b) free moment. Error bars show \pm sd for Turf 1

4.4.2 Movement: STOP

The mean GRF loading profiles displayed in Figure 4.6a show that one peak force occurred in both the vertical and horizontal directions during the *STOP* movement. These peaks occurred during the early phases

of stance phase: approximately 20% stance phase (40ms) for the vertical GRF peak; approximately 15-25% stance phase (30-50ms) for the horizontal GRF. For the remainder of the stance phase, the subjects' forward momentum was significantly retarded as they were stepping off the force platform. This resulted in no further significant peak forces for the rest of the stance phase.

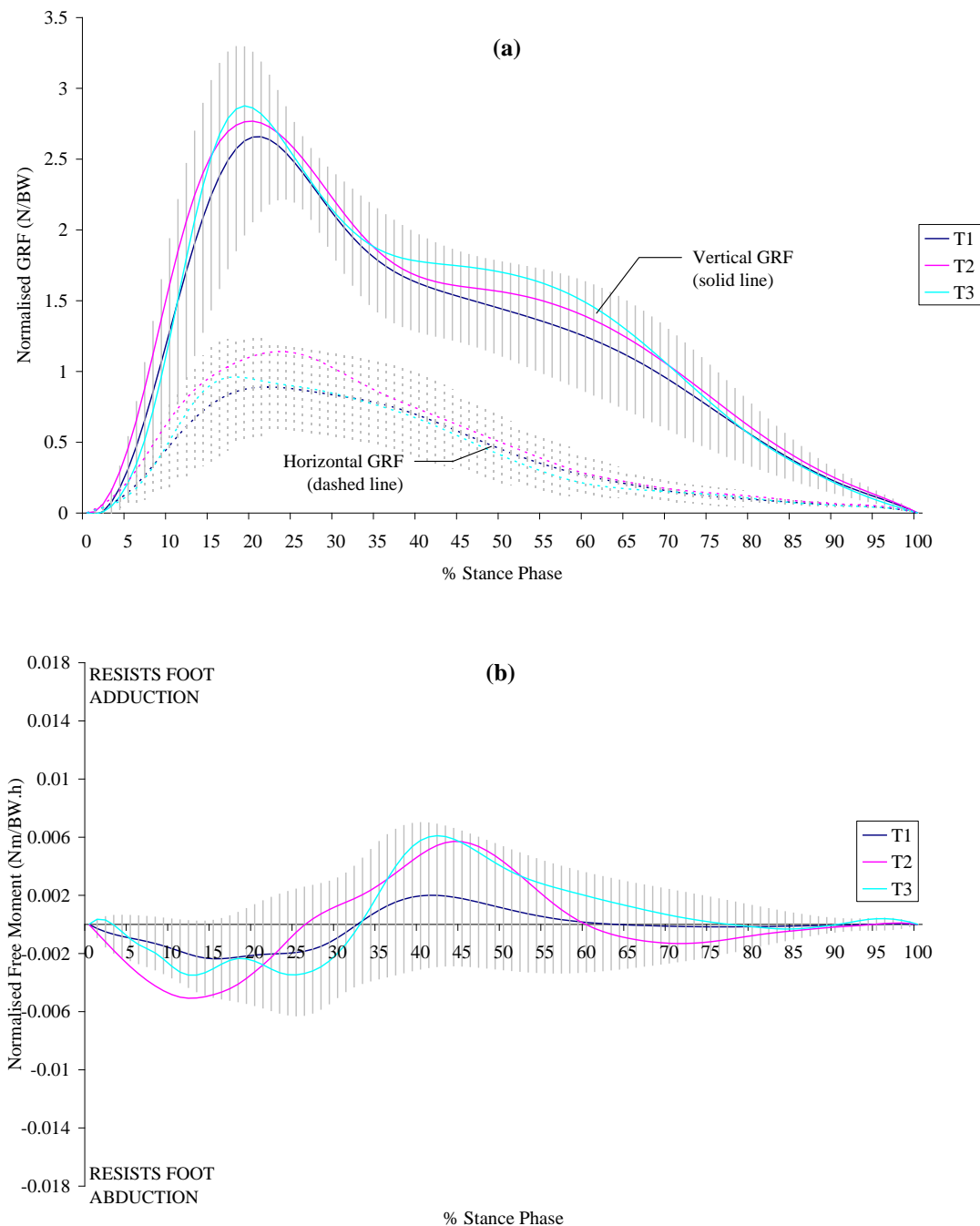


Figure 4.6 Mean normalised ground loadings on each surface during the STOP movement: a) vertical and horizontal GRF; b) free moment. Error bars show \pm sd for Turf 1

Figure 4.6b shows two phases of free moment loading. During the first 25-35% stance phase (50-65ms), a free moment resisting foot abduction was measured, with a peak occurring at approximately 15% stance phase (30ms). A free moment resisting foot adduction was present during approximately 30-60% stance phase, with a peak occurring at about 40-45% stance phase (75-85ms). No other significant free moment was apparent for the remaining 35% of the stance phase.

4.4.3 Movement: 45-degree turns

Figure 4.7(a, b) and Figure 4.8(a,b) show the mean GRF-vs-time and free moment-vs-time patterns for the *45L* and *45R* movements, respectively. Similar loading profiles were observed for both the *45L* and *45R* movements.

The free moment loading profile for both *45L* and *45R* movements was relatively consistent on all three turfs (Figure 4.7b and 29b). However, there was variability between subjects. Generally, three peaks were observed in the first 40% of stance phase. In both types of movement, the stance phase could be broken down into 4 periods, with regards to the free moment: 0-10%; 10-20%; 20-40%; and the remaining 60% stance phase.

In general, a small free moment resisting foot adduction occurred in the first period of stance phase (0-10%). A free moment resisting foot abduction occurred between 10-20% stance phase and a free moment resisting foot adduction occurred between 20-40% of stance phase. No significant free moment was present during the final 40-100%, except for on Turf 1, where a small, consistent free moment resisting foot adduction occurred.

As with the other movements, the direction of the free moment was not consistent between subjects for the two 45° turns. For example, the mean free moment peak that occurred at approximately 15% stance phase was less prominent for the *45L* movement (Figure 4.7b), where a free moment resisting foot adduction was measured in about only half of the subjects. In contrast, in the *45R* movement (Figure 18b), a free

moment resisting foot adduction occurred for 2 subjects (H2 and H3) on Turf 1 and Turf 2. During the *45R* movement on Turf 3, a free moment resisting foot abduction peak at 10-20% stance phase was present for all subjects.

During the 20-40% period of stance phase, most of the subjects typically produced a free moment resisting foot adduction. For the *45L* on Turf 3, one subject (R4) produced a free moment resisting abduction during this period and throughout the remainder of stance phase. For three of the subjects on Turf 1 (R3, F3 and H4) during the *45R* moment, a peak was not observed and the free moment was reduced to zero.

For the remainder of the stance phase (40-100%), there were no consistent trends apparent in the data. This was due to the variation between subjects and turfs in the magnitudes and direction of the free moment. In general for the *45L*, a predominately positively directed free moment resisting foot adduction, was present in four subjects (F1, F2, H3, R1); a predominantly negative free moment, resisting foot abduction, was displayed in three subjects (F3, F5, R3); and the direction of the free moment changed between surfaces for the other six subjects.

For the *45R*, a predominately positively directed free moment resisting foot adduction was present in four subjects (H1, R1, R2, R4); a prominently negative free moment, resisting foot abduction, was displayed in four subjects (F1, F4, H2, R3); and the direction of the free moment changed between surfaces for another four subjects. One other subject (H3) did not produce a substantial free moment for the final stages of the stance phase for either 45° turn

4.4.3.1 Movement: 45L

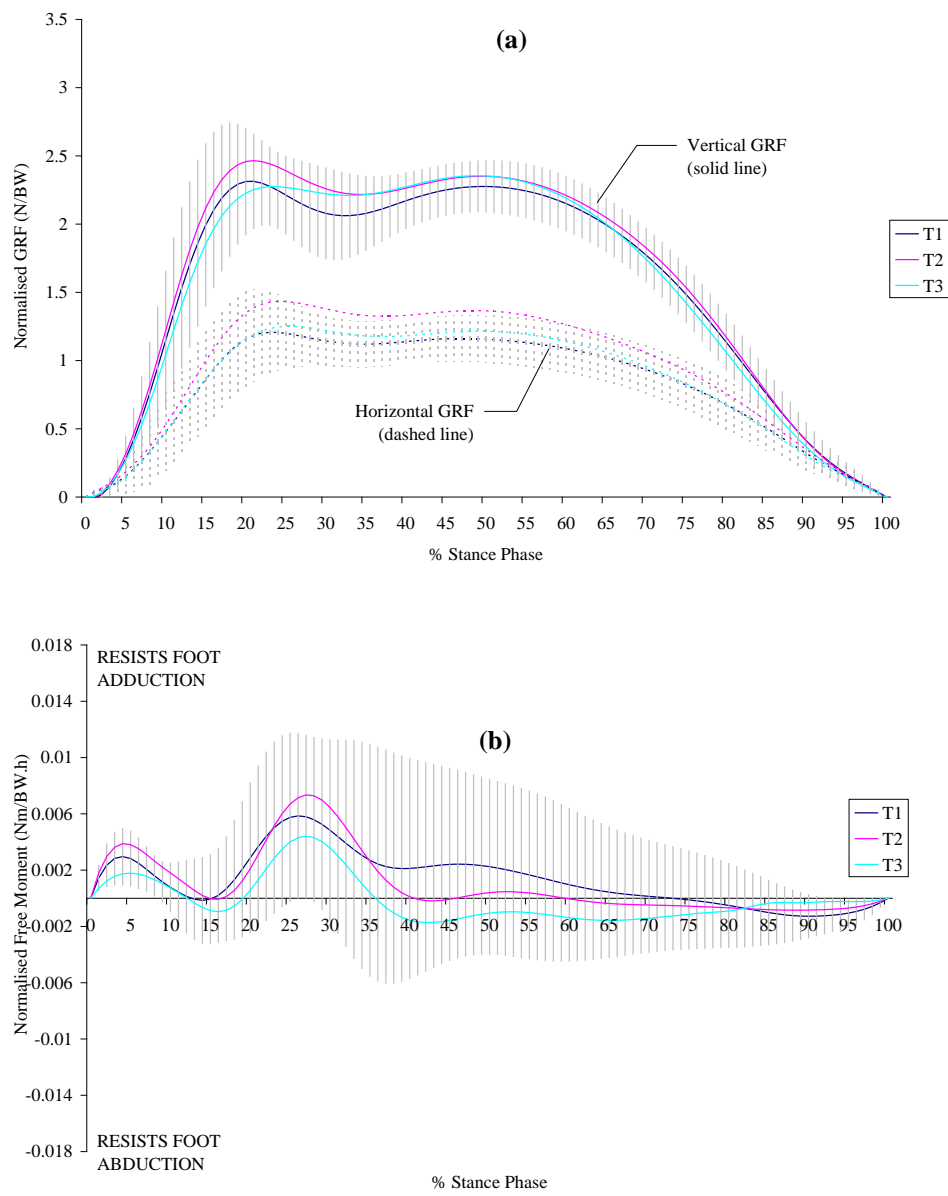


Figure 4.7 Mean normalised ground loadings on each surface during the 45L movement: a) vertical and horizontal GRF; b) free moment. Error bars show \pm sd for Turf 1

4.4.3.2 Movement: 45R

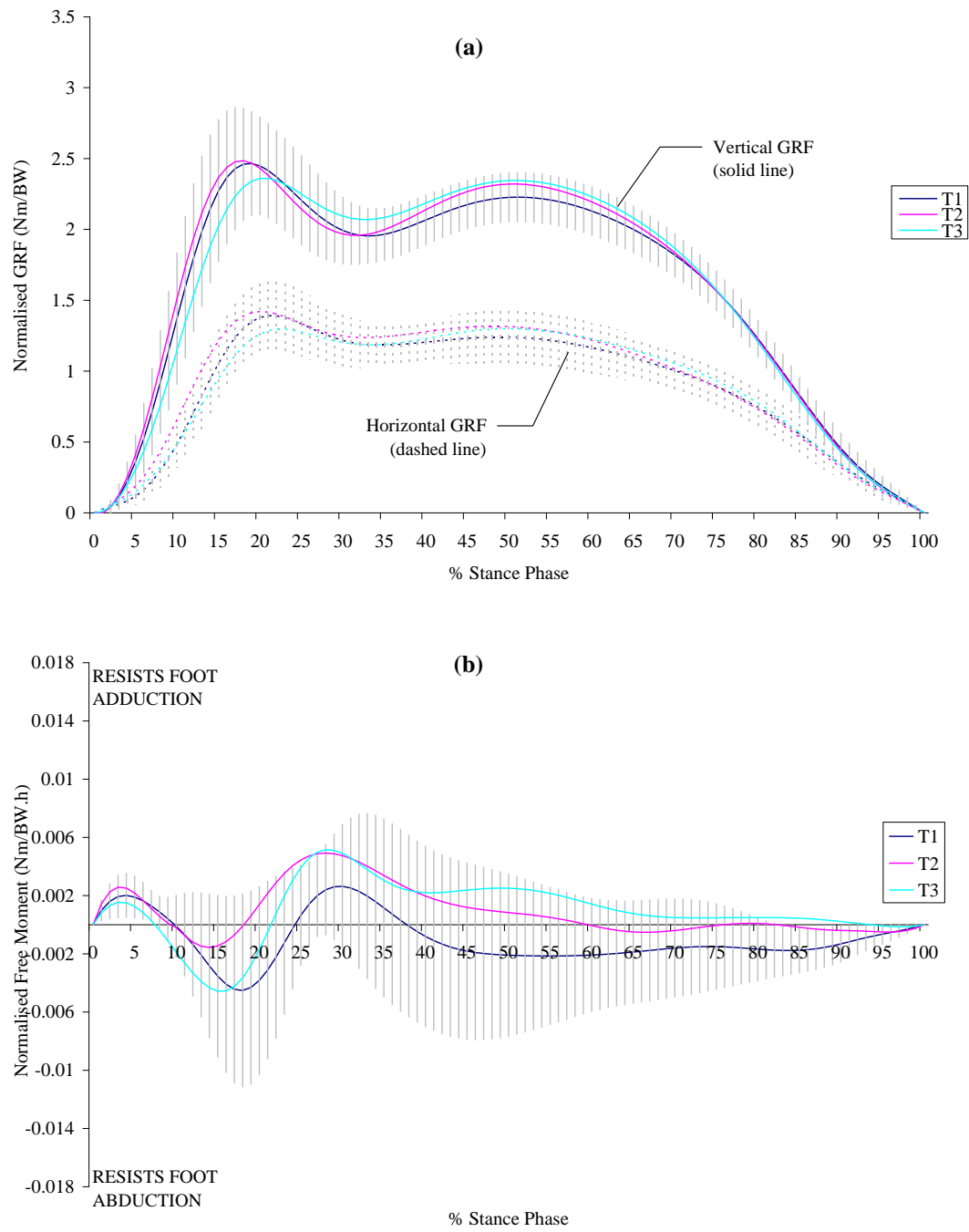


Figure 4.8 Mean normalised ground loadings on each surface during the 45R movement: a) vertical and horizontal GRF; b) free moment. Error bars show \pm sd for Turf 1

4.4.4 Movement: 90-degree turns

Figure 4.9 (a,b) and Figure 4.10 (a,b) show the mean GRF-vs-time and free moment-vs-time patterns for all subjects on all three turfs for the *90L* and *90R* movements, respectively.

Similar loading profiles were observed for both the *90L* and *90R* movements. The 90° turns also had similar vertical GRF loading profiles to the *RUN* movement (Figure 4.9a and Figure 4.10a). However, the magnitude of the vertical GRF was generally lower than the *RUN* movement.

In the first 15-20% stance phase (40-50ms), a small peak was observed in both the vertical and horizontal GRFs. Also, a free moment resisting foot adduction was observed during this period for both the *90L* and *90R* (Figure 4.9b and Figure 4.10b).

During the middle 20 to 60% stance phase (50-160ms), as the subject turned and transferred forward momentum to a lateral direction, an increasing vertical GRF was applied in both the *90L* and *90R* movements. The horizontal GRF remained relatively constant for the *90R* movements (Figure 4.10a), whereas it tended to decrease slightly for the *90L* movement (Figure 4.9a). A sustained free moment, resisting foot abduction, was applied during this period for both movements (Figure 4.9b and Figure 4.10b); although the magnitude of the free moment resisting foot abduction was generally lower for the *90R* movement.

A second, larger vertical GRF peak occurred at approximately 60% stance phase. This corresponded with a peak in the free moment curve. The graphs suggest that the free moment was lower on Turf 1 than on the other two turfs. However, this difference was statically insignificant.

4.4.4.1 Movement : 90L

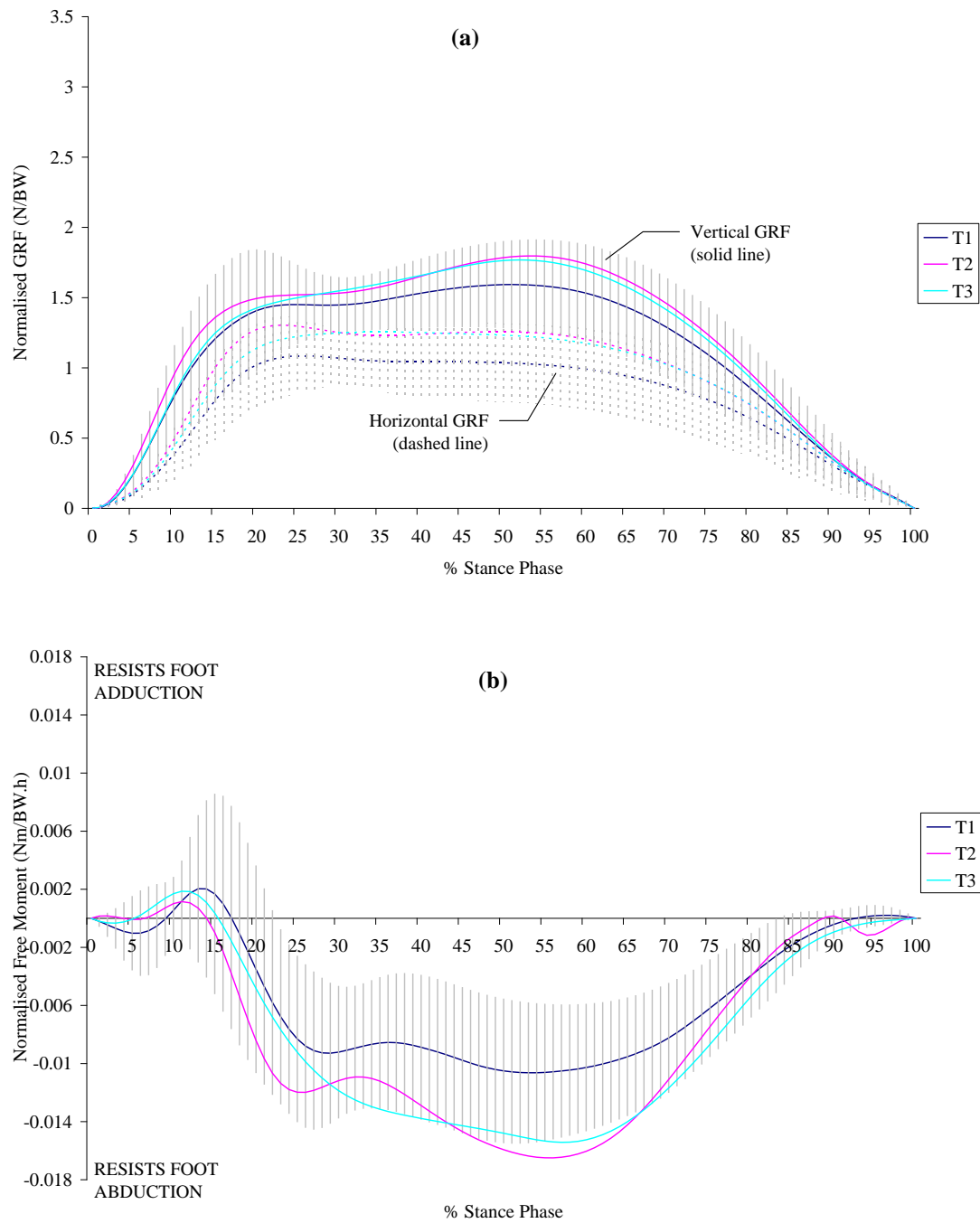


Figure 4.9 Mean normalised ground loadings on each surface during the 90L movement: a) vertical and horizontal GRF; b) free moment. Error bars show \pm sd for Turf 1

4.4.4.2 Movement: 90R

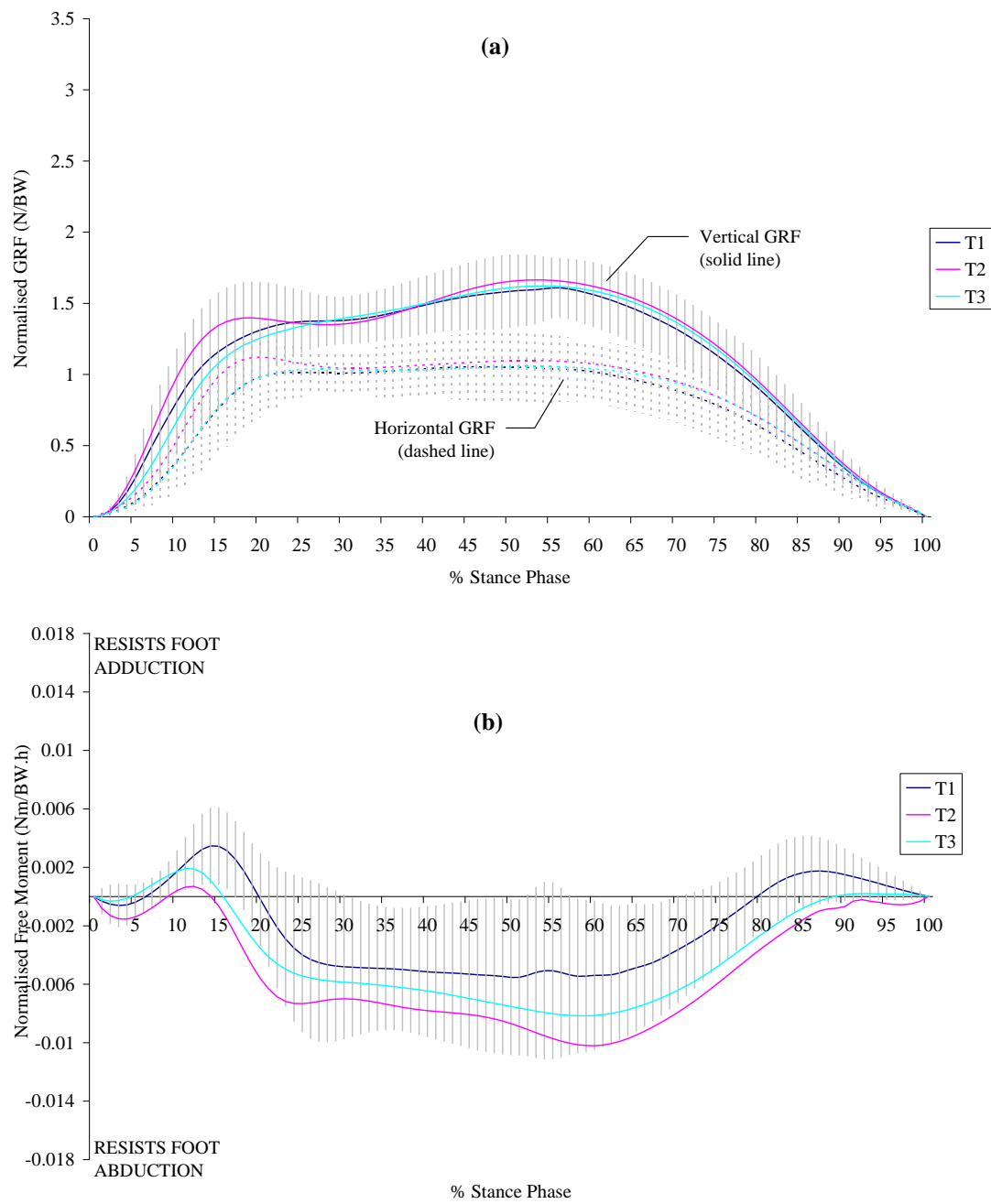


Figure 4.10 Mean normalised ground loadings on each surface during the 90R movement: a) vertical and horizontal GRF; b) free moment. Error bars show \pm sd for Turf 1

4.4.5 Movement: 180T

Figure 4.11 (a,b) show the mean GRF-vs-time and free moment-vs-time patterns for all subjects on all three turfs for the 180T movement.

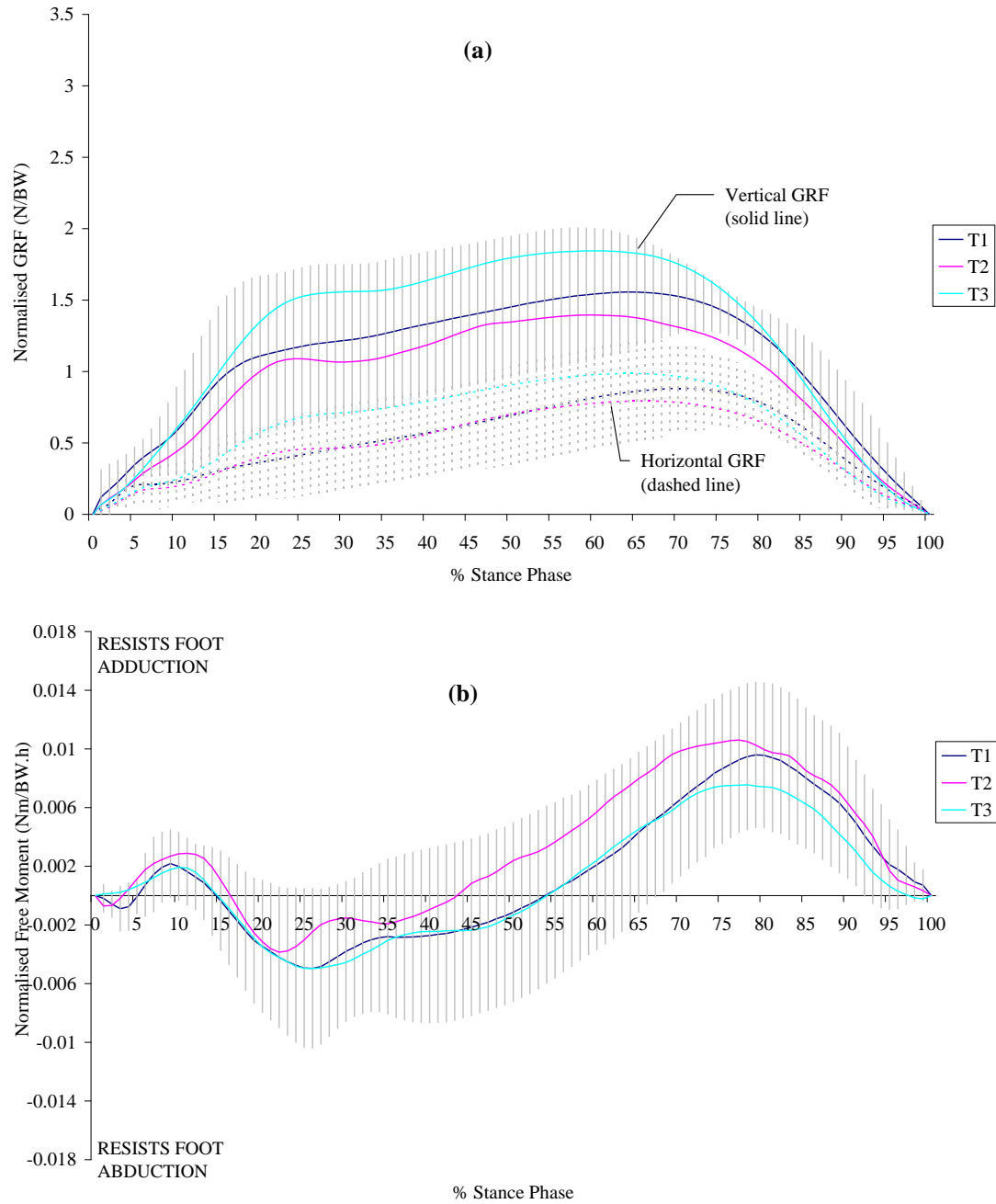


Figure 4.11 Mean normalised ground loadings on each surface during the 180T movement: a) vertical and horizontal GRF; b) free moment. Error bars show \pm sd for Turf 1

During the initial weight acceptance phase of the *180T* movement (0-30% stance phase; approximately 0-140ms), a peak vertical GRF of 1-1.5BW was observed (Figure 4.11a). Generally, the horizontal GRF slowly increased in magnitude during this period with some subject producing small peaks. In the first 30% stance phase, the free moment that was applied switched from an initial moment resisting foot adduction to one that resists foot abduction (Figure 4.11b).

Peak loadings were observed at approximately 65-80% stance phase (260-340ms). This corresponded to the subject completing the 180° turn and pushing off in the opposite direction. The magnitudes of the peaks were 1.4-1.8BW and 0.8BW for the vertical and horizontal GRF, respectively. The magnitude of the free moment was approximately 0.01Nm/BWh and its direction reversed back to one that resisted foot adduction.

4.5 Peak Ground Loadings

4.5.1 Phases of peak loadings

As can be seen from section 4.4, multiple loading peaks occurred during the stance phase for each of the movements. Typically two significant peaks occurred: one in the impact phase (*impact peak*) and one in the propulsion phase (*propulsion peak*) of the movement. The magnitudes of the peaks in the two phases would often be similar. For example, the vertical GRF in the *RUN* and 90° turns. In contrast, impact peak of the 45° turns were generally greater than the propulsion peak. However, there did not seem to be consistency between subjects in which of the phases the greatest peak would occur.

The ground loading profiles of each movement were visually inspected to obtain an estimation of the times when the impact and propulsion phases typically occurred (Table 4.2). Peaks were only measured during the respective phases if there was a definite peak in the data (as opposed to a continuing rise in the force or moment as between the defined end of impact phase and start of propulsion phase). As such, the defined phases are broad enough to allow the calculation of the times of the ground loading peaks.

It was observed that in several instances clear vertical or horizontal GRF impact peak were not produced. This was often inconsistent between the separate performances on the different turfs. Therefore, it was not always possible to conduct a repeated measures analysis to measure statistical differences between turfs and movements. However, the times of the impact and propulsion phases were relatively consistent between turfs.

The defined impact phase of the RUN movement (0-50ms) was shorter than the other movements, due to the shorter stance time. For most movements, the impact phase generally occurred during the first 35% of stance. The defined impact phase for the 180T was longer due to the greater range of times when impact peaks occurred.

Movement	Impact Phase		Propulsion Phase	
	ms	% Stance	ms	% Stance
RUN	<50ms	0-30	>50ms	31-100
STOP	<70ms	0-35	>70ms	36-100
45L & 45R	<70ms	0-35	>70ms	36-100
90L & 90R	<80ms	0-32	>80ms	33-100
180T	<150ms	0-50	>150ms	51-100

Table 4.2 Times of the impact and propulsion phases for each movement

4.5.2 Vertical GRF

Table 4.3 displays the absolute peak vertical ground loading magnitudes in the impact and propulsion phases, respectively, for each movement on the 3 turfs. The times to the peak load in each of phase are also presented. Vertical GRFs normalised to bodyweight are presented in Figure 4.12..

The largest vertical GRF was measured for the STOP movement during the impact phase ranging from 3-3.5BW over the 3 turfs, approximately 2300-2800N. The straight sprinting (RUN) and the cutting turns (45R, 45L) produced similar vertical GRFs. The RUN ranged from 2.3-2.4BW, whereas the 45L and 45R were slightly higher with 2.5-2.7BW. Vertical impact GRFs for the 90L, 90R and 180T movements were markedly lower. The 90° ‘cross’ turns (90L, 90R) had a range of 1.3-1.7BW and the 180° turns had a range of 1.3-1.5BW (1000-1200N).

The vertical impact GRF peaked at approximately 40-50ms for all movements, except for the 180T

where it occurred between 64-74ms. However, impact peaks were not consistently produced during the movements on the different turfs by all subjects. Furthermore, only 2 of the subgroup of 8 subjects selected for statistical analysis produced impact GRFs peaks for all movements on all turfs, so there was insufficient data to perform a repeated measures analysis for statistical differences between turfs and movements.

Movement		Vertical GRF					
		Impact Phase			Propulsion Phase		
		T1	T2	T3	T1	T2	T3
RUN	Absolute (N)	1743 (429)	1784 (551)	1892 (491)	1808 (371)	1773 (444)	1964 (360)
	Times to peak (s)	0.043 (.005)	0.040 (.006)	0.042 (.007)	0.088 (.010)	0.090 (.010)	0.085 (.009)
STOP	Absolute (N)	2312 (684)	2816 (999)	2707 (791)	1329 (572)	1358 (506)	1416 (462)
	Times to peak (s)	0.040 (.005)	0.038 (.005)	0.041 (.007)	0.104 (.026)	0.093 (.015)	0.095 (.013)
45L	Absolute (N)	1955 (438)	2062 (544)	2064 (579)	1804 (327)	1863 (435)	1834 (421)
	Times to peak (s)	0.045 (.007)	0.044 (.008)	0.043 (.006)	0.102 (.010)	0.098 (.010)	0.100 (.011)
45R	Absolute (N)	2049 (451)	2075 (517)	2035 (524)	1749 (414)	1833 (416)	1902 (349)
	Times to peak (s)	0.042 (.005)	0.041 (.006)	0.043 (.005)	0.111 (.011)	0.109 (.013)	0.105 (.009)
90L	Absolute (N)	1231 (336)	1305 (458)	1262 (566)	1357 (268)	1461 (394)	1492 (336)
	Times to peak (s)	0.048 (.008)	0.047 (.009)	0.045 (.014)	0.137 (.017)	0.127 (.022)	0.129 (.024)
90R	Absolute (N)	1067 (118)	1234 (351)	991 (606)	1337 (336)	1332 (384)	1362 (301)
	Times to peak (s)	0.044 (.006)	0.049 (.009)	0.047 (.016)	0.135 (.027)	0.149 (.020)	0.145 (.024)
180T	Absolute (N)	1013 (671)	1206 (874)	1225 (896)	1364 (364)	1567 (448)	1671 (441)
	Times to peak (s)	0.074 (.045)	0.069 (.029)	0.064 (.031)	0.288 (.173)	0.221 (.075)	0.244 (.122)

Table 4.3 Mean (sd) magnitude and times of peak vertical GRFs during the impact and propulsion phases of 7 movements performed on 3 different artificial turfs

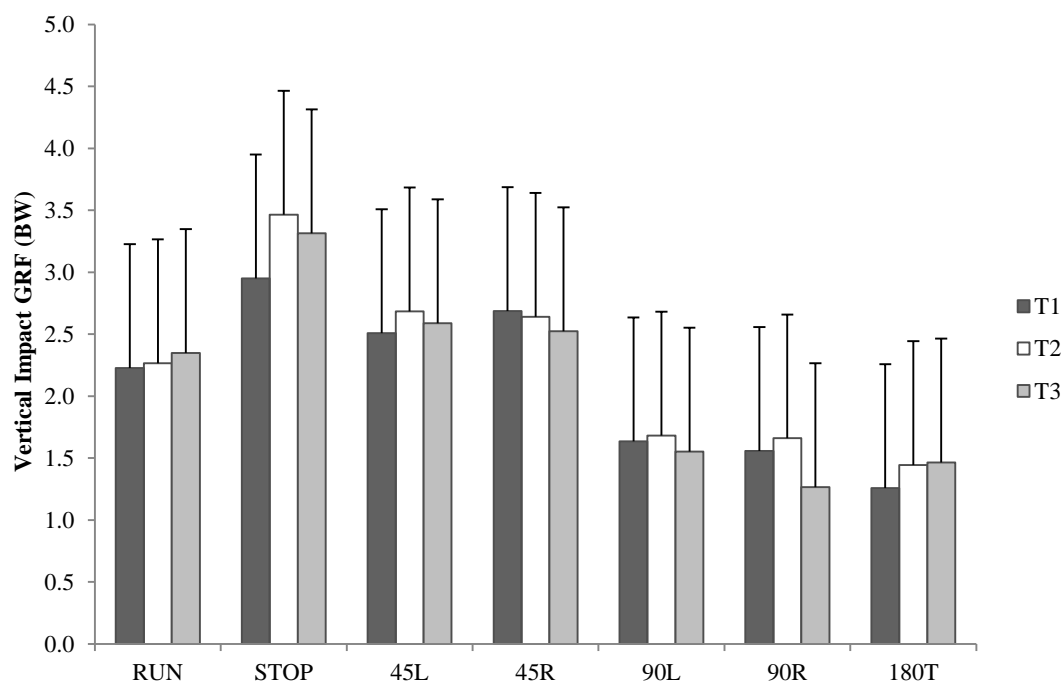


Figure 4.12 Vertical impact GRFs for 7 movements performed on 3 artificial turfs (values are normalised to subjects' bodyweight (BW))

In the propulsion phase, there was no significant difference in peak vertical GRFs between the 3 turf conditions ($P=0.125$). The largest peak was observed in the *RUN* (2.3-2.4BW), *45L* (2.1-2.4BW) and *45R* (2.3-2.4BW) (Figure 4.13). These 3 movements produced significantly higher vertical propulsion peaks than the *90L* (1.7-1.9BW) and *90R* (1.7BW) movements ($P<0.002$). The *RUN* and *45R* also produced significantly higher vertical propulsion peaks than the *180T* (1.7-2.1BW) ($P<0.042$).

The peak vertical GRFs in the 90° and 180° turns were greater in the propulsion phase than during the impact phase. The opposite was the case for the 45° turns. The ground loading data for the *STOP* movement during the propulsion phase was disregarded as the movement does not have a propulsive function. There was no significant difference in vertical propulsion peaks between the 3 turf conditions ($P=0.125$). Furthermore, there was no significant interaction between turfs and movements on the peak vertical GRFs.

There was a greater range in the timings of the propulsion peaks between the movements compared to the impact phase. They ranged from 85-90 ms (*RUN*) to 244-288ms for the *180T*. For the 45° turning movements, ground loading peak values occurred at approximately 98-111ms. The peaks occurred slightly

later for the 90° turning movements at approximately 127-149ms.

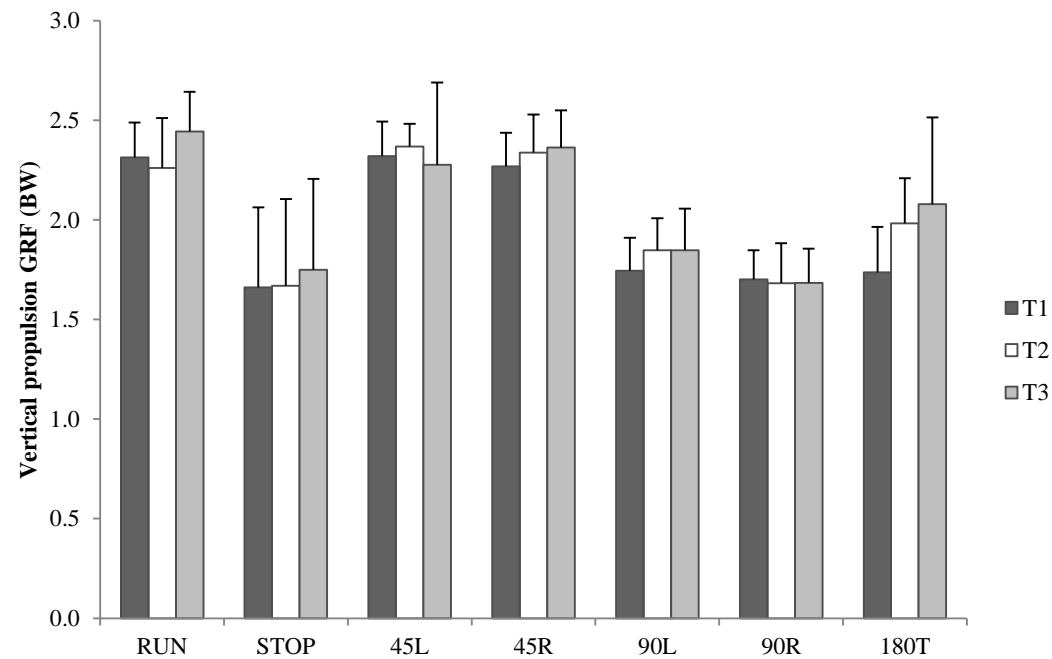


Figure 4.13 Vertical propulsion GRFs for 7 movements performed on 3 artificial turfs (values are normalised to subject's bodyweight (BW))

4.5.3 Horizontal GRF

Peak horizontal forces and the corresponding times of the peaks during the impact and propulsion phases are presented in Table 4.4. Propulsive peaks were similar magnitudes to the impact peaks, except for the *RUN* and *180T* movements in which the propulsive peaks were approximately 50% greater.

Mean horizontal GRF impact peaks are shown in Figure 4.14. For all movements except the *RUN* and the *180T*, the peak horizontal impact GRF was greater than 0.9BW. The horizontal impact GRF of the *RUN* movement (0.3-0.4BW) was lower than the running movements and occurred earlier in stance (30ms). The *180T* movement ranged between (0.4-0.6BW) across the 3 turfs and occurred later in stance (60-75ms). Impact magnitudes were greatest for the *STOP*, *45L* and *45R* movements, ranging from 1.1-1.5BW, at approximately 40ms. Horizontal impact GRFs for the *90L* and *90R* movements were 1.0-1.4BW (at 40-50ms) and 0.9-1.2BW (at 45-50ms), respectively. As with the vertical impact GRF, there was insufficient

data to perform a repeated measures analysis for statistical differences between turfs and movements.

Movement		Horizontal GRF					
		Impact Phase			Propulsion Phase		
		T1	T2	T3	T1	T2	T3
RUN	Absolute (N)	224 (70)	261 (48)	234 (46)	501 (146)	514 (135)	502 (86)
	Times to peak (s)	0.034 (.011)	0.030 (.011)	0.029 (.007)	0.126 (.014)	0.134 (.015)	0.127 (.011)
STOP	Absolute (N)	876 (371)	1196 (657)	1018 (467)	324 (316)	294 (320)	360 (245)
	Times to peak (s)	0.045 (.011)	0.041 (.008)	0.041 (.011)	0.121 (.054)	0.124 (.042)	0.109 (.033)
45L	Absolute (N)	948 (361)	1076 (541)	932 (509)	914 (245)	1096 (307)	994 (220)
	Times to peak (s)	0.047 (.011)	0.043 (.015)	0.037 (.013)	0.102 (.010)	0.094 (.011)	0.095 (.007)
45R	Absolute (N)	1058 (365)	1133 (411)	1039 (398)	1003 (272)	1064 (263)	1065 (243)
	Times to peak (s)	0.043 (.007)	0.041 (.008)	0.043 (.007)	0.103 (.011)	0.101 (.009)	0.101 (.008)
90L	Absolute (N)	769 (507)	1095 (615)	1031 (528)	936 (210)	1088 (383)	1089 (302)
	Times to peak (s)	0.039 (.021)	0.050 (.009)	0.046 (.017)	0.121 (.030)	0.109 (.025)	0.123 (.030)
90R	Absolute (N)	764 (202)	879 (323)	676 (525)	920 (232)	899 (254)	931 (243)
	Times to peak (s)	0.049 (.011)	0.049 (.010)	0.045 (.021)	0.128 (.027)	0.142 (.033)	0.147 (.032)
180T	Absolute (N)	364 (344)	518 (499)	532 (519)	775 (278)	916 (334)	894 (338)
	Times to peak (s)	0.075 (.053)	0.060 (.027)	0.066 (.033)	0.324 (.169)	0.255 (.081)	0.276 (.124)

Table 4.4 Mean (sd) magnitude and times of peak horizontal GRFs during the impact and propulsion phases of 7 movements performed on 3 different artificial turfs

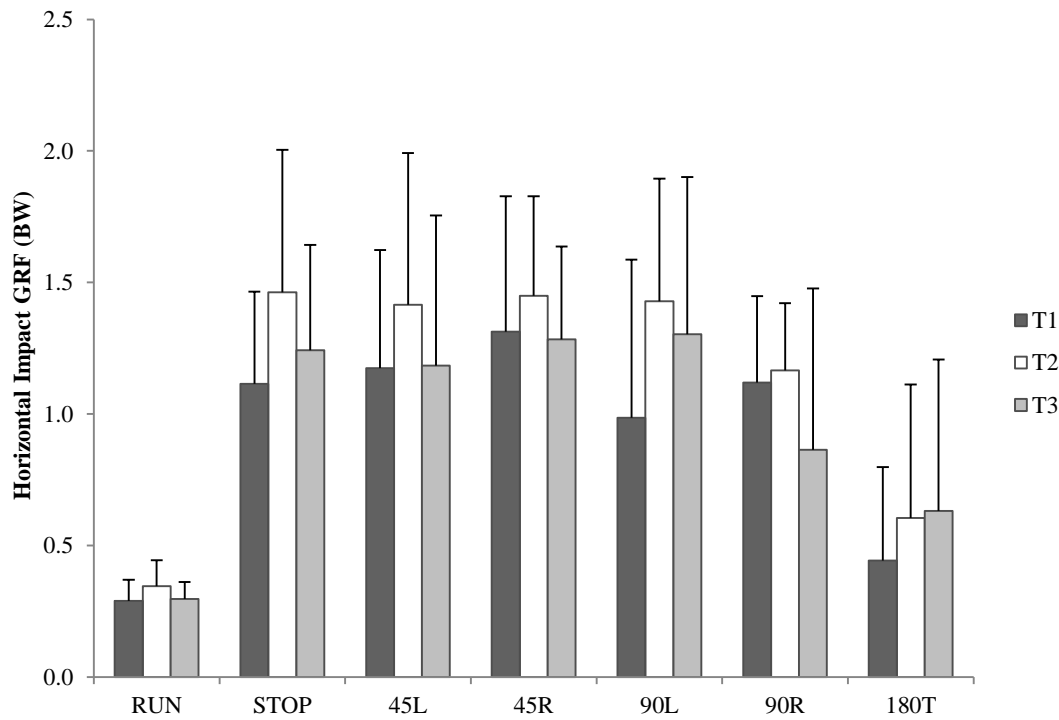


Figure 4.14 Horizontal impact GRFs for 7 movements performed on 3 artificial turfs (values are normalised to subjects' bodyweight (BW))

Mean horizontal GRF propulsion peaks are shown in Figure 4.13. The *RUN* movement (0.63-0.66BW at 130ms) produced significantly lower magnitudes than all other movements ($P<0.004$). Horizontal propulsive peaks for the 45° turns ranged from 1.2-1.4BW (at approximately 100ms). The *90L* (1.2-1.35BW) produced significantly larger peaks than the *90R* (1.14-1.16BW) ($P=0.015$). The *90L* peak also occurred earlier in stance than the *90R* (approximately 120ms compared to 140ms). Peak horizontal propulsion GRFs occurred later in the *180T* movement than any other movement (1.0-1.15BW at 260-320ms) but these values were quite variable.

Statistical analysis of the subgroup of the 8 subjects showed that an overall statistical difference existed between the turf conditions across the movements ($P=0.033$). Post-hoc pairwise comparison tests (using a Bonferri adjustment) were used to identify where this overall difference lay; however, the analysis did not identify statistical differences between two individual turfs. Peak horizontal propulsive GRFs on Turf 2 were 0.083BW higher than on Turf 1 ($P=0.83$) and 0.067BW higher than on Turf 3 ($P=0.158$). Furthermore, there was no significant interaction between turf and movements on the peak horizontal GRFs.

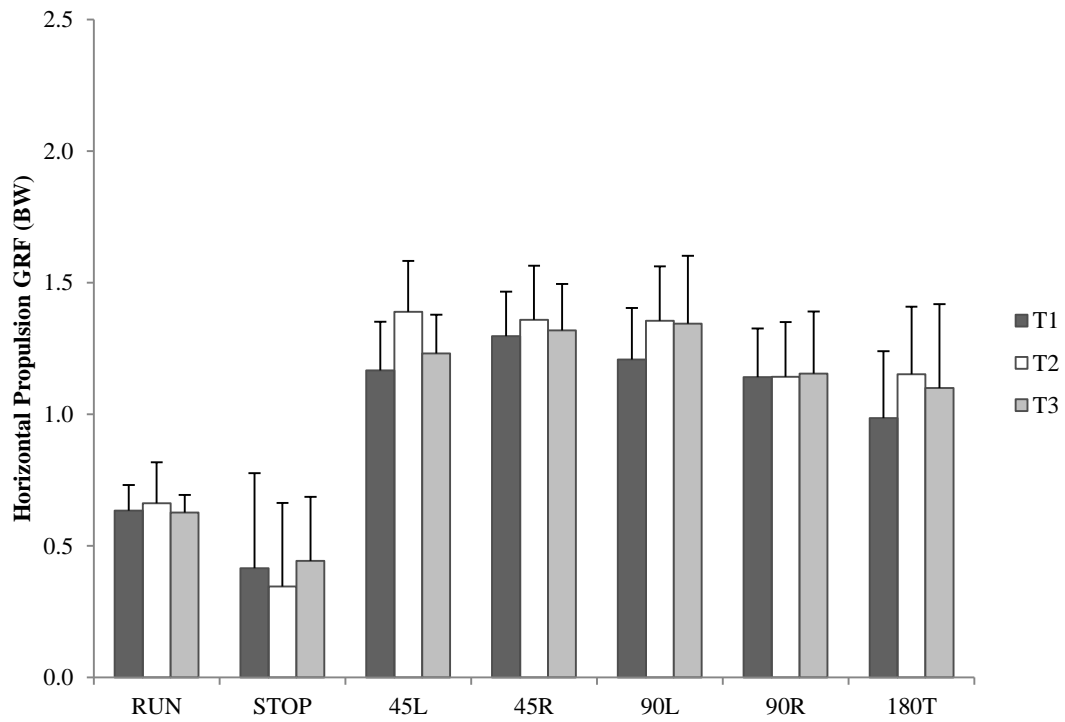


Figure 4.15 Horizontal propulsion GRFs for 7 movements performed on 3 artificial turfs (values are normalised to subjects' bodyweight (BW))

4.5.4 Free Moment

The peak free moment was highly variable in both the impact and propulsion phases (Table 4.5). This was still apparent when the values were normalised for the subjects' bodyweight and height (Figure 4.16 and Figure 4.17). Therefore, peak values will be described in terms of the perhaps more meaningful absolute free moment in the following section (Table 4.5).

Movement		Free Moment					
		Impact Phase			Propulsion Phase		
		T1	T2	T3	T1	T2	T3
RUN	Absolute (Nm)	8.7 (5.0)	7.7 (4.7)	9.5 (7.3)	8.6 (5.6)	10.7 (11.1)	6.3 (4.2)
	Times to peak (s)	0.039 (.011)	0.038 (.012)	0.042 (.011)	0.100 (.013)	0.096 (.014)	0.097 (.017)
STOP	Absolute (Nm)	9.0 (5.5)	8.2 (3.2)	9.4 (8.0)	8.9 (5.1)	10.3 (6.2)	10.6 (7.3)
	Times to peak (s)	0.037 (.010)	0.031 (.006)	0.038 (.008)	0.087 (.015)	0.089 (.014)	0.086 (.013)
45L	Absolute (Nm)	12.0 (9.9)	13.7 (7.5)	11.5 (6.5)	13.2 (6.7)	12.9 (6.1)	10.4 (6.4)
	Times to peak (s)	0.033 (.018)	0.039 (.013)	0.040 (.010)	0.108 (.028)	0.096 (.020)	0.098 (.019)
45R	Absolute (Nm)	11.2 (5.5)	10.2 (3.5)	11.5 (5.6)	13.0 (6.4)	12.8 (7.4)	11.0 (5.3)
	Times to peak (s)	0.036 (.007)	0.032 (.012)	0.040 (.010)	0.096 (.018)	0.108 (.032)	0.102 (.022)
90L	Absolute (Nm)	7.6 (7.2)	6.5 (4.0)	9.2 (7.9)	18.6 (2.9)	26.2 (10.0)	27.7 (12.9)
	Times to peak (s)	0.034 (.010)	0.032 (.008)	0.034 (.009)	0.120 (.038)	0.126 (.039)	0.124 (.033)
90R	Absolute (Nm)	7.9 (2.4)	9.6 (7.7)	6.8 (3.6)	13.7 (3.0)	17.4 (5.0)	15.5 (4.8)
	Times to peak (s)	0.041 (.007)	0.037 (.012)	0.040 (.013)	0.125 (.040)	0.149 (.033)	0.131 (.040)
180T	Absolute (Nm)	11.4 (7.1)	12.1 (5.3)	10.5 (5.9)	17.4 (7.6)	19.1 (5.0)	16.5 (6.1)
	Times to peak (s)	0.104 (.076)	0.067 (.026)	0.085 (.030)	0.321 (.174)	0.263 (.059)	0.269 (.120)

Table 4.5 Mean (sd) magnitude and times of peak free moments during the impact and propulsion phases of 7 movements performed on 3 different artificial turfs

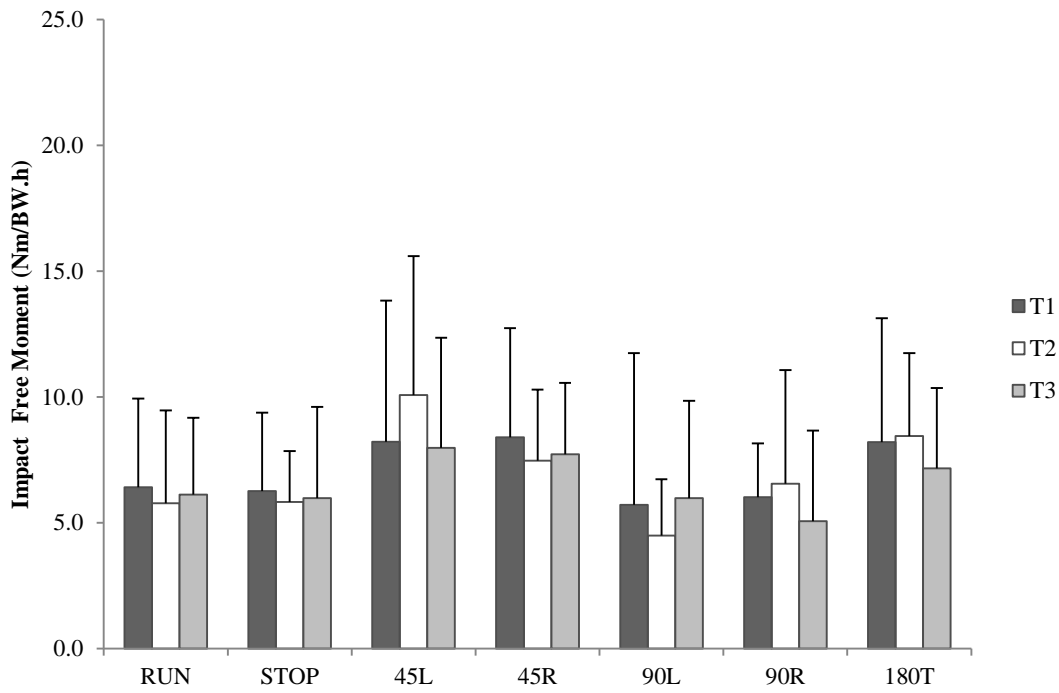


Figure 4.16 Impact Free Moments for 7 movements performed on 3 artificial turfs (values are normalised to subjects' bodyweight and height (Nm/BW.h))

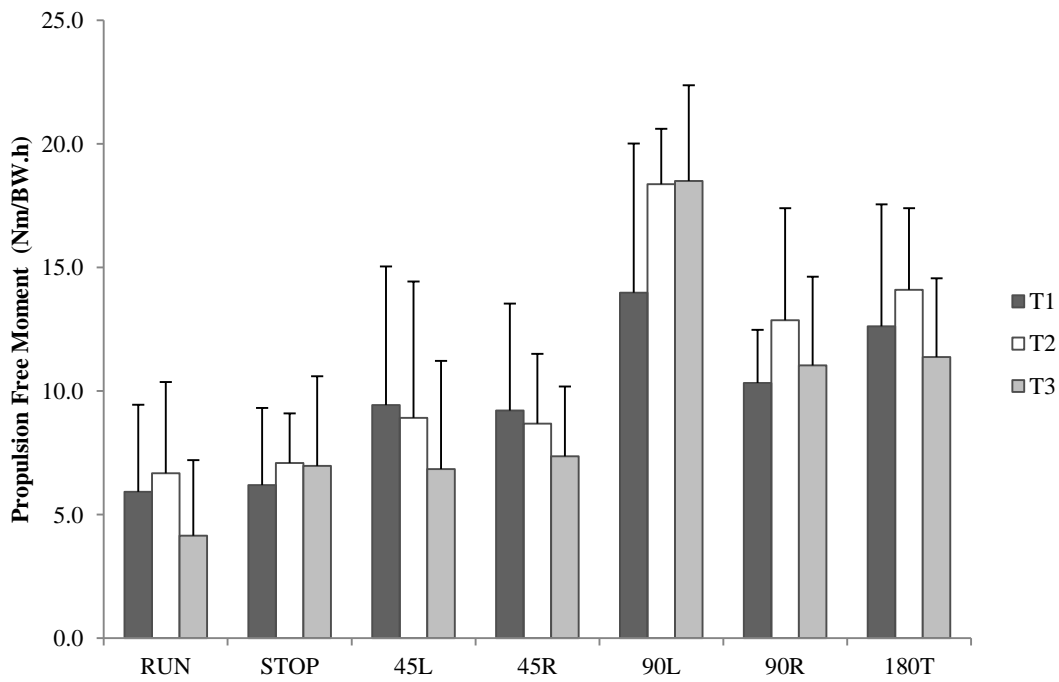


Figure 4.17 Propulsion Free Moments for 7 movements performed on 3 artificial turfs (values are normalised to subjects' bodyweight and height (Nm/BW.h))

The largest free moment in the impact phase was produced in the 45L, 45R and 180T movement: ranging

between 10-14Nm. The *RUN* and *STOP* produced similar magnitudes to the 90° movements, ranging from 6.5-9.6Nm. The time of the peak impact free moment was approximately 30-40ms for all movements, except for the 180T (70-100ms). While an overall significant difference in normalised peak free moments between all movements was calculated ($P=0.13$), pair-wise comparisons did not identify any significant differences in free moments between individual movements. This may be a result of the high variability in the peak free moments data. Also, there were no significant differences for the movements across the three turf conditions ($P=0.652$), nor any significant turf-movement interaction.

The peak propulsion free moments were similar in magnitude to the impact free moments, except in movements with a large angle of turn. The 90° and 180° turns produced higher free moments in the propulsion phase compared to the impact phase. The *90L* movement produced the largest free moments (18.6-27.2Nm). All the other movements produced free moments less than 20Nm.

Statistical analysis of the normalised data showed that significant differences in the peak propulsion free moment with respect to movement ($P<0.001$). The propulsion free moment produced in *90L* movement was significantly greater than the *RUN* (6.3-10.7Nm), *45L* (10.4-13.2Nm), *45R* (11.0-13.0Nm) movements ($P<0.007$) (Figure 4.17). The *90L* free moment was also greater than the *90R* (13.7-15.4Nm) ($P=0.046$).

While there were no significant differences in the normalised peak free moments for all movements across the three turf conditions, there was slight interaction between the types of turfs and the movements on peak propulsion free moments ($P=0.022$). However, the multi-factorial nature of the data and its variability make it difficult to interpret this interaction.

Peak free moments occurred earlier in the propulsion phase during the *RUN* and 45° turning movements (approximately 100ms). For the 90° and 180° turns, they occurred later, approximately 120ms and 260-320ms, respectively.

4.6 Vertical Loading Rates

Peak absolute and normalised (to body weight (BW)) vertical loading rates are shown in Table 4.6. The seven

movements may be divided into two groups, with the *RUN*, *STOP*, *45L* and *45R* movements produced significantly greater vertical loading rates than the *90L*, *90R* and *180T* movements ($P<0.048$).

The largest vertical loading rate was observed during the *STOP* movement, ranging between 102-134 kNs^{-1} (130-172 N/BWs, normalised). The smallest vertical loading rate was observed during *180T* movement, ranging between 28-41 kNs^{-1} (35-52 N/BWs, normalised). There were no significant differences in peak vertical loading rates for all movements between the three different turfs ($P=0.28$).

Movement	Vertical Loading Rate (kNs^{-1})			Normalised Vertical Loading Rate (N/BWs)		
	T1	T2	T3	T1	T2	T3
RUN	63.0 (22.1)	69.8 (25.1)	69.2 (28.4)	80.7 (26.1)	89.5 (26.5)	85.5 (25.7)
STOP	101.5 (48.4)	144.4 (101.7)	133.7 (71.1)	130.8 (60.3)	171.7 (83.6)	162.9 (83.8)
45L	86.9 (37.7)	85.2 (30.6)	81.0 (31.4)	109.5 (32.3)	109.9 (30.4)	100.0 (28.3)
45R	92.4 (29.3)	93.2 (30.3)	79.2 (24.4)	120.3 (31.5)	120.4 (30.4)	99.7 (30.0)
90L	38.7 (14.5)	40.7 (18.0)	42.4 (22.9)	50.95 (21.29)	51.74 (18.44)	51.59 (20.05)
90R	38.1 (16.4)	38.4 (13.7)	34.0 (13.0)	51.32 (26.38)	50.70 (19.01)	42.46 (14.19)
180T	27.4 (14.4)	40.8 (20.0)	28.4 (16.8)	35.16 (21.62)	51.98 (27.40)	34.17 (14.01)

Table 4.6 Mean (sd) peak vertical loading rates for the movements on each artificial turf for all subjects

4.7 Linear and Rotational Traction

Table 4.7 presents the traction coefficients (linear and rotational) for each movement across the three turfs. The statistical analysis did not indicate any significant differences in either of the traction coefficients across the three turfs ($P=0.15$ (linear), $P=0.32$ (rotational)). Across all movements, the mean linear and rotational traction coefficients for all 3 turfs were approximately 0.6 and 12mm, respectively.

The linear traction coefficient (LTC) remained below 0.8 for all movements. The *90L* and *90R* movements produced the highest traction than any of the other movements, approximately 0.80 ($P<0.01$). The LTC produced during the *RUN* and *STOP* movements were lowest: 0.39 and 0.44, respectively. The

45L, 45R and 180T movements all produced similar coefficients of approximately 0.6.

The rotational traction coefficient (RTC) remained below a value of 20mm for all movements. As with the peak free moment values, the movements could be divided into groups: the RTC for the 90L, 90R and 180T movements were generally greater than for the RUN, STOP, 45L and 45R movements. The 90L movement produced the highest RTC of approximately 18mm, which was significantly greater than the RUN, STOP, 45L and 45R movements ($P<0.002$). In addition, the 90L produced higher traction coefficients than the 90R, but the difference was statistically insignificant ($P>0.05$).

Movement	Linear traction			Rotational traction (mm)		
	T1	T2	T3	T1	T2	T3
RUN	0.39 (0.07)	0.38 (0.03)	0.38 (0.03)	7.7 (3.1)	6.1 (2.9)	6.0 (2.7)
STOP	0.42 (0.09)	0.46 (0.13)	0.39 (0.09)	7.6 (2.6)	8.4 (4.0)	7.5 (2.9)
45L	0.55 (0.07)	0.61 (0.07)	0.55 (0.07)	10.7 (4.0)	9.3 (2.8)	8.2 (2.8)
45R	0.58 (0.05)	0.60 (0.05)	0.57 (0.06)	8.8 (2.6)	8.9 (3.5)	8.0 (2.4)
90L	0.74 (0.09)	0.82 (0.10)	0.81 (0.08)	16.7 (3.4)	17.9 (4.1)	18.7 (4.8)
90R	0.73 (0.10)	0.76 (0.12)	0.77 (0.08)	12.3 (3.3)	15.8 (3.7)	13.5 (4.0)
180T	0.59 (0.11)	0.60 (0.06)	0.60 (0.05)	17.4 (5.9)	17.6 (4.0)	14.5 (6.2)

Table 4.7 Peak linear and rotation traction coefficients. The values display the mean (\pm sd) measurements for all the subjects on each artificial turf.

4.8 Knee Angles

The following section summarises the knee angle profiles throughout each movement, the mean knee angles at initial contact with the ground, and finally mean peak values.

4.8.1 Knee Angle Profiles

The profiles of the sagittal and frontal plane knee angles during stance phase for all 7 movements are presented in Figure 4.18 and Figure 4.19, respectively. For the RUN and STOP movements, the frontal knee angle maintained a relatively neutral position. During the *RUN*'s impact phase, the knee was in approximately 40° flexion, which gradually increased in the middle of stance and then extended to approximately 15° of flexion by the end of the movement. The knee was straighter at the start of the *STOP* and increased in flexion for the remainder of stance.

For the 45° turns, the sagittal plane knee angle profiles were similar in shape to the *RUN*. In the frontal plane, the knee tended to go into an increasingly abducted position during the impact phase and then returned to a general neutral position for the remainder of stance.

For the 90° turns, the knee was typically abducted at initial contact, moving towards an adducted position during the first 20% stance, and in a neutral position for the remainder of stance. In the sagittal plane, the change in knee flexion was less than the other movements. Starting from approximately 30-45°, knee flexion gradually increased to a peak in the middle of stance, and extended slightly towards the end of the movement.

For the 180T, the average frontal knee angle was neutral for the most of the movement. In the sagittal plane, the knee maintained between 45-65° of flexion for the first 60% of stance, before extending rapidly for the remainder of the movements.

For all movements, there was a trend for the knee to go into abduction towards the end of the stance. This was more marked in the *180T* movement.

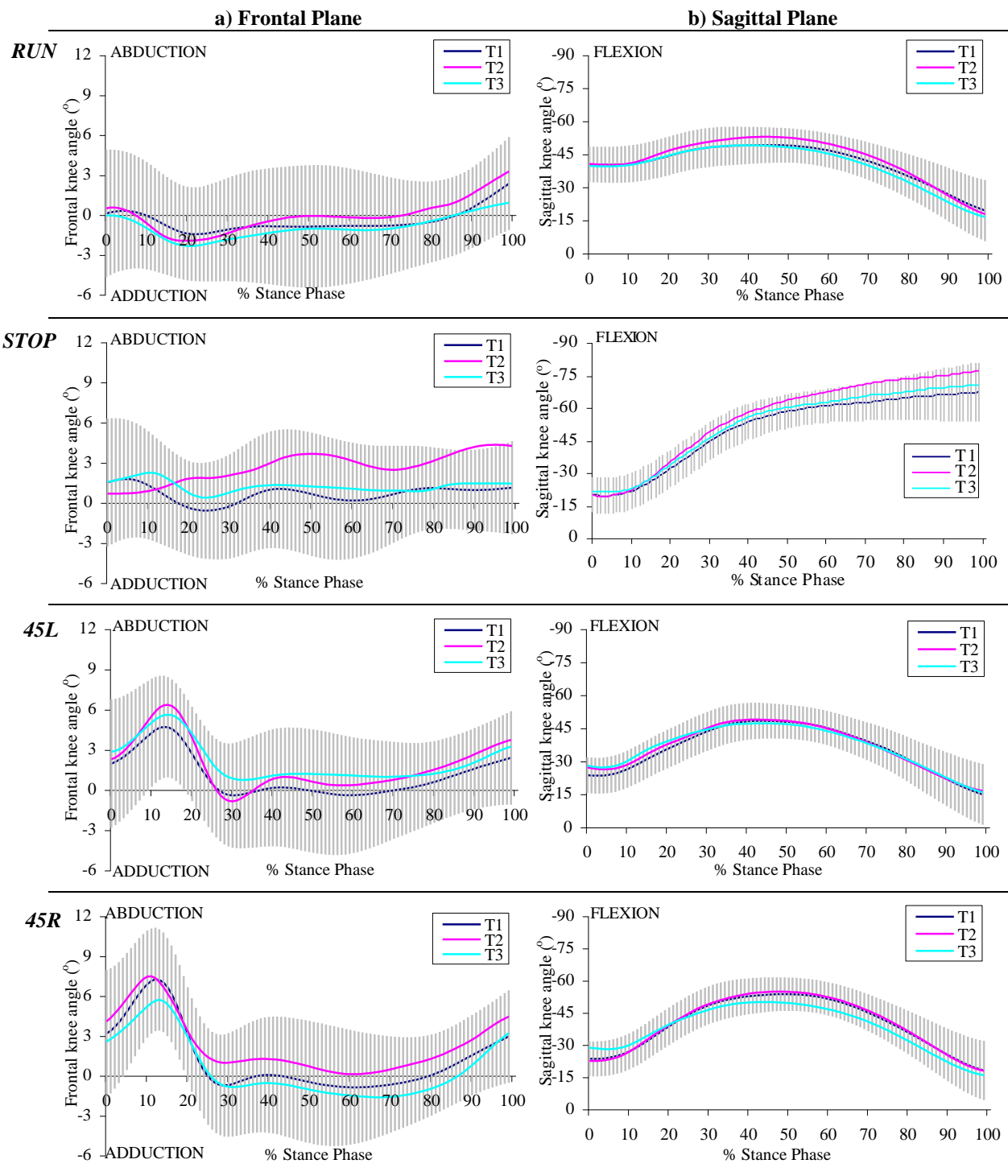


Figure 4.18 Knee angles for the *RUN*, *STOP*, *45L* and *45R* movements in the a) frontal plane; b) sagittal plane. Error bars show \pm sd for Turf 1

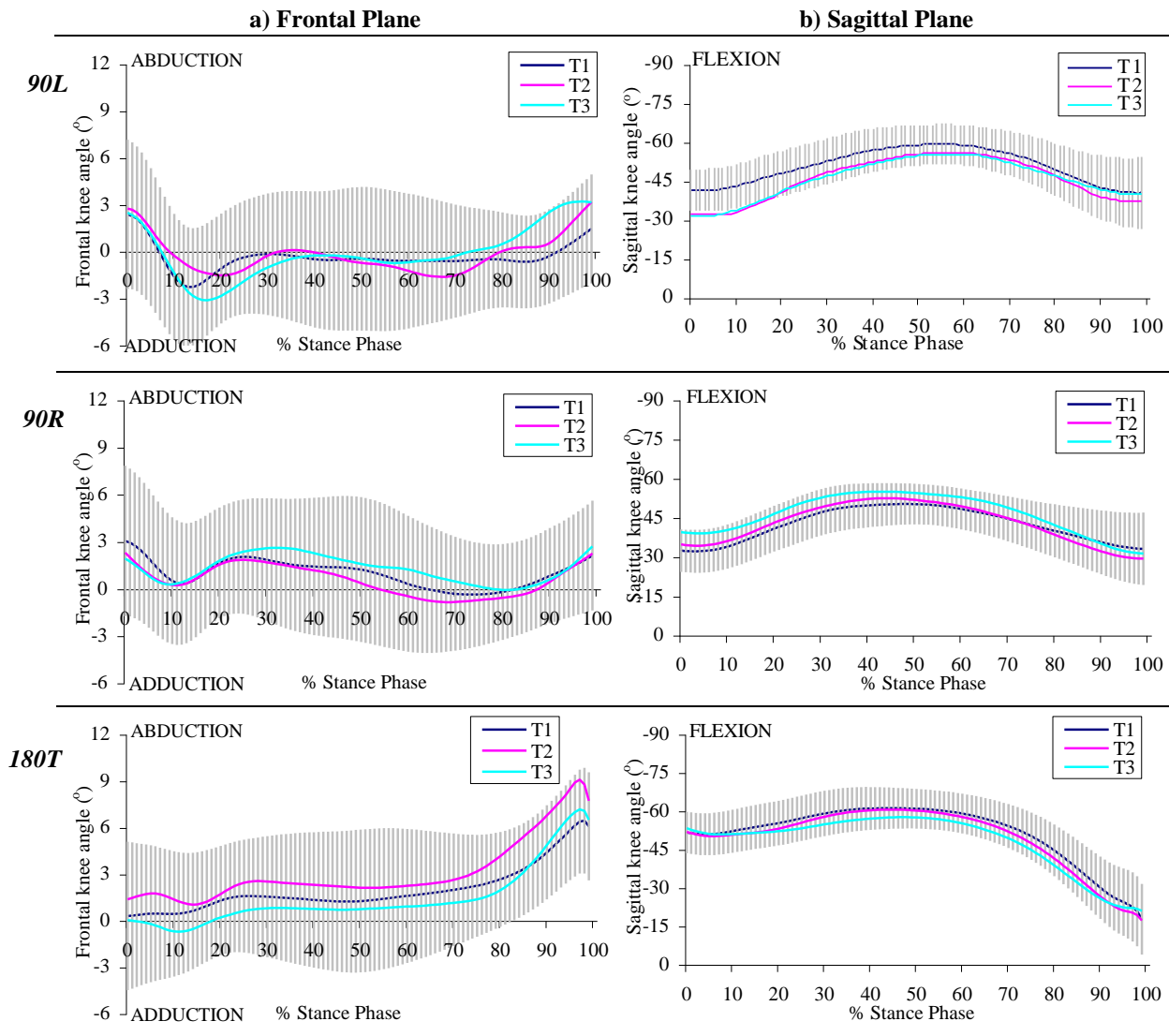


Figure 4.19 Knee angles for the *90L*, *90R* and *180T* movements in the a) frontal plane; b) sagittal plane. Error bars show \pm sd for Turf 1

There was a relatively large variation in the frontal knee angle direction between subjects. This is indicated by the large error bars in Figure 4.18 and Figure 4.19. For individual movements, some subjects had an abducted knee throughout the movement; some had an adducted knee, while for the others the knee angle interchanged between abduction and adduction. Also, the direction of the knee angle at initial contact and peak knee angle for several individuals was not consistent across the different turf conditions (Table 4.8). For many individual subjects, the direction changed on the different turfs. However, the knee was abducted during the initial contact phase of the 45° turns for the majority of subjects.

		RUN	STOP	45L	45R	90L	90R	180T
Initial Contact	Adduction on all 3 turfs	4	3	0	1	1	0	2
	Abduction on all 3 turfs	3	6	8	9	8	4	5
	Variable over 3 turfs	6	4	5	3	4	9	6
Peak angle	Adduction on all 3 turfs	4	3	1	1	6	1	1
	Abduction on all 3 turfs	5	7	7	6	3	3	8
	Variable over 3 turfs	4	3	5	6	3	9	4

Table 4.8 Consistency of the direction of initial contact and peak frontal plane knee angle for each movement in the 3 turf conditions

4.8.2 Knee Angles at Initial Contact

The mean knee frontal and sagittal knee angles at the initial contact for each movement are shown in Figure 4.20 and Figure 4.21, respectively. Due to the individual variation in the direction in the frontal plane between subjects – some players had abducted knee while others were adducted (see section 4.8.1), the mean absolute knee angle rather than mean abduction/adduction angles are shown. While it may be preferable to present mean knee angles, it was felt that in this case, because of the individual variation, the magnitude of the knee angle (in either abduction or adduction) would not be represented adequately, i.e. the individuals with abducted knee angles at initial contact would ‘cancel out’ those with adducted knee angles.

The mean frontal plane knee angles at initial contact was similar for all of the movements, ranging from approximately 2.5-5° ($P=0.09$), and between the three turfs ($P=0.251$).

Similarly, the three turfs did not appear to affect the knee flexion angles at initial contact ($P=0.167$). However, the magnitude of knee flexion at initial knee contact varied between the movements performed. The largest angles were observed in the *180T* and *RUN* movements, with 52° and 40° flexion, respectively. The *STOP* movement produced significantly lower knee flexion angles at initial contact than all of the other movements, except for the *45L* ($P<0.032$). For the other movements, the *45L* and *45R* produced significantly lower flexion angles than the *RUN*, *90R* and *180T* ($P<0.018$).

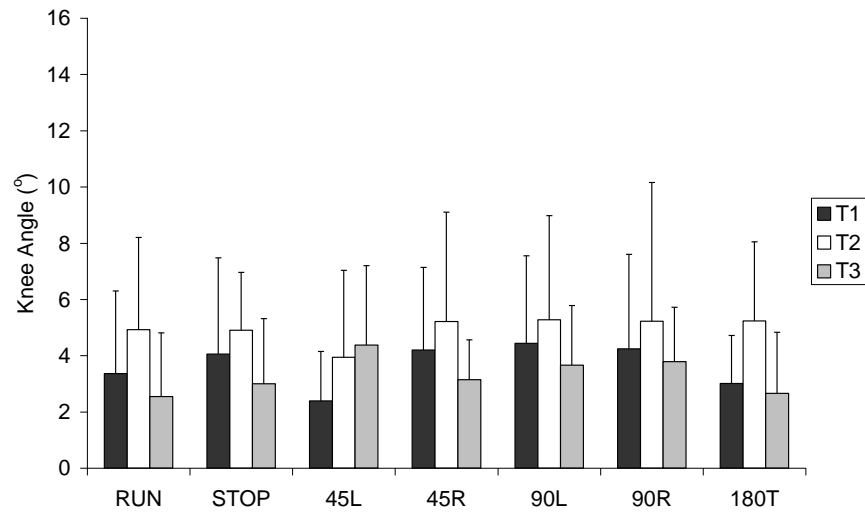


Figure 4.20 Frontal knee angle at initial contact (mean absolute values)

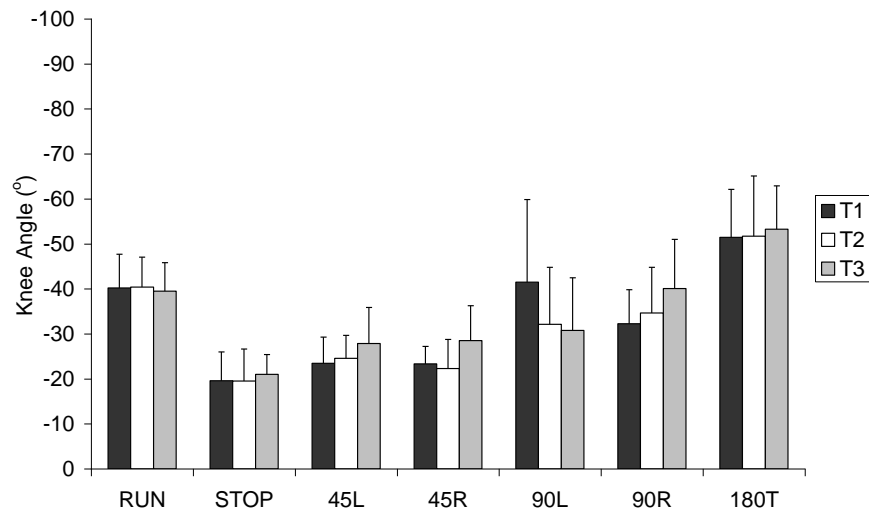


Figure 4.21 Sagittal knee angle at initial foot contact (mean values)

4.8.3 Peak Knee Angles

The mean peak frontal and sagittal knee angles during the whole of the respective movements are shown in Figure 4.22 and Figure 4.23, respectively. Similar to the initial contact results and for the individual variability in the direction of the knee angle in the frontal plane (see section 4.8.1), mean absolute values for peak frontal knee angles are given.

There were no significant differences in mean peak knee flexion angles between different turfs, in

either the frontal or sagittal plane ($P=0.650$, frontal; $P=0.292$, sagittal). Peak frontal knee angles during movements on Turf 2 were 1.5° to 2° greater than on Turf 1 and Turf 3, respectively, but this was not significant ($P=0.321$ and $P=0.91$, respectively).

All of the movements produced peak frontal knee angles of between 6° and 11° . The *180T* movement produced significantly greater abduction angles than the *RUN* movement of approximately $6-8^\circ$ ($P=0.024$), occurring towards the end of the movement. The *45R* also produced significantly greater knee abduction angles than the *RUN* movement ($P=0.021$). The peak abduction angles for the *45L* and *45R* movements occurred during the first 20% of stance phase.

In the sagittal plane, peak knee flexion angles typically occurred during the middle of the stance phase for most movements. However, the greatest knee flexion of approximately $70-80^\circ$ for the *STOP*, occurred towards the end of the stance phase. This was significantly greater than all other movements, except for the *90L* and *90R* ($P<0.034$). The *45L* movement produced the smallest degree of knee flexion (approximately 48°) compared to the other movements ($P<0.025$), and was $4-5^\circ$ less than the *45R* movement. In addition, peak knee flexion during the *RUN* and *45R* was significantly lower than the *90R* and *90L*, respectively ($P=0.022$ and $P=0.025$, respectively).

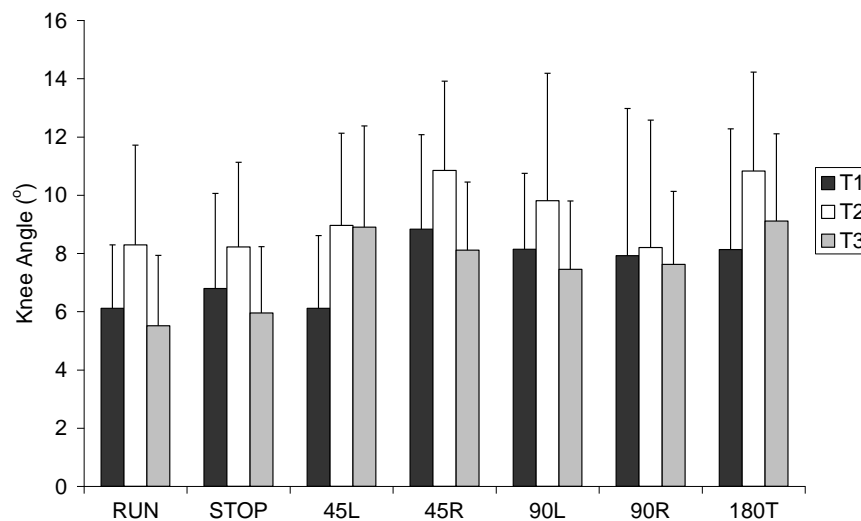


Figure 4.22 Peak frontal knee angle during stance phase (absolute values)

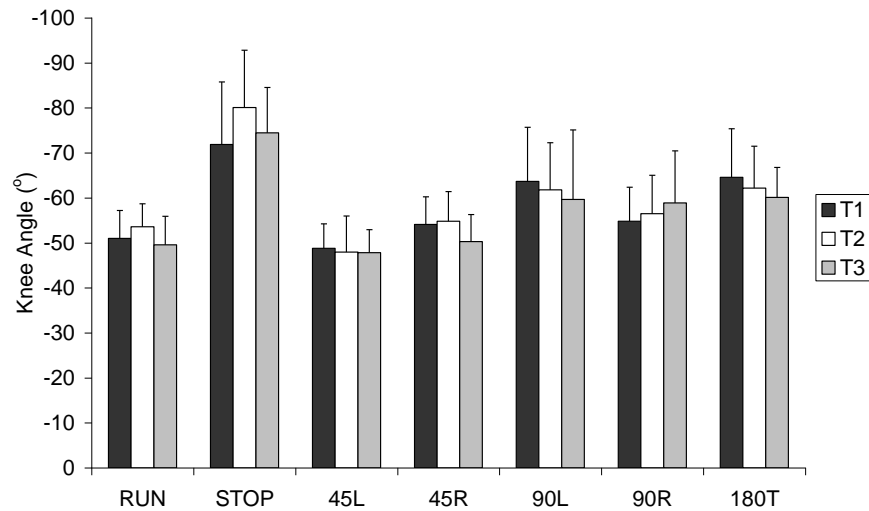


Figure 4.23 Peak sagittal knee angle during stance phase (mean values)

4.9 Internal Knee Moments

4.9.1 Knee Moment Profiles

The three-dimensional (frontal (X), transverse (Y) and sagittal (Z)) internal knee moments during the whole stance phase of the 7 movements performed on the 3 turf condition are shown in Figure 4.24 to Figure 4.27. Similar to previous charts, the error bars shown are for the T1 condition and provide an indication of the variability between individual subjects (the standard deviation for all 3 turf conditions were similar).

4.9.1.1 Frontal Plane

All movements produced a frontal knee moment peak during the impact phase. The *RUN*, *90L* and *90R* (Figure 4.24a, and Figure 4.26) tended to produce an abductor moment, while the *45L*, *45R* and *180T* tended to produce an adductor moment (Figure 4.25 and Figure 4.27). The direction of the frontal plane moment varied between subjects during the *STOP* movement (Figure 4.24b) (also see Appendix D for individual data). Knee moment magnitudes were generally greater during this phase than the rest of stance for most movements, except for the *STOP*.

During the middle, early propulsive phase of stance, all movements produced abductor knee moments. These peaked at approximately 40-60% stance phase but at a lesser magnitude than during impact phase.

Towards the end of stance phase (80%-100%), the magnitude of the frontal plane knee moment reduced to a minimum in all movements, except for the *180T*. Here, an adductor moment was produced with a magnitude similar to that observed during the impact phase. Small adductor moments were also observed in the *RUN*, *90L* and *90R*.

4.9.1.2 *Transverse Plane*

A small external rotator moment of approximately 0.1- 0.2 Nm/kg was applied to the knee during the initial contact with the surface and throughout the impact phase in the *STOP*, *45L*, *45R* and *180T* movements. Smaller internal rotator knee moments were applied during the *RUN*, *90L* and *90R* movements at initial contact.

A small external rotator peak was observed during the impact phase in the *45L* and *45R* movements. This corresponded with the knee adductor moments in the same period. Similarly, the external rotator peak in the *90L* and *90R* movements corresponded with a peak abductor moment during the weight acceptance phase. For the *RUN* movement, the knee moment changed from internal to external moment during this period.

The variability in the data continued to increase during the propulsion phase of the movements. For the *RUN* and *STOP* movements, a general external rotator moment and a smaller internal rotator was applied to the knee during the middle phase of stance, respectively. The data was extremely variable for both the *45L* and *45R*, with a general external rotator moment being applied to the knee. For the *90L* and *90R*, the direction of the knee moment changed from an internal rotator peak at about 30% stance to an external rotator peak at about 70-75% of stance phase. During the *180T*, the knee moment also changed direction through the propulsion phase from an external rotator moment to an internal rotator peak at approximately

80% stance.

4.9.1.3 *Sagittal Plane*

At initial contact, a flexor moment was exerted to the knee in all movements, except for the 180T. During the impact phase, the direction of the knee moment changed from a flexor to an extensor moment during the first third of stance phase. Knee moment magnitudes during this impact phase were slightly greater than at initial contact, although this is not always apparent from the aggregated data shown.

For the 180T, a flexor knee moment tended to be applied at initial contact and in the impact phase. However, some subjects produced a small extensor moment just after initial contact before returning sharply to a flexor moment.

In the propulsive phase, all movements tended to produce an extensor peak at approximately 30% to 50% of stance. After this point, the internal knee moment tended to reduce completely at about 80% stance and maintained a minimal amount of loading for the remainder of stance.

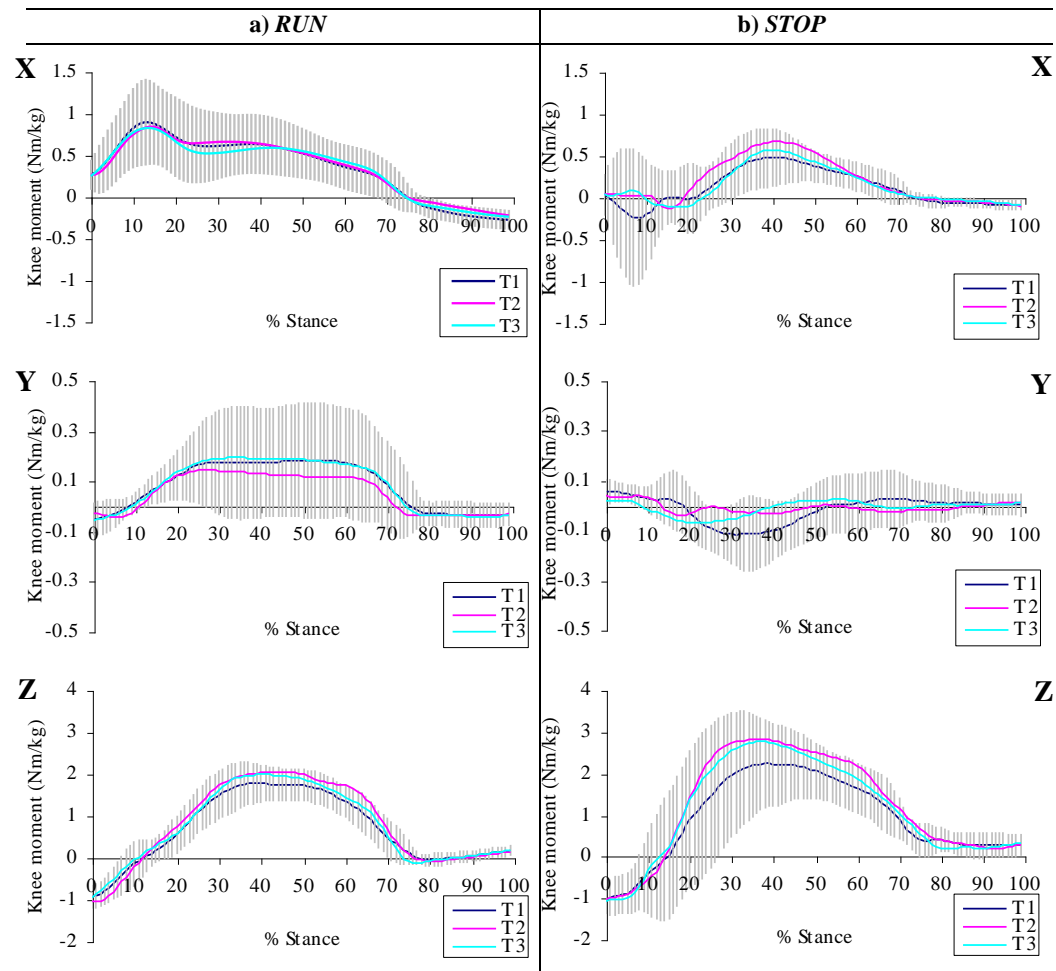


Figure 4.24 Knee moments during movements performed on 3 artificial turf surfaces: a) RUN movement, b) STOP movement. Moments displayed are internal moments (X= frontal plane: +ve= abductor moment, -ve= adductor moment; Y=transverse plane: +ve= external rotator moment, -ve= internal rotator moment; Z=sagittal plane: +ve= extensor moment, -ve=flexor moment)

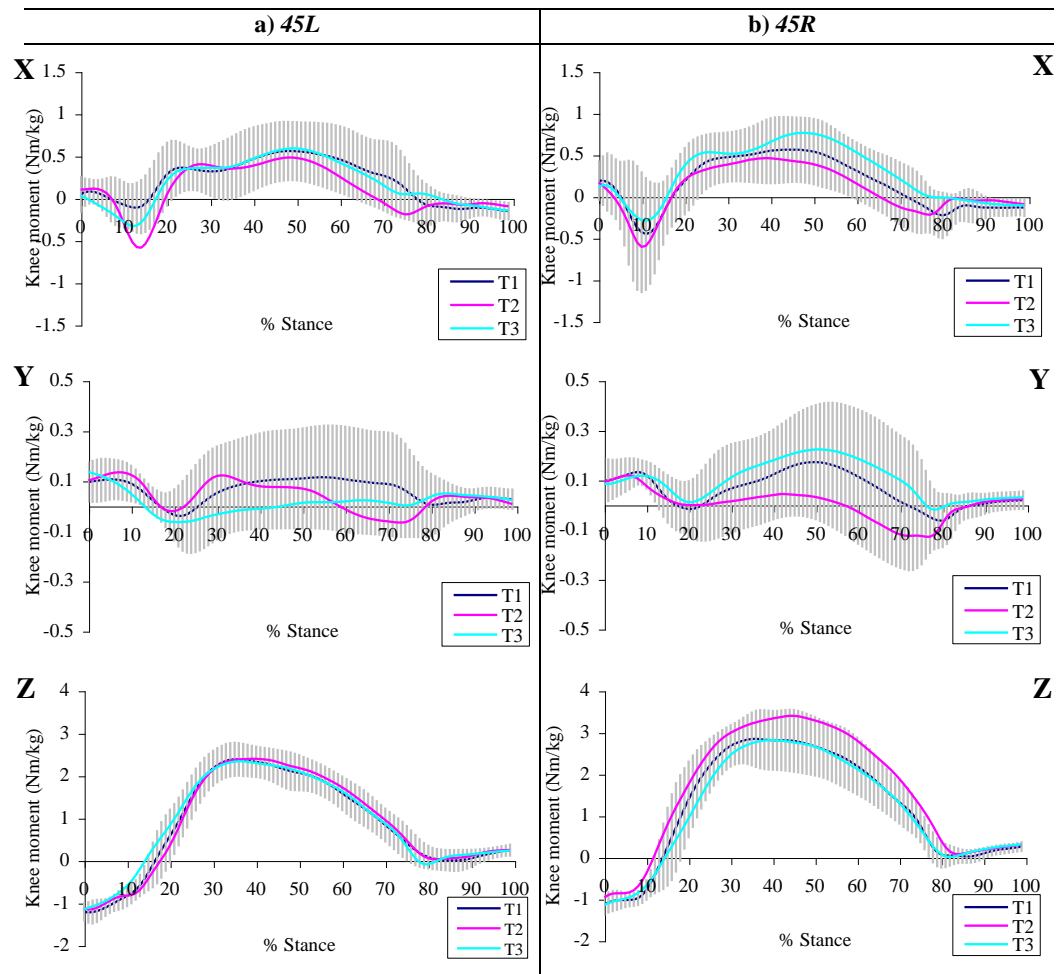


Figure 4.25 Knee moments during movements performed on 3 artificial turf surfaces: a) 45L movement, b) 45R movement. Moments displayed are internal moments (X= frontal plane: +ve= abductor moment, -ve= adductor moment; Y=transverse plane: +ve= external rotator moment, -ve= internal rotator moment; Z=sagittal plane: +ve= extensor moment, -ve=flexor moment)

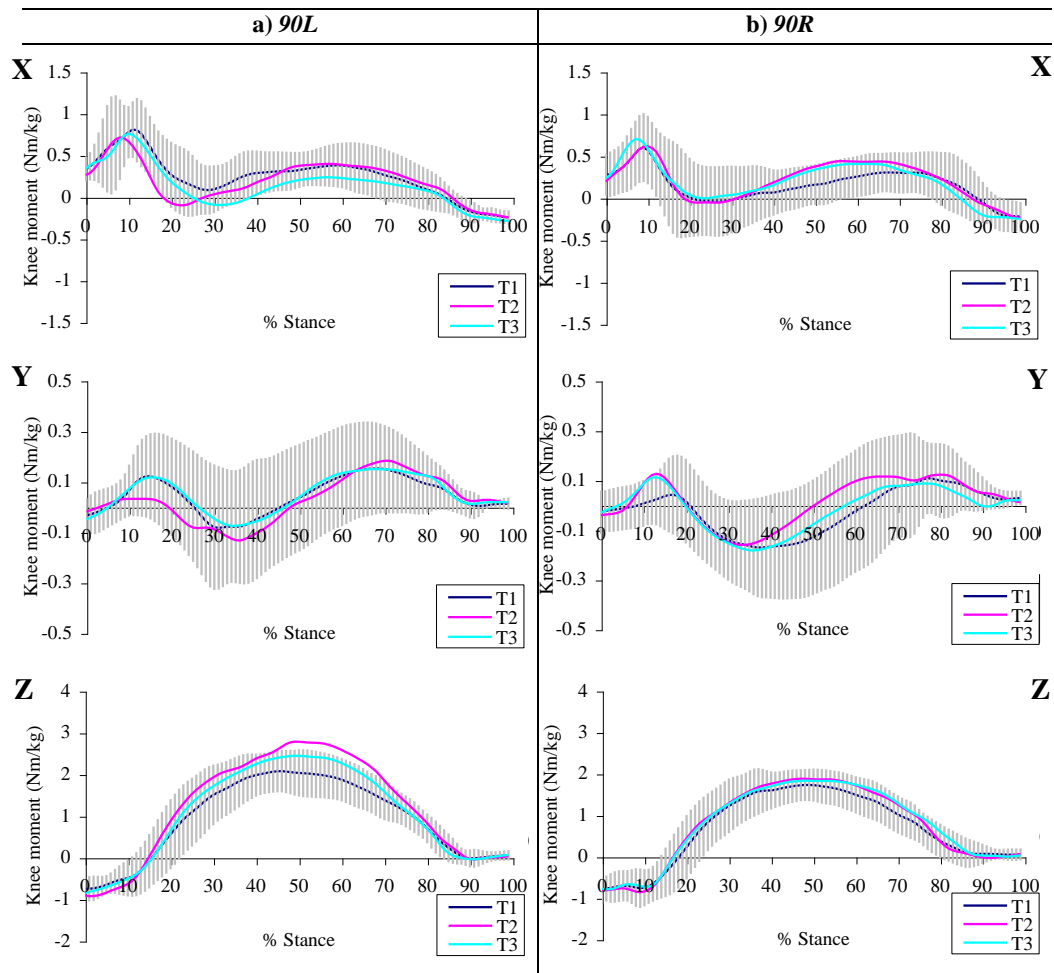


Figure 4.26 Knee moments during movements performed on 3 artificial turf surfaces: a) 90L movement, b) 90R movement. Moments displayed are internal moments (X= frontal plane: +ve= abductor moment, -ve= adductor moment; Y=transverse plane: +ve= external rotator moment, -ve= internal rotator moment; Z=sagittal plane: +ve= extensor moment, -ve=flexor moment)

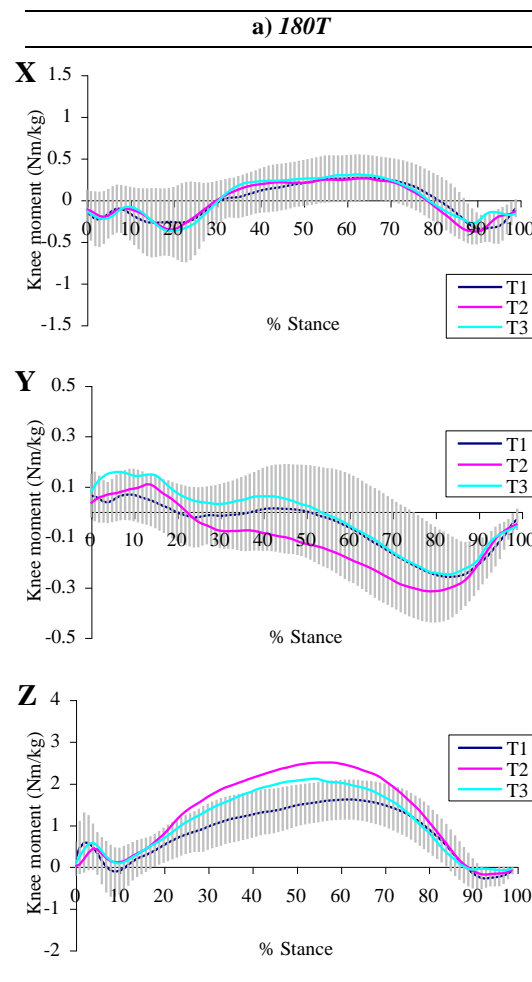


Figure 4.27 Knee moments during 180T movement performed on 3 artificial turf surfaces. Moments displayed are internal moments (X= frontal plane: +ve= abductor moment, -ve= adductor moment; Y=transverse plane: +ve= external rotator moment, -ve= internal rotator moment; Z=sagittal plane: +ve= extensor moment, -ve=flexor moment)

4.9.2 Peak Knee Moments

The mean peak internal knee moments during the initial contact (Figure 4.28), impact phase (Figure 4.29) and propulsion phase (Figure 4.30) are shown below. Knee moment calculations are given with respect to the movement phases identified from the ground reaction forces (see Section 4.5).

Mean peak absolute values for the frontal, transverse and sagittal plane knee moments are provided. This indicates the magnitude of the internal knee moment but does not take into account its direction. As shown in Appendix D, the knee moment direction varied between individual subjects. For some movements, aggregating the positive and negative signed peak values (indicating its direction) would cancel each other

out and therefore reduce the magnitude of the mean knee moment. The direction of the knee moments is provided in the summary of the knee moment profiles (section 4.9.1).

4.9.2.1 *Initial Contact*

Figure 4.28 shows the mean peak knee moments, normalised to bodyweight, during the initial contact phase. Frontal knee moments were below 0.4 Nm/kg for all movements. The largest knee moment was observed during the *90L* and *90R*. The smallest peak moment occurred during the *STOP* (approximately 0.15Nm/kg).

The magnitudes of transverse knee moments were comparable for all movements on the different turfs, ranging between approximately 0.1 to 0.2Nm/kg. The 45° and 180° turns produced slightly higher magnitudes, although there was no significant difference between movements. Transverse knee moments were slightly lower on Turf 3 (except for the *45L* movement) but this was not significant.

The *45L* and *45R* produced the greatest flexor moment at initial contact of 1.2 Nm/kg, followed by the *RUN* and *STOP*. The *90L* and *90R* produced flexor moments of approximately 0.8Nm/kg – significantly lower than the *45L* and *45R* ($P<0.05$). A small extensor moment was produced for this *180T* movement with a magnitude of 0.3 to 0.5 Nm/kg.

No statistical differences in initial contact knee moments across movements existed across turf conditions.

4.9.2.2 *Impact Phase*

During the impact phase, the *RUN* and *90L* produced slightly greater frontal knee moments than the other movements, peaking at approximately 1.1Nm/kg. The frontal knee moments in the *90R* were generally lower than the *90L* during this impact phase, although this was not statistically significant. The *STOP* movement produced slightly lower frontal knee moments than all the other movements at approximately 0.55Nm/kg. However, the frontal plane knee moments were extremely variable between subjects.

The magnitude of transverse knee moments during this phase ranged approximately from 0.1 to 0.3

Nm/kg. The *90L* movement produced the highest moments and the *RUN* and *STOP* produced the lowest moments. Any differences between movements were not statistically significant, although the data was relatively variable.

All movements produced a sagittal knee moment generally greater than 1.0Nm/kg. The *STOP* (1.2-1.3Nm/kg), *45L* (1.2-1.4Nm/kg) and *45R* (1.2-1.3Nm/kg) produced slightly greater knee moments than the other movements. No statistical differences in initial contact knee moments for all the movements existed across turf conditions.

4.9.2.3 *Propulsion Phase*

Frontal plane knee moments in the propulsion phase ranged approximately from 0.6 to 0.8 Nm/kg. These magnitudes were generally less than during the impact phase. No statistical differences existed between movements, although the *90L* and *90R* were generally lower.

The magnitudes of the peak transverse moments were slightly greater during the propulsion phase than the impact phase. All movements produced similar peak knee moments (0.3 to 0.4 Nm/kg).

The sagittal plane knee moment was highest during the propulsion phase. The *STOP* and *45R* produced the greatest knee extensor moment at approximately 3 to 3.5Nm/kg. The *STOP* extensor moment was significantly greater than the *RUN* and *90R* moments ($P<0.01$). The *45R* moment was significantly different from the *RUN*, *90L*, *90R* and *180T* ($P<0.05$). The *45R* and *90L* was slightly greater than the same movements conducted on the contralateral leg (*45L* and *90R*, respectively). However, these differences were not statistically significant.

While no overall significant differences in peak propulsion knee moments existed between all three turfs when analysed together, movements on Turf 2 tended to produce greater transverse than Turf 1 (mean difference = 0.108Nm/kg) and Turf 3 (mean difference = 0.131Nm/kg). Sagittal plane moments were also generally higher on Turf 2. Turf 1 produced generally lower knee extensor moments than Turf 3 but these results were not statistically significant. No significant differences between turfs existed in the frontal plane

knee moments.

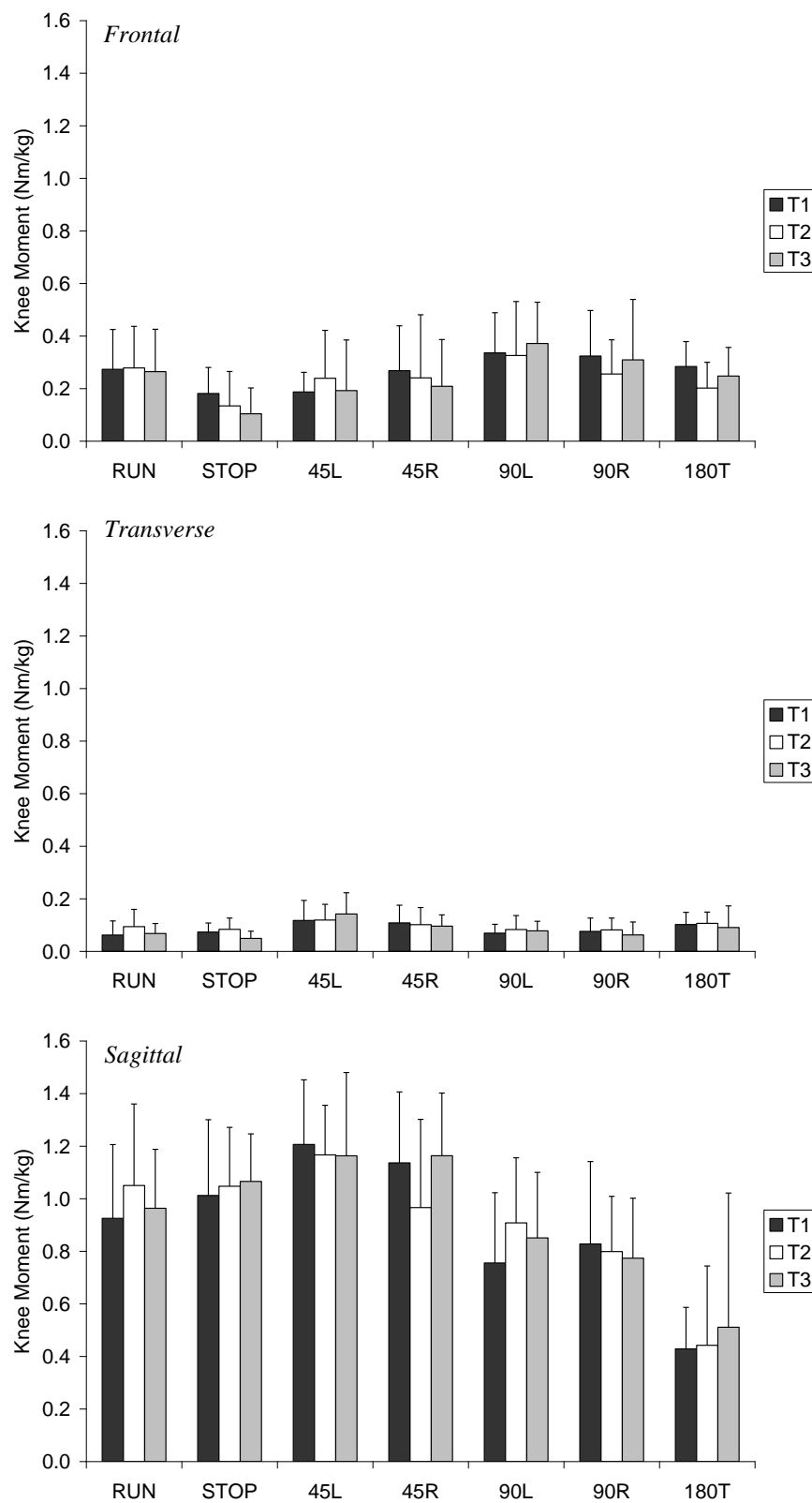


Figure 4.28 Normalised knee moments at initial contact for movements performed on the three artificial turfs

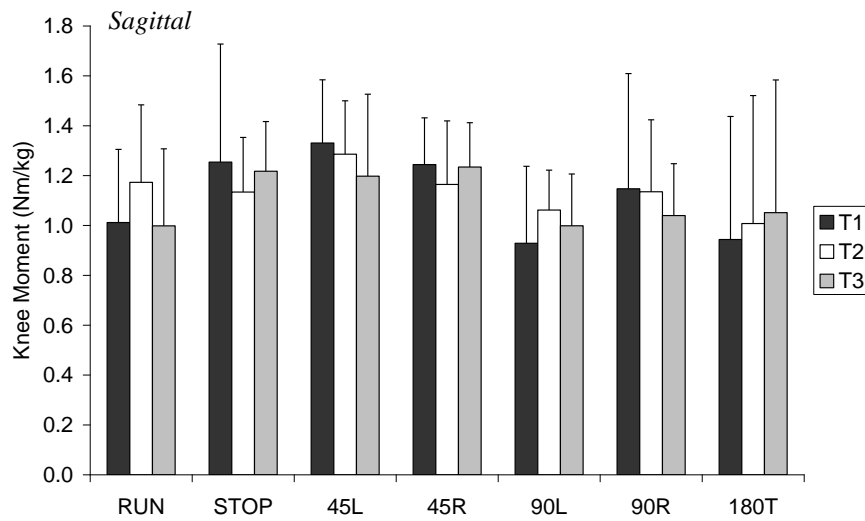
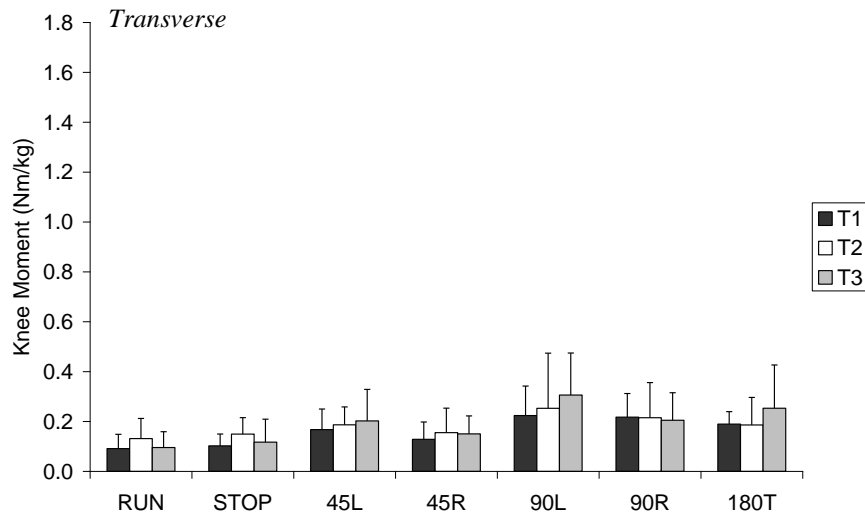
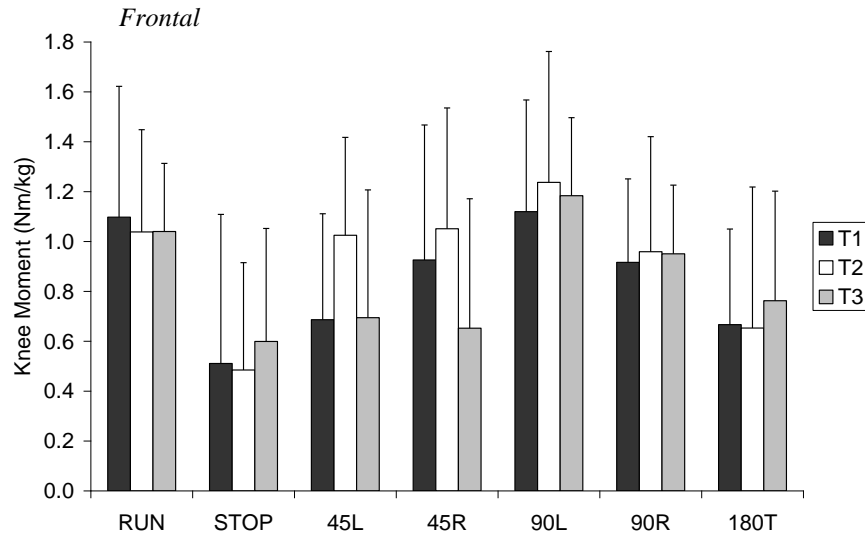


Figure 4.29 Peak, normalised knee movements during the impact phase of stance (1-20%) for movements performed on the three artificial turfs

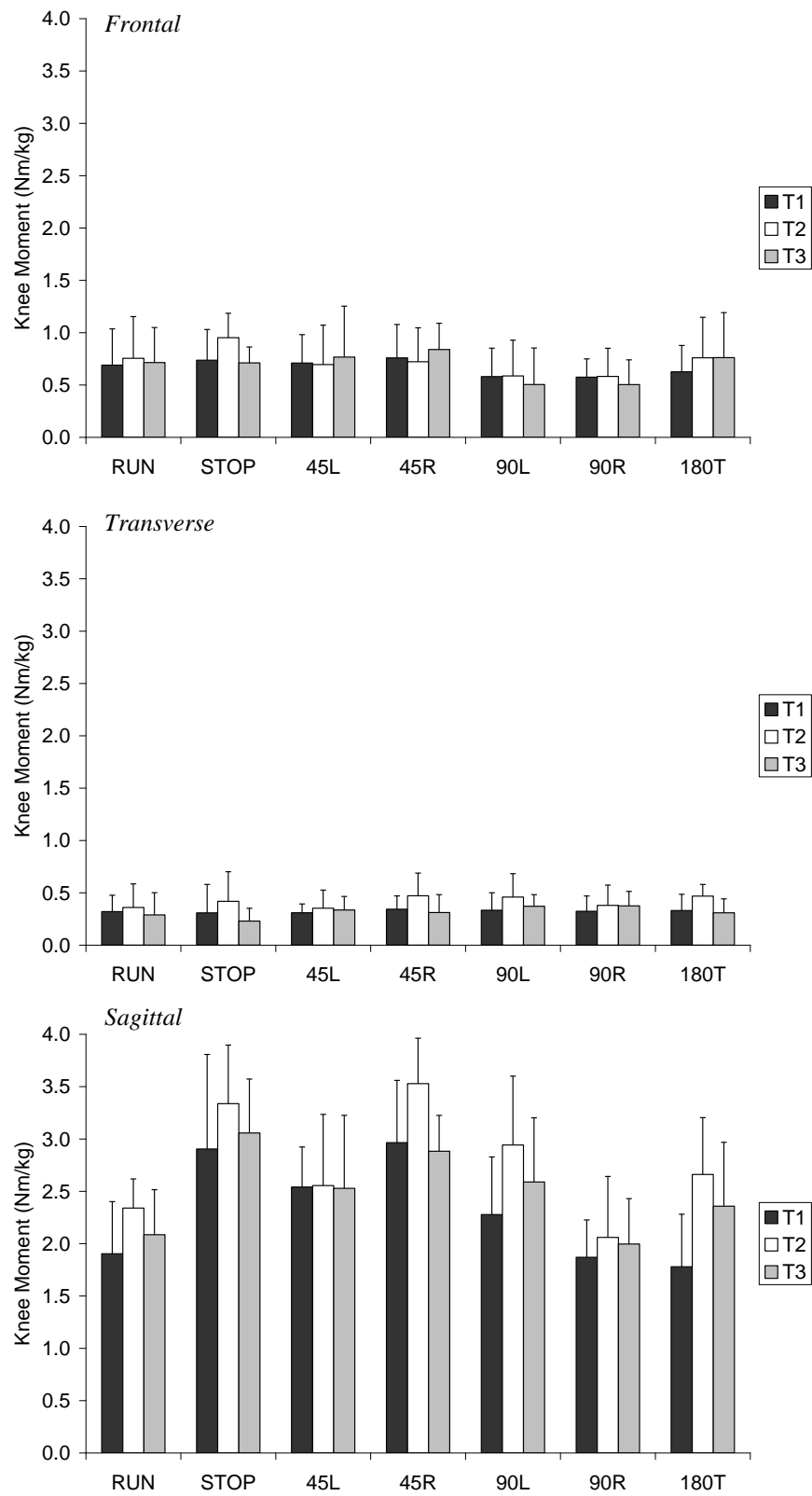


Figure 4.30 Peak, normalised knee moments during the propulsion phase of stance (20-100%) for movements performed on the three artificial turfs

4.10 Validation of Biomechanical Data

It was important that the movements which subjects performed in the controlled environment of a laboratory were executed in a similar style and manner as would be expected in the natural environment of an outdoor sports pitch. The biomechanical data collected in the laboratory was partially validated by comparing with the output of the electrogoniometer, positioned over the subject's left knee, and the two accelerometers, positioned on the shank and pelvis, collected during the lab and field-testing of the sports players. This proved a quantifiable link between the movements performed in the laboratory and outside in a natural playing environment. In addition, subjective analysis of the video data confirmed that the subjects generally performed the movements in the same way.

Unfortunately, a technical fault developed in the electrogoniometer during the outdoor testing sessions, which resulted in absent data for all subjects on Turfs 7, 8 and 9, for seven subjects on Turfs 4, 5 and 6. As a result, there was insufficient data to provide a robust validation of the indoor testing based on the electrogoniometer data.

Nevertheless, the remaining data from 5 subjects was analysed to provide as reasonable substantiation of the data collected in the laboratory as possible. Knee flexion angles at initial foot contact from movements conducted on Turf 2 and a similar surface outdoors (Turf 4: wet and dry conditions) were compared. In addition, data from the short natural grass surface (Turf 6) is presented in Figure 4.31.

4.10.1 Knee angles

Table 4.9 shows the mean difference in knee angles during matched movements performed on comparable surfaces outside the laboratory (T4 dry) and inside the laboratory (T2) was less than 5°. It also shows that the knee angles on artificial turf are comparable with those on a dry natural grass surface. The movements performed on the artificial surface during wet conditions (T4), however, produced slightly greater

differences in knee angles.

Data from one subject (F5) is provided as a typical example of the knee angles before and after foot strike for each of the movements performed on laboratory based turf (T2) and a similar outdoor turf (T4) (Figure 4.32).

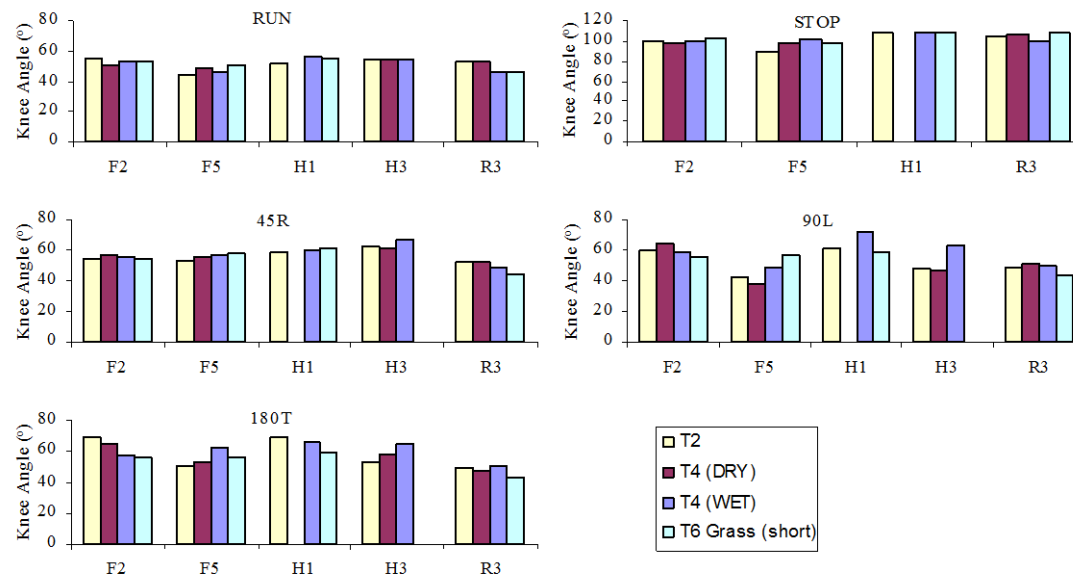


Figure 4.31 Comparison of peak knee angles during movements performed by 5 subjects in laboratory conditions (T2) and on outdoors surfaces (T4, T6).

	T4 (dry) (n=19)	T4 (wet) (n=24)	T6 (grass) (n=20)
Initial knee angle	4.8 (\pm 3.0)	8.4 (\pm 7.1)	6.4 (\pm 5.7)
Peak knee angle	3.1 (\pm 2.0)	5.2 (\pm 4.7)	5.8 (\pm 3.3)

Table 4.9 Mean difference in knee angles in outdoors (T4, T6) conditions from laboratory conditions (T2). Shown is the aggregated data is from 5 subjects performing *RUN*, *STOP*, *45R*, *90L* and *180T* movements

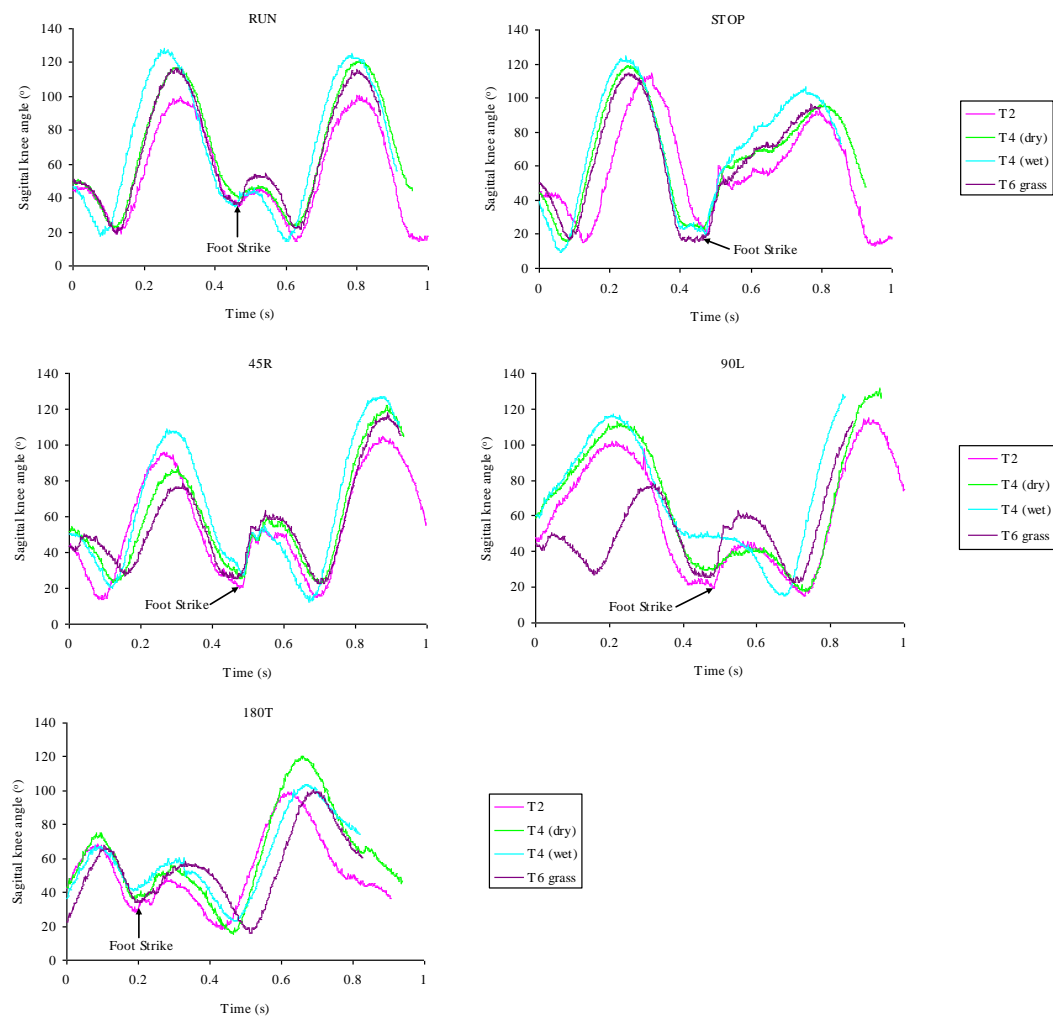


Figure 4.32 Typical knee angles before and after foot strike on the laboratory based and outdoor surfaces (Subject F5)

4.10.2 Shank and pelvic acceleration

The analysis of the shank and pelvic acceleration formed part of another thesis about an experimental/computational investigation of the interaction between athletes and playing surfaces by (Brachet, 2005). The reader is referred to this thesis for a full description of the accelerometer results.

In summary, four activities (*RUN*, *STOP*, *45R*, *90L*) performed by eight subjects were examined to compare peak shank and pelvic acceleration. The acceleration data was variable between subjects. The mean peak shank acceleration was 5.5g, 7.6g, 12.6g and 4.8g for the straight-line sprinting, stopping, 45R and 90L movements, respectively. The mean peak pelvic accelerations were 1.2g, 2.3g, 1.7g and 1.7g for the

same movements, respectively. No significant differences for shank or pelvic accelerations were observed between comparable surfaces: Turf 2 (lab) and Turf 4.

CHAPTER 5. DISCUSSION

This first part of the study examined biomechanical parameters of the player/surface interaction during seven types of movement that commonly occur during field sports such as football, rugby and hockey. These included straight running and turning movements.

This section will discuss the main findings and advances of the study in the light of published data and theories. It will also discuss the limitations of the study, the implications for the development of artificial turf testing and new opportunities offered by these findings for future research.

5.1 Summary of Main Results

The main findings can be summarised as follows:

1. **The surface type did not generally tend to affect the ground loadings or knee biomechanics:**

- The profiles and peak values of ground loading, knee kinematics and knee kinetics were generally similar between surfaces for the seven movements analysed.

2. **Highly dynamic movements increased ground loadings:**

- There was a large range in ground loading parameters for the 7 movements analysed.
- Greater vertical GRFs were measured in faster movements (*RUN*, *STOP*, 45° cuts)
- Greater horizontal GRFs, free moments and traction coefficients were measured in turning movements (45° cuts and 90° crossover turns).

3. **Highly dynamic movements increased knee kinematics and kinetics:**

- Movements with a greater change in momentum (*STOP*, 90 and 180 degree turns) produced higher peak knee flexion.
- Peak frontal plane knee angles were higher in 45 degree turns and 180T, although there individual variations in the abduction/adduction direction.
- Movements with large turns produced larger frontal and transverse knee moments, but high

individual variation was present.

- Faster movements produced larger sagittal plane knee moments.

5.2 Comparability of Results with Other Studies

The ground loading and knee mechanics results for the different movements are generally comparable with similar biomechanical studies of player interactions on artificial turf.

However, direct comparisons are difficult due to differences in study methodologies. For example, the type of movement, approach velocities, turning angles, shoes worn by participants, and the type of artificial turf used often vary between studies. Furthermore, the definition of GRF parameters can be different. There are often two vertical GRF peaks in running movements: the passive (impact) peak and active (propulsive). This study presents results on the peak vertical GRF throughout the whole of stance, while others have presented the impact GRF peak.

Straight line running is the most commonly analysed movement and was therefore the easiest movement to compare between studies, although running velocities are not always comparable. While there are differences between study designs, Table 5.1 and Table 5.2 shows GRFs and knee biomechanical parameters during the RUN movement measured in this study were comparable with published data. Although frontal knee moments in the present study were slightly greater than other studies, this confirms that the kinetics and kinematics of running and turning on artificial turf have been satisfactorily reproduced.

For the other movements, comparisons with the literature are presented as appropriate throughout the discussion section below.

GRF parameter (peaks)	Present study	Other studies*
Vertical GRF (BW)	2.39	1.89-3.00
Horizontal GRF (BW)	0.63	0.2-0.8
Free moment (Nm)	7.91	5.9-12
Vertical loading rate (BWs ⁻¹)	86.4	50-100
Linear traction coefficient	0.39	0.1-0.69
Stance time (ms)	175	250
Approach velocity (ms ⁻¹)	5.9	3.4-6.9

*(Bobbert *et al.*, 1992b; Cavanagh, 1990; Cavanagh & LaFortune, 1980; Clarke *et al.*, 1983; De Wit *et al.*, 2000; Dixon *et al.*, 2000; Garcilazo, 2007; Guisasola, 2008; Holden & Cavanagh, 1991; Meijer *et al.*, 2006; Milner *et al.*, 2006; Novacheck, 1998; Shorten and Mientjes, 2003; Stiles *et al.*, 2007; Stiles & Dixon, 2006; Stucke *et al.*, 1984; Vaughan, 1984; Zifchock *et al.*, 2006)

Table 5.1 Ground loading data from the present compared with other studies

Knee kinematics (peaks)	Present study	Other studies*
Sagittal knee angle (degrees)	49.6-53.6	35-47.2
Frontal knee angle (degrees)	1.2-3.9	3.0-6.0
Sagittal knee moment (Nm/kg)	1.90-2.34	1.0-2.5
Frontal knee moment (Nm/kg)	1.04-1.10	0.20-0.80
Transverse knee moment (Nm/kg)	0.29-0.32	0.06-0.40

*(Besier *et al.*, 2001b; Dixon *et al.*, 2000; Ferber *et al.*, 2003; Guisasola, 2008; Novacheck, 1998; Winter, 1990)

Table 5.2. Knee kinematic and kinetic data from the present study compared with other studies

The following sections discuss the main findings summarised in Section 5.1.

5.3 The Impact of Artificial Turf on Ground Loadings

This study found no consistent differences in ground loadings and traction coefficients between the three artificial turfs. The test-retest reliability of movement performances between the testing conditions, based on approach velocities and stance times, was shown to be high suggesting that the subjects executed the movements in a similar fashion between testing sessions.

Similar peak vertical GRF, free moments, loading rates, linear traction coefficients, or rotational traction coefficients were observed between the 3 types of surfaces for the group of movements examined. However, movements performed on Turf 2 did produce higher peak horizontal GRFs than the other two surfaces. However, the differences were very small (0.067 to 0.083 BW; approximately 4.7N to 5.8N for a 70kg person) and regarded as insignificant. This may be a result of measurement error from the force plates and/or inertial force of the turfs (see Appendix A for details of an investigation of the inertial force of artificial turf).

By including a range of different types of movements, including straight line running and turning

movements, this study provides further evidence towards the argument that GRFs are independent of the surface type. Other studies have also reported comparable findings (Clarke *et al.*, 1983; Dixon *et al.*, 2005; Dixon *et al.*, 2000; Ferris *et al.*, 1998; Nigg, 2001; Nigg & Wakeling, 2001; Verlhest *et al.*, 2009). This result may be explained by body's central nervous system using muscle tuning to keep the ground reaction force (GRF) constant in order to minimise soft tissue vibrations regardless of surface hardness (Nigg, 2001).

This overall finding suggests that, in terms of ground loadings, the biomechanical interaction between the player and the surface is similar for different surfaces. This also suggests that a mechanical test rig which applies a biomechanically valid single force (or combination of forces) that simulate specific sports movements could be applied to characterise different surfaces.

This general result is in contrast to recent studies conducted by the University of Exeter which have reported differences in GRF parameters on different surfaces. Stiles and Dixon (2007) found significant differences in the peak and mean loading rates of vertical and horizontal GRF during running on three types of artificial turf, matching mechanical rankings of surface cushioning. In another study by Stiles and Dixon (2007) on different natural turf surfaces, peak active vertical force and impact loading rates were significantly different but peak horizontal GRFs were similar.

A study by Guisasola (2008) also on natural surfaces with varying cushioning properties discovered significant differences on vertical rates of loading and the time they occurred, but none in peak vertical or horizontal GRFs. Stiles *et al* (2006) reported significantly higher peak vertical GRF and lower peak horizontal GRF on a baseline surface with no cushioning (force plate surface) compared to three natural turf surfaces. Low (2010) found that during turning movements on natural turfs, the peak impact force (taken using an in-shoe pressure system) was significantly lower on the more cushioned surfaces. However, when subjects performed turning activities in the current study no significant differences in GRF parameters were found.

Interestingly, equine studies examining the biomechanical response of horses to surfaces reported

differences in GRF parameters on synthetic racetrack surfaces compared to natural surfaces (Chateau *et al.*, 2010; Robin *et al.*, 2009; Setterbo *et al.*, 2009; Thomason and Peterson, 2008). However, these studies have measured GRF with an accelerometer and a dynamometric horseshoe and not force plates. This suggests that the method of GRF measurements may have an effect on the observed biomechanical response.

In order to discuss the significance and validity of the results of this study, the factors which may have influenced the ground loadings measured on the different surfaces are considered. There are four main factors that may potential influence the ground loading results: 1) the mechanical properties of the surfaces tested; 2) the player-shoe-surface interaction; 3) the kinematic and kinetic response of the player (see Section 5.4); and 4) the limitations of the testing procedure (see Section 5.8). The influence of the mechanical properties of the surfaces tested and the player-shoe interface are further discussed, as follows.

5.3.1 Influence of the Surface Mechanical Properties on Ground Loadings

Mechanical testing of all the surfaces was not conducted during this study. Therefore, it is possible that all three may have had similar mechanical characteristics under these loading conditions. This may have led to the indifferent ground loading observed, assuming that the kinematic response remains constant for similar surface characteristics. However, a previous study has shown that the Tarkett-Sommer surface (as used for T2) is harder (i.e. gives greater peak deceleration during impact) than FieldTurf (as used for T3) (Baker and Woolacott, 2005). Clegg Hammer test results for hardness ranged from 120-135 gravities for FieldTurf and 165-211 gravities for Tarkett-Sommer. Rotational traction was similar for both surfaces. Brosnan et al (2009) found that AstroTurf (as used for T1) was harder and produced greater rotational traction than FieldTurf.

As already stated, mechanical testing of hardness and traction was not conducted prior to the biomechanical evaluation. On one hand, it seems perfectly logical to have baseline measurements of the surfaces, so that prior knowledge of the mechanical characteristics of the surfaces under evaluation is obtained. However, one is still faced to the uncertainty whether ‘standard’ mechanical tests (such as the

Clegg Hammer or Berlin Athlete test) represent the loadings applied by players during ‘in game’ situations. Therefore, this creates a circular argument and any baseline measurement may become irrelevant. Until standardised, biomechanically validated and reliable mechanical artificial tests are fully developed, it may be just as appropriate to consider the players’ perceptions of the surface characteristics as the baseline for biomechanical testing.

There is a general anecdotal view that players perceive surfaces differently to others. For example, 3G surfaces are generally viewed to be less hard and provide more traction than sand infilled 3G ‘Astroturf’-type surfaces, but there is only limited empirical evidence to support this. Fleming *et al* (2005) found that field hockey players perceive differences in surface hardness and friction properties of pitches. Stiles *et al* (2007) reported that a player’s perception of surface cushioning is significantly correlated with loading rates of vertical ground reaction force and also matched mechanical ratings of cushioning. Research into different types of 3G turf suggest that players perceive turf filled with Styrene Butadiene rubber granules as less hard and abrasive than turf filled with thermoplastic rubber granules (Zanetti, 2009).

It seems that research on players’ perception of different surfaces has focussed on hardness. Apart from research conducted in the 1980s on 1G surfaces (Baker and Bell, 1986) and other anecdotal evidence, there appears to be a lack of recent research regarding players’ perceptions of the frictional properties of artificial turfs.

The suggestion that the observed differences in ground loading between the turfs in this study was because the turfs have similar mechanical properties appears misplaced. Previous research on the mechanical testing and players’ perceptions of surfaces informs us that the hardness and frictional properties of the surfaces used in this study are different.

The age of the respective turfs may have contributed to results of the biomechanical testing. The turfs used in the study were of different ages, although the exact ages were not known. Turf 1 was likely to be the oldest (perhaps a few years old) and Turf 3 was brand new. Age-related effects in the surface response to

loading have been described by other authors but this appears to be mainly related to the degree of infill compaction *in-situ* pitches (Naunheim *et al.*, 2004; Zanetti, 2009).

5.3.2 Influence of the Shoe-Surface Interface

The analysis of ground reaction forces to evaluate the interaction of footwear with surfaces is beyond the scope of this study. However, the footwear is an important component of the player-footwear-surface interaction triad. Subjects wore different types of shoes in this study. Some wore shoes designed specifically for artificial turf while others wore their normal training shoes. Some of the shoes had cleats (or studs) while other did not. In the interests of experimental research, it is important that only one variable (i.e. the surface) is different between testing conditions and all other variables are controlled for. However, the requirement for the subjects to perform movements as naturally as possible and to a maximum level was also a high priority for this study. It was felt that controlling the footwear may result in the subjects wearing footwear they were unaccustomed to and felt uncomfortable performing in. So, in balance, it was decided to allow subjects to conduct the trials in their own footwear.

Theoretically, the properties of the shoe should have an effect on the ground loadings. For example a hard sole should increase the impact peak and decrease the time to impact. Previous research has shown that the effect of footwear is to generally delay the peak impact forces, compared to barefoot running. Shoes with softer midsoles delay peak impact forces more than shoes with harder midsoles (Zhang *et al.*, 2005) . However, peak forces later in stance phase are not thought to be affected by footwear construction. Some authors have suggested that the biomechanical analysis of the shoe-surface interaction using force plates to differentiate shoe types provides the same inconclusive results as described before about the biomechanical response to different surfaces (Hamill, 1996).

The significant higher peak horizontal GRFs measured on Turf 2 compared to Turf 1 in this study may have been a result of interaction of Turf 2 on the different shoe types worn by the subjects. However, analysis of individual subjects found that there was no particular shoe-type effect (cleated or non-cleated).

It has been demonstrated in other studies that cleat or stud design impacts on the rotational traction during mechanical testing of different artificial surfaces (Livesay *et al.*, 2006; Villwock *et al.*, 2009) and biomechanical evaluations of the shoe interface have shown a shoe-effect on joint kinetics. For example, increased shoe traction significantly increased ankle and knee joint moments (Wannop *et al.*, 2010). However, in terms of injuries, Drakos *et al* (2010) reported there was no difference in biomechanical variables measured during a simulated cut made with cleats or turf shoes on the modern playing turf.

Any shoe-surface interaction ought to be taken into consideration in the construction of a mechanical test rig which replicates human movements. The properties of the rig's test foot that comes into contact with surfaces should reflect the appropriate footwear worn by players. The properties of the test-foot that are likely to influence the shoe-surface interaction include the material, shape, contact surface area, grip or cleat design and arrangement.

5.4 The Impact of Artificial Turf on Knee Biomechanics.

Theoretically, kinematic changes that alter a joint's stiffness and force coupling can influence the ground loading measured at the player-ground interface. However in this study, there were no statistical differences in the knee angle between surfaces when all the movements were analysed together. This was for both the sagittal and frontal planes at initial contact and maximal knee angle during stance, respectively. Nor did the different artificial turfs significantly affect knee moments.

5.4.1 Knee kinematics

These findings suggest that players did not alter knee kinematics in response to performing movements on the three different surfaces tested. This supports other authors (Stiles *et al.*, 2008; Stiles & Dixon, 2007) who reported that changes in the properties of natural turf did not yield any significant differences in ankle or knee biomechanics. They argued that humans prefer to maintain similar geometries when running on a variety of natural turf surfaces. It could be also suggested that any differences in mechanical properties

between the surfaces may not have been sufficient to elicit changes in the kinematic response during the movements.

There is a contrasting argument which suggests that a kinematic adjustment may occur prior to, or at, impact in order to attenuate the force imparted by harder surfaces. Several studies have shown that a player adapts their movement in response to performing on different surfaces (Dixon *et al.*, 2005; Dixon *et al.*, 2000; Frederick, 1986; Gerritsen *et al.*, 1995; Hardin *et al.*, 2004). For example, Hardin *et al.* (2004) showed that running on surfaces with increased stiffness resulted in increased hip and knee extension at contact, while peak hip flexion angle decreased and peak knee flexion angle remained unchanged. Hardin *et al.* (2004) also showed that increased ankle, knee, and hip flexion velocities occurred on harder surfaces, as a result of an uncontrollable response to the impact forces. A more extended knee at initial contact was thought to stiffen the leg in order to minimise the effect of the higher flexion velocities that may increase maximal knee flexion, which would increase the effort required during push off. It is also reported that a stiffer leg at contact is likely to increase the vertical ground reaction force and the impact shock transmitted through the body (Gerritsen *et al.*, 1995; Hardin, 2000). From the limited accelerometry data available in this study, the accelerations measured at the pelvis (which is approximate to the body's centre of gravity) are attenuated to a similar magnitude across surfaces.

In this study, there was evidence of an individual kinematic response to a particular surface and between surfaces. This was most evident with the frontal knee angle at initial contact with the ground. For the same movements, some players had adducted knees while others were abducted (Figure 4.18, Figure 4.19 and Appendix C). Also, the direction of the frontal plane knee angle at initial contact was different on different surfaces for the same player. The type and mechanism of kinematic adaptations response to changes in surface properties may be individualistic and, therefore, individual subject analyses are recommended (Dixon *et al.*, 2005).

A study by Dixon *et al.* (2000) concluded that the mechanism of adaptation varies among individuals

and recommended the need to perform individual subject analyses . In a later study, Dixon *et al* (2005) also found individual variations in knee kinematics on different surfaces but they reported individual increases in knee flexion on stiffer surfaces.

Comparison of frontal and transverse plane kinematic adaptations in response to performing on artificial turf with other studies of similar types of movements is difficult due to the limited amount of literature.

5.4.2 Knee kinetics

This study found no consistent differences in knee moments between the three artificial turfs. As no other published research on the impact of different artificial turfs on knee loading could be identified, it is difficult to state the comparability and/or generalisability of this finding. As such, this is perhaps one of the first studies of knee moments in sports movements performed on different artificial turfs; and any findings should, at this stage, be viewed as cautionary until other research is conducted to confirm or refute them.

The consistent knee moments over the different surfaces observed in this study may be a result of kinematic adaptations of joints not measured in this study, such as the ankle or hip. While no kinematic adjustment of the knee was observed in this study, any other joint adaptations may have occurred in order to maintain similar GRFs and attenuate the loading of the knee and other joints. This suggests that subjects adapted to the varying surface hardness in a similar fashion to optimise the efficiency of locomotion. To explore this notion further, any future research must include a full body biomechanical analysis, including both kinematic and kinetic assessment of the ankle, knee, and hip joints.

There must also be consideration to the muscle theory proposed by Nigg and supported by other authors (Nigg & Liu, 1999; Wakeling *et al.*, 2001; Wakeling *et al.*, 2003; Zadpoor & Nikooyan, 2010). It suggests that the ground loadings act as an input to produce a muscle reaction, or *tuning*, shortly before the next contact with the ground to minimise soft tissue vibration and/or reduce joint and tendon loading. In

response to changes in the impact interface conditions, the muscle activity adapts to maintain a constant joint movement pattern for given movements (Boyer *et al.*, 2007; Nigg, 2001). Zadpoor (2010) suggests that the central nervous system uses muscle tuning to keep the ground reaction force (GRF) constant regardless of shoe or surface hardness, wherever possible.

5.4.3 Methods of biomechanical analysis

The contrasting findings relating to whether there are knee biomechanical adaptations in response to surface conditions may be due to the methodological differences between the studies. For example, the accuracy and reliability of skin marker placement in biomechanical analyses has been documented previously (Cappozzo *et al.*, 1996; Reinschmidt *et al.*, 1997). The large inter-subject variation observed in this study may be due to the skin marker placement. For cutting movements, the absolute error of skin-marker derived frontal plane knee kinematics has been reported to be 6.7° (± 5.4) at foot-strike, 5.9° (± 3.1) at mid-stance, and 13.1° (± 9.8) at toe-off (Benoit *et al.*, 2006).

Markers placed on bony prominences or areas with a high degree of muscle contraction can often lead to erroneous movement of the marker with respect to underlying bony landmarks and calibrated bone embedded reference frames. The use of marker clusters and compression bandages on the subjects' shank in this study was an attempt to reduce inter-marker movement and minimise relative soft tissue movement. Secure and reliable placement of markers that minimises relative skin movement is vital to accurate and repeatable kinematic data.

5.4.4 Summary of biomechanical response to artificial turf

Any kinematic and kinetic adaptation in response to a different surfaces, either systematic or individual, is likely to have an impact of potential injuries. Regular training and performance on a particular surface may reduce the likelihood of injuries. However, if players are performing at a maximal level on different surfaces

without the necessary time to adapt to it, it may intensify the strain placed on joints and the potential for injuries may increase.

5.5 The Impact of Movement Type on Ground Loadings

The GRF results indicate that the type of movement had an effect on the ground loading parameters. In particular, the magnitude of the peak ground loadings varied considerably between the different movements. The impact of movement type on each GRF parameter is described below.

5.5.1 Vertical GRF and Loading Rates

Firstly, there were differences in the peak vertical GRF and vertical loading rates between movements. This is likely to be due to the different approach velocities at the initial impact with the force platform, even though the subjects were instructed to perform each movement as fast as possible. Other studies have also found that vertical ground reaction forces increased linearly with gait speed. (Hunter *et al.*, 2005; Keller *et al.*, 1996).

The movements with the fastest approach velocities tended to produce the highest vertical GRFs and loading rates. These were the *RUN*, *STOP*, *45L* and *45R* cutting turns. These movements whose approach velocities ranged from 5 to 6ms⁻¹ produced GRFs ranging from approximately 1900 to 2800 N (2.4 to 3.5BW) and peak vertical loading rates ranging from approximately 60 to 144kNs⁻¹ (80 to 170kN/BWs).

Similarly Meijer *et al* (2006) found speed of movement impacts vertical ground loadings and reported comparable peak vertical GRFs of 2.6 to 2.7BW for fast velocity running movements (4.8 to 6.9 ms⁻¹). The high speed movements also tended to have the most rapid increase in the vertical GRF following impact during the weight acceptance phase of stance, as indicated by the higher vertical loadings rates of up to 144kNs⁻¹ (170kN/BWs) and times to the peak impact force (38 to 40ms).

Movements with slower approach velocities (approximately 4ms⁻¹), such as the 90° cross turns (*90L*,

90R), produced lower vertical GRF of 1400 to 600N (1.7 to 1.9BW). Slower movements had statistically lower peak vertical GRFs than the other movements. It could be viewed that a slower approach velocity may be required for the player to prepare and align their body appropriately to allow them to complete the turning movements effectively and safely.

Approximate vertical GRF limits could be applied to categories of movement, based on their approach velocities. For slower turning movements, with approach velocities less than 4.5ms^{-1} , a limit of 2BW could be applied. For movements faster than 4.5ms^{-1} or those requiring less speed reduction prior to impact, an upper limit could be set at 3.5BW to take into account the variations in the vertical GRF observed between individual subjects. To illustrate this point, the *STOP* movement which had the highest approach velocity and the largest change in momentum (forward velocity reduced to zero within two steps) produced the highest vertical GRF and loading rates.

5.5.2 Horizontal GRF

Another major finding was the large horizontal GRFs measured in some of the movements. Cutting-type turning movements produced the highest peak horizontal forces of approximately 1.6BW. This equated to approximately 50% of the vertical GRF in the 45° 'cut', for example. Other studies have also shown high horizontal forces in turning movements. Morag *et al* (2001) reported peak horizontal GRFs of 1.17BW (~860N) during a cutting turn. Horizontal GRFs of approximately 0.9BW (660N) were measured during a running 180° turn at 3.8ms^{-1} by Dixon *et al* (2006). Guisasola *et al* (2008) also analysed a running 180° turn at 3.8ms^{-1} and reported horizontal GRFs of approximately 0.87BW (640N) compared to the 1.3 to 1.5BW measured in the present study. These results are not directly comparable as the *180T* conducted in the present study did not involve a run-up.

Therefore, movements with a significant change in momentum tended to produce higher horizontal GRFs. A change in momentum could be either a change in direction in turning movements and/or a reduction in velocity. Energy from the subject's forward momentum is transferred to a different horizontal

direction producing the high horizontal GRFs. The effect is to retard the forward momentum (during the *STOP*, for example) and minimise over-rotation of the body during turning movements, thus allowing the player to control the manoeuvre.

Movements which involve a change of direction combined with deceleration to produce high horizontal GRF, such as the cutting manoeuvres, are likely to be a risk factor for a non-contact ACL injury. For example, Alentom-Geli *et al* (2009) described the most common mechanism for a non-contact ACL injury includes “movements consisting of high deceleration combined with high knee internal extension torque and dynamic valgus rotation with the body weight shifted over the leg and the plantar surface of the foot fixed on the playing surface”. Other common ACL injury mechanisms include landing from a jump in or near full extension, or pivoting with knee near full extension and a planted foot.

5.5.3 Free moment of rotation

As may be expected, the movements involving turns tended to produce the highest free moments (and rotational traction coefficients). The free moment of rotation typically remained below an approximate limit of 30Nm for all movements, although some individual subjects achieved higher values.

This 30Nm limit is slightly higher than free moments reported in other studies. For example, in one of the earliest studies of free moments in sporting movements, Stucke (1984) reported moments of rotation kept below a limit of about 25Nm in tests with subjects. However, this is not directly comparable as the approach velocities were considerably lower and the movements were performed on a cinder surface. Valiant (1987) described free moments of 17.2Nm during cutting movements on artificial turf. During cutting and running 180° movements, Stefanyshyn *et al* (2010) reported free moments of 10 to 20Nm.

The magnitude of the peak free moments observed in this study fall comfortably within the upper limit of 50Nm specification for “rotational traction” on artificial turf set by the sporting governing bodies. Taking a simplistic view, this observation suggests that the 50Nm regulatory limit may be too high and such a high limit may have the potential to cause injuries, particularly ACL damage. For example, if too much

rotational force is required before the foot can turn on the surface, very high moments and stresses could be placed on the internal structures of the ankles and knees and increasing injury risk. However, the 50Nm limit is based on BS EN 15301-1:2007 Torque Wrench Test to measure rotational traction, which does not apply forces and use test shoe materials observed in a real athletic situation. Therefore, it is difficult to compare this mechanically-derived rotational traction limit with the free moments observed in this biomechanical study. Consequently, it may be more appropriate to suggest that the 30Nm rotational traction limit that is based on either a biomechanical analysis of an artificial turf or a biomechanically validated testing procedure may be a suitable limit for regulatory bodies to consider. In light of this, however, it is recognised that the present study included only a small cross section of all the possible types and speeds of movements.

The rotation results suggest that subjects demonstrated evidence of limb dominance. It is interesting to note that the moments of rotation (and rotational traction values) for the 90L were generally higher than those for the 90R. Similar phenomena have been reported by Garcilazo (2007). All of the subjects in the present study were right-foot dominant so it could be speculated that the subjects demonstrated superior proprioceptive control when their left foot is used as the stabilising stance/turning foot when performing tight turns, and therefore felt more comfortable turning to the left. The relatively low values for rotation on the 45° turns may indicate that the foot rotation during this movement is less than the 90° turns.

5.5.4 Linear and rotational traction

The range of linear traction coefficients for the same surface supports the theory that sports surfaces do not follow the classic laws of friction, in that they are affected by the normal (vertical) load and the relative velocities of the player and surface. It was evident that during some of the turning activities, a high resistance to linear movement was produced at the player-surface interface, resulting in higher traction coefficients. For all the movements included in this study, the linear traction coefficients (LTC) tended to remain below a value of 0.8 but remain above 0.35. Although, the lower limit is less, these are comparable with the recommended values for *slip resistance* ($\mu = 0.6$ to 1.0) set by the governing bodies for football,

rugby and hockey (Fédération Internationale de Football Association, 2009b), (International Rugby Board, 2010) (Federation Internationale de Hockey, 2008).

These values are similar to the “peak force ratios” on artificial turf, reported by Valiant (1990) but lower than the traction coefficients for cutting movements reported by Shorten (2003). It was expected prior to testing that the *STOP* movement would produce a higher LTC, due to the abrupt reduction of forward momentum. However, the *STOP* LTC was similar to the *RUN*. The lower than expected traction value in the *STOP* may have been due to the high horizontal GRF to vertical GRF ratio produced in this movement.

Also, the LTC may have been much higher if the player had completely stopped on the force plate so that all the braking horizontal forces were measured. However, it is extremely difficult to stop completely in one step following a sprint and there may be a high chance of injury to try to attempt this. Higher LTC may have occurred in the 2 or 3 steps following the force plate before the player’s motion ceased fully but these subsequent steps were not measured.

The rotational traction coefficients (RTC) clearly show that more grip was required when performing tight-angled turns, such as the 90 degree turns than compared to 45 degree cutting movements. A RTC limit of approximately 20mm could be applied for these higher-angled turning movements, and 10mm for all the other movements. Differences between this result and other comparable studies may also exist because it difficult to control the contact surface area between the players shoe and the surface which is known to have an effect on the free moment generated (Andreasson *et al.*, 1986).

There is a need for sports surfaces to achieve a traction balance. Too much traction may lead to injury, while too little traction may lead to reduced performance. For example, there is a higher incidence of ACL injuries with increased resistance to movement at the shoe-surface interface (Myklebust *et al.*, 1998). Understanding which movements have a higher traction requirement on artificial surfaces is important for reducing the injury risk and increasing performance. Secondly, it may allow the development of specific training regimes to improve technique in sports where turning quickly and safely is vital.

5.6 The Impact of Movement Type of Knee Biomechanics

Similar to the ground loadings, there was a large range in knee kinematics and kinetics between different movements. A discussion of each follows.

5.6.1 Kinematics

In general, movements with the largest change in momentum (e.g. *STOP*, 90° and 180° turns) tended to produce the highest peak knee flexion. In particular, the *STOP* movement produced very high flexion angles compared to the other movements. From a relatively straight 20° at initial contact with the turf, the knee flexion increased throughout stance to a maximum of approximately 80°. This high degree of flexion can act to attenuate the high impact forces and forward momentum of the movement.

The magnitude of the turning angle also tended to have an impact on peak knee flexion. For example, 90 and 180 degree turns tended to produce greater impact and peak knee flexion than 45 degree turns. These sharper turning movements also tended to produce an increased abducted knee at initial contact. In contrast, more extended knees and less knee abduction tended to occur as the approach velocity increased and turning angle decreased.

In general, the knee angle data in the present study were representative of typical values for comparable movements presented in the literature. Knee angle data for the following movements performed on artificial turf and other surfaces are comparable with the literature:

- *RUN*: the data for the *RUN* was comparable with several author studies (Dixon *et al.*, 2000; Guisasola, 2008; Hardin *et al.*, 2004; Novacheck, 1998; Stiles *et al.*, 2008). The knee angles reported by Guisaola (2008) were lower than the present study but the movement was performed at approximately half the speed
- 45-degree cuts: the data was comparable with Sigward and Powers (2006), Mclean *et al* (1999);

and Pollard *et al* (2004) (knee abduction). Data from the present study was within the ranges reported by Kaila *et al* (2007) for 30° and 60° cuts.

No studies could be identified that have examined the knee kinematics for a comparable STOP movement, 90° turns or 180 degree turn from a standing start performed on artificial turf.

This study identified that these other movements had different knee kinematics than running fast in a straight line. All of the movements which included a run up and a significant change in momentum produced lower knee flexion angles at impact compared to straight line sprinting. This was against prior expectations and in contrast to data published by Besier (2001b). However, in Besier's study subjects performed movements on an uncovered force plate and turning angles and running velocities were different from the current study. Also, kinematic adaptations which may have taken place in other joints (e.g. hip) to reduce impact were not examined in the current study.

One may hypothesize that in preparation to either change direction or slow down abruptly the body would adopt a more flexed knee, in order to cushion the impact. This would tend to reduce the stiffness of the kinetic chain (a term referring to the body as a system of linked rigid bodies) and increase shock absorption. Derrick (2004) commented that a more extended knee angle at initial contact can increase the forces experienced by the body and therefore increase injury potential. Increased knee flexion may give the runner a larger margin for dealing with kinematic errors but this benefit could have an associated metabolic cost that will reduce performance. It must be noted, however, that peak knee flexion angles during the remainder of stance in all movements were comparable with the literature.

Turning movements tended to affect the magnitude of frontal plane kinematics. Increased peak frontal plane knee angles in the 45° and 180° turns tended to place the knee into a more abducted position compared to running in a straight line (which was typically in a neutral position).

However, these generalised results should be taken with caution considering the large individual variation in knee kinematics observed between subjects performing the same movement. In particular, the

initial knee angles at initial contact were highly variable, suggesting that there may be individual adaptations for different types of surface.

5.6.2 Kinetics

The knee moments reported in the current study were generally comparable with published data. However, although knee biomechanics during running has been extensively researched, little kinetic data is available on other types of movement or on movements performed on artificial turf, and no studies were identified that compared knee moments during sports movements on different types of artificial turf.

Knee moments for the 45° cut were comparable with studies of natural turf (Besier *et al.*, 2001b; Pollard *et al.*, 2003; Sigward and Powers, 2006). For similar artificial turf studies, transverse and frontal plane moments were slightly higher than the mean peak values reported by Stefanyshyn *et al* (2010) and Kaila *et al* (2007), This may be due to differences in the types, execution and velocity of the movements included in the studies. Peak knee moments were, however, comparable with the greatest mean peak values for 30° and 60° cuts presented by Kaila (2007). Knee moments were also similar to Wannop (2010) but the type of surface was not described in detail.

In summary, large internal knee extensor moments were measured in all movements. Movements which involved a rapid deceleration and/or a change in direction (*STOP* and 45° turning movements) tended to produce the largest knee moments. For all movements, however, extensor knee moments measured approximately 1 to 1.5Nm/kg during the impact phase and 2 to 3.5Nm/kg during the propulsion phase. In comparison, peak knee moments in normal walking are typically 0.6Nm/kg (Lee and Hidler, 2008). It must be noted, however, that separation of sagittal plane knee moments into impact and propulsion phases is rather arbitrary. Typically, no peaks were observed in the impact phase as the extensor moments tended to continue to increase throughout the impact phase into the propulsion phase (see Section 4.9).

In general, knee flexor moments were observed in all movements during initial contact (except for the *180T*). The impact of the external ground reaction force tending to extend the knee at initial contact

causes contraction of the knee flexor muscles to counteract the external force and prevent knee hyperextension. This may have a specific impact in sports where players obtain injuries when stopping suddenly or turning quickly. For example, the large flexor moments observed during the initial phases of the *STOP* movement and 45° turns may indicate a requirement for players to undertake specific muscle strengthening exercises to prevent the knee flexor (hamstring) injuries common to field sports like football and rugby.

For most of the remaining stance phase, all movements tended to produce an extensor moment as the direction of the ground reaction force passes behind and tended to flex the knee, causing the subject's quadriceps to contract to propel the body forward. The highest sagittal plane moments were observed during this stage and have the potential to significantly load the knee ligaments increasing the risk of injury.

Frontal and transverse moments were more variable. Although some significant differences were observed in knee moments between movements, this variability suggests that movements may not have been performed consistently between subjects or was due to the effect of intra marker movement, as discussed earlier. Alternatively, the variability in the frontal and transverse knee moments may indicate an individual response to performing these movements on artificial turf, as described by Dixon *et al.* (2005).

For all movements, frontal knee moments were typically greater during the impact phase. Frontal plane moments were highest for the 90° turns, reaching a mean peak of 1.1Nm/kg during the impact phase. However, the direction of frontal plane moments was also variable between movements. For example, in the impact phase, the *RUN* and 90° turns tended to produce abductor moments while the 45° turns tended to produce adductor moments.

Biomechanically, the abductor moments in the *RUN* and 90° turns indicate that the knee abductors and lateral ligaments act to resist the external adduction moment caused by the ground reaction force passing inside the knee. The adductor moment observed in the early phases of a 45° turn, indicate that the external ground reaction force passes laterally to the knee, imparting an external abduction moment, causing the knee

adductors, such as the semitendinosus and gracilis, to resist knee abduction, control joint movement and maintain joint stability. This suggests that for sports where particular types of movements are common (such as the 45° cutting turns for wingers in rugby, for example), players ought to carry out specific training to strengthen the knee muscles and ligaments to cope with the rapid frontal loading moments that occur during the initial phases of some movements.

Peak transverse plane moments were approximately 0.4Nm/kg (approximately 30Nm), with more acute turning movements, such as the 90° and 180° turns, tending to produce the higher transverse moments. The marked rise in internal rotator moments during the impact phase of these types of movements indicates the knee's response to the high horizontal ground forces causing to turn the knee outwards. The combination of the high external forces, increased knee abduction and external knee rotation in these movements may place the knee at risk of injury. Besier *et al* (2001a; 2001b) also reported increased valgus and internal rotation moments for similar turning movements.

In the anatomical sense, high internal rotator loading of the knee is likely to twist and strain the anterior cruciate ligaments to a level where injury may occur (Drakos *et al.*, 2010). The rapid change in the direction of the transverse moments from external to internal rotator in many of the movements (and back again in the 90° turns) will also likely place the cruciate ligaments under great strain.

The ultimate aim of measuring loading to anatomical structures in biomechanical sports studies is usually to either a) improve performance, or b) reduce injury potential. However for the latter, it can be difficult to equate the type and level of knee loading obtained from biomechanical studies that have the potential to cause injury. This is probably because of the ethical and practical difficulties to conduct such *in vivo* studies. So, the level of loading that will strain muscles, tendons and ligaments to the point when an injury can occur, is unknown.

The study by Drakos *et al.* (2010) is one of the few identified that attempted this. Using a mechanical testing apparatus, the effect of different loading at the shoe-surface interface on the loading of cadavers'

anterior cruciate ligaments was investigated. Simulated cutting turns with certain shoe-surface combinations (such as AstroTurf-cleats compared to natural grass-cleats) caused significantly more strain in the ACL and could potentially cause knee injury. Drakos *et al.* (2010) reported a linear relationship between moment and ACL strain. This cadaveric model was able to demonstrate that performing a cut on certain shoe-surface combinations (such as AstroTurf-cleats compared to natural grass-cleats) causes significantly more strain in the ACL and thus has the potential to be more deleterious to the knee. Further research is required to investigate the relationship between knee loadings (or any other joints) and injuries, and how mechanical artificial turf testing apparatus can mimic this relationship.

5.7 Study Originality and Importance

This study has added to the understanding of the biomechanical interaction with artificial turf during a variety of movements commonplace in field sports, such as football, hockey and rugby. Other studies have examined similar movements and reported comparable results. However, many of these studies included only a few movements in their research design and the different methodologies make it difficult to compare results. For example, some studies have controlled the approach velocity during subject's movements (with timing gates), while others have not. Similarly, some studies have specified and controlled the turning angle of movements, while others have examined turns in one direction only.

In addition, there is a lack of studies that have examined ground loadings during very high velocity (e.g. sprinting) or high impact movements (e.g. landing from a running jump or stopping or turning abruptly). This study has provided data on two of these types of movements, namely the *STOP* (stopping suddenly after a maximum velocity run) and the *180T* (turning 180° from a standing start). Injury prevalence is high for these types of movements. In particular, high velocity and impact movements is a risk for acute knee cruciate ligament injury (Alentorn-Geli *et al.*, 2009). This information from this study will add to the understanding of how players perform various types of movements on artificial turf. This may, in turn, help prevent injuries or assist in the design of new artificial turfs to minimise injuries.

The inclusion of a range of movement types in the same study has allowed a comparison of the resultant ground loadings. Although insignificant differences were observed between the different surfaces for the individual movements, there was a substantial range of ground loadings between movement types. The results indicate that the grounded loadings are affected by the combination of the approach velocity and the degree of the subject's momentum change. As momentum is a vector quantity that has a magnitude and a direction, turning movements can be described to be a change in momentum.

This is the first study of its kind to measure the biomechanical interactions of sports player movements on artificial turf and use this data as the input to the design and construction of a test rig, which mimicked these biomechanical interactions. In particular, no other studies have investigated the impact of performing a range of sports movements on different artificial turfs on the moments generated around the knee. This understanding has allowed the development of a biomechanically validated test rig (see Chapter 6) that simulates the typical ground loading profiles and resultant knee loading.

5.8 Limitations of the Testing Procedure

The biomechanical study had several limitations related to the study design, methodology and conduct. These are summarised as follows:

- Firstly, the number of subjects was relatively small and this may impact the generalisability of the results. A higher number of subjects performing in all testing conditions is likely to increase the statistical rigour. However, the inclusion of 10 to 15 subjects is not unusual in these types of the biomechanical studies.
- A further possible limitation may be the low number of trials performed by each subject for each movement. However, due to the requirement to include as wide a range of movements as possible, the number of trials was limited to allow the completion of individual testing sessions within two hours to not overly fatigue the subjects.
- The execution of the test movements may have been affected by the range of the subjects' skill level,

age and sport. All subjects performed to a high standard of competition but the professional and more experienced players may have executed the movements more efficiently. Also, rugby players may perform some of the turning movements slightly differently to football or hockey players, for example. However, all of the movements included in the study commonly occurring in different field sports and were not considered to be complex.

- Fully establishing the reliability of the subject's movement execution between the testing sessions is challenging. While the approach velocities and stance time showed good correlation between the three turfs, other factors such as the consistency of movement technique, style and speed is difficult to determine.
- The type of shoe worn by the subjects was not controlled. Doing so may have led to unnatural or uncomfortable movements and, pragmatically, there was not enough time during the testing sessions for the subjects to get used to a type of shoe which may have been completely different from the one usually worn.
- The effect of the laboratory and all the testing equipment is an unnatural environment for sports players to execute movements naturally and this may have had an impact on the data. Also, movements and ground reaction forces may have been impacted by subjects targeting the turning area (force plate).

There were also a few methodological constraints in the data collection systems:

- As force plates, in essence, only acts as a whole body accelerometer, their use in this study may have led to masking of the effects of cushioning by shoes and/or surface of the impact force by superimposing the low frequency motions of the centre of mass as described by Shorten (2002). It is also possible that the 120Hz sampling frequency may have been too low to observe some of the higher frequency events during the impact phase (i.e. heel strike transient).
- The marker system used in the current study did not include any markers on thigh segments. This

restricted the calculation of internal/external rotation of the knee. Furthermore, the accuracy of anatomical and joint centre reference frames may have been affected by the following factors: locating anthropometric landmarks; the marker attachment method; soft tissue movement; and the complex nature of very high frequency impacts during the movements performed.

5.9 Implications for Artificial Turf Design

The large ground loadings observed during high velocity movements in this study may have consequences on the design of artificial surfaces for sports where high velocity movements occur frequently. This information is required in order to design surfaces that can optimise performance and reduce the risk of non-contact injuries, particularly ACL injuries.

High-velocity movements have a major role in many types of competitive sports. For example, it has been shown that, on average, professional football players will sprint 15m every 90 seconds (Reilly and Thomas, 1976) and conduct a bout of high-intensity activity every 60 seconds (Strudwick *et al.*, 2002). In total, football players can perform up to 1km of high intensity running (Di Salvo *et al.*, 2009) and execute 726 ± 203 turns during a single match (Bloomfield *et al.*, 2007). However, the influence of surface cushioning on attenuating the impact is not fully understood and further research on methodologies to measure localised impact forces may be required.

There is not a consensus on the relationship between the cushioning properties of surfaces and subsequent injury rates. A review by Nigg (2001) stated that there is little evidence to suggest that impact forces are important factors in the development of chronic and/or acute running-related injuries. Until there is better understanding of these issues, combined with the methodological matters regarding injury aetiology, the challenge of designing and prescribing suitable artificial turfs will remain. More research on these issues is required.

As observed in this study, others have also shown that the effect of surface (or shoe) cushioning on

impact forces is insignificant when measured using a force plate (Dixon *et al.*, 2000; Shorten *et al.*, 2003). However, further research is required on techniques to measure the impact of surfaces on localised impact forces to the joints of the lower extremities and along the kinetic chain. For example, Low (2010) reported that, using an in-shoe pressure system, peak impact forces were reduced on more cushioned surfaces.

The national governing bodies for football, hockey and rugby have all set linear traction limits for artificial playing surface from 0.6 to 1.0. The findings from this study suggest that these limits are slightly too high and do not take into account movements which require less traction, such as straight line sprinting and stopping abruptly. However, the linear traction guidelines are appropriate for the other types of movements examined in this study. Injuries caused by a surface with higher than required traction properties may be less likely for normal running but may have considerable potential for injury in more dynamic movements, like stopping.

5.10 Implications for the Future of the Mechanical Testing of Artificial Turf

Current, standard methods for the mechanical testing of artificial turf apply loads usually in one direction or within the same plane, and are typically not relevant to the player-surface interaction. This study has provided further evidence to this claim. Future mechanical testing methods should apply biomechanically relevant loads to characterise and test artificial turf. The information obtained from this study was required for the development of a new mechanical test rig that did just this. Therefore, the findings from the biomechanical study had implications on how the test was designed, in terms of the type, magnitude and direction of forces generated by the rig.

The biomechanical results indicate that players impart similar whole-body ground loadings on different artificial turfs for the same movements. This suggests that in order to mechanically replicate a player's ground loadings that exist in a particular movement performed on different surfaces, it is appropriate to apply a single force magnitude in a given direction (vertical, horizontal or rotation around the vertical axis). There appears to be no requirement to apply different force magnitudes according to the type

of surface tested. The magnitude of the applied forces ought to represent the highest forces that occur for a particular movement. This further suggests that the magnitude of forces applied in a mechanical test rig could be standardised. Additionally, identifying when peak loads occur during movements is particularly important for replicating loads in an appropriate time frame which represents the period for the greatest loading of the knee or other joints.

The biomechanical results also confirm that sports movements are very 3-dimensional. Fast turning movements such as the 45° cutting manoeuvre, for example, produce very high horizontal ground reaction forces and free moments, as well as considerable vertical ground reaction forces. It seems, therefore, logical that in order to truly replicate the real-life situation, the mechanical test rig should be able to apply forces to the surface in a combination of directions within the same action.

This study has further demonstrated the wide range and large magnitude of forces and moments that are applied to the turf by players when performing a range of highly dynamic movements. The non-linear loading response of many artificial surfaces suggests that they respond differently to different loading magnitudes and timescales. As such, mechanically applied loads ought to mimic the magnitude and timescales of the player-surface ground loadings that occur in a range of movements. Therefore, a new mechanical test rig ought to be able to apply a range of load combinations to a surface to replicate those occurring in different sports movements.

5.11 Implications for Future Research

It is problematic to compare the ground loadings from this study with those reported in studies where they have been measured using mechanical test rigs. It is generally accepted that traction is dependent on the magnitude of the normal force but many of the mechanical test rigs apply normal loads much lower than what is observed in biomechanical studies. For example, Kuhlman *et al* (Kuhlman *et al.*, 2010) reported on the use of a newly developed test rig and found that using normal loads above 1776 N caused damage to the

surface.

With consideration to previous research, the results from the current study have identified a number of questions that can be addressed by future research:

1. How do the biomechanical response of players performing on artificial turf compare with performing on natural turf?
2. Which biomechanical properties differentiate surface types and how do these parameters correlate with mechanical properties of surface hardness and traction?
3. How does the players' perception of surface impact their performance?
4. How do artificial turfs respond over extended periods of time and how does this impact the testing of surfaces?
5. Is the biomechanical interaction of different surfaces different when local impact forces on the individual joints (ankle, knee and hip, for example) are considered?
6. What is the clinical relevance to ground loadings in relation to injury mechanisms?
7. Is there an ipsilateral preference in sports movements on artificial turf (difference between left and right-footed stance foot) and what is the significance, if any?

Finally, the non linear response of artificial turfs is well established but much of the prior research has concentrated on straight line running. Sports consist of many other types of player-surface interaction, not just running based activities. Little is known about the response of artificial turfs to other types of interaction, many of which are sports-specific. For example, the sliding tackle in football can lead to serious abrasion injuries on high friction surfaces but there is a lack of research about the effect of different surfaces on a player's ability to perform sliding tackles or the potential for abrasion injuries. In football, other movements could include kicking a ball and the large range of movements performed by goalkeepers. Rugby is a classic example of a sport with multiple movement types. Maintaining a good foothold to drive forward during movement such as scrummaging or mauling is vital to keep possession and gain territory.

However, there is little biomechanical data on these types of complex movements and further research on the biomechanical responses during a wider variety of high impact and turning movements is required.

CHAPTER 6. DEVELOPMENT AND INITIAL TESTING OF A PROTOTYPE ARTIFICIAL TURF TEST RIG

6.1 Introduction

The purpose of this second section of the study was to develop and initially test a new rig for the assessment of sport turfs. The aim was to design and construct a rig that mimicked the 3-dimensional loading actions of a sports player. This chapter describes the design, manufacture and application of the new test rig.

As previously described, current sports turf testing procedures are not biomechanically validated. Many of the tests are laboratory based, which on one hand make it easier to control for temperature and humidity; but they may not reflect the real-life situation of an installed surface on which players actually perform. During this study, it was aimed to develop a functional sports surface testing rig and testing procedures to be used on sports surfaces *in situ*.

There were four main objectives to this part of the study:

1. Design and manufacture a new sports turf testing rig and develop testing procedures.
2. Validate the output of the rig with biomechanical data.
3. Apply the test rig to assess different types of surfaces.
4. Generate mechanical characteristics of the surface tested.

The design of the test rig was based on data collected during the biomechanical analysis of artificial turf conducted earlier in this study (Chapters 3-5). As discussed in section 5.10, findings from the biomechanical analysis indicated the following governing principles for the design of an artificial turf test rig:

1. The loads should be applied by the test rig simultaneously in different directions to replicate the 3-dimensional nature of players' movements.
2. A single load magnitude should be applied by the test rig in each direction to replicate the similar whole body player-surface loadings observed on different surfaces for the same movements.
3. The magnitude of the loads applied by the test rig can be standardised to replicate the highest player-

surface loadings for a given movement

4. The loading rate of the loads applied by the test rig should replicate a similar time frame in which the greatest player-surface loading occurs
5. The test rig should apply a range of load combinations to replicate the different player-surface loadings which occur in different movements.

6.1.1 Design Specifications

Using the above governing principles as the starting point for the design of the new test rig, the following specifications were developed to guide the formulation of design concepts. These were as follows:

- The rig must be portable to allow testing of artificial and natural turfs *in situ*
- The rig must apply vertical, shear and torque loadings (around a vertical axis) in one impact action
- The rig must apply biomechanically valid loads that will mimic the loads observed during the biomechanical analysis of sports movements (Chapter 4), in terms of magnitude and timescales.
- Due to the non-linear response of artificial turfs to loading, the loads applied by the test rig must reflect the peak loads applied by an athlete to the surface (Walker, 2003). It is also recommended that the applied mechanical loads should reflect the ‘top end’ of peak ground loadings during a player surface interaction (Shorten, 2002). Therefore, the upper quartile of ground loadings measured during the biomechanical tests was used as the input for the test rig instead of the mean peak values (Table 6.1).
- The loads applied by the test rig must be accurate and reliable
- An accurate, reliable and recordable measure of the impact loading and turf displacement must be provided. Turf displacement was measured as it would allow calculation of the surface stiffness – an important property in understanding the mechanical characteristics of a material

- The device must be safe to use.

Direction	Peak Load	Approximate Time to Peak Load
Vertical	3500N	25-50ms
Horizontal	1600N	25-50ms
Torque	40Nm	25-50ms

Table 6.1 Approximate load criteria for test rig, based on upper quartile Ground Reaction Force results obtained during the biomechanical testing of artificial turf

6.2 Design Concepts Considered

6.2.1 Concept A: Drop weight and 'tilting wedges'

Concept: The basic function of this design involved the use of a mass, released from a height down a cylinder. Castors, located at the bottom of the drop weight, would strike a circular test foot with wedges tilted at opposite angles to each other (Figure 6.1).

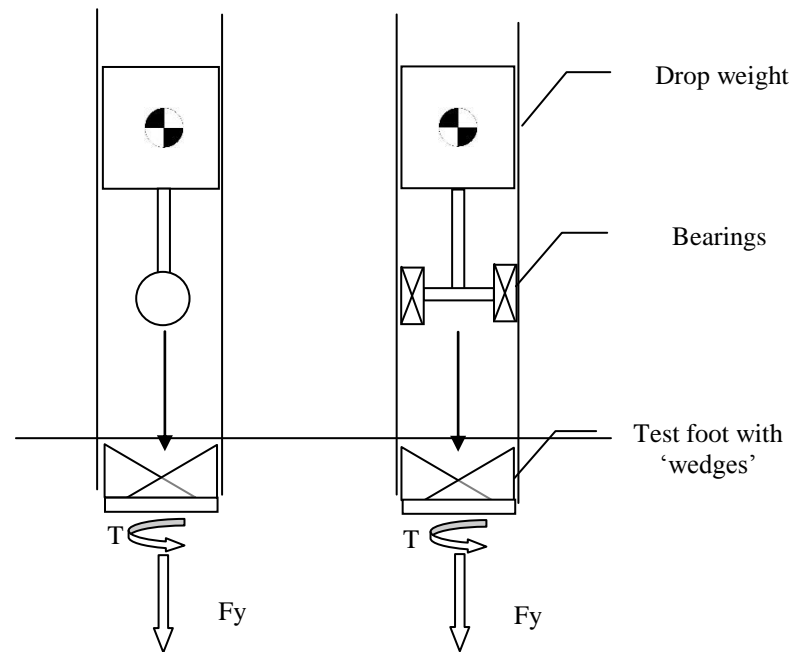


Figure 6.1 'Tilting wedges' concept

Observations:

- Vertical force and torque generated
- No net shear force generated
- Concerns regarding impact forces on castor bearings
- Concerns regarding castor friction within the cylinder.

6.2.2 Concept B: Two drop weights with pulleys and rotating disc

Concept: Two drop weights of unequal mass are released from a height. One of the drop masses impact with a test foot to apply a vertical force. Cables are attached to the top of the drop weights and passed through a

pulley system to apply unequal couple to a rotating disc on top of the test foot. This unbalanced couple would produce a torque and net shear force to the test foot (Figure 6.2).

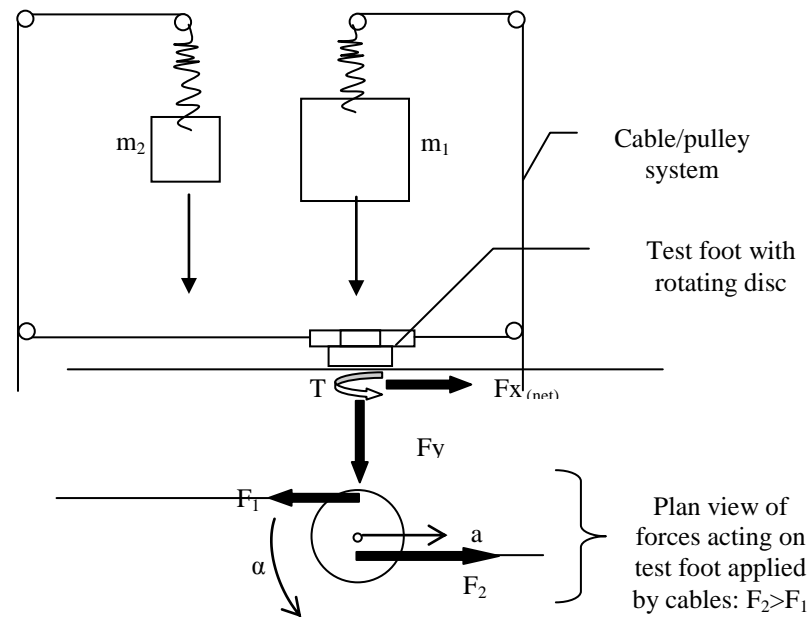


Figure 6.2 Two drop weight pulley concept

Observations:

- Vertical force, shear force and torque could be generated simultaneously and force couple is efficient for torque generation
- Concerns regarding cable lengths and strengths, pulley strength and system friction
- Could this method produce high enough net shear forces?

6.2.3 Concept C: Weighted pendulum and flywheel

Concept: A weighted pendulum is released to impact a tilted surface or 'wedge' located at the top of a test foot. The angle of the tilted surface would provide the magnitude of the vertical and horizontal force components. A flywheel is also attached to the test foot and generates the required torque. The rotation of the flywheel remains independent of the test foot (which remains still on the surface) until the weighted pendulum impacts and engages gears on the shaft of the test foot. This would transfer the torque generated

by the flywheel to the test foot (Figure 6.3).

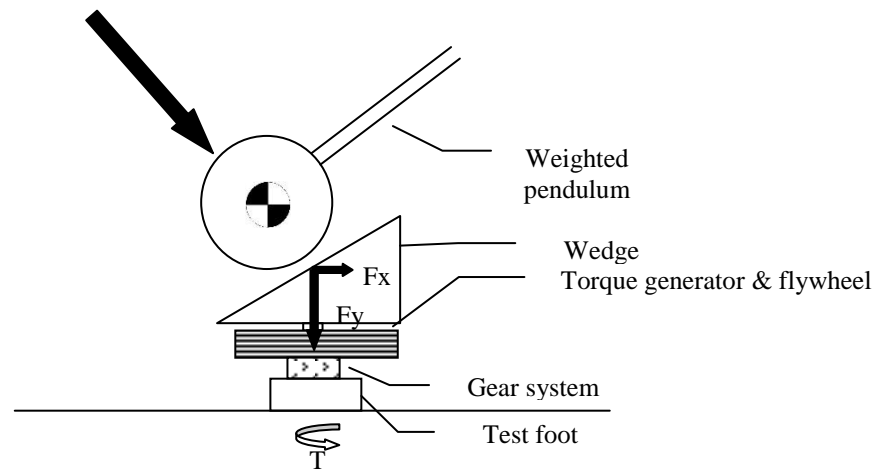


Figure 6.3 Weighted pendulum and flywheel

Observations:

- Vertical force, shear force and torque generated. Loads applied simultaneously
- Heavy masses can be easily released and winched back up using a pendulum system. A cylinder for a drop-weight to fall within is not required.
- The placement and powering of the torque generator is problematic. A battery-powered generator may be required for the *in situ testing*
- Other limitations: the gear timings required; wedge proportion will dictate ratio of shear to vertical force- less flexibility for different ranges of forces.

6.2.4 Concept D: Drop weight with hydraulic rams

Concept: A drop weight is released to fall through a cylinder, which impacts with a shaft attached to the test foot. This provides the vertical load. Hydraulically powered rams apply an unbalanced couple to a disc attached to the test foot, which produces the shear force and torque. The pressurising of the rams is triggered by the impact of the drop weight onto a pressure sensor/contact located on the central shaft (Figure 6.4).

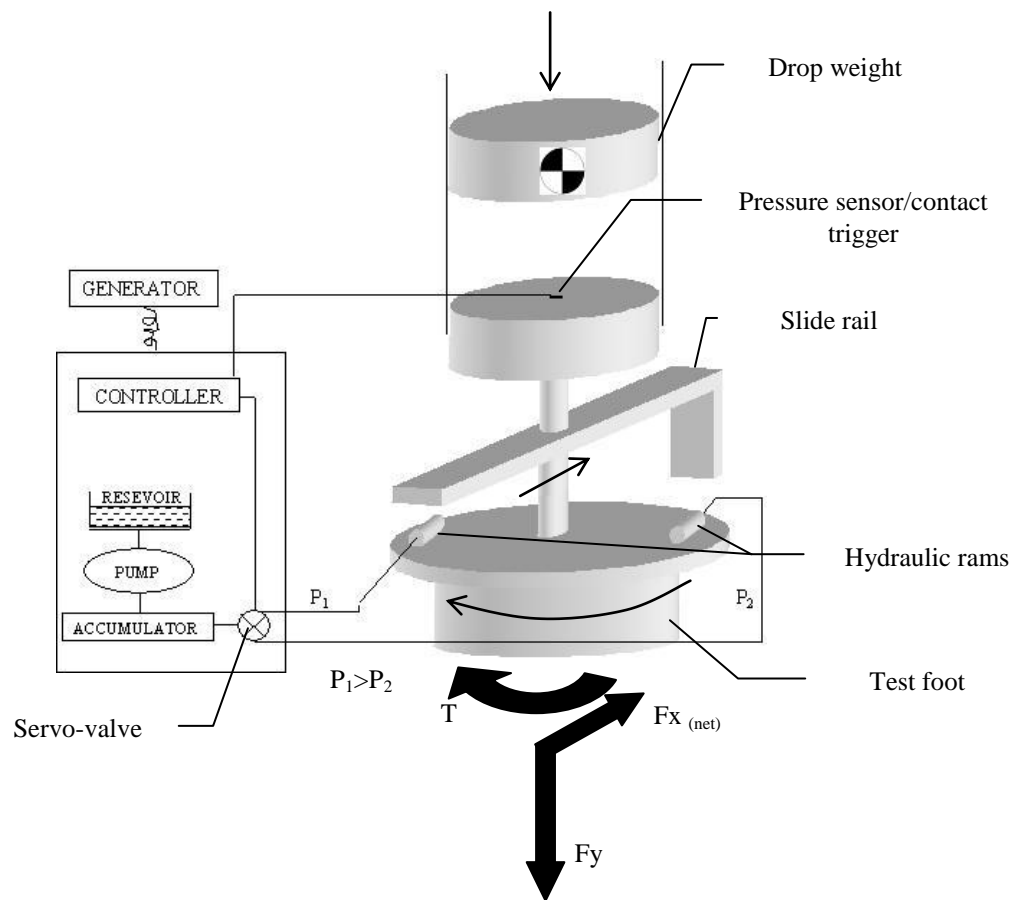


Figure 6.4 Drop weight with hydraulic rams

Observations:

- Vertical force, shear force and torque generated.
- Potentially high shear forces could be generated through hydraulic system.
- Doubtful whether shear force and torque could be generated fast enough following impact of drop weight. May take 0.5 seconds for rams to pressurise fully.
- Hydraulic fluid may be difficult to transport and there could be a potential for spillage onto the sports surface.

6.2.5 Concept E: Multiple drop weights with cable system

Concept: Three independent drop weights are released from a height. One drop weight impacts with the test foot, applying a vertical force. The other two drop weights of different masses, impact with separate L-crank levers. Cables attached to the levers transfer the vertical force into horizontal forces. The other ends of the cables are attached to a circular test foot offset from the vertical axis. This will produce an unbalanced couple imparting a net shear force and torque to the test foot (Figure 6.5).

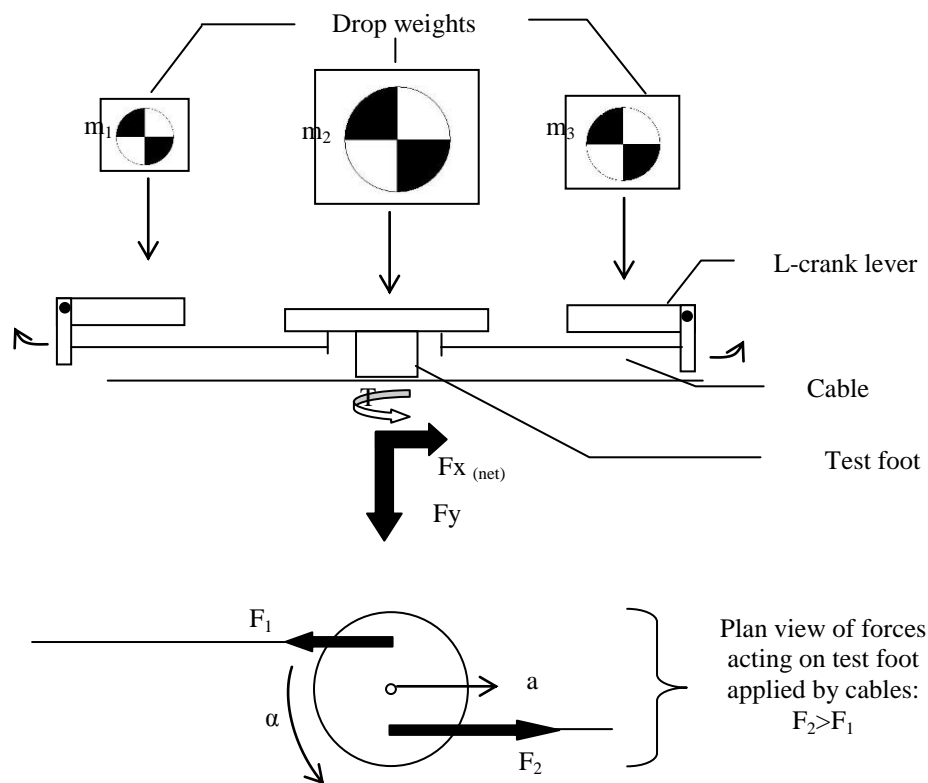


Figure 6.5 Multiple drop-weights with cable system

Observations:

- Force couple is efficient for torque generation
- The release of three drop-weights may be problematical.
- The use of three drop-weights may be excessive and add additional weight to the total rig weight. This would be difficult to use in practice and transport.
- The size of the whole rig to accommodate all parts may be too large.

- Cables would need pretension to ensure that the forces are transferred simultaneously.
- This position of the cable attachments to the test foot can be easily altered to vary the magnitude of torque applied.
- The factors affecting force the magnitude of the applied loads include the mass of the drop-weights, the length of the levers and the attachment of the cables.

6.2.6 Concept F: Multiple drop-weights and lever system

Concept: This is a variation of Concept E. The cables are eliminated and the L-crank levers are turned around. The middle drop-weight applies the vertical force, as before. The other two drop-weights (of unequal mass) impact with L-crank levers, which directly transfer the force to the test foot, horizontally. The unequal horizontal force will produce an unbalanced couple to the test foot, resulting in a net shear force and torque (Figure 6.6).

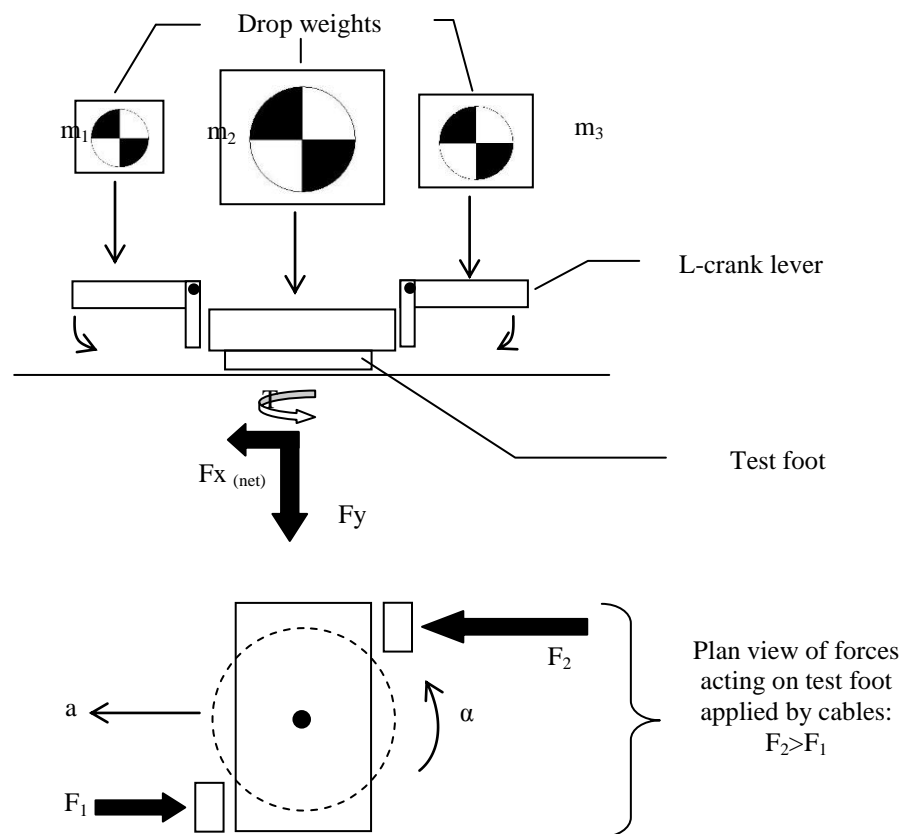


Figure 6.6 Multiple drop-weights with L-crank levers

Observations:

- The level configuration will allow a more compact rig design than Concept E.
- No pretension of cables required, impact timings should be more precise
- Force couple is efficient for torque generation. However, will the net shear force produced be large enough?
- Difficult to vary position of horizontal forces applications in order to vary level of torque. Would have to vary the drop-weight mass.
- The release of three drop-weights may be problematical.
- The use of three-drop weights may be excessive and add additional weight to the total rig weight. This would be difficult to use in practice and transport.
- The factors affecting force the magnitude of the applied loads include the mass of the drop-weights, the length of the levers.

6.3 Strathclyde Sports Turf Testing Rig

6.3.1 Basic concept

The concept chosen as the basis for the Strathclyde Sports Turf Testing Rig (SSTTR) combined the use of pendulums from Concept C and the L-crank lever with cable system Concept E. In this concept, two weighted pendulums, of equal length, are used to load the test foot. If the pendulums are released at the same time, one weighted pendulum impacts a vertical shaft located directly above the test foot to apply a vertical force. The other pendulum strikes an L-crank lever. A cable is attached at the other end of the L-crank lever and with the test foot (attachment offset to vertical axis of rotation) to transfer the force horizontally and apply torque.

The vertical shaft is supported in a block containing a system of bearings that allows unrestricted movement of the test foot in a vertical and rotational direction (rotation around the vertical axis). The block

also contains a system of linear bearings to allow the test foot to move in a horizontal fashion along two parallel, horizontal shafts.

Observations:

- A vertical force, shear force and torque are generated. The loads are applied simultaneously
- The heavy masses can be easily released and winched back up using a pendulum system. A cylinder for a drop-weight to fall within is not required.
- It employs simple mechanical concepts.
- The attachment of the cable can be varied in order to change the magnitude of the applied torque

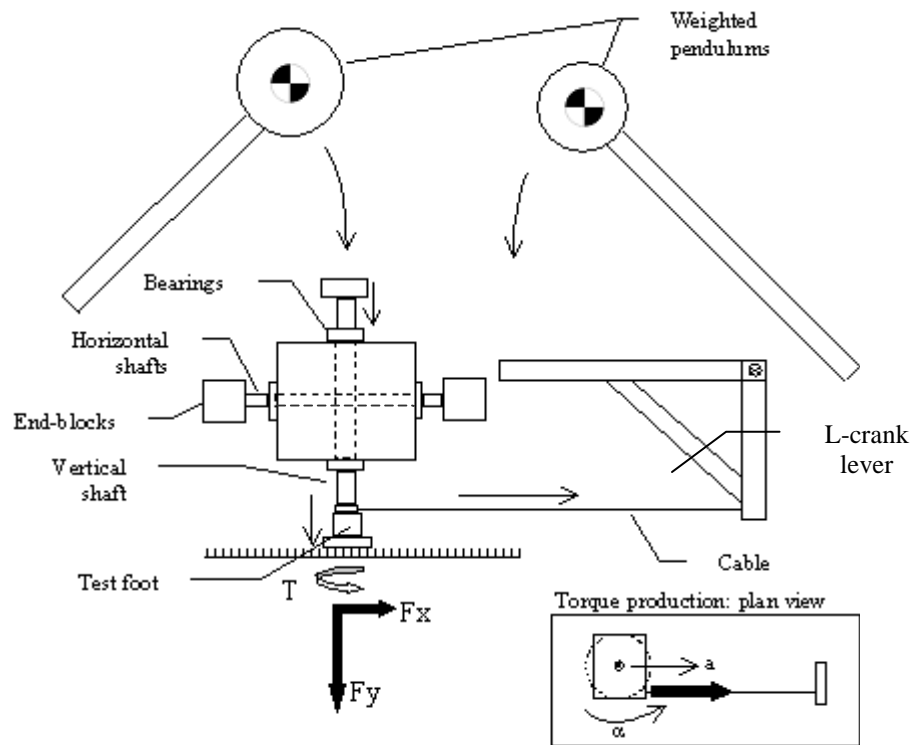


Figure 6.7 Double weighted pendulums with L-crank lever/cable system

6.3.2 Strathclyde Sports Turf Testing Testing Rig Components

Figure 6.7 illustrates the 3D design drawing for the Strathclyde Sports Turf Testing Rig, shown from above and below. The main components of the rig are summarised in Figure 6.8.

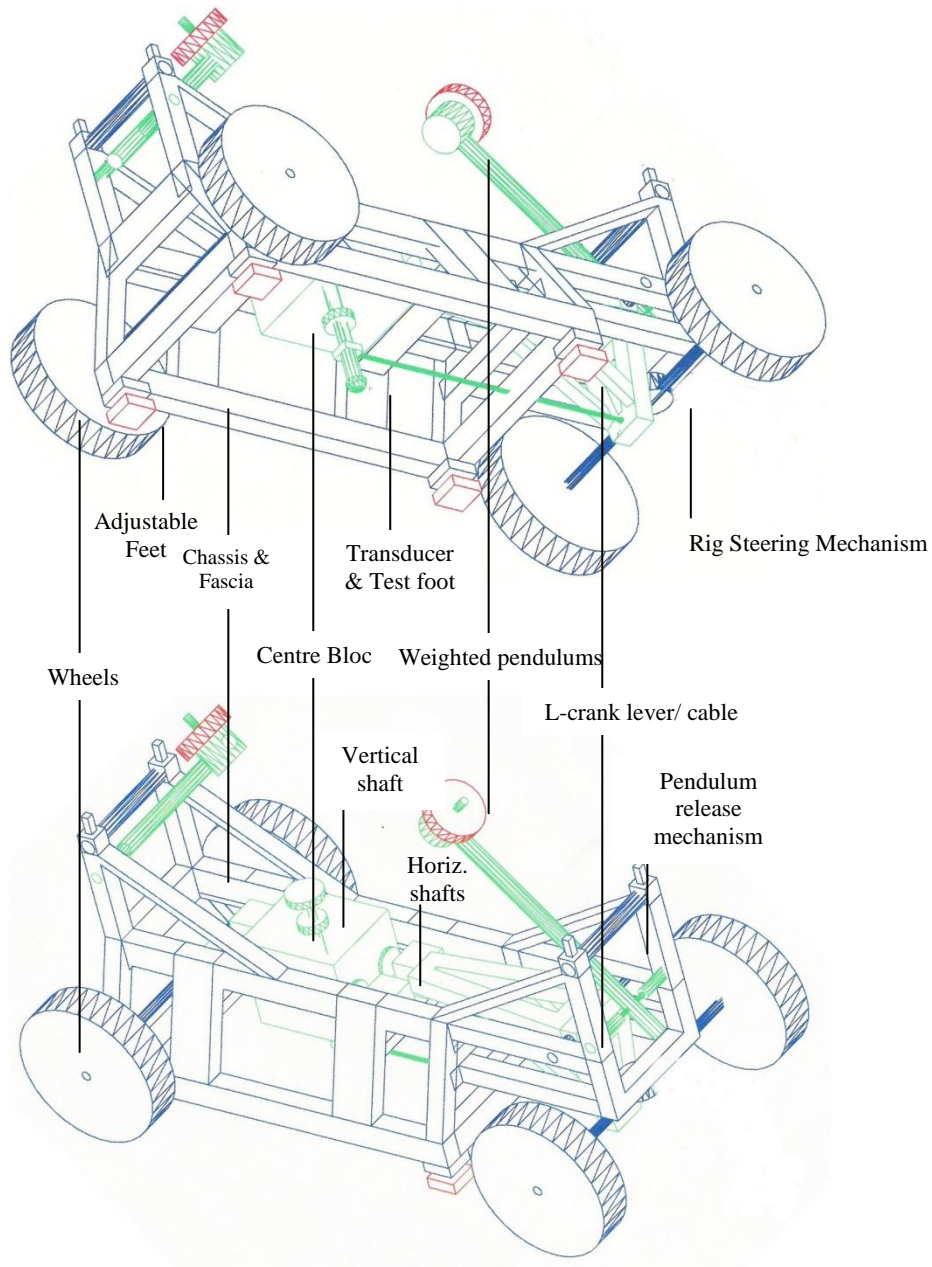


Figure 6.8 3D schematic of SSTTR, from above and below

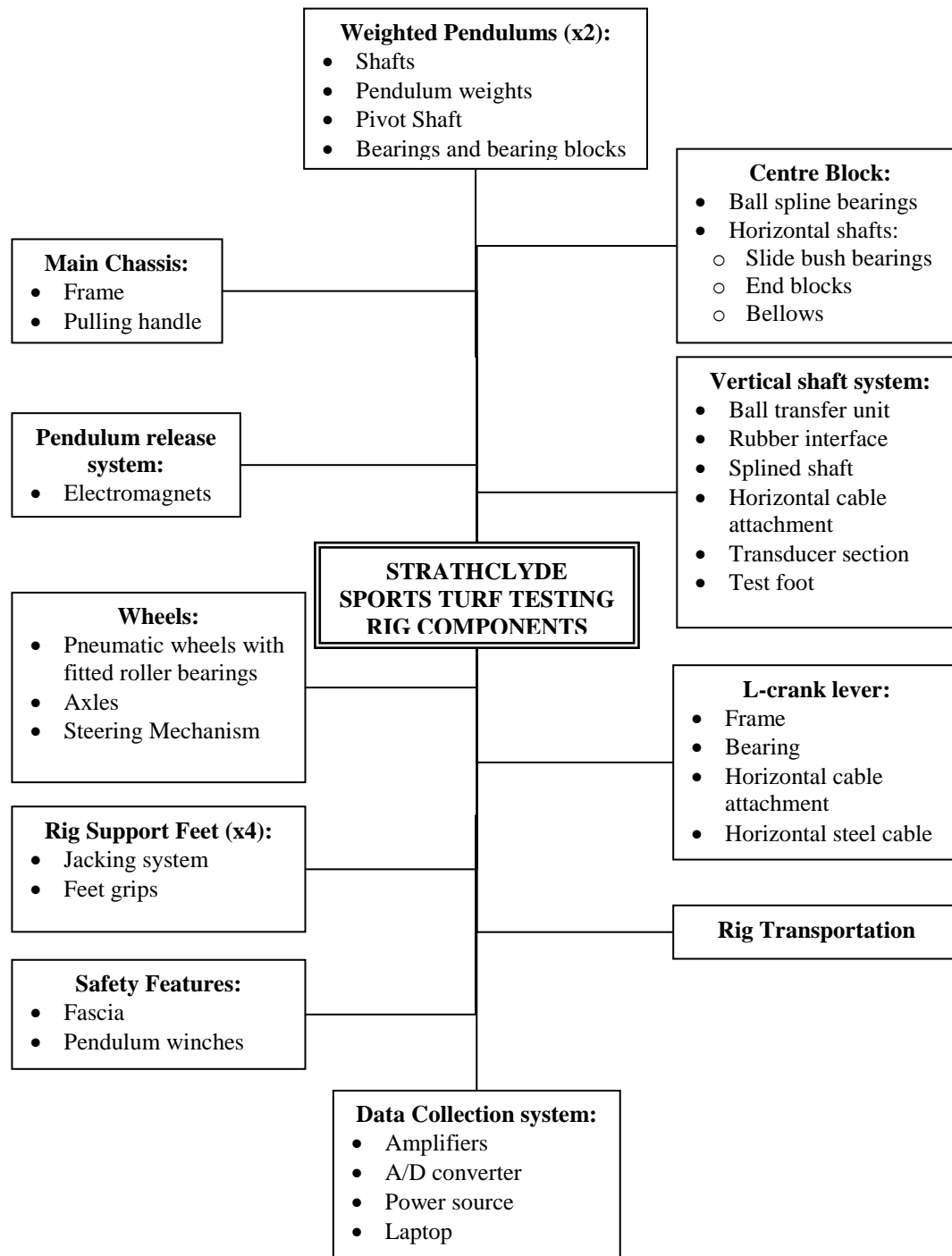


Figure 6.9 Mind map of the SSTTR components

6.3.2.1 Chassis

The main chassis of the rig was constructed of square aluminium tubing. This material allowed the rig to remain rust-free and be relatively lightweight (approximately 80kg in total), which was important when manoeuvring the rig around different locations of a test surface. The rig consisted of 31 individual parts, welded together using aluminium welding techniques. The general dimensions of the chassis were 1500x600x715mm.

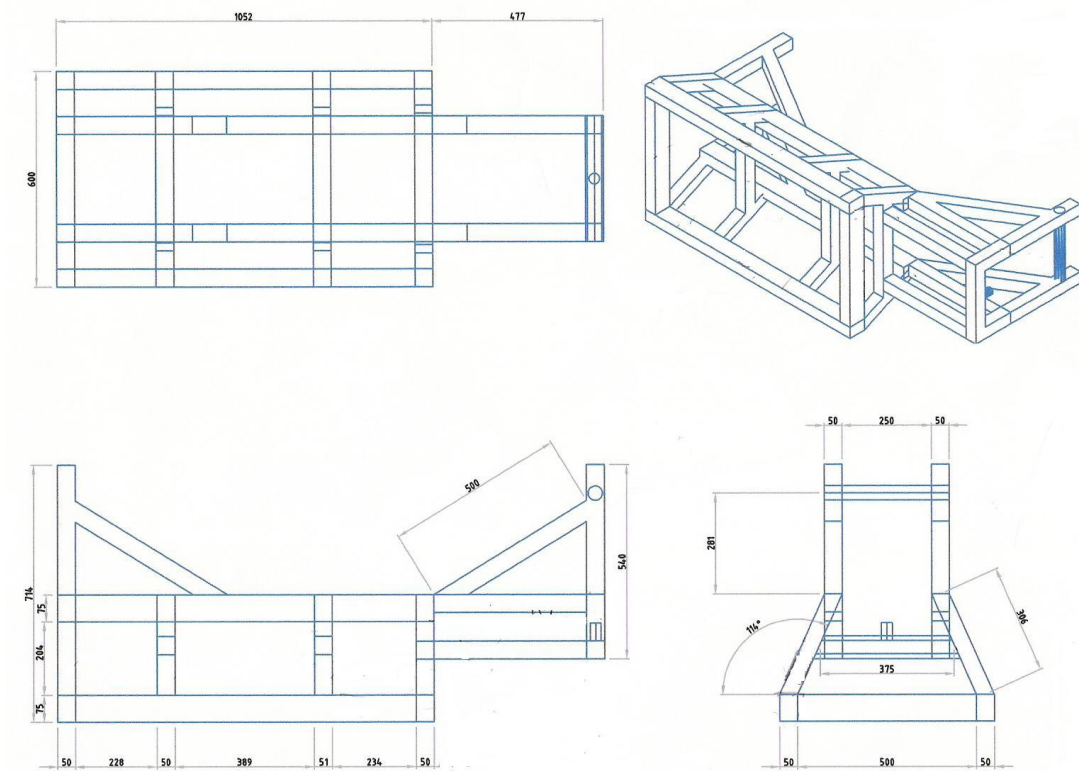


Figure 6.10 Aluminium chassis

6.3.3 Weighted Pendulums

Two weighted pendulums were utilised on the rig. Each weighted pendulum consisted of a pendulum head, shaft and a bearing system (Figure 6.11). The pendulum shafts were constructed from 25mm steel square tubing. The shafts were angled at 45° so that the impact point (i.e. the bottom of the pendulum head) was level with the pendulum's axis of rotation. This ensured that the applied force was as vertical as possible, minimising the effect of any horizontal force components.

The shaft was firmly attached to a perpendicular $\text{Ø}30\text{mm}$ solid steel shaft. The smooth rotation of the pendulum was achieved using $\text{Ø}30\text{mm}$ single row radial bearings, located in bearing blocks at each end of the perpendicular steel shaft.

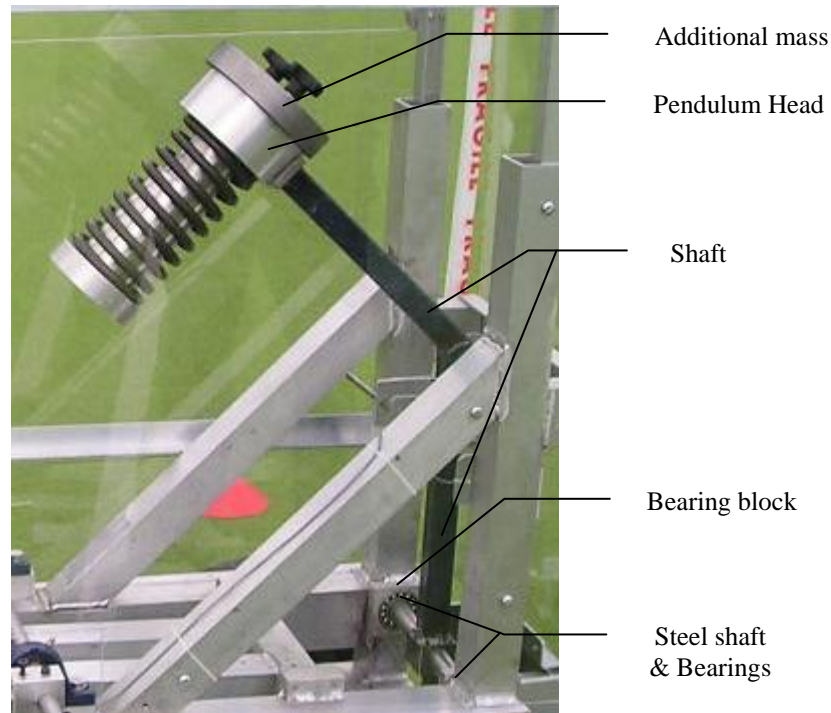


Figure 6.11 Weighted Pendulums

Each of the pendulums was raised using winches and pulleys. The winch was bolted onto the main chassis. A 3mm steel cable with an eyelet at the end was connected to a rod on the back of the pendulum. The cable passed over a small pulley, which was positioned at the same height as the cable connection with the pendulum, and was wound around the pulley.

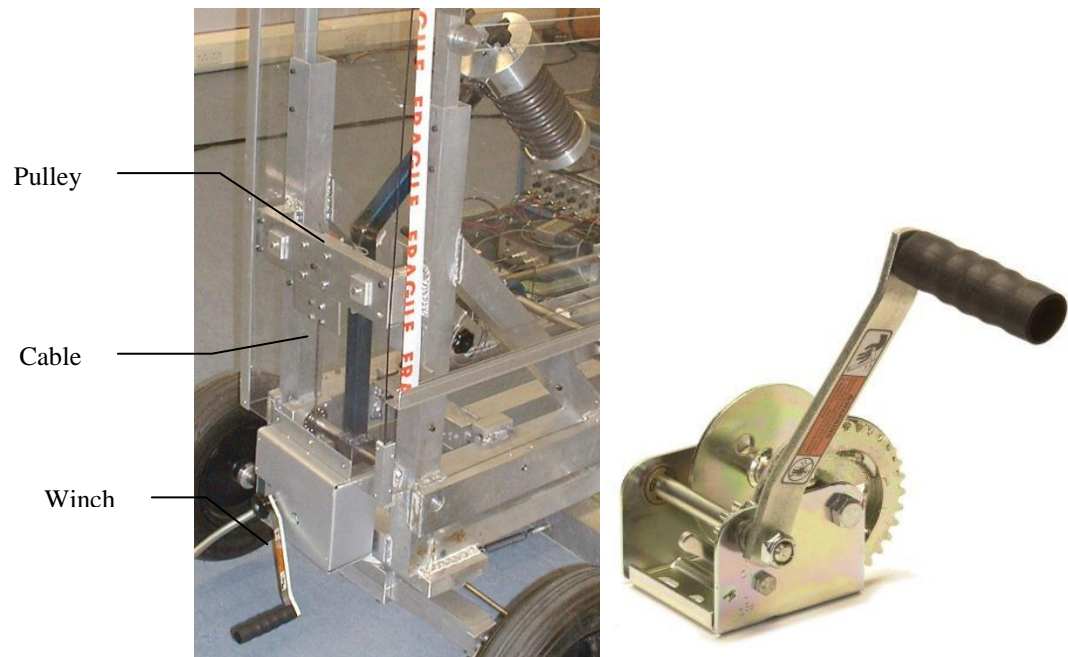


Figure 6.12 Pendulum winch

When the pendulums were released, the cable was unwound from the winch drum, which freely rotated. This prevented any restriction of the natural freefall of the pendulum.

The main components of the pendulum heads consisted of a top section, a middle section that slid inside a lower section, a spring and an additional mass (Figure 6.13). The spring–piston design of the pendulum head allowed a controlled loading rate following impact. Following the release of the pendulum, the lower section of the pendulum head was the point of impact. The change in momentum of the heavy top section of the pendulum head provided the majority of the load transferred to the test foot. As the fillet part of the top section slid inside the lower section, the spring acted to control the loading rate and retard the momentum of the top section.

The mass of the lower section was kept as low as possible in order that the effective mass applying the significant load was contributed by the mass of the top section. The forces applied by the pendulums could be increased by fastening additional masses to the pendulum heads by locating them on two bolts protruding from the upper surface of the top section.

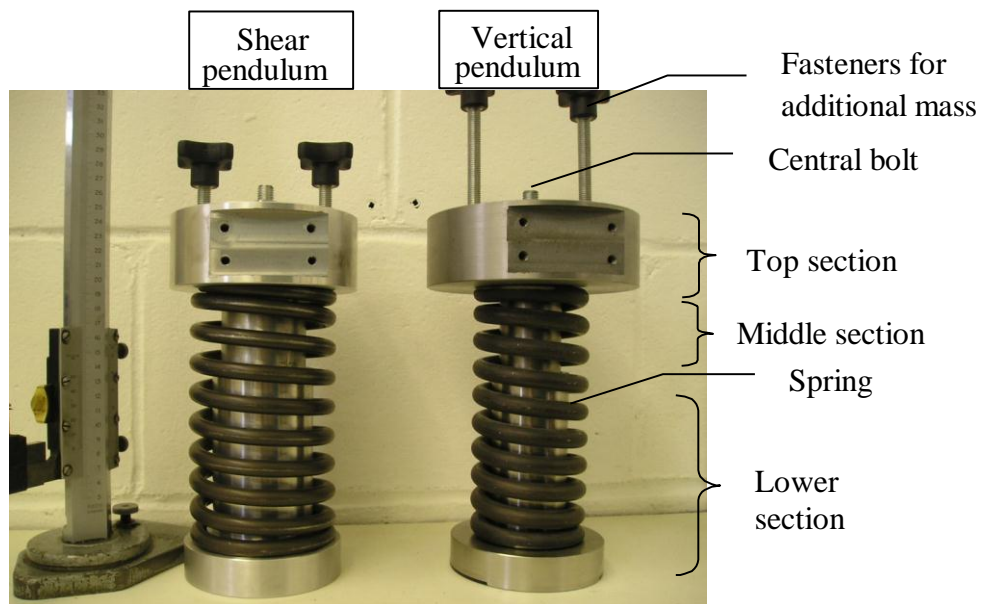


Figure 6.13 Pendulum heads

The middle section was bolted to the top section. A locked nut at the top of the central bolt, which passed right through the middle of the pendulum head complex, prevented the top section and lower section from coming apart.

The two pendulums had pendulum heads of different masses. The pendulum that applied a vertical force to the test foot will be referred to as the ‘vertical pendulum’. The pendulum that applied a force resulting in a horizontally applied force to the test foot will be referred to as the ‘shear pendulum’. The mass of the vertical pendulum was greater than the mass of the shear pendulum due to the larger forces that were applied vertically.

The dimensions of each pendulum head were primarily governed by the specification of the springs that were purchased. The type of springs and the calculation of the required spring constants for each pendulum head are described in Section 6.3.3.1. The springs in each pendulum head was initially compressed by 2mm.

The effective mass of the vertical pendulum head (not including the additional mass) was approximately 14kg. The top section ($\text{Ø}150\text{mm} \times 50\text{mm}$) of was constructed from mild steel, in order to permit a high mass within reasonable dimensions. The middle section ($\text{Ø}44\text{mm} \times 113\text{mm}$) and the lower

section ($\text{Ø}110\text{mm} \times 25\text{mm}$) were both constructed of stainless steel to allow a smooth piston operation.

An additional 11kg mass ($\text{Ø}150\text{mm} \times 80\text{mm}$) was manufactured out of mild steel. Two bolt holes were produced in order that the additional mass could be located on the top section of the pendulum head and fastened down with knobs. A centre hole was also produced through the additional mass to allow the passage of the centre bolt through it as the spring-piston complex deflected following impact.

The shear pendulum was manufactured entirely from aluminium. This reduced its effective mass to approximately 3.5kg. The basic dimensions were as follows: top section ($\text{Ø}130\text{mm} \times 50\text{mm}$), middle section ($\text{Ø}59\text{mm} \times 113\text{mm}$) and lower section ($\text{Ø}110\text{mm} \times 25\text{mm}$).

As with the vertical pendulum, an additional mass could be attached to the shear pendulum to increase the load transferred to the test foot. A section of mild steel ($\text{Ø}150\text{mm} \times 25\text{mm}$) was manufactured, which could increase the effective mass of the shear pendulum by 3.1kg.

6.3.3.1 *Analysis of pendulum mechanics*

In order to generate a series of tests that encompassed the range of forces applied by a player during various sports movements, an iterative process, using an analysis of simple harmonic motion and the principle of energy conservation, was conducted to calculate the masses of the pendulums, the drop heights and spring constants required to apply the appropriate loading profiles.

In the following, the pendulum is defined as a simple pendulum and ignores the small relative mass of the pendulum shaft.

It was suggested that the applied loads should reflect the ‘top end’ of ground loadings during a player surface interaction (Shorten, 2002). Therefore, the upper quartile of ground loadings measured during the biomechanical tests was used as the input for the test rig instead of the mean values.

As described in the analysis of the ground reaction forces in the biomechanical tests, the different sports movements could be grouped into high, medium and low dynamic movements, according to the

magnitudes of the ground loadings. This information was used to define the magnitude of the loads to be generated and applied to the test foot by the rig (Table 6.2).

Group	Movements	Required Loads (approximate)		
		Vertical (N)	Shear (N)	Torque (Nm)
High	Stopping, Kicking, Heading	3500	1600	15-25
Medium	Running, Turning	2400	1300	20-35
Low	Walking, Hockey Hit	1200	500	6-20

Table 6.2 Approximate loads to be applied by the turf testing rig

The deflection-extension cycle of a fixed spring under loading can be described simple harmonic motion. Following impact, the spring located on the pendulum head was compressed as a result of the mass of the pendulum. The compression of the spring, from a starting spring length to the maximum compression was described as a quarter of the spring's full compression-extension cycle (Figure 6.14).

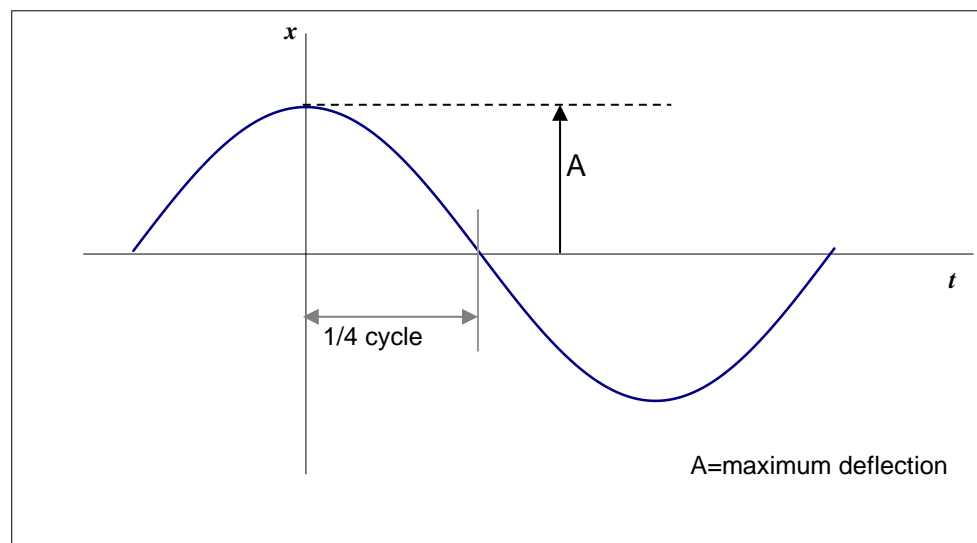


Figure 6.14 Displacement (spring deflection) versus time in simple harmonic motion

The motion of the pendulum head spring can be described as follows:

$$x = A\cos(\omega t) \quad [\text{Eq 6.1}]$$

$$v = \frac{dx}{dt} = -A\omega\sin(\omega t) \quad [\text{Eq 6.2}]$$

$$a = \frac{d^2x}{dt^2} = -Aw^2 \cos(wt) \quad [\text{Eq 6.3}]$$

where:

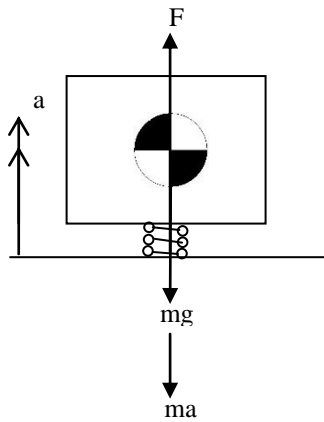
A = amplitude of deflection (m); w = angular velocity (rads^{-1}); t = time (s)

The time (t_f) taken from the moment of impact of the pendulum head to when the applied force reaches a peak value is one quarter of the *period time* (t_p) of simple harmonic motion for the spring to complete one full compression-extension oscillation.

$$t_p = 4 \times t_f \quad [\text{Eq. 6.4}]$$

$$1 \text{ cycle} = 2\pi \text{ rads in } t_p \quad [\text{Eq. 6.5}]$$

Therefore: $w = \frac{2\pi}{t_p} \text{ rad.s}^{-1} \quad [\text{Eq. 6.6}]$



This illustrates the impact of the pendulum head and the maximum compression of the spring. At the extremes of simple harmonic motion, the acceleration (a) of the mass (m) is directed towards the midpoint of its motion.

$$F = mg + ma \quad [\text{Eq. 6.7}]$$

$$a = \frac{F - mg}{m} \quad [\text{Eq. 6.8}]$$

where:

F =force applied by the pendulum head; m =mass of the pendulum head

At the peak force (F_{\max}) applied by the pendulum, the spring compression is at its maximum (A_{\max}) and time (t) = 0. Therefore, using the approximate required peak loads to be applied from Table 6.2, the compression of the spring was calculated by:

$$\frac{F_{\max} - mg}{m} = -A_{\max} \omega^2 \times 1$$

$$A_{\max} = \frac{F_{\max} - mg}{m\omega^2} \quad [\text{Eq. 6.9}]$$

Subsequently, the required spring stiffness or constant (k) for the pendulum head was calculated by:

$$k = \frac{F_{\max}}{A_{\max}} \quad (\text{N}\cdot\text{m}^{-1}) \quad [\text{Eq. 6.10}]$$

For any given peak force, pendulum head mass, time to peak force and calculated maximum spring deflection, the height that the pendulum needs to be released from was calculated by:

$$v_{\max} = A\omega \quad [\text{Eq. 6.11}]$$

$$\frac{1}{2}mv^2 = mgh$$

$$\text{Therefore: } h = \frac{\frac{1}{2}(A\omega)^2}{g} \quad [\text{Eq. 6.12}]$$

It is noted that the above is a simple model of pendulum mechanics and ignores rotational inertia. An iterative process was conducted using an Excel spreadsheet to calculate maximum spring deflections, spring constants and pendulum release heights from defined peak forces required to be applied by the pendulum, pendulum head masses and times to peak forces. The required peak forces were 3500N and 2400N for the vertical pendulum, and 1100N and 900N for the shear pendulum. Due to the L-crank lever configuration (see Section 6.3.8), these vertical forces applied by the shear pendulum were transferred horizontally to

apply approximately 1600N and 1300N to the test foot, respectively.

A suitable spring constant value was selected for each pendulum. This value ensured that both of the required peak loads could be applied using a reasonable mass within an appropriate time frame for the vertical and horizontally pendulum, respectively.

The spring constant for the vertical and horizontal pendulums was 90kNm^{-1} and 25kNm^{-1} , respectively. The iterative process was reversed in order to calculate the exact pendulum head masses required, using these spring constants and a defined release height of 0.354m (Table 6.3). The effective length of the pendulum shaft was 0.5m. If it is released from a 45° angle, the release height = $0.5 \sin 45^\circ = 0.354\text{m}$.

It is noted that the ‘load pulse times’ or times to the peak loading were somewhat shorter than what was set out in the design objectives to mimic the player-surface loadings (times to peak=25-50 msec). However, given the constraints of the springs (and spring constants) available when sourcing materials for the rig construction, it was felt that the calculated time to peak loads was not unreasonable. It was also expected that friction between the two sections of the pendulum would contribute to the pendulum’s ‘stiffness’ and further delay the time to peak load.

Pendulum	Required Force (N)	Spring Constant (k)	Deflection (m)	Height (m)	Velocity (ms^{-1})	Mass (kg)	Angular Velocity (rads^{-1})	Time to Peak (s)
Vertical	3500	90826	0.039	0.354	2.636	25.00	65.47	0.024
Vertical	2400	90826	0.026	0.354	2.636	14.80	94.32	0.017
Shear	1100	25001	0.044	0.354	2.636	6.50	60.19	0.026
Shear	900	25001	0.036	0.354	2.636	3.40	84.15	0.019

Table 6.3 Pendulum mechanics

The calculated masses were used as the criteria for the design of the pendulum masses.

6.3.4 Pendulum release mechanism

For the multi-directional loads to be applied to a surface during the same interval of time, the pendulums must impact at the same time. Therefore, the pendulums were required to be released simultaneously and fall under the force of gravity. A permanent holding GMP magnet with D.C. electromagnet release (*Emessen*

Solenoid Company, Surrey, UK) was utilised for each pendulum. The Ø50mm magnets held a permanent magnetic force with a nickel armature plate fixed in the back of each pendulum, until the magnets was electrically triggered simultaneously with the same 24V supply voltage. The electrical impulse was provided by 2x12V batteries.



Figure 6.15 Electromagnet

The magnets had a maximum holding force of 435N at 0mm air gap between the magnet and armature plate. For the purposes of safety, a safety factor of 4 was used to calculate a maximum holding load of 109N.

Following an electrical impulse, the magnet retained a residual holding force of 70N with a 0mm air gap between the magnet and armature plate. However, the magnet and armature plate would have to be perfectly aligned to achieve a 0mm air gap. It was agreed that this was not practically possible during the normal operation of the rig. It was assumed that a very small air gap would be present when the pendulums are repeatedly released and then raised by the winches.

Figure 6.16 shows the results of an experiment conducted on an Instron testing machine to measure the effect of the air gap on the magnet's holding force. The presence of an air gap had a significant effect on the holding force of the magnet. Assuming that an air gap may be present, the position of the armature plate on the elbow of the pendulum shaft (on the lower section of the shaft) was calculated to minimise the load to be held by the magnet during a non-energised state. With a 20kg pendulum mass, the holding load on the

magnet was 76N.

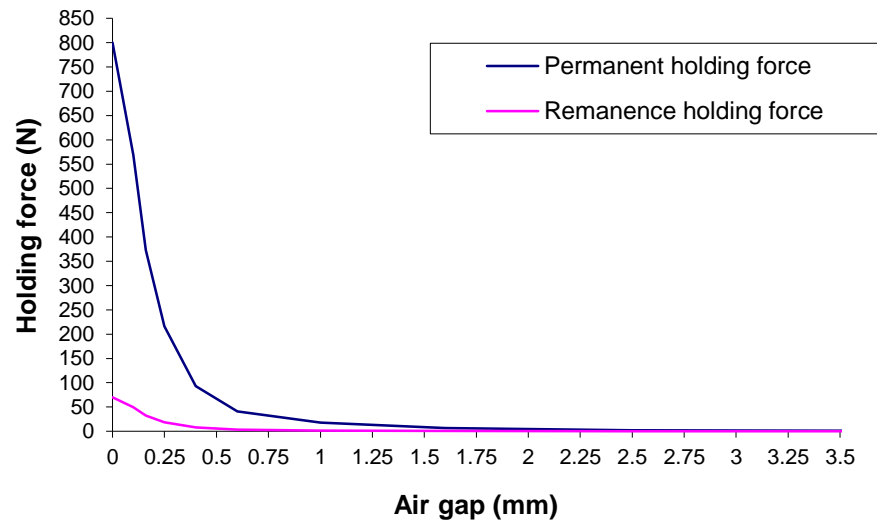


Figure 6.16 Instron test results examining the effect of the air gap on magnetic holding force

6.3.5 Centre Block

The Centre Block was a main component of the rig. The main function of this component was to encapsulate a system of bearings that permitted the three degrees of freedom of the test foot as a result of the loads applied to it. The Centre Block was manufactured from a single piece of aluminium and represented a cross shape. The general outer dimensions of the block were 290x290x250mm (Figure 6.17). Three bore holes were manufactured out of the block. One was for the vertical shaft and bearings. This was situated through the centre of the block running top to bottom. The other two shafts holes ran perpendicular to the vertical shaft hole and parallel to each other. Horizontal shafts and bearings were located in these bore holes.

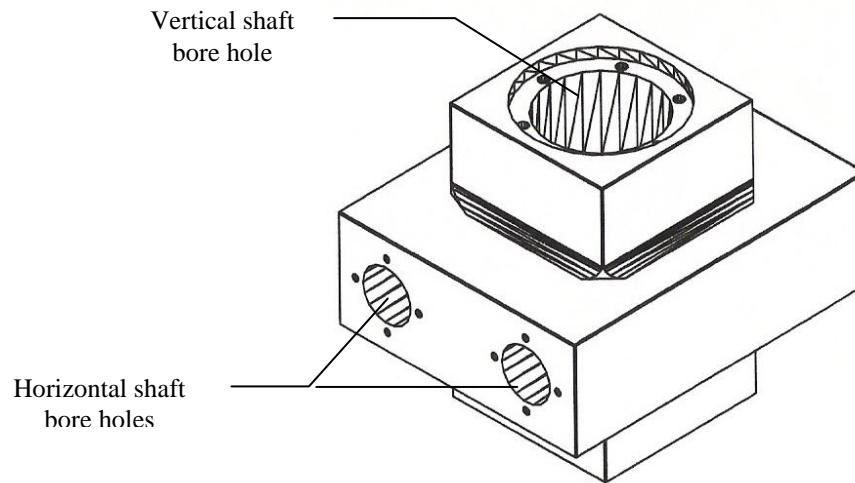


Figure 6.17 Schematic of centre block

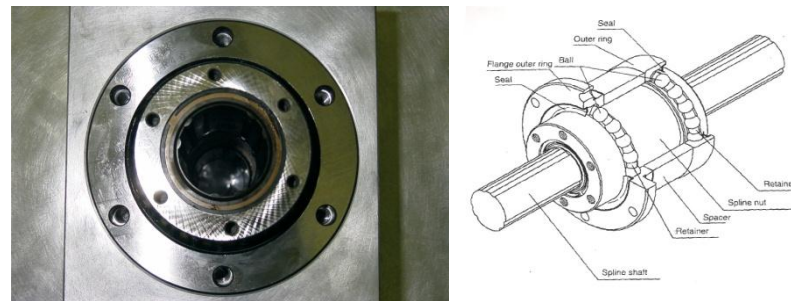


Figure 6.18 Rotary Spline Bearing

A rotary spline bearing was located at either end of the vertical shaft bore hole. The configuration of this bearing allowed the vertical movement of the shaft, in addition to rotation of the shaft around the vertical axis. The bearings were sealed to prevent any foreign matter entering the bearing.

Linear bearings permitted the centre block (viz. test foot) to move in a horizontal direction along two parallel steel shafts (Figure 6.19). The length of the steel shafts allowed an approximate 60mm horizontal displacement of the test foot. A bearing was placed at either side of the centre block for each steel shaft. Shaft end blocks secured the steel shafts in place to the rig. Rubber bellows were used to protect the shafts and bearings from dirt particles.

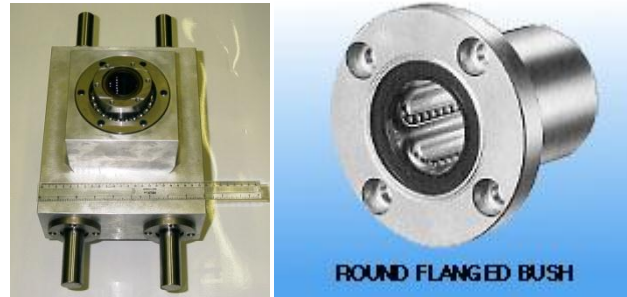


Figure 6.19 Linear bush bearings for the horizontal shafts

6.3.6 Vertical shaft system

The function of the vertical shaft system was to transfer the vertical force applied by the ‘vertical’ pendulum to the test foot positioned on the surface to be tested. A transducer was also located on the vertical shaft to measure the applied loads and the acceleration of the test foot.

As can be seen from Figure 6.20, the vertical shaft system consisted of six main components: a ball transfer unit, a rubber interface, a splined steel shaft, a horizontal cable attachment, a transducer and a test foot.

6.3.6.1 *Ball Transfer Unit*

The ball transfer unit (BTU) transferred the load applied by the ‘vertical’ pendulum to the shaft. The heavy duty BTU had a load capacity of approximately 10kN. The ball configuration of this component maximised the transference of the vertical load from the pendulum and allowed the vertical shaft to move horizontally and rotationally, even under high vertical loading. The BTU was screwed into the top of the vertical shaft.

6.3.6.2 *Rubber Interface*

A rubber interface was used to minimise the very high frequency transient shock caused by the metal on metal impact of the ‘vertical’ pendulum striking the steel ball of the BTU. A 76x76x10mm piece of neoprene padding, with a shore hardness of 60 Duro, was used.

6.3.6.3 Splined shaft

The shaft consisted of a $\text{Ø}40\text{mm} \times 430\text{mm}$ splined steel shaft. The spline worked in conjunction with the rotary bearings to enable the shaft and test foot to move vertical and rotate at the same time.

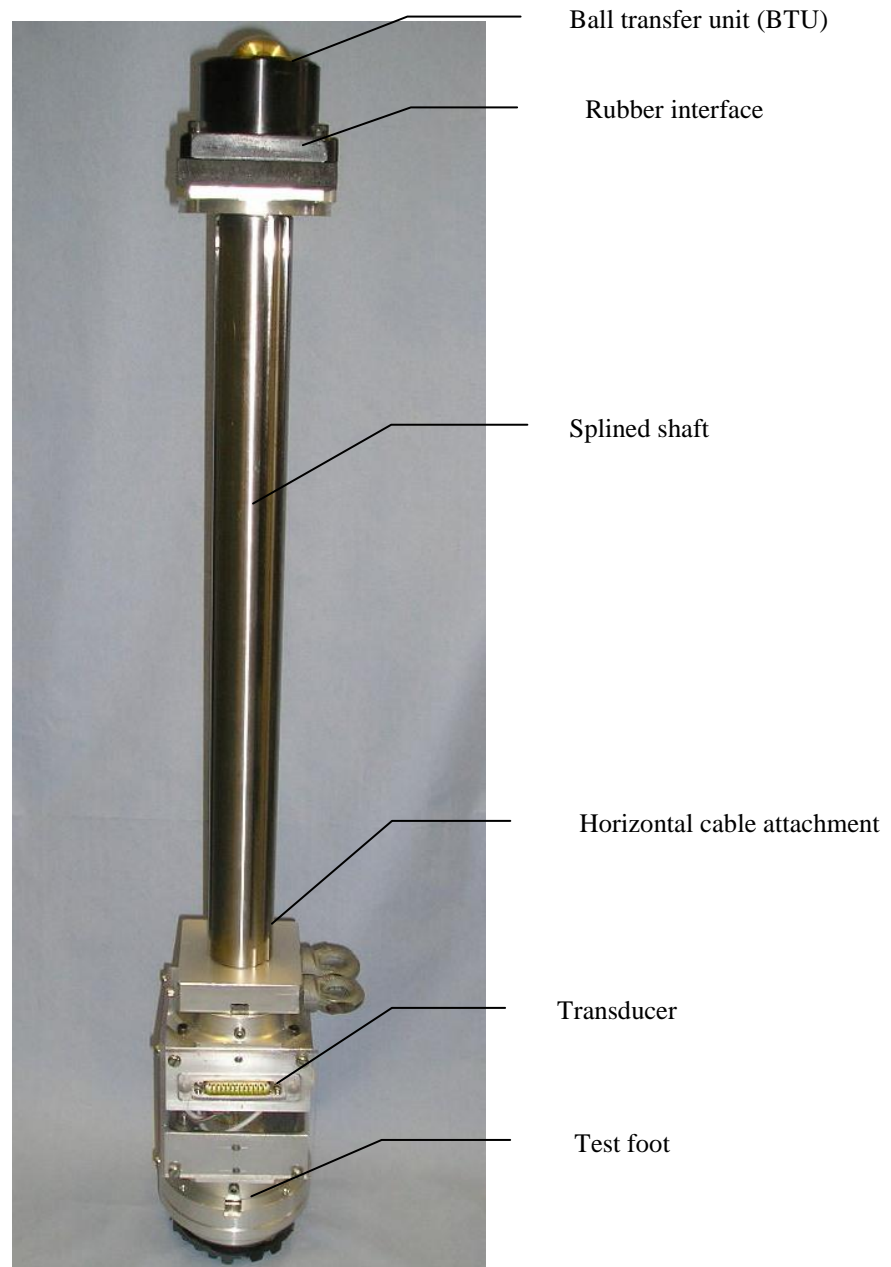


Figure 6.20 Vertical shaft system

6.3.6.4 *Horizontal Cable Attachment Block*

A horizontal cable attachment block was positioned at the end of the splined shaft. This allowed a stainless steel cable to be attached to the vertical shaft. This attachment block consisted of two eyebolts screwed into an aluminium block. One eyebolt was positioned along the vertical axis of the vertical shaft. This was referred to as eyebolt A. The attachment of the cable to this eyebolt using a thimble eye ensured that only a horizontal load was transferred to the test foot.

The centre of the second eyebolt was offset 30mm to the side of the vertical axis of the vertical shaft. This was referred to as eyebolt B. The attachment of the cable to this eyebolt allowed a horizontal force plus a torque to be applied to the test foot.



Figure 6.21 Horizontal cable attachment block

6.3.6.5 *Transducer Section*

The transducer section was located just above the test foot. The vertical shaft was screwed into this transducer section, securing the horizontal cable attachment block in place. The transducer section consisted of a 4- channel pylon force transducer and a complex of three accelerometers attached within an aluminium housing (Figure 6.22). The 4 channels of the transducer corresponded to the measurement of a vertical force,

2 perpendicular horizontal forces and torsional moment (around the vertical axis).

One of the accelerometers corresponded to the measurement of a vertical acceleration. The placement of the other two accelerometers allowed the measurement of a horizontal acceleration and an angular acceleration around the vertical axis. The output of the transducer was relayed to an amplification and data collection system through a D-connector located on the housing of the transducer.

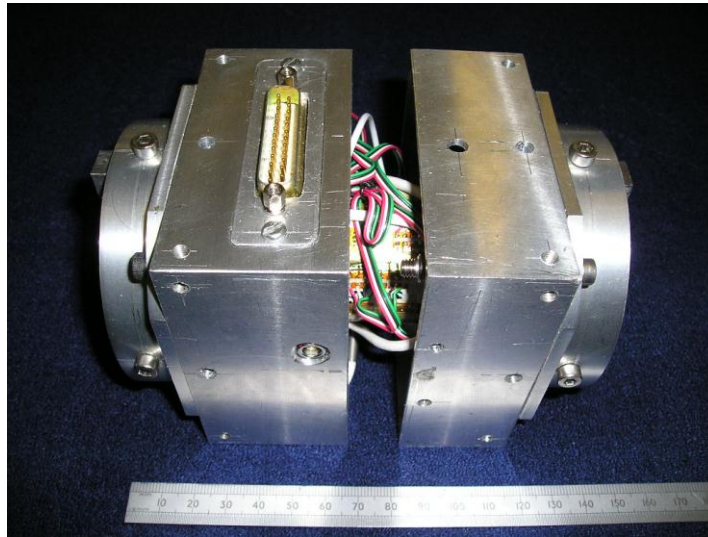


Figure 6.22 Instrumented transducer

The pylon transducer was previously developed in a study by Runciman and Nicol (1993), in which the transducer specifications are described in detail. During loading, strain deformation of strain gauges located on the pylon produced an electrical output, from which a calculation of the applied load can be conducted.

The original pylon transducer consisted of a series of 16 foil electrical resistance type strain gauges, arranged in two rows around the pylon circumference, forming 6 channels. The configuration of each channel consisted of a full wheatstone bridge. The channels corresponded to the loads applied through the pylon transducer in all 6 degrees of freedom: F_x , F_y , F_z , M_x , M_y , M_z . The current study only required the three forces and one moment around the vertical axis (M_y) to be measured (Figure 6.23). Therefore, the cabling of the pylon transducer was modified to only include the output of the required channels. This also freed up available pins on the D-connector for the output of two of the accelerometers.

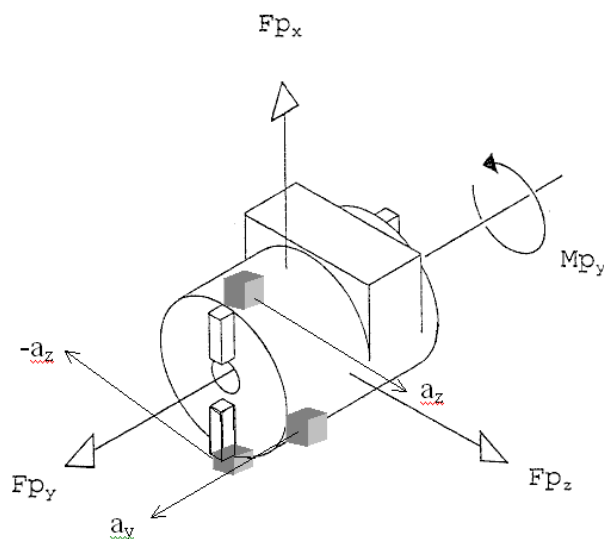


Figure 6.23 Instrumented pylon transducer with positive loading conventions shown. These are positive as applied by the transducer to the test foot. Three accelerometers are also shown in place

The range of the two EGCS accelerometers (*Entran, Herts, UK*) that measured horizontal acceleration (a_z) was $\pm 50g$. They had a sensitivity of $4mV/g$ and a frequency response of 0 to 600Hz. These were the same accelerometers that were used during the biomechanical testing. Vertical acceleration (a_y) was measured with a $\pm 100g$ 8704B K-shear accelerometer (*Kistler, Winterthur, Switzerland*). This accelerometer's sensitivity was $50mV/g$ and had a frequency response of 0.6 to 9000Hz.

Each accelerometer was securely fixed onto the inside of the transducers aluminium housing using mounting studs that were tightened to a mounting torque of 2Nm, as per manufacturer's specifications. The two $\pm 50g$ accelerometers were positioned directly opposite of each other on the vertical midline of the transducer, so that their sensitive axes were parallel with the horizontal z-axis of the transducer. The $\pm 100g$ accelerometer was positioned so that its sensitive axis was parallel with the vertical axis of the transducer.

6.3.7 Test Foot

The SSTTR was to be employed on a variety of surfaces, natural and artificial. Players wear different types of footwear, which are suitable to the surface to be played on. In general, players who perform on grass or longer pile surfaces tend to wear studded (cleated) footwear. Players who perform on shorter pile, artificial

surfaces, for example hockey players, tend to wear footwear with pimples soles.

For the test rig to be adaptable to many types of surfaces, the test foot utilised during an assessment of the surface must represent the type of footwear players actually wear on that surface. Following discussion with the subjects who participated in the biomechanical assessment, it was decided that two types of test foot would be manufactured for the initial design of the test rig.

For the assessment of grass or longer pile surfaces, a studded test foot was used. For the assessment of the shorter pile, artificial surfaces a pimpled test foot was used (Figure 6.24). The studded test foot consisted of 4 standard plastics studs of height 13 ± 1 mm, equally positioned at a distance of 30mm from the centre of the test foot. The configuration of the studs was such to replicate the stud position found on the midfoot (metatarsals) section of conventional studded footwear. For the purposes of this study, a conventional football boot was used to base the stud configuration.

An additional 4 holes were tapped into the test foot at an equal distance of 20mm from the centre. This was to allow a different configuration of studs to be used, if required.

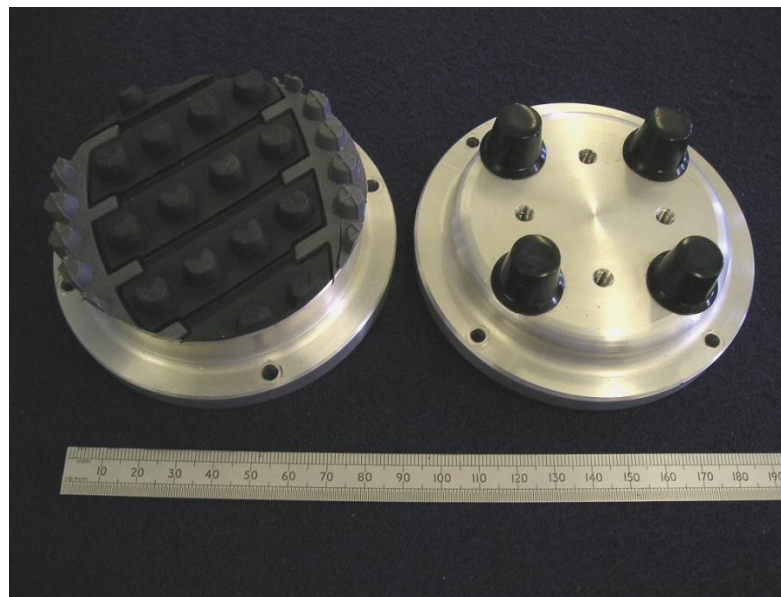


Figure 6.24 Test feet: pimpled (left) and studded (right)

The pimpled test foot consisted of a $\text{Ø}60$ mm diameter, 11 ± 1 mm thick piece of pimpled rubber. The pimpled rubber was obtained from the midfoot (metatarsal) region of an UK size 10 *Adidas Bracara TF* artificial turf

sports shoe sole.

The effective contact area of both test feet approximate the midfoot (metatarsal) region of a UK size ten foot. The midfoot (metatarsal) region was selected as it is recognised that foot strike patterns change from being predominantly rear-foot to predominantly midfoot strikers at higher running speeds (Keller *et al.*, 1996). As the the SSTTR was designed to mimic high impact and highly dynamic movements, it was felt that the area of the midfoot region would be an appropriate contact area for the test foot.

The edges of the test feet were rounded so that no sharp edges were present that could damage any test surface. The test feet were bolted into the bottom part of the transducer section.

6.3.8 L-crank lever system

The L-crank lever system allowed the vertical force that is applied by the ‘shear’ pendulum to be transferred horizontally to the test foot. Eleven pieces of 50x50mm aluminium tubing was welded together to construct the L-crank lever (Figure 6.25). With a longer lever arm at the pendulum contact side, the lever arms of the crank were designed to efficiently transfer the horizontal force to the test foot.

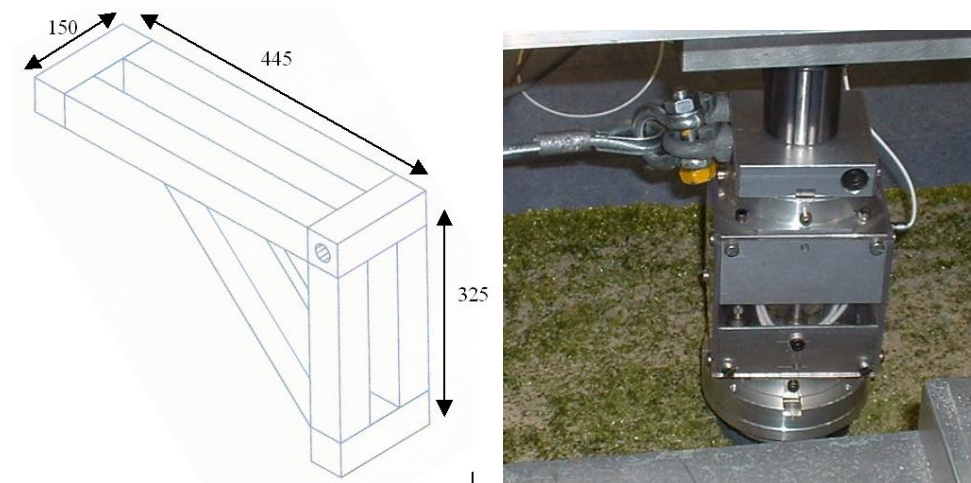


Figure 6.25 L-crank lever (left) and steel cable attachment to the vertical shaft (right)

A Ø25mm steel shaft was fixed in a shaft hole in the corner of the L-crank lever. This allowed the lever to rotate within Ø30mm single row radial bearings placed either end of the shaft. The bearings were held in

place with bearing blocks, which were welded to the main chassis.

A Ø4mm x 750mm stainless steel cable (1x19, SWL: 3kN) was attached to an eye-bolt at the lower section of the L-crank lever, using a rigging screw. The other end of the cable was attached to the eyebolts screwed into the cable attachment block via a thimble and a bow shackle. The cable could be attached to either eyebolt on the cable attachment block to vary the amount of torque applied to the test foot by using the bow shackle. The heights of the attachment points at either end of the steel cable were equal to ensure that the cable was horizontal. A spring was attached to the back of the bottom section of the L-crank lever to the main chassis to apply a small amount of pretension to the steel cable. This was done to maximise the rigidity of the L-crank lever system.

6.3.9 Rig Support Feet

Due to the highly dynamic nature of the testing process, the rig was required to have a stable base for its operation. Also, due to the size of the test feet and transducer heights, the whole rig was required to be raised to ensure that the steel cable was kept horizontal. Therefore, the rig was designed with four support feet that could jack the rig up so that wheels were 55mm off the ground.

Figure 6.26 displays the rig support feet *in situ* and also in isolation to show their design more clearly. Each support consisted of two aluminium bars connected with a simple hinge joint with sintered “Oilite” bearings. The lower section of the support leg passed through within an aluminium block, which was bolted onto the main chassis. The block guided the vertical movement of the lower section of the support leg. A 80x80x25mm solid piece of aluminium, which formed the support foot, was welded to the bottom of the lower section. A 3mm thick piece of ridged rubber was stuck to the bottom of the support foot to provide a protective interface between the rig and the surface.

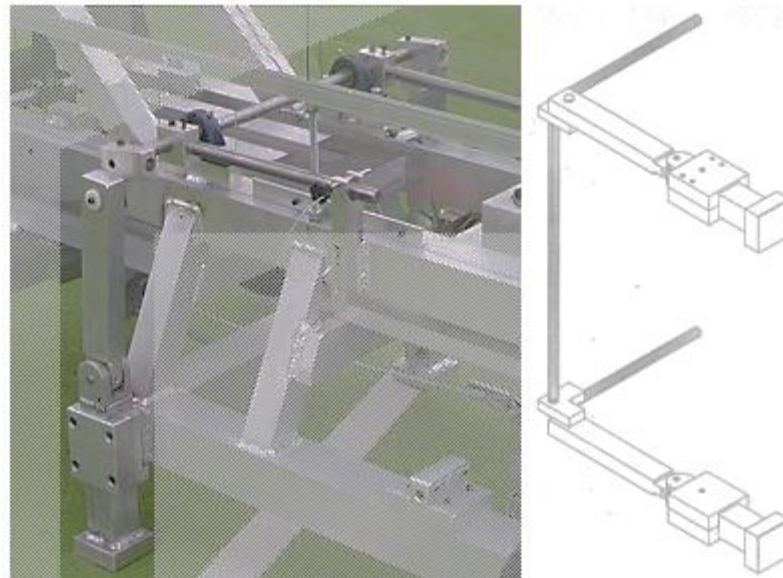


Figure 6.26 Rig support feet

The support feet were raised and lowered by rotating a handle that was connected to the upper section of the support via a L-crank lever system. A full 180° rotation of the handle moved the support vertically by the required distance. A steel rod passing through two pillow block bearings and connecting to the L-crank levers allowed the support feet on opposite sides of the rig to be raised simultaneously (Figure 6.26).

The design of the support feet provided a stable base of support. The support feet were locked in position by inserting steel pins through the guiding blocks and the lower section of each support leg. Also, the handles were secured in cradles using steel pins.

6.3.10 Wheels

One of the main design specifications of the rig was that it should be portable and be able to test different areas of a test surface. Therefore, the rig was supplemented with four Ø395mm wheels, with integrated roller bearings and pneumatic tyres, positioned at each corner of the rig. The two wheels at the rear ('vertical' pendulum end) were located on Ø25mm axles securely fixed to the main chassis. At the front of the rig, a simple steering mechanism was designed to allow the front wheels to turn. A towing handle was fitted to the front axle to allow the rig to be manoeuvred manually.

6.3.11 Safety features

The rig underwent the required assessment conducted by the department safety committee. Risk assessments concerning the operation of the test rig were also conducted. The highly dynamic and potentially dangerous nature of the rig necessitated certain safety features. While in a non-operative state with the pendulums raised, three mechanisms prevented the pendulums from any accidental release.

Firstly, the holding force of the magnets should prevent the pendulums from releasing. Secondly, the winch system contained a locking mechanism to secure the pendulum in place. Finally, a mechanical stop consisting of a steel rod was located through brackets bolted onto the main chassis and passed in front of the pendulums. When required, the rig operator released the winch lock and pulled out the mechanical stop when required to prime the pendulum 'ready for release'. A limiter on the steel rod of the mechanical stop prevented it from being pulled out completely.

It was essential to prevent any access to the moving parts in the working area of the rig, while the rig was in operation. A fascia constructed of polycarbonate was bolted to the main chassis and completely covered the upper section of the rig. Some controlled access to the pendulum was required to be able to add extra weights to the pendulum head when required. This accessibility was governed by two sliding doors on one side of the polycarbonate fascia. A pulley system allowed the two doors to be opened simultaneously and restricted only one door from being opened on its own.

The doors could only be opened when the rig was in a non-operative state, following a release of the pendulums with them resting still in a down position. The doors were prevented from opening when the pendulum were ready to be released, the doors were prevented from opening as a result of the mechanical stop being pulled out, restricting the movement of the doors.

An additional guard was placed both of the winch systems to prevent any access to the cable and the cogs of the winch when the pendulums were released and raised.

6.3.12 Transportation

A box trailer was used to transport the rig to different test sites. A long ramp was constructed that fitted on the back of the trailer so that the rig could be easily wheeled up. The trailer was hooked to the back of the department's Vauxhall Astra Estate car. For transportation purposes, the rig was jacked up onto its support legs while in the trailer to prevent it moving around. The front legs of the rig were removed prior to loading onto the trailer to allow the rig to be pushed over the top of the ramp.



Figure 6.27 Strathclyde Sports Turf Testing Rig (SSTTR)

6.3.13 Data Collection System

Due to the portable nature of the rig, the data collection system required to be portable also. The function of the data collection system was to provide a power supply, initiate an impulse for the magnets, provide

amplification of the transducer signals and collect the resulting data.

Figure 6.28 shows the components of the custom made Data Collection System. The main unit consisted of the six strain gauge amplifiers (*RS Components, Corby UK*) on an in-house built printed circuit board. These corresponded with the four channels from the force transducer, plus the two 50g accelerometers. The amplification systems provided gain and bridge supply together with an offset control. The gain and bridge voltage settings for each channel are detailed in Table 6.4.

Two 12V high capacity lead acid batteries provided a dual power supply for the strain gauge amplifiers. The batteries also provided the power supply required for the magnet excitation.

The smaller unit provided the power supply and low impedance coupler for the 100g accelerometer. The passive *Piezotron 510A* low impedance coupler (*Kistler, Winterthur, Switzerland*) served as an interconnecting device, simultaneously providing conditioned power to the low impedance accelerometer and a measured signal to the recording equipment. Two 12V high capacity lead acid batteries provided the power supply to the accelerometer.

An Inspiron 1100 Pentium 4 2.2GHz CPU 512Mb RAM laptop computer (*Dell, Bracknell, UK*) with an integrated 16-bit A/D card (*National Instrument, Newbury, UK*) and a custom written LabView v.7.0 programme (*National Instruments, Newbury, UK*) was used to commence the test procedure by initiating the impulse sent to the magnets, collect and filter the outputted data from the transducer and calculate the applied loads and accelerations. The sampling frequency for collecting data was 3000Hz.

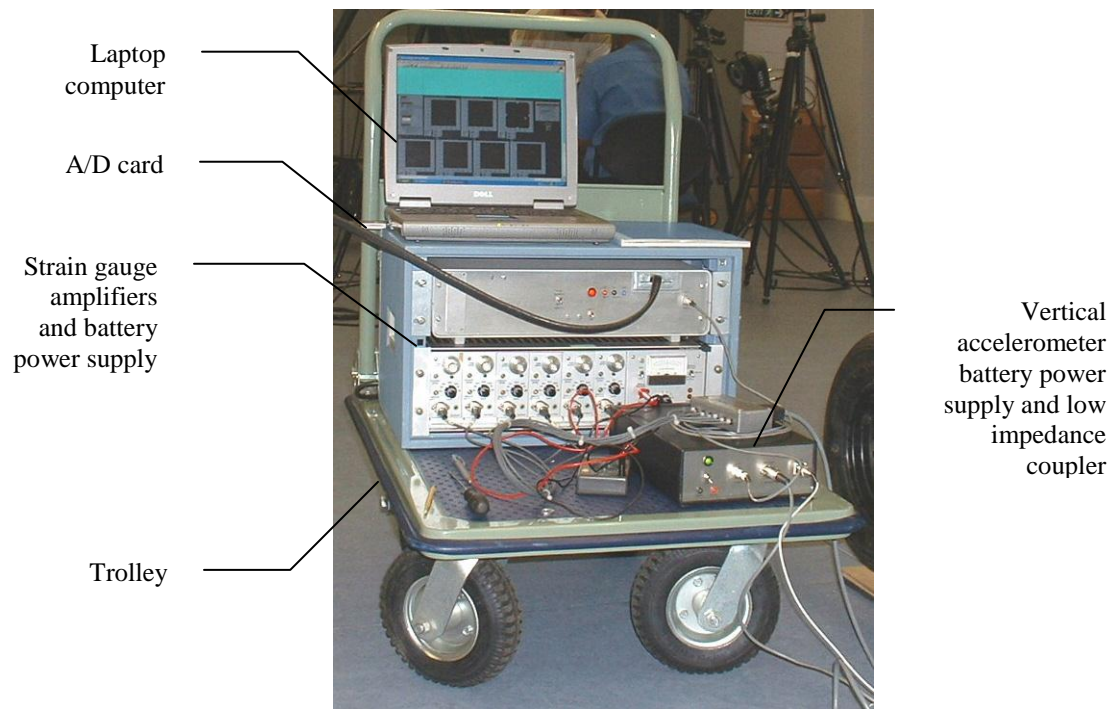


Figure 6.28 Data collection system

Channel No.	Channel name	Bridge Voltage (V)	Amplifier Gain
0	Horizontal accelerometer A	5	0
1	Horizontal accelerometer B	5	0
2	My	5	2000
3	Fx	5	10,000
4	Fy	10	10,000
5	Fz	5	10,000

Table 6.4 Total amplifier gain and bridge excitation voltages used for the instrumented pylon transducer during testing and calibration sessions

Figure 6.29 displays a screenshot from the LabView data collection programme. The voltage outputs of the 7 channels are displayed individually. The applied loads are calculated using a calibration matrix derived from the calibration process, described in Section 6.3.15. Accelerations were calculated from the calibration equations provided by the manufactures of the devices.

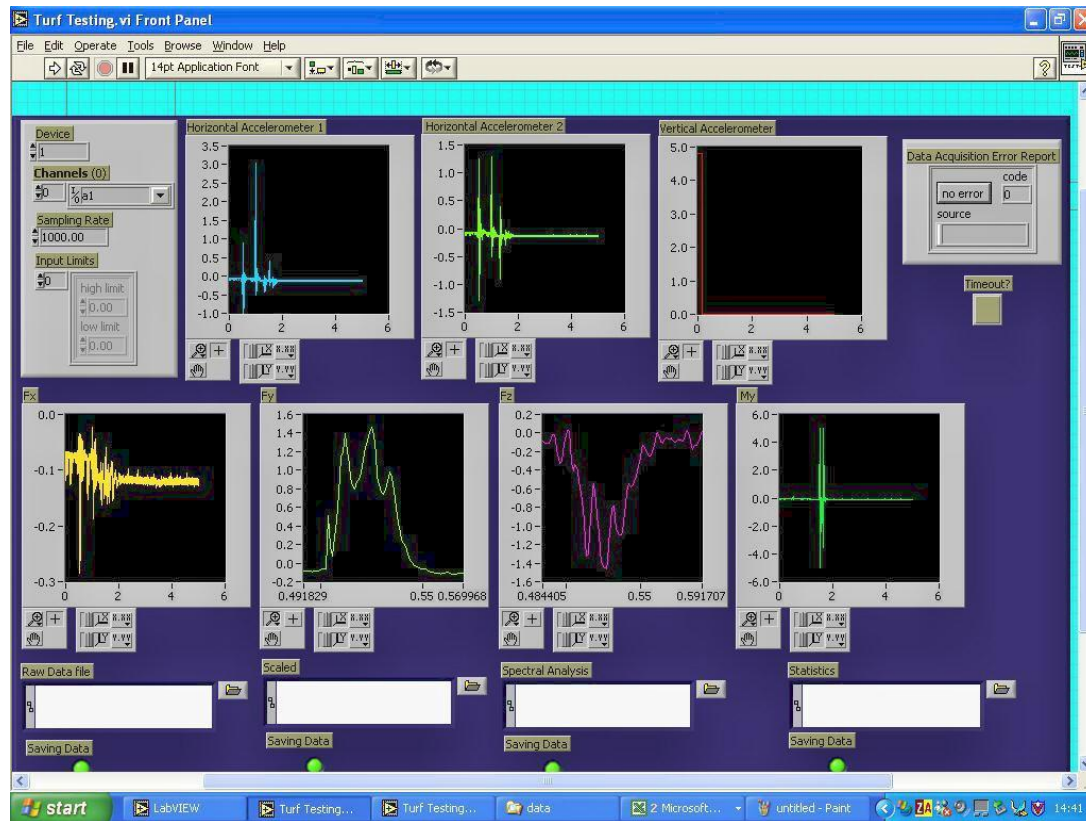


Figure 6.29 Screenshot from LabView data collection programme

6.3.14 Data filtering

During the initial collection and processing of the data, the signals remained unfiltered. Filtering is the process of removing any unwanted noise from the required data. However, due to the complex and unknown nature of high impact collisions such as was presented during the rig tests, it can be difficult to distinguish between the systematic noise and the signal content. As a result, over rigorous filtering may remove some of the proper signal. Therefore, a visual inspection of the raw data was conducted to determine if any filtering was appropriate.

It was decided to leave the signal from the strain gauges measuring applied forces in 3 dimensions and axial torque unfiltered. The observed signal was relatively smooth around the peak that was of interest to this study. On the other hand, very high frequency transients were observed in the accelerometer signals. These transients corresponded with the initial impact of the vertical and shear pendulum heads with the ball transfer unit or the L-crank lever, respectively.

Through a process of trial and error with different filter cut-off frequencies, appropriate filters were adopted that minimised the initial shock transient at the impact event while maintaining the magnitude of the smooth acceleration peak which corresponded with the peak loading rate phase. An 8th order low-pass Butterworth filter was chosen. For the horizontal accelerometers, a cut off frequency of 100Hz was used. For the vertical accelerometer, a cut-off frequency of 250Hz was used.

6.3.15 Pylon Transducer and Calibration

A full description of the pylon force transducer calibration process is given by Runciman (Runciman and Nicol, 1993). The same linear calibration procedures were followed in this study to verify that the original calibration matrix was still valid. The calculation of the applied loads from the measured output signals require the use of a *cross-talk* or *calibration matrix* derived from the calibration curves of each load channel on the transducer.

It is assumed that the output signal [S] can be expressed as the linear combination of the applied load components. The signal for each output channel of the transducer would be the linear combination of the combined effects of the loading (Runciman, 1993). A matrix is used to take into account any cross talk on the other channels that is present in the output signal. Each signal is a combination of the components of the applied loads that are to be measured: Fp_x , Fp_y , Fp_z and Mp_y :

$$S_i = \sum_{j=1}^4 M_{ij} L_j \quad [\text{Eq. 6.25}]$$

where, S_i = Output signal ($i = 1 \dots 4$)
 L_j = Applied load ($j = 1 \dots 4$)
 M = Cross-talk matrix

The output signal for each channel is derived from the cross product of the cross-talk coefficients and the input signal (applied load).

$$[S] = [M][L] \quad [\text{Eq. 6.26}]$$

where,

$$[S] = \begin{bmatrix} SF_x \\ SF_y \\ SF_z \\ SM_y \end{bmatrix} \quad [M] = \begin{bmatrix} m_{11} & m_{12} & m_{13} & m_{14} \\ m_{21} & m_{22} & m_{23} & m_{24} \\ m_{31} & m_{32} & m_{33} & m_{34} \\ m_{41} & m_{42} & m_{43} & m_{44} \end{bmatrix} \quad [L] = \begin{bmatrix} Fp_x \\ Fp_y \\ Fp_z \\ Mp_y \end{bmatrix}$$

In normal use, the applied loads would be the parameters that are required to be calculated. To determine the applied load from the output signal, equation 6.26 is rearranged:

$$[L]=[C][S] \quad [\text{Eq. 6.27}]$$

where $[C]$ is the inverse of the cross talk matrix $[M]$ ($[C] = [M]^{-1}$). The matrix $[C]$ is referred to as the calibration matrix. Units for the parameters $[L]$, $[S]$ and $[C]$ were N or Nm, volts, and N/volt or Nm/volt, respectively.

The components of the initial cross talk matrix $[M]$ were calculated by applying known loads to each channel of the transducer (F_x , F_y , F_z and M_y) and measuring the corresponding output signals. The transducer was securely fixed to a mounting base in different orientations. Masses were suspended from the transducer using a hanger and a weights pan. The different configurations enabled axial loads (F_{p_y}), shear loads (F_{p_x} and F_{p_z}) and torsional loads (M_{p_y}) to be applied to the transducer. For full description of the procedures used, see Runciman (Runciman & Nicol, 1993).

The resulting output signals for each loading condition was plotted against the load that was applied in each condition. The slope of the line for each output was analysed using linear regression techniques to determine the corresponding components of a column of the cross talk matrix $[M]$. Correlation coefficients were calculated for each output signal to determine the linearity of the output signals. R-squared values for the F_{p_x} , F_{p_y} , F_{p_z} and M_{p_y} data were greater than 0.999.

The calibration matrix $[C]$, calculated from the inversion of the cross talk matrix $[M]$, was as follows:

$$[C]=\begin{bmatrix} -229.57 & 0.60 & -7.04 & 0.16 \\ 0.20 & 389.78 & -3.80 & -27.73 \\ -8.47 & -3.76 & 226.13 & -4.12 \\ 0.05 & 0.07 & -0.13 & 32.79 \end{bmatrix}$$

6.4 In Situ Pitch Testing

Initial testing of the SSTTR was conducted *in situ* at eight different test sites on sports pitches used for football, hockey and rugby. The test sites were located in and around the Glasgow region. Six of the test sites had artificial surfaces; one had a natural grass pitch (normally used for rugby); and the other test site had a hybrid turf pitch (natural turf, reinforced with synthetic fibres, normally used for football). The types of artificial turf surfaces including the following:

- 1 x nylon carpet surface (analogous to a first generation type turf)
- 1 x short pile, sand-infilled turf (similar to the second generation T1 surface used in the biomechanical assessment)
- 1 x *Tarkett Sommer* medium pile, sand-dressed surface (similar to *the second generation T2* surface used in the biomechanical assessment)
- 2 x third generation, long pile, sand-rubber infill surfaces (1 x *FieldTurf* surface similar to the T3 surface used for the biomechanical assessment; the manufacturer of the other surface was unknown).
- 1 x water-based hockey surface

Permission was obtained from the site owners prior to any testing taking place. Due to safety requirements and the use of sophisticated electronics, testing took place on dry days; however the natural grass surface was slightly wet on the day of testing.

In addition, the rig was tested on a sample of the TI turf used in the biomechanical assessment to provide a reference. The turf was secured firmly on top of the force plate, as described in section 3.2.1. The same testing procedures were conducted as for the *in situ* testing (section 6.4.3). Data from the laboratory testing are referred to as *sand infill (lab)* in section 6.4.

6.4.1 Pitch Areas

To enable an overall assessment of the whole pitch surface, tests were conducted in different areas around

the pitch. These were standardised into the following six areas, as shown in Table 6.5 and Figure 6.30:

Test Area	Football Pitch	Rugby Pitch	Hockey Pitch
1	6-yard box A	Try line A	Goal area A
2	Penalty box	22-yard line	25-yard line
3	Centre Circle	Centre line	Centre line
4	6-yard box B	Try line B	Goal area B
5	Wing	Wing	Wing

Table 6.5 Standardised test areas

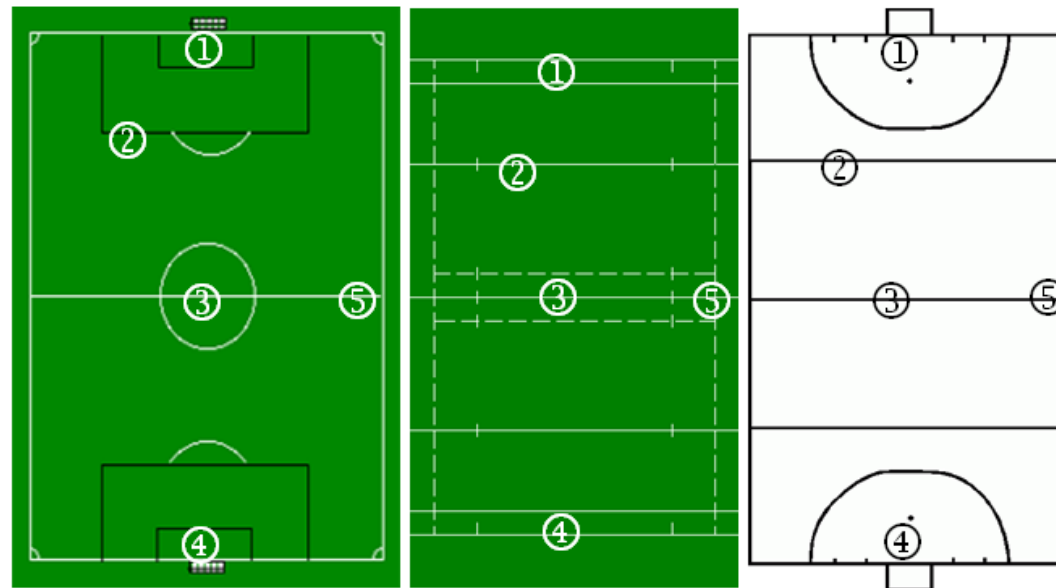


Figure 6.30 Standardised pitch areas for football (left), rugby (middle) and hockey (right) pitches

6.4.2 Types of Test

The flexible operation of the rig allowed different types of test to be conducted on each test surface. A test battery consisting of six individual types of tests were devised. These tests allowed a surface to be loaded in a combination of directions. As a result, the response to unidirectional and multidirectional loads could be assessed. The six tests are described as below, using the pendulum configurations as follows:

- 25kg vertical pendulum = 14kg vertical pendulum head plus 11kg additional mass
- 14kg vertical pendulum = vertical pendulum head only
- 6.6kg shear pendulum = 3.5kg shear pendulum head plus 3.1kg additional mass
- 3.5kg shear pendulum = shear pendulum only.

6.4.2.1 *Test 1: Linear Traction (Under Static Vertical Loading) Test*

In this test, a dynamic shear force is applied to the surface while being loaded with a static vertical load. The test foot was preloaded with a static vertical load of 250N. The 25kg vertical pendulum provided this static load. The horizontal cable was attached to the eyebolt A on the cable attachment block. The 6.6kg shear pendulum was subsequently released to impart a dynamic shear force to the test foot. A traction coefficient was calculated as a ratio of the shear force to the vertical force.

6.4.2.2 *Test 2: Linear Traction (Under Dynamic Vertical Loading) Test*

In this test, the surface was loaded with a dynamic shear force and dynamic vertical force. The 25kg vertical pendulum and 6.6kg shear pendulum were used. The horizontal cable was attached to the eyebolt A on the cable attachment block. The pendulums were released simultaneously so that the impacts occurred at the same time.

6.4.2.3 *Test 3: Combined Linear & Rotational Traction Test*

Test 3 consisted of a dynamic shear force and torque while being loaded with a static vertical load, partially replicating the action of a 'foot' sliding and twisting on the surface. The test foot was preloaded with a static vertical load of 250N. The 25kg vertical pendulum provided this static load. No additional masses were applied to the 3.5kg shear pendulum. The horizontal cable was attached to the eyebolt B offset 30mm to the side of the vertical axis of the vertical shaft on the cable attachment block so that the applied shear force produced a torque. Linear and rotational traction coefficients were calculated as a ratio of the peak shear force to the peak vertical force and the peak torque to the peak vertical force, respectively.

6.4.2.4 *Test 4: Vertical impact test*

The test consisted of the application of a dynamic vertical force only to the surface, using the 25kg vertical pendulum. The shear pendulum was not used during this test.

6.4.2.5 *Test 5: Low Impact 3D Test*

In this test, the surface was dynamically loaded with a combined vertical force, horizontal force and torque. This test replicated a low impact turning movement, such as the 90° cross turn, and measured vertical loading with a sliding and twisting test. The 14kg vertical pendulum was used for a vertical force, the 3.5kg shear pendulum was used to produce a shear force and a torque was produced as in section 6.4.2.3. The pendulums were released simultaneously so that the impact and loading occurred at the same time.

6.4.2.6 *Test 6: High Impact 3D Test*

In this test, the surface was dynamically loaded with a combined vertical force, horizontal force and torque. This test replicated a high impact turning movement, such as the 45° cross turn, measuring high vertical loading with a sliding and twisting test. The 25kg vertical pendulum was used for the vertical force; the 3.5 kg shear pendulum was used to produce a shear force; and a torque was produced as in section 6.4.2.3. The pendulums were released simultaneously so that the impact and loading occurred at the same time.

6.4.3 Rig Testing Procedure

One trial of each of the six tests was conducted in the five different areas of the pitch (Table 6.5; Figure 6.30). The tests were conducted in the order described in section 6.4.2. At each test site, 30 successful trials were conducted, totalling 240 trials for all eight outdoor sites and the laboratory tests.

To replicate the actual sporting environment as close as possible, the test foot appropriate to the surface was used in the tests. Therefore, the pimpled test foot was used for the short pile surfaces (sand-infilled, sand-dressed, nylon, water-based surfaces). For the longer piled surfaces (3G, hybrid, natural turf), the studded test foot was used (see section 6.3.7 for a description of the test feet). Furthermore, some of the pitch owners did not permit the studded test foot to be used on the short-pile surfaces.

To allow consistent testing and prevent compacting of the surface, the rig was moved slightly between tests so that test foot rested on a untested piece of surface.

6.4.4 Data analysis

To characterise the sports surfaces tested by the SSTTR, Table 6.6 shows the parameters calculated during the data analysis of the six tests. Table 6.7 describes how the parameters are calculated.

Parameter (peak value)	Test 1	Test 2	Test 3	Test 4	Test 5	Test 6
Shear force (N)	✓	✓	✓		✓	✓
Vertical force (N)				✓	✓	✓
Torque (Nm)			✓		✓	✓
Time to peak forces/torque (s)	✓	✓	✓		✓	✓
Shear force loading rate (kNs ⁻¹)	✓	✓	✓		✓	✓
Vertical force loading rate (kNs ⁻¹)				✓	✓	✓
Torque loading rate (kNms ⁻²)			✓		✓	✓
Linear traction (under static vertical loading) (μ_s)	✓		✓			
Linear traction (under dynamic vertical loading) (μ_d)		✓			✓	✓
Rotational traction (under static vertical loading) (λ_s)			✓			
Rotational traction (under dynamic vertical loading) (λ_d)					✓	✓
Horizontal displacement (mm)	✓	✓	✓		✓	✓
Horizontal acceleration (g)	✓	✓	✓		✓	✓
Vertical displacement (mm)				✓	✓	✓
Vertical acceleration (g)				✓	✓	✓
Angular displacement (rad)			✓		✓	✓
Angular acceleration (rads ⁻²)			✓		✓	✓

Table 6.6 Parameters calculated for each of the six tests

Parameter	Description
Shear force (N)	Peak value
Vertical force (N)	Peak value
Torque (Nm)	Peak value
Time to peak forces/torque (s)	Time in seconds
Shear force loading rate (kNs ⁻¹)	Shear force/time
Vertical force loading rate (kNs ⁻¹)	Vertical force/time
Torque loading rate (kNms ⁻²)	Torque/time
Linear traction (under static vertical loading) (μ_s)	Peak shear force / vertical force at peak shear*
Linear traction (under dynamic vertical loading) (μ_d)	Peak shear force / vertical force at peak shear
Rotational traction (under static vertical loading) (λ_s)	Peak torque / vertical force at peak shear*
Rotational traction (under dynamic vertical loading) (λ_d)	Peak torque / vertical force at peak shear
Horizontal acceleration (g)	Peak value (see 0)
Horizontal displacement (mm)	Double integration of the horizontal acceleration (see 0)
Vertical acceleration (g)	Peak value
Vertical displacement (mm)	Double integration of the vertical acceleration
Angular acceleration (rads ⁻²)	Peak value (see 0)
Angular displacement (rad)	Double integration of the angular acceleration (see 0)

Table 6.7 Description of the test parameters calculations

* Static linear traction should theoretically be calculated as peak shear force ÷ static vertical force. However, as can be seen for the force profile in Figure 6.32, the vertical force did not remain 'static' during the impact. Therefore, the vertical force at the moment of the peak shear force magnitude was used as the divisor

As stated in section 6.4.3, five trials of each six test were conducted at each test site. For each parameter in the data analysis, an average of the five trials was calculated. However, for Test 3, Test 5 and Test 6, a successful trial was defined as when the two pendulums impacted within 10 ms of each other; an average of these successful trials was calculated.

6.4.4.1 Calculation of horizontal and angular acceleration and displacement

The location of the two accelerometers was critical to allow the calculation of the horizontal (a_z) and angular (α_y) (around a vertical axis) accelerations. Figure 6.31 displays the accelerations acting on the test foot caused by the applied shear forces and torques.

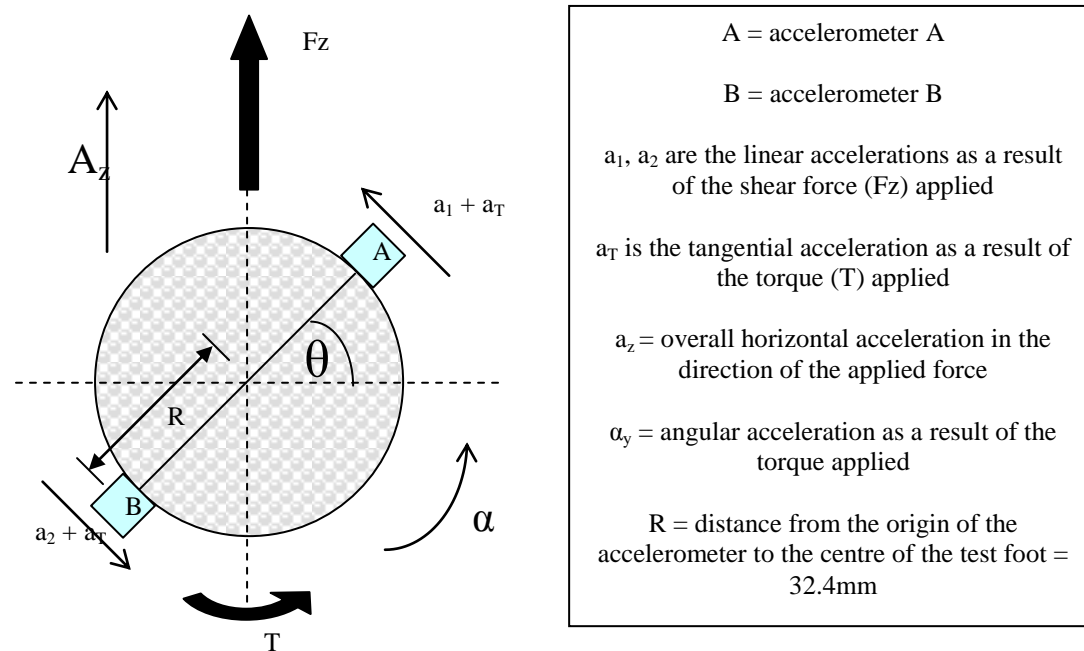


Figure 6.31 Plan view of accelerations acting on the test foot

The outputs from accelerometers A and B contained the acceleration caused by the application of the shear force plus a tangential acceleration caused by the torque applied to the test foot. Therefore, $A = a_1 + a_T$ $B = a_2 + a_T$.

In order to calculate the magnitude of the tangential acceleration:

$$\mathbf{a}_2 = -\mathbf{a}_1 \quad [\text{Eq. 6.13}]$$

$$\mathbf{A} = \mathbf{a}_1 + \mathbf{a}_T \quad [\text{Eq. 6.14}]$$

$$\mathbf{B} = -\mathbf{a}_1 + \mathbf{a}_T \quad [\text{Eq. 6.15}]$$

[Eq. 6.14] + [Eq. 6.15]:

$$\mathbf{A} + \mathbf{B} = 2\mathbf{a}_T \quad [\text{Eq. 6.16}]$$

$$\mathbf{a}_T = \frac{\mathbf{A} + \mathbf{B}}{2} \quad [\text{Eq. 6.17}]$$

To calculate the angular acceleration (α_y) around the vertical axis:

$$\alpha_y = \frac{\mathbf{a}_T}{R} \quad [\text{Eq. 6.18}]$$

The angle (θ) that the test foot rotates can be calculated from the double integration of the angular acceleration:

$$\theta = \int \omega \, dt = \iint \alpha \, dt \quad [\text{Eq. 6.19}]$$

$$\omega = \int \alpha \, dt = \alpha t \quad [\text{Eq. 6.20}]$$

$$\begin{aligned} \theta &= \int \omega \, dt = \int \alpha t \, dt \\ &= \frac{\alpha t^2}{2} \quad [\text{Eq. 6.21}] \end{aligned}$$

When the test foot acted upon by an offset horizontal force, the test foot is turned by an angle θ . The overall horizontal acceleration (a_x) in the direction of the horizontal force is given by:

$$\begin{aligned} \mathbf{a}_x &= \mathbf{a}_1 \cos \theta - \mathbf{a}_2 \cos \theta \\ &= (\mathbf{A} - \mathbf{a}_T) \cos \theta - (\mathbf{B} - \mathbf{a}_T) \cos \theta \\ &= \mathbf{A} \cos \theta - \mathbf{B} \cos \theta \quad [\text{Eq. 6.22}] \end{aligned}$$

The horizontal displacement (s) and rotational displacement (θ) of the test foot were given by the double integration of the horizontal and angular accelerations, respectively:

$$s = \iint a_x dt \quad [\text{Eq. 6.23}]$$

$$\theta = \iint \alpha_y dt \quad [\text{Eq. 6.24}]$$

6.5 Results and Discussion

6.5.1 Linear Traction (Under Static Vertical Loading)

For the tests conducted on the artificial turfs, the shear force profile was generally characterised by an inverted ‘V’ curve (Figure 6.32). The shear force profile produced from the test conducted on the natural grass surfaces was much less uniform in shape (Figure 6.33)

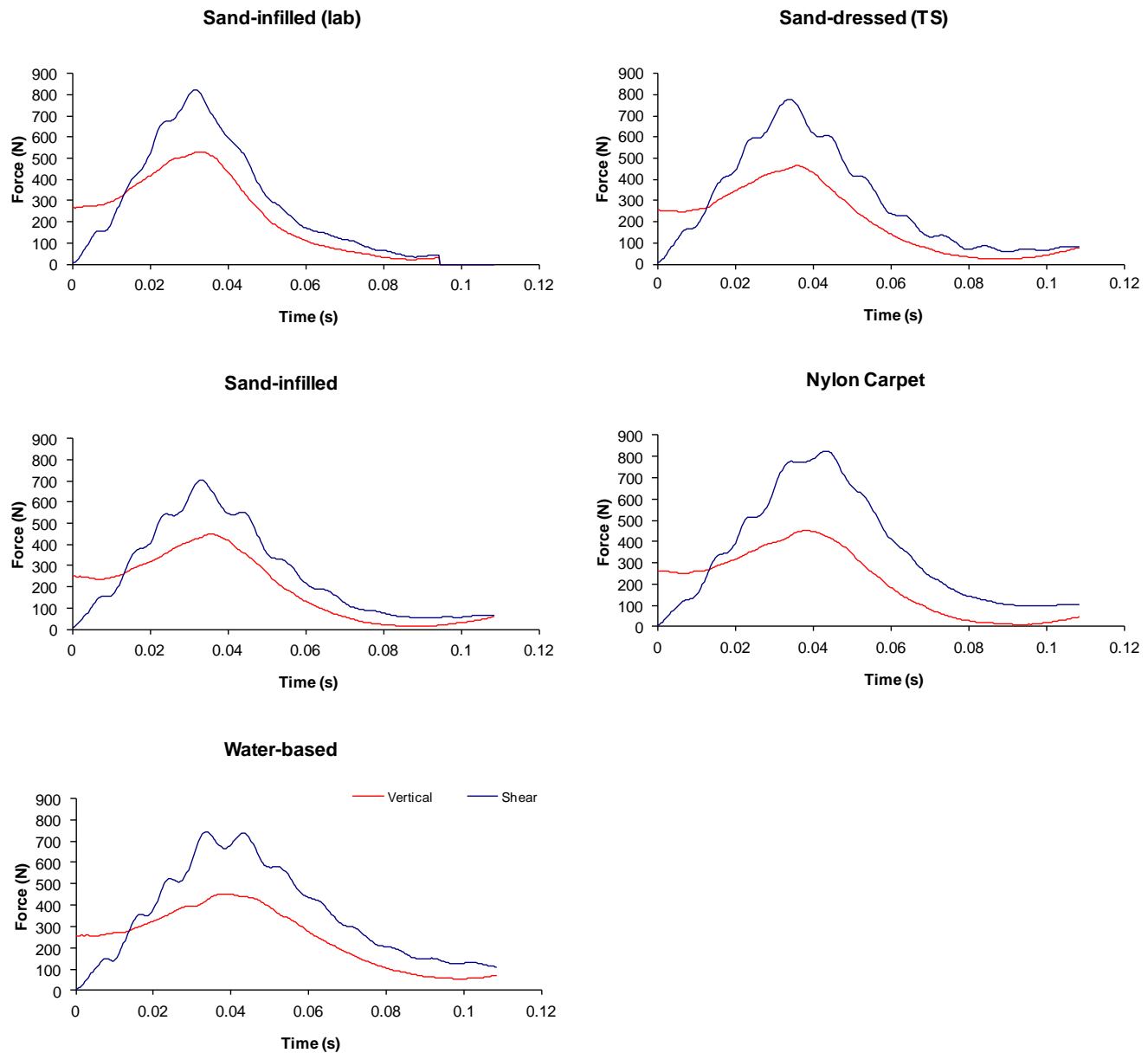


Figure 6.32 Linear Traction (Under Static Vertical Loading) Test: Force profiles on surfaces tested with pimped test foot

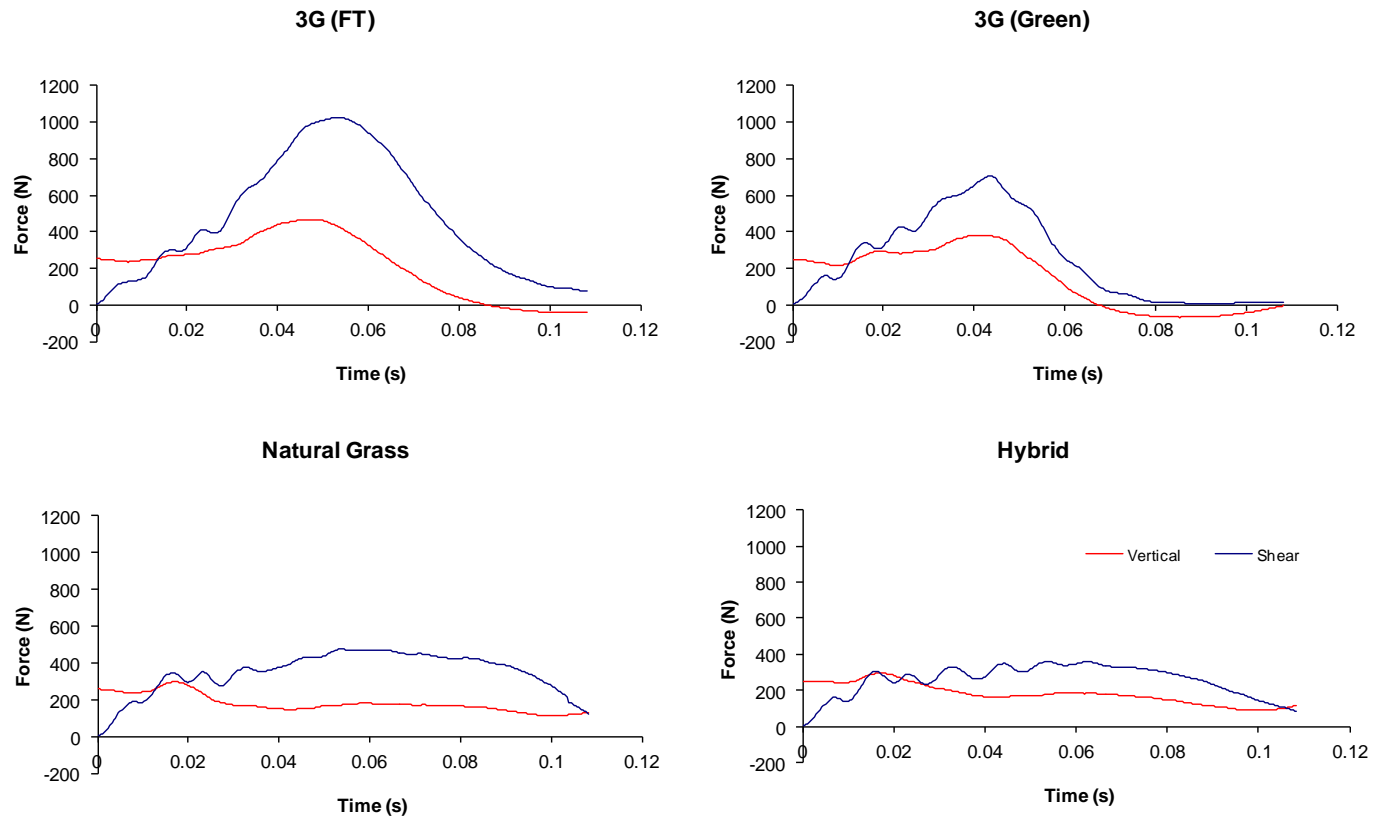


Figure 6.33 Static linear traction test: force profiles on surfaces tested with studded test foot

Site	Test foot	Peak Shear Force (N)			Vertical Force at Peak Shear (N)			Linear Traction (μ_s)		
		Mean	Min	Max	Mean	Min	Max	Mean	Min	Max
Sand-infill (lab)	Pimpled	821	723	888	527	496	559	1.56	1.46	1.66
Sand-dressed (TS)*	Pimpled	780	731	817	453	415	488	1.73	1.6	1.84
Sand-infilled	Pimpled	709	630	844	460	389	632	1.57	1.22	1.76
Nylon carpet	Pimpled	834	792	879	425	396	449	1.97	1.83	2.18
Water based	Pimpled	785	728	868	440	405	472	1.79	1.66	1.92
3G (FT)	Studded	1060	996	1153	443	388	512	2.43	1.9	2.89
3G (Green)	Studded	714	583	832	390	293	485	1.86	1.65	2.07
Natural Grass*	Studded	490	454	522	185	162	214	2.7	2.12	3.2
Hybrid	Studded	427	367	478	221	202	243	1.93	1.82	1.99

* Trial 1 not included in statistics

Table 6.8 Peak forces and traction coefficients for the linear traction (under static vertical loading) test

Table 6.8 displays the mean peak shear forces obtained during the linear traction (under static vertical loading) test on each of the surfaces. In addition, the vertical force and linear traction coefficient corresponding with the peak shear force are also presented. The mean peak shear forces measured on all the

surfaces ranged between approximately 430N to 1060N. The times to the peak shear force from the moment of impact ranged from 32ms to 53ms. Different results were observed for the test conducted with the pimpled test foot and the studded test foot (Figure 6.32 & Figure 6.33). This was to be expected due to the different frictional properties of the two test feet. For the tests conducted with the pimpled test foot, the mean peak shear forces ranged from 709N to 834N. A greater variation in peak shear forces was observed on the surfaces tested with the studded test foot, with mean values ranging from 427N to 1060N. The shear forces measured on the natural and hybrid grass surfaces were considerably lower than on the longer pile 3G artificial turfs.

For the tests conducted with the pimpled test foot, the shear force reached a peak of approximately 800N at 35-45ms following impact. The greatest mean shear force was observed on nylon carpet (834N). The lowest mean shear force was observed on the sand-infilled turf (709N).

The force profile charts show that during the application of the shear force, a vertical force measured altered from the static 250N vertical force that was applied to the test foot at the start of the test (Figure 6.32 and Figure 6.33). The vertical force at the moment of the peak shear force ranged from 425N to 527N and 185N to 443N for the tests conducted with the pimpled and studded test foot, respectively. The vertical force was increased from the static vertical force on the artificial surfaces, but not for the natural and hybrid grass surfaces. With regards to the artificial surfaces, this increased vertical force could indicate the test foot was pushed into the ground when the shear force was applied.

For the grass surfaces, 2 periods of peak shear forces was observed (Figure 6.33). The first peak occurred at about 20ms following impact at a magnitude of approximately 350N. After the first peak, there was a smoother rise to a second peak of approximately 400N, about 60ms following impact. The vertical force reached a peak at the same period as the first shear force peak. Subsequently, the vertical force was reduced below the applied static force, indicating that the test foot may have been initially pulled down into the turf and was then pulled up.

The tests conducted with the pimpled test foot generally produced lower traction coefficients. These ranged from 1.56 (sand-infilled surfaces) to 1.97 (nylon carpet surface). For the tests conducted with the studded test foot, the traction coefficient ranged from 1.86 to 2.7. The natural grass turf and 3G (green) surfaces produced the highest and lowest traction coefficients, respectively.

The time to the peak shear force were generally shorter for the surfaces tested with the pimpled test foot (Figure 6.34). Times ranged from 32-43ms and 44-53ms for the pimpled test foot and studded test foot, respectively.

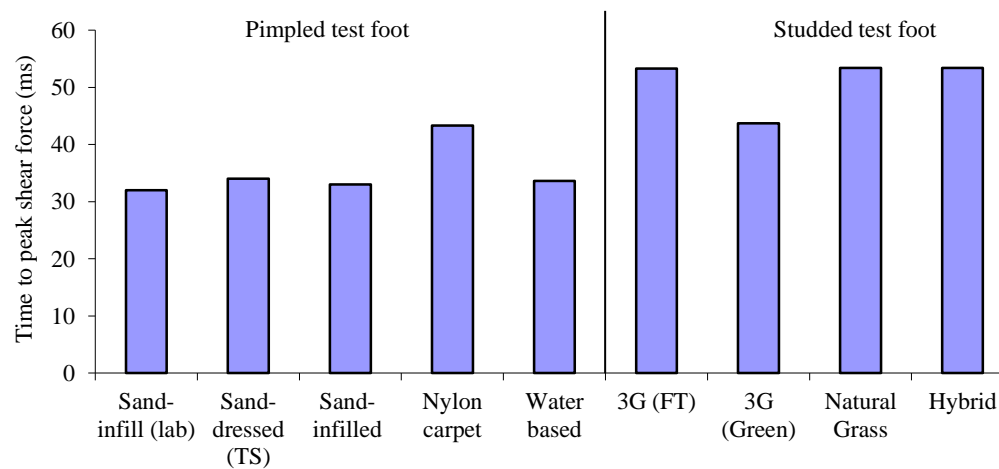


Figure 6.34 Static linear traction test: time to peak shear force

For the pimpled test foot, the shortest time to peak shear force was 32ms on the sand-infill (lab) surface. The longest time was 43.3ms, measured on the nylon carpet surface.

For the studded test foot, the shortest time to peak shear force was 43 ms on the 3G (Green) surface. The 3G (FT), natural grass and hybrid grass surface all had similar times to the peak shear force of approximately 53ms.

For the pimpled test foot tests, the greatest peak loading rate of 56kNs^{-1} was observed on the sand-infill (lab) surface (Figure 6.35). The lowest peak loading rate was observed on the sand-dressed (TS) surface (51kNs^{-1}).

For the tests conducted with the studded test foot, the 3G (green), natural grass and hybrid grass surfaces

produced similar shear force loading rates, ranging from 46kNs^{-1} to 49kNs^{-1} . The 3G (FT) surface produced the shear force loading rates of all the longer pile turfs with a value of 55kNs^{-1} .

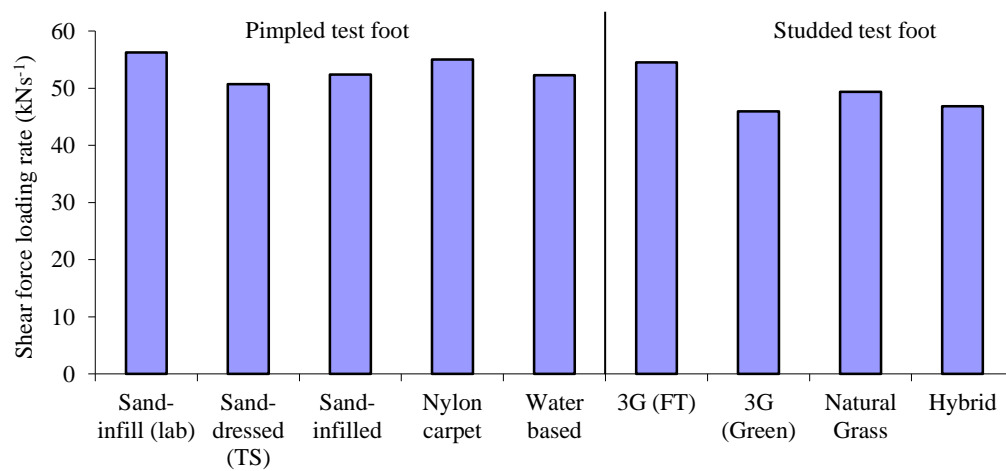


Figure 6.35 Static linear traction test: shear force loading rates

The horizontal acceleration of the test foot across the turf ranged from 5g to 11g for all the surfaces (Figure 6.36). For the pimpled test foot trials, the greatest horizontal acceleration was measured on the sand-infilled surface conducted outdoors. However, the lowest peak horizontal acceleration was measured on the sand-infilled (lab), conducted indoors. The horizontal acceleration data ranged from 11g to 14g for the outdoor tests conducted with the pimpled test foot and 7g to 10g for the tests conducted with the studded test foot. The 3G (FT) and hybrid grass turfs produced lower peak acceleration values than the other two surfaces.

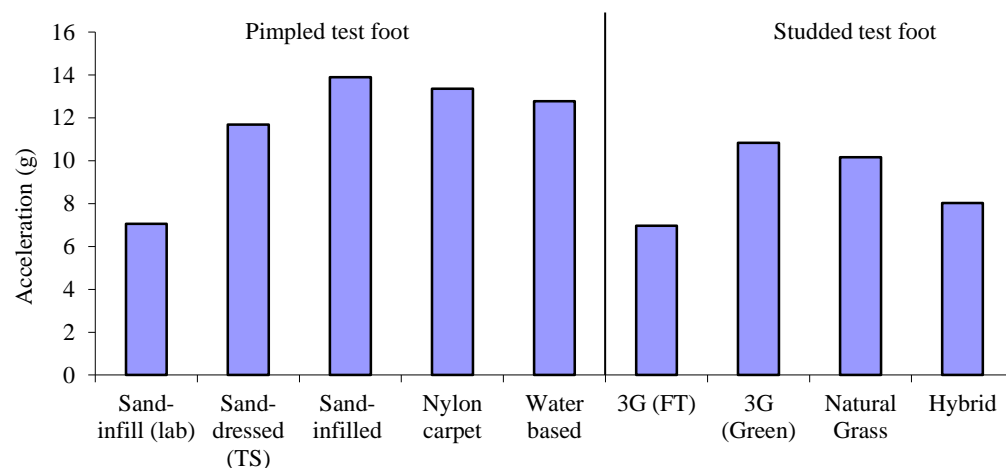


Figure 6.36 Linear Traction (Under Static Vertical Loading) Test: Mean peak horizontal acceleration

The peak horizontal displacements of the test feet are presented in Table 6.9. The pimped foot test produced greater displacements than the studded foot tests. However, the results were variable, with the displacements from the five trials ranging up to 55mm. The tests conducted with the pimped test foot on the sand-infilled and sand-dressed surfaces produced similar average displacements of approximately 30mm. The greatest displacement was observed on the water-based surface and the lowest displacement was on the nylon carpet.

For the tests conducted with studded test foot, the average displacement on the 3G (FT) was slightly lower than the other surfaces at 15mm. The displacement on the other turfs ranged from 22-25mm. However, many of the trials produced very low displacements, possibly due the studs getting locked in the turf.

The results indicated that the artificial surfaces tested with pimped test foot tended to have more traction than the new generation surfaces and natural grass turfs where studded footwear is conventionally worn. However, the pimped test foot tended to slide on the surface farther and with more acceleration. This is an unexpected finding as one might expect that surfaces with higher traction coefficients would result in less and slower movement of the test foot. One possible reason is that the high impacts and ground reactions involved may have caused the test rig to move or bounce leading to the pimped test foot losing contact with the surface more on the shorter pile turfs than the longer studded test foot on the longer pile surface. However, due to the different test foot used on the different surfaces, it is hard to compare all surfaces together and explain this contradiction further.

Site	Test foot	Peak Shear Displacement (mm)		
		Mean	Min	Max
Sand-infill (lab)	Pimped	30.6	24	35
Sand-dressed (TS)	Pimped	30.3	17.1	53.4
Sand-infilled	Pimped	32.5	23.9	51.8
Nylon carpet	Pimped	22.2	2	50.4
Water based	Pimped	45.4	27.1	63.8
3G (FT)	Studded	15.4	3.7	43.8
3G (Green)	Studded	22.1	4.7	44.3
Natural Grass	Studded	22.3	7.4	37.3
Hybrid	Studded	25.5	4.2	60.6

Table 6.9 Linear Traction (Under Static Vertical Loading) Test: Mean peak horizontal displacement

6.5.2 Linear Traction (Under Dynamic Vertical Loading) Test

The vertical force measured during the dynamic linear traction test generally presented two peaks (Figure 6.37 & Figure 6.38). The first peak occurred at about 15ms and the second peak occurred at about 30ms. For some surfaces, the first peak was greater than the second. For other surfaces, the opposite was observed.

The shear force produced during the dynamic linear traction test produced a smooth, one-peak profile. The magnitude and time of the peak shear force varied across the surfaces and between test foots.

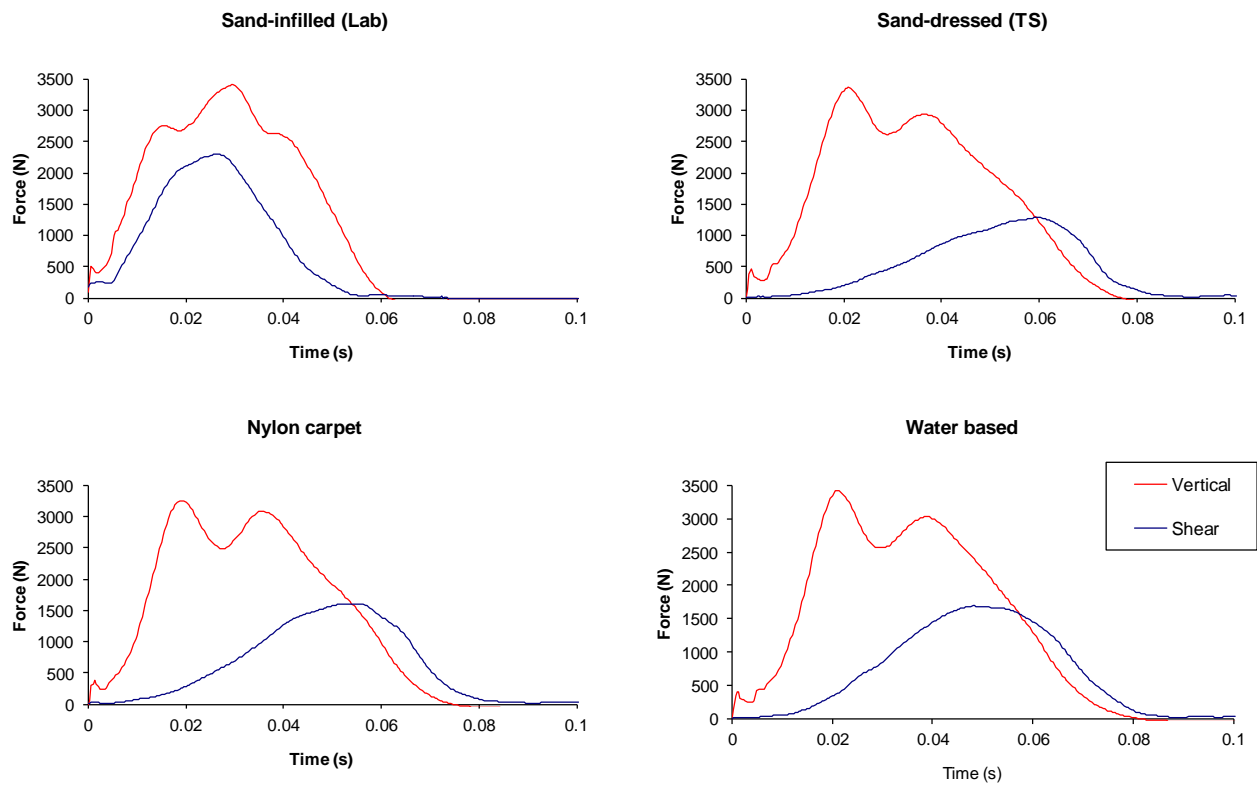


Figure 6.37 Linear Traction (Under Dynamic Vertical Loading) Test: force profiles on surfaces tested with pimped test foot

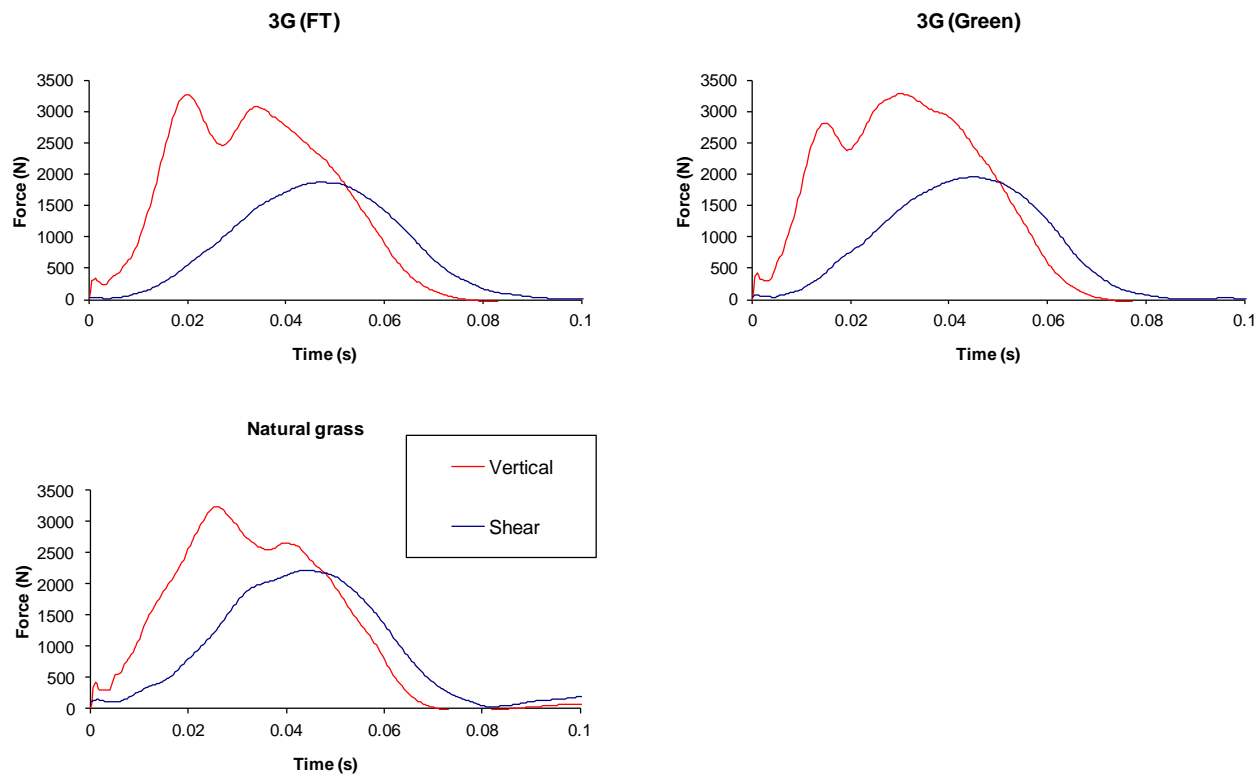


Figure 6.38 Linear Traction (Under Dynamic Vertical Loading) Test: force profiles on surfaces tested with studded test foot

Not all surfaces are presented in Figure 6.37 and Figure 6.38. On some of the tests, it appeared that the impact of the shear pendulum occurred up to 40ms following the impact of the vertical pendulum. This delay in impact times was not always consistent in one set of trials on a particular surface. For example, for the tests conducted on the sand-infilled surface outdoors, the shear pendulum impacted at the same time as the vertical pendulum for three of the five trials conducted. For the other two trials, the shear pendulum impacted 30ms later.

As a result of the mistiming error, the peak shear force occurred at different magnitudes of vertical force. It was apparent that higher magnitudes of shear force were measured when the vertical force was higher. This indicates that as the test foot is forced more into the turf vertically, it took greater force to pull it horizontally.

For four out of the five trials conducted on the natural grass turf, the shear force pendulum impacted

approximately 70ms before the vertical pendulum impacted.

As a result of these factors, the data was analysed from trials where the impact times of the vertical and shear pendulums occur within 10ms of each other. These impact times were identified from the accelerometer data.

For some of the trials on the sand-infilled turf (lab) surface and one trial on the 3G (FT) surface, the signal measured on the shear force channels saturated at a level of approximately 2300N, i.e. the output exceeded 10V. These trials were not included in the analysis of the results. However, in the case of the sand-infilled (lab) surface, the trials where the signal saturated at the very apex of the force peak were analysed. Table 6.10 shows the peak forces and traction coefficients for the linear traction test (under dynamic vertical loading). For the tests conducted with the pimped test foot, the mean peak shear force measured ranged from 1708N to 2320N. The lowest peak shear force was measured on the water-based surface. The highest peak shear force was measured on the sand-infilled (lab) surface.

The magnitude of the vertical force measured at the peak shear force ranged from 2044N to 3274N. The lowest was measured on the nylon carpet surface and the highest peak vertical force was measured on the sand-infilled (lab) surface.

The traction coefficient for the dynamic traction test ranged from 0.71 to 0.93. The lowest value was for the sand-infilled (lab) surface. The highest traction coefficient was observed on the nylon carpet surface.

For the tests conducted with the studded test foot, the mean peak shear force measured ranged from 1862N to 2209N. The lowest shear force was observed on the 3G (FT) surface. The highest shear force was observed on the natural grass turf. The magnitude of the vertical force at the peak shear force was lowest for the 3G (FT) surface at 1983N, and highest for the natural grass turf (2428N). The traction coefficients were similar for all turfs tested with the studded test foot. These ranged from 0.91 to 0.94.

Site	Test Foot	Peak Shear Force (N)			Vertical Force at Peak Shear (N)			Linear Traction (μ_a)		
		Mean	Min	Max	Mean	Min	Max	Mean	Min	Max
Sand-infilled (lab)	Pimpled	2320	2223	2477	3274	3142	3342	0.71	0.69	0.74
Sand-dressed (TS)*	Pimpled	1862	1846	1879	2172	1983	2361	0.87	0.8	0.93
Nylon carpet**	Pimpled	1883	1805	1974	2044	1908	2312	0.93	0.85	0.98
Water based	Pimpled	1708	1598	1901	2229	1782	2575	0.78	0.67	0.9
3G (FT)***	Studded	1862	1707	1968	1983	1917	2098	0.94	0.87	1
3G (Green)	Studded	1989	1737	2258	2229	1782	2573	0.91	0.72	1.17
Natural grass****	Studded	2209	2209	2209	2428	2428	2428	0.91	0.91	0.91

*data from trials 1 & 5; **data from trials 2,3,5; ***data excluding trial 4; ****data from trial 1

Table 6.10 Peak forces (N) and traction coefficients for the linear traction (under dynamic vertical loading) test

Table 6.11 shows the peak horizontal acceleration and displacement during the linear traction (under dynamic vertical loading) test. The magnitude of the peak horizontal accelerations ranged from 11g to 13g on the surfaces tested with the pimpled foot, and 7.5g to 11.7g on the surfaces tested with the studded foot.

Site	Test Foot	Peak Horizontal Acceleration (g)			Peak Horizontal Displacement (mm)		
		Mean	Min	Max	Mean	Min	Max
Sand-infill (lab)	Pimpled	7.05	6.11	8.73	30.6	24	35
Sand-dressed (TS)	Pimpled	11.68	9.12	12.67	30.3	17.1	53.4
Sand-infilled	Pimpled	13.9	11.8	16.2	32.5	23.9	51.8
Nylon carpet	Pimpled	13.35	10.16	18.38	22.2	2	50.4
Water based	Pimpled	12.78	9.8	19.69	45.4	27.1	63.8
3G (FT)	Studded	6.96	5.55	9.78	15.4	3.7	43.8
3G (Green)	Studded	10.83	5.54	14.04	22.1	4.7	44.3
Natural Grass	Studded	10.16	5.45	16.4	22.3	7.4	37.3
Hybrid	Studded	8.02	4.11	14.46	25.5	4.2	60.6

Table 6.11 Linear Traction (Under Dynamic Vertical Loading) Test: Peak horizontal acceleration and displacement

From the limited data available, it is difficult to characterise the surfaces in terms of their linear tractional properties. However, the results indicate that the 3G turfs produce similar traction coefficients to the natural turf surface. The sand-infilled and water based surfaces appear to produce lower traction coefficients than the other two surfaces tested with the pimpled test foot.

6.5.3 Combined Linear & Rotational Traction Test

The combined linear and rotational traction test applied a dynamic shear force and torque to the test foot, which was loaded with a static 250N vertical force. During this test, the shear force reached a peak at approximately 40-50ms. Across all the turfs tested, with both test feet, the peak shear force ranged from 411N to 686N (Figure 6.39 and Figure 6.40).

Two peaks were observed in the measured torques. The magnitude of the greater of the two peak torques applied to the turfs ranged from 13.1 to 20Nm. This peak torque occurred at about 20-30ms from the moment of impact of the shear pendulum. In addition, a smaller peak occurred at about 8ms, with a magnitude ranging from 10Nm to 15Nm. This may have coincided with the initial impact of the pendulum and the tightening of the steel cable connecting the L-crank lever to the test foot. The application of the shear force and torque appeared to also pull the test foot down into the turf. This is evident from the increase in the measured vertical force, from the static 250N to a peak ranging from 274N to 392N. The vertical force increased the most when the applied torque reached a peak.

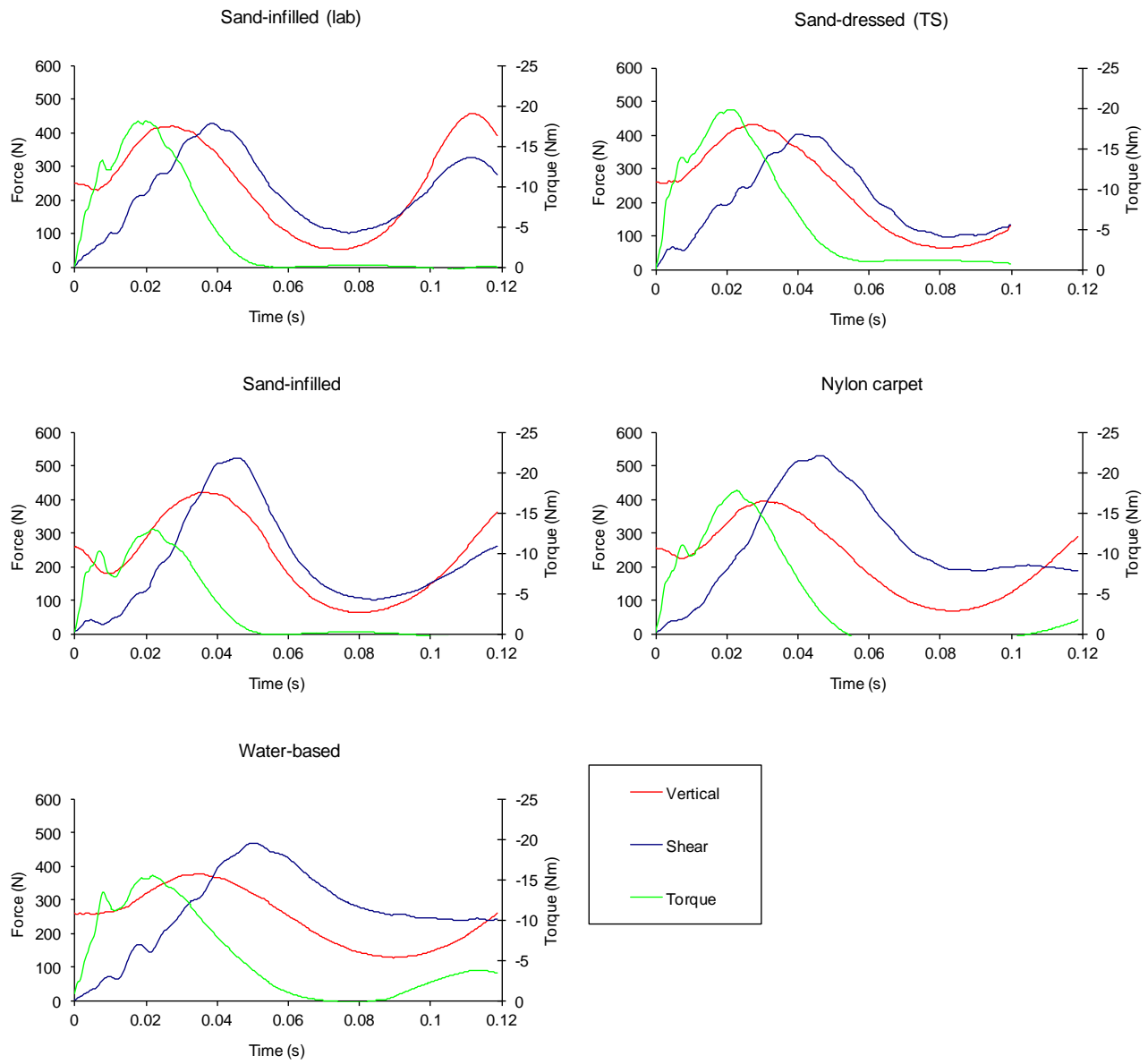


Figure 6.39 Combined Linear & Rotational Traction Test: force profiles on surfaces tested with pimped test foot

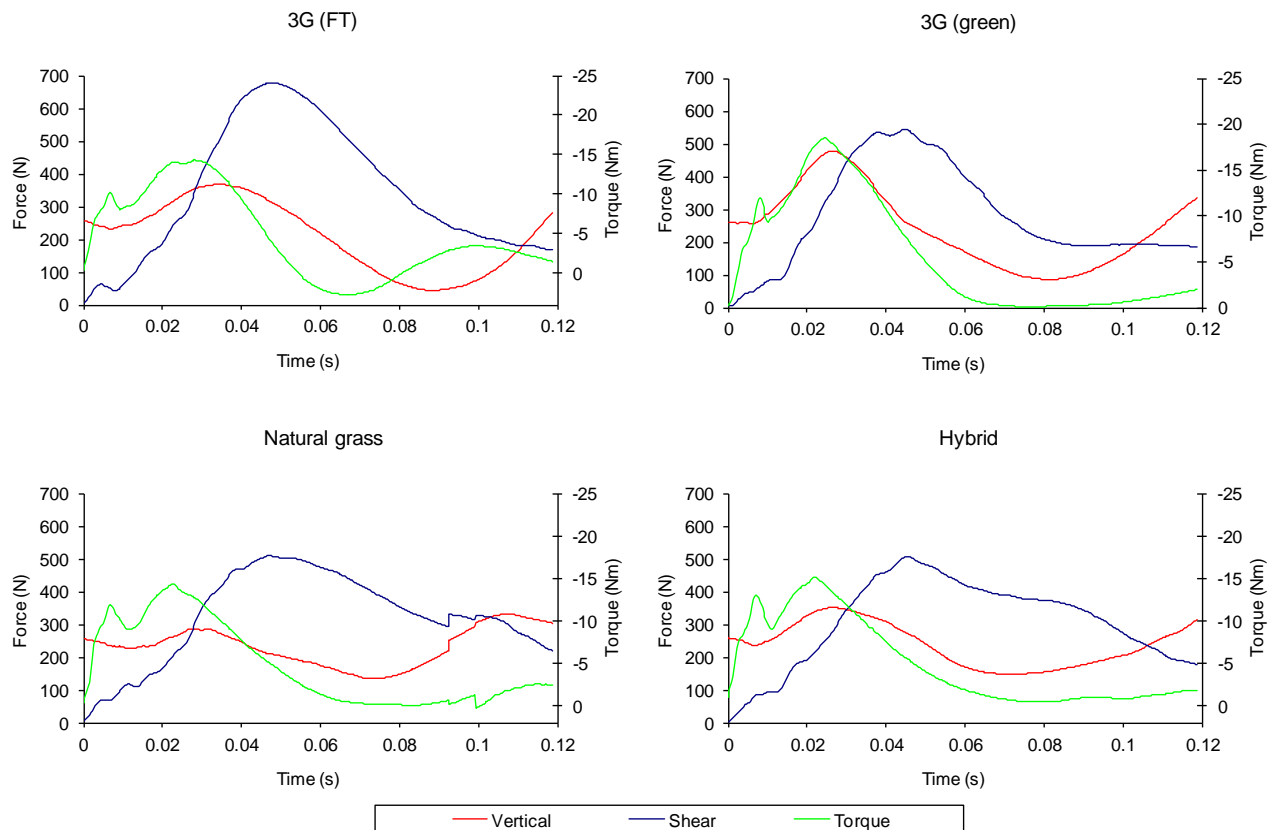


Figure 6.40 Combined linear and rotational traction test: force profiles on surfaces tested with studded test foot

The peak shear forces, linear traction ratios, peak torques and rotational traction ratios for the combined linear and rotational traction test for all surfaces are shown in Table 6.12.

For the tests with the pimples test foot, the lowest peak shear force of 411N was measured on the sand-dressed (TS) surface. The greatest mean peak shear force was observed on the nylon carpet surface. The outdoor sand-infilled pitch produced slightly lower shear values.

This result corresponds with the values for the linear traction coefficient. The highest traction coefficient was observed on the nylon carpet, with a linear traction coefficient of 1.72. The lowest linear traction coefficient was calculated on the sand-dressed surface (1.19).

The largest torque was measured on the sand-dressed surface with a value of 20Nm. The lowest torque of 13.1Nm was measured on the sand-infilled surface. The sand-infilled (lab) and the nylon carpet surface produced similar torques of 18.4Nm and 18.1Nm, respectively.

Rotational traction was calculated as the peak torque normalised to the vertical force measurement. The sand-infilled (lab) and the water-based surfaces produced the same value of 0.053m. The sand-infilled surface tested outdoors produced the lowest rotational traction value of 0.042m. The sand-dressed (TS) and nylon carpet produced similar rotational tractions of 0.049m and 0.051m, respectively.

For the tests conducted with the studded test foot and similar to the linear traction (under static vertical loading) test, the trials conducted on the natural grass and hybrid surfaces produced much more varied results than the artificial surfaces. For example, the peak shear force and torque measured on the natural grass surface ranged from 374N to 884N and from 11Nm to 18.3Nm, respectively. Therefore, any comparison between the natural and artificial turfs must be taken as indicative.

The magnitudes of the shear forces were higher for surfaces tested with the studded test foot compared to the pimped test foot. The peak shear forces were higher on the 3G (FT) compared to the 3G (green), although the results for the latter were quite varied (Table 6.12). With respect to the linear traction coefficients, the 3G (FT) produced similar values to the natural grass surface: 2.23 and 2.12, respectively. The other two surfaces produced lower but similar traction coefficients: 1.76 and 1.74, respectively.

The 3G (green) surface produced the largest peak torque value of 18.6Nm. The 3G (FT) produced the lowest torque. Examining the torque values, normalised to the vertical force, the two 3G surfaces produced the lower rotational traction values of 0.43 and 0.39, compared to the natural grass and hybrid surfaces.

Due to the smaller mass on the horizontal pendulum, the linear traction coefficient measured during the combined static linear and rotational test was on average 20% lower than the traction coefficient measured during the linear traction (under static vertical loading) test. However, the pattern of results between the two tests was similar. The nylon carpet surface produced the highest traction coefficient in both tests. Also, the water-based pitch produced higher traction coefficients than the sand-dressed and sand-infilled surfaces.

Site	Test Foot	Peak Shear Force (N)			Vertical Force at Peak Shear (N)			Linear Traction (μ_s)		
		Mean	Min	Max	Mean	Min	Max	Mean	Min	Max
Sand-infill (lab)	Pimpled	430	409	461	337	296	393	1.29	1.08	1.43
Sand-dressed (TS)	Pimpled	411	372	455	345	308	405	1.19	1.12	1.24
Sand-infilled	Pimpled	538	438	610	392	353	437	1.37	1.24	1.55
Nylon carpet	Pimpled	553	469	592	310	289	335	1.72	1.56	1.84
Water based	Pimpled	475	416	534	316	304	329	1.5	1.34	1.66
3G (FT)	Studded	686	624	714	308	293	328	2.23	2.09	2.44
3G (Green)	Studded	599	394	693	347	269	490	1.76	1.41	2.11
Natural Grass	Studded	565	374	854	274	177	351	2.12	1.29	2.97
Hybrid	Studded	559	401	758	316	247	390	1.74	1.62	1.94

Site	Test Foot	Peak Torque (Nm)			Vertical Force at Peak Torque (N)			Rotational Traction (λ_s)		
		Mean	Min	Max	Mean	Min	Max	Mean	Min	Max
Sand-infill (lab)	Pimpled	18.4	18.0	18.7	352	300	415	0.053	0.045	0.062
Sand-dressed (TS)	Pimpled	20.0	18.1	22.6	408	367	444	0.049	0.051	0.048
Sand-infilled	Pimpled	13.1	12.5	13.7	315	301	330	0.042	0.039	0.046
Nylon carpet	Pimpled	18.1	15.5	19.8	357	325	373	0.051	0.048	0.054
Water based	Pimpled	15.7	15.1	16.3	302	254	345	0.053	0.064	0.044
3G (FT)	Studded	14.5	13.5	16.5	342	300	415	0.043	0.040	0.048
3G (Green)	Studded	18.6	14.8	22.3	471	400	558	0.039	0.037	0.043
Natural Grass	Studded	15.8	11.3	23.8	294	221	400	0.052	0.048	0.060
Hybrid	Studded	16.7	12.9	22.8	342	248	499	0.050	0.046	0.052

Table 6.12 Combined linear & rotational traction test: results

For the surfaces tested with the pimpled test foot, the shortest time to the peak force was observed on the sand-infilled (lab) surface, followed by the sand-dressed (TS) surface. The water-based pitch produced the longest time (50ms) to the peak shear force (Figure 6.41). However, the peak shear loading rate was also greatest on the water-based surface. The shear loading rates ranged from 29.6kNs^{-1} to 43.2kNs^{-1} for the surfaces tested with the pimpled test foot (Figure 6.42a). The sand-infilled surfaces produced similar shear loading rates of 31kNs^{-1} and 32kNs^{-1} .

The time taken to reach the peak torque ranged from 20ms to 23ms, across all 5 surfaces tested with the pimpled test foot (Figure 6.41). As such, the torque loading rates resembled the same pattern of results as the peak torque measurements. The range of torque loading rates was 3.8kNms^{-1} to 5.6kNms^{-1} . The greatest torque loading rate was measured on the sand-dressed surface. The lowest torque loading rates were measured on the sand-infilled surfaces that were tested indoors and outdoors.

For the surfaces tested with the studded test foot, the times to the peak shear force and torque were similar to the surfaces tested with the pimples test foot, ranging from 45-48ms (shear force) and 22-28ms (torque) (Figure 6.41). The peak shear force loading rates were also similar, ranging from 32kNs^{-1} to 43kNs^{-1} (Figure 6.42), with the longest time being on the 3G (Green) surface and the shortest time on the Hybrid surface. Except for the 3G (FT) surface, the loading rates for the surfaces tested with the studded test foot were higher than the pimples test foot. The peak torque loading (Figure 6.43) was lowest on the 3G (FT) surface at 4.1kNms^{-1} and greatest on the natural grass surface at 5.7kNms^{-1} .

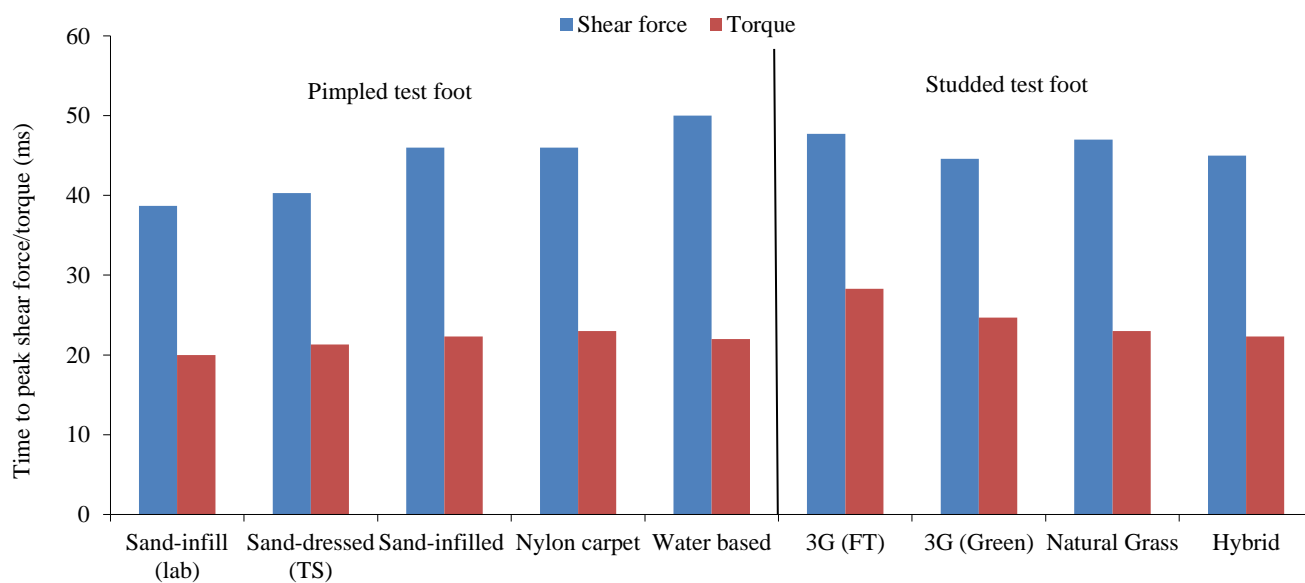


Figure 6.41 Combined linear & rotational traction test: time to peak shear and peak torque

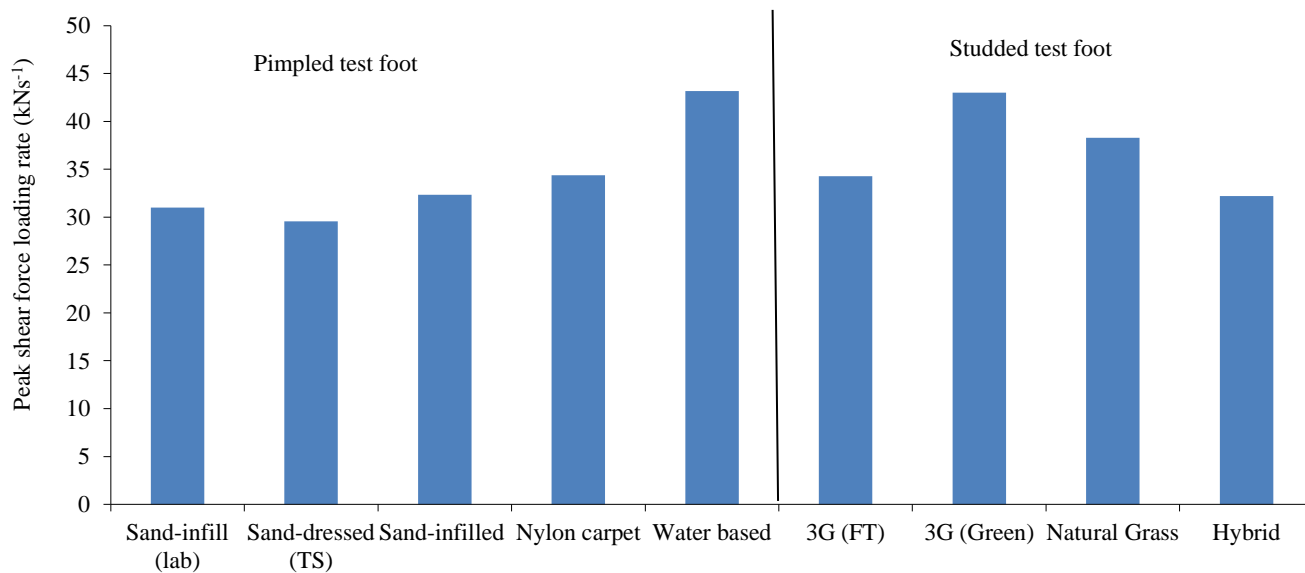


Figure 6.42 Combined linear & rotational traction test: shear force loading rate

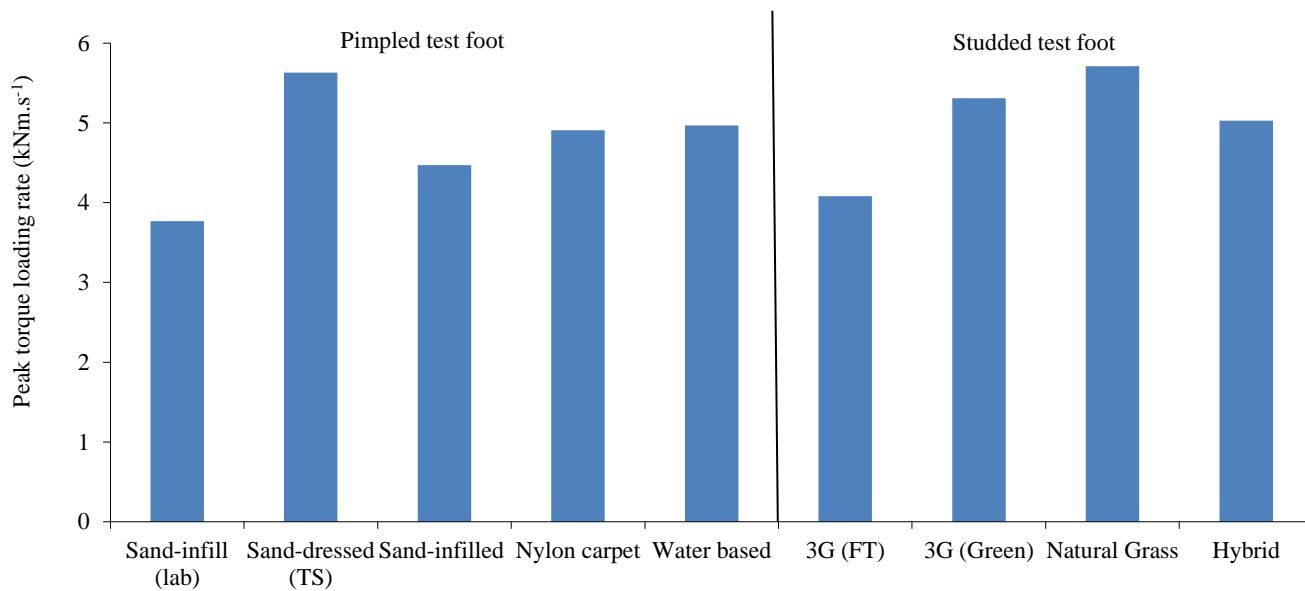


Figure 6.43 Combined linear & rotational traction test: torque loading rate

The resultant horizontal accelerations ranged from 17g to 29g, and the angular accelerations ranged from 2608 rads⁻² to 4454 rads⁻², for all surfaces (Figure 6.44 and Figure 6.45). As the angular acceleration was calculated from the output of the single axis accelerometers, the pattern of the results of linear and angular accelerations between the surfaces resembled each other. For the surfaces tested with the pimpled test foot,

the lowest accelerations were measured on the sand-infilled (lab) surface; the highest on the water-based surface. For the surfaces tested with the studded test foot, the peak accelerations were similar for all turfs, except for the hybrid turf. For the 3G surfaces and the natural grass turf, the horizontal and angular accelerations ranged from 27 to 29g and 4018 to 4345 rads⁻², respectively. The acceleration values for the hybrid surface were lower at 23g and 3425 rads⁻².

The horizontal and angular displacements of the test foot are shown in Table 6.13. The average displacements of the test foot ranged from 71mm to 89mm horizontally, and 1.0 rad to 1.4 rad rotationally. There were no differences in the displacement of the test foot between surfaces tested with the pimpled test foot and studded test foot.

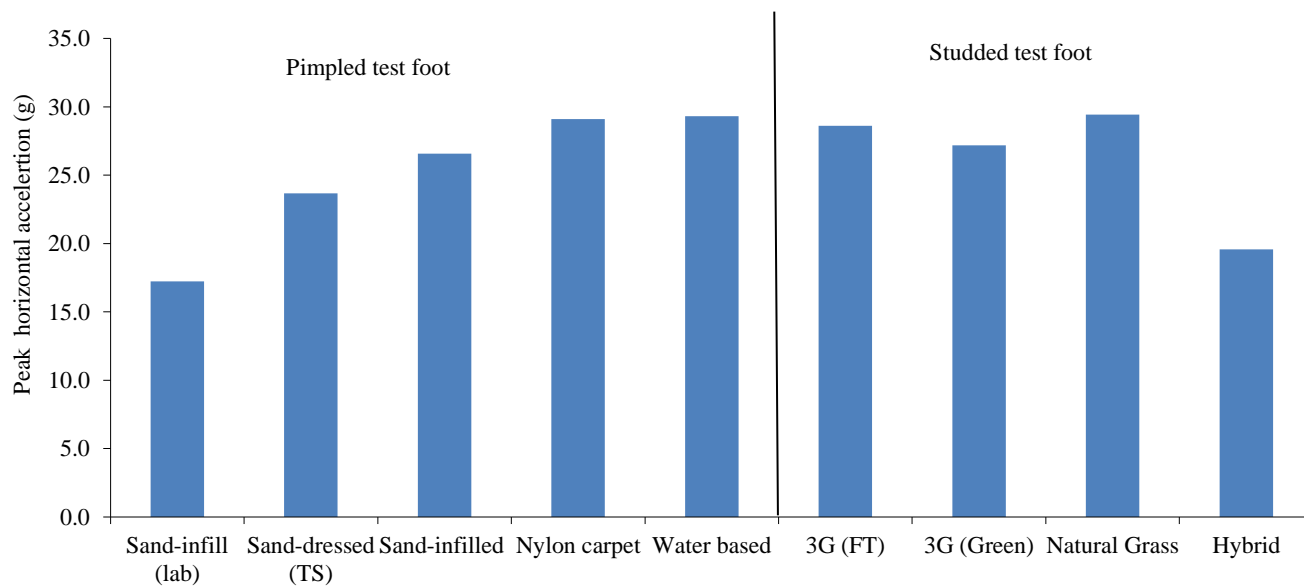


Figure 6.44 Combined linear & rotational traction test: peak horizontal acceleration of the test foot

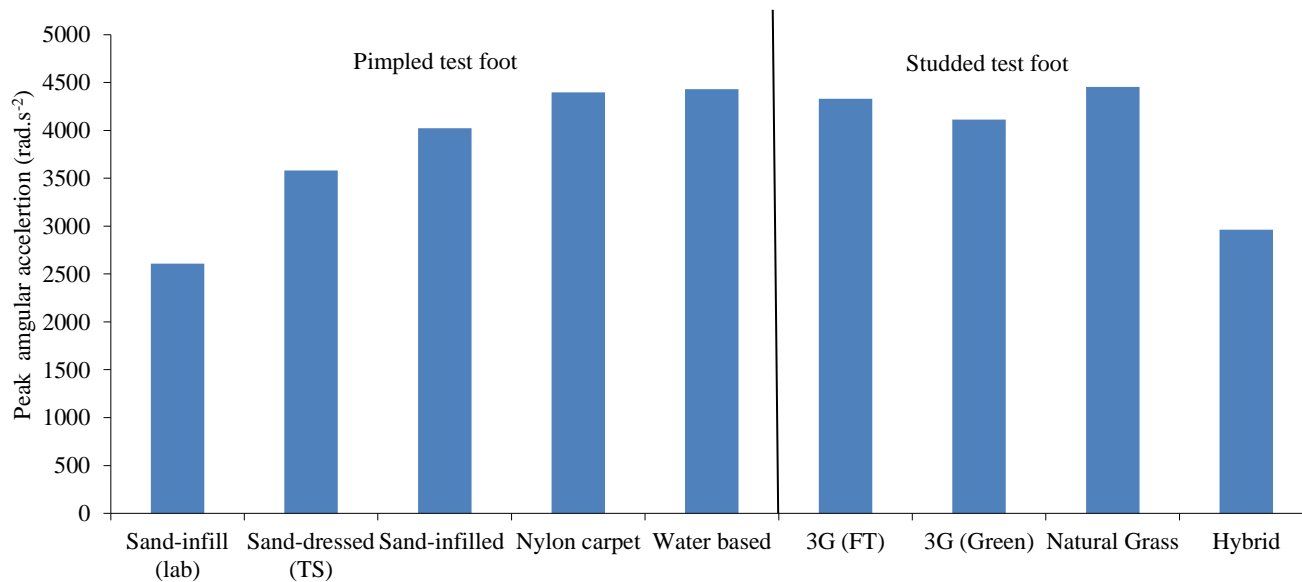


Figure 6.45 Combined linear & rotational traction test: peak angular acceleration of the test

Site	Test Foot	Peak Horizontal Displacement (mm)			Peak Angular Displacement (rad)		
		Mean	Min	Max	Mean	Min	Max
Sand-infill (lab)	Pimpled	85	80	89	1.31	1.23	1.37
Sand-dressed (TS)	Pimpled	63	58	69	0.97	0.90	1.06
Sand-infilled	Pimpled	86	74	92	1.32	1.15	1.41
Nylon carpet	Pimpled	67	59	76	1.03	0.92	1.18
Water based	Pimpled	82	75	95	1.26	1.15	1.46
3G (FT)	Studded	77	70	81	1.19	1.08	1.25
3G (Green)	Studded	71	54	91	1.10	0.83	1.40
Natural Grass	Studded	81	59	102	1.25	0.91	1.58
Hybrid	Studded	89	53	125	1.37	0.82	1.93

Table 6.13 Combined linear & rotational traction test (pimpled foot): Peak horizontal displacement and rotational displacement

6.5.4 Vertical Impact Test

6.5.4.1 Reference Surface (concrete)

A test using the 'vertical' pendulum with the 20kg mass was conducted on a concrete surface to provide reference value for the vertical force and as a basic comparison with the Berlin Athlete test. The concrete surface was the floor of the mechanical workshop of the Bioengineering Unit. One trial of the test was

performed.

The vertical impact test conducted on the concrete surface produced very sharp transient shocks just after impact, up to approximately 8000N (Figure 6.46). This was ignored as mechanical noise caused by the high frequency impact. The first significant peak occurred at 16.3ms following impact with a magnitude of 4300N. A second peak of 3600N occurred at 29ms.

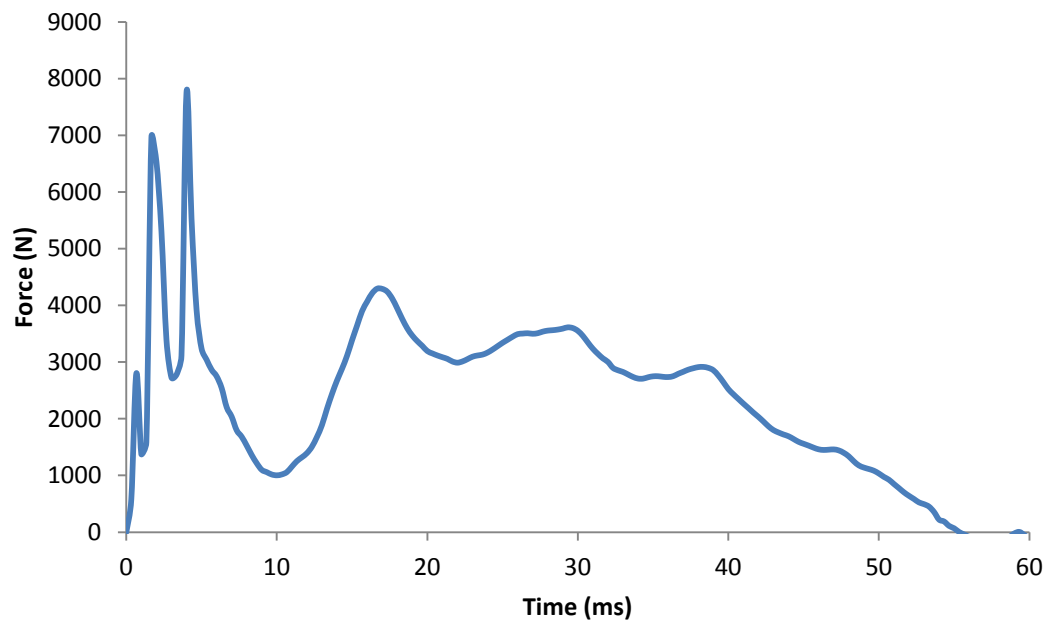


Figure 6.46 Vertical impact test: vertical force profile on concrete

6.5.4.2 Pitch Tests

The force profile for produced during the vertical impact test can be generally characterised by a curve containing three peaks (Figure 6.47 and Figure 6.48). The first, sharp peak can be regarded as an insignificant event of the whole test. It is the result of the initial impact of the base of the pendulum head on the top of the test foot shaft. Following this initial impact, the effect of the spring in the pendulum head retarded the loading rate.

The first significant peak force occurred at approximately 20ms following the impact of impact. The magnitude of this peak force ranged from 2888N to 3440N for all the tests conducted. A second significant peak was observed on all surfaces, except for the hybrid grass surface. This peak occurred at approximately

33ms from the moment of impact. The magnitude of this peak force ranged from 3081 to 3350N.

The two peaks may have been caused by either the pendulum head ‘bouncing on the ball transfer unit or by the turf bottoming out with the test foot contacting a harder surface used as a base underneath the turf. Further investigation of this phenomenon is required to explore the origins of these two vertical force peaks and their impact on the testing process. It was assumed that the first peak was of most importance as this signifies the initial impact of the pendulum/test foot system with the surface. Therefore, the following discussion of the results will focus on the first vertical force impact peak.

As with the other tests, the evaluation of the results from the tests conducted with the pimped test foot and the studded test foot was conducted separately. It could be assumed that any differences in the material properties of the rubber used for the two test feet tread would not significantly affect the outcome of this test. Future work should be conducted to quantify if this factor significantly alters the vertical force propagation.

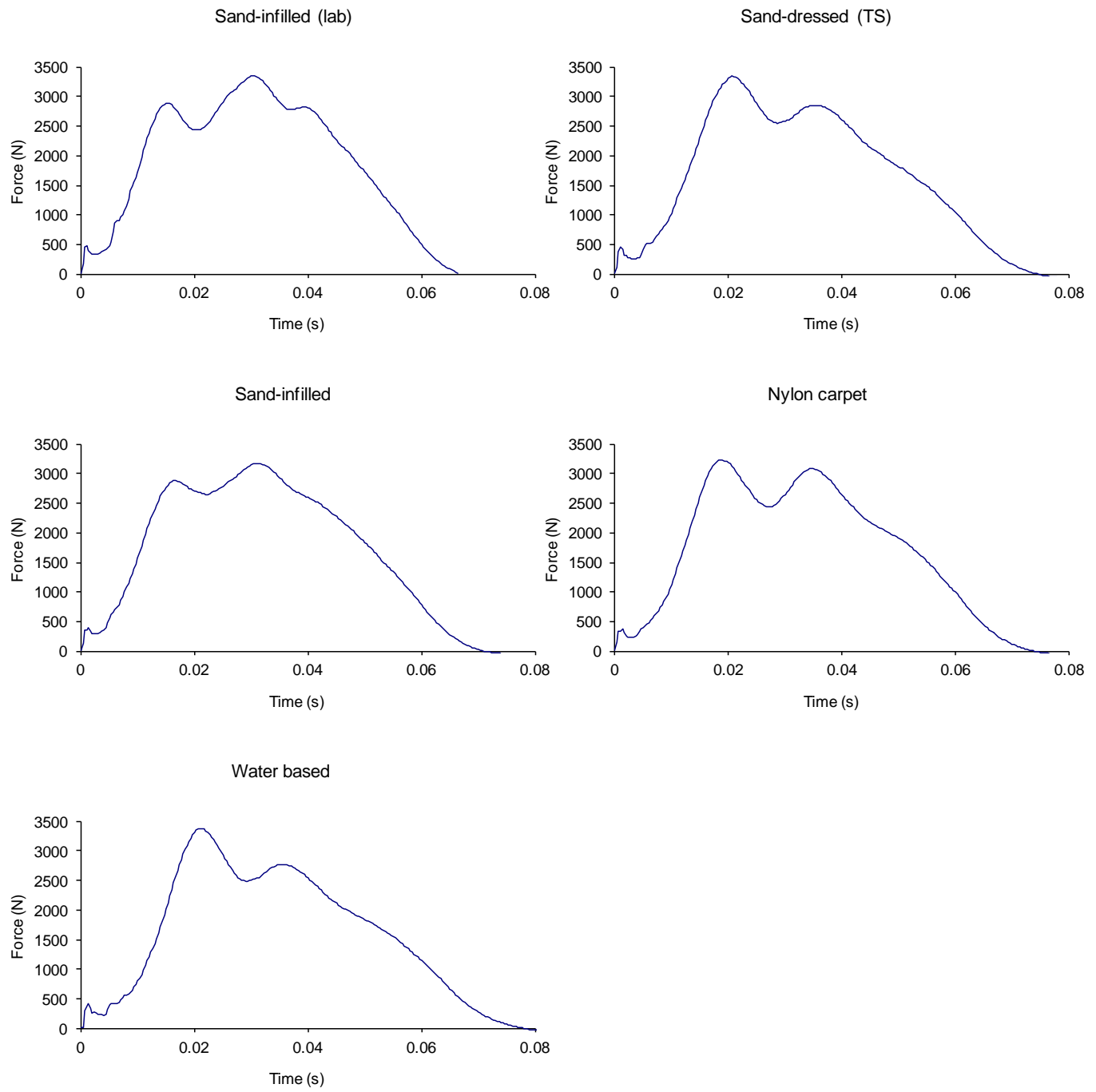


Figure 6.47 Vertical impact test: vertical force profiles (pimpled test foot)

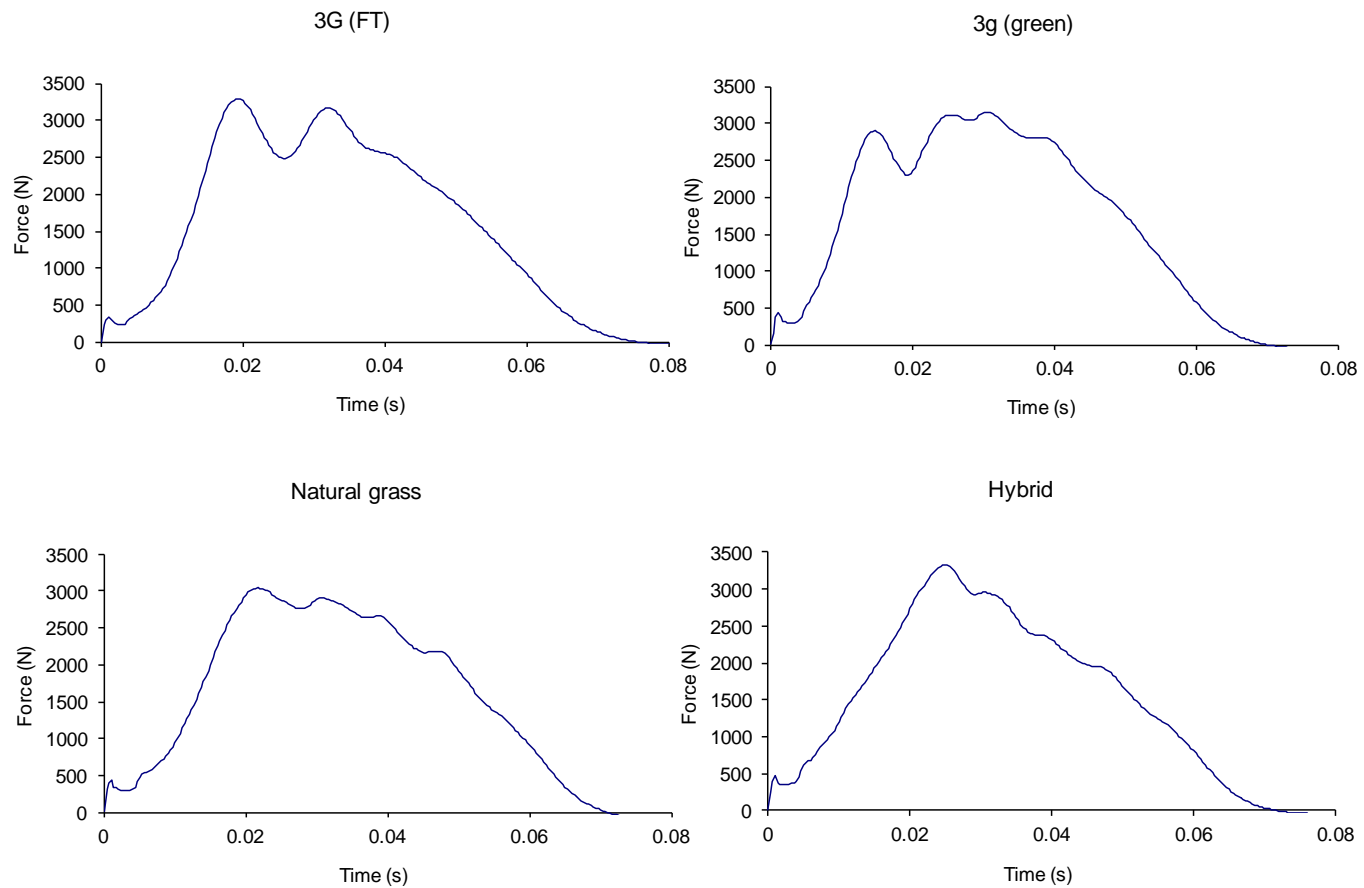


Figure 6.48 Vertical impact test: vertical force profiles (studded test foot)

The data from the vertical impact tests were analysed by examining the magnitude of the first significant peak and the time taken from the moment of impact to this first peak (Table 6.14). The maximum loading rate was also calculated over the time period from 6ms following impact to the first peak. The first 6ms was not included in order to remove the transients shocks, described previously, from the data.

Site	Test Foot	Peak 1 Force (N)			Peak 1 time (ms)			Loading rate (kNs ⁻¹)		
		Mean	Min	Max	Mean	Min	Max	Mean	Min	Max
Sand-infill (lab)	Pimpled	2888	2758	2962	16	15	16	450	423	485
Sand-dressed (TS)	Pimpled	3362	3250	3447	21	19	22	319	307	328
Sand-infilled	Pimpled	2931	2854	3034	17	15	18	325	294	350
Nylon carpet	Pimpled	3242	3203	3307	19	18	20	333	315	345
Water based	Pimpled	3440	3362	3513	21	19	23	352	315	389
3G (FT)	Studded	3326	3252	3405	19	19	20	351	324	370
3G (Green)	Studded	2926	2848	2994	15	14	15	392	365	426

Site	Test Foot	Peak 1 Force (N)			Peak 1 time (ms)			Loading rate (kNs ⁻¹)		
		Mean	Min	Max	Mean	Min	Max	Mean	Min	Max
Natural Grass	Studded	3355	3226	3478	22	18	26	313	238	418
Hybrid	Studded	3357	3179	3494	25	24	26	241	205	273

Site	Test Foot	Peak Vertical Acceleration (g)			Peak Vertical Displacement (mm)		
		Mean	Min	Max	Mean	Min	Max
Sand-infill (lab)	Pimpled	8.4	5.8	10.3	4	1	7
Sand-dressed (TS)	Pimpled	13.6	12.9	14.2	11	6	21
Sand-infilled	Pimpled	9.3	7.5	10.5	11	3	31
Nylon carpet	Pimpled	13.1	11.5	14.5	16	6	26
Water based	Pimpled	16.2	14.6	17.7	7	6	8
3G (FT)	Studded	15.8	14.5	16.6	7	3	11
3G (Green)	Studded	11.1	9.0	12.3	5	5	6
Natural Grass	Studded	13.8	8.5	19.0	9	7	11
Hybrid	Studded	9.0	7.5	10.2	16	10	24

Table 6.14 Vertical impact test: Results

For the tests conducted with the pimpled test foot, the sand-infilled surfaces produced the lowest peak forces.. These surfaces had the shortest time to the peak force of 16-17ms. The greatest peak force was measured on the water-based pitch with a magnitude of 3440N. The loading rate greatest on the sand-infilled surface tested on the lab (450kNs⁻¹). The other surfaces had similar loading rates, ranging from 319kNs⁻¹ to 351kNs⁻¹.

It was expected that for the tests conducted with the studded test foot on the ‘softer’ longer pile surfaces that the vertical forces would be lower than the ‘harder’, short pile surfaces tested with the pimpled foot. However, this was not the case. This may be due to the increased shore hardness of the studs than the rubber pimples.

The 3G (FT), natural grass and hybrid grass surfaces produced similar peak forces of 3326-3357N. The vertical force measured on the 3G (Green) surface was noticeably lower than the other surfaces with a magnitude of 2926N.

The mean times to the peak force were lower and the mean loading rates were higher on the artificial turfs compared to the grass surfaces. The loading rate that was measured on the natural grass surface was

variable, ranging from 237kNs^{-1} to 418kNs^{-1} . The loading rates on the 3G (FT) surfaces were much lower and fell within the limits produced by the natural grass surfaces. The wet pitch conditions during the testing of the hybrid grass surfaces were reflected in the considerably lower loading rates measured on this surface. It appears that the shorter the time to the peak force and the higher the loading rate, the lower the peak force.

6.5.5 3D Low Impact Test

During this test, the mass of the pendulum that provided the vertical loading was reduced to 10kg. This was provided a vertical load of approximately. Unfortunately, following the analysis of the results of this test, it was apparent that the two pendulums heads (providing the vertical and horizontal loads) did not impact within 10ms of each other for any of the trials conducted on the different surface. Therefore, it was decided to discard the results of this test from the study, as they would not represent an accurate 3D impact test. The reason for the disparity between the impacts of the two pendulum heads will be discussed during the next section.

6.5.6 3D High Impact Test

The force profiles measured during the combined, 3D (three directional) loading are displayed in Figure 6.49. The shapes of the profiles were similar to those observed in the other, unidirectional tests. Two vertical force peaks were produced on the artificial turfs, while only one peak was produced on the natural grass turf.

The magnitude of the first vertical force peak ranged from 3000N to 3400N (Table 6.15) and the time taken to this first peak was approximately 15-20ms. The shear force reached a peak at approximately 35-50ms with a magnitude ranging from 1400-1600N. The measured torque reached a peak of approximately 34-42Nm at 15-35ms following impact. The surfaces tested with the pimpled test foot produced similar torque values of 39Nm and 42Nm. For the surfaces tested with the studded test foot, the 3G (FT) surface produced noticeably lower torques than the natural grass surfaces, 34Nm compared to 42Nm.

The sand-infilled surface produced lower peak vertical forces and torques but higher peak shear

forces than the nylon carpet surface. The 3G (FT) surface produced a lower peak vertical force and torque but similar shear forces compared to the natural grass surface.

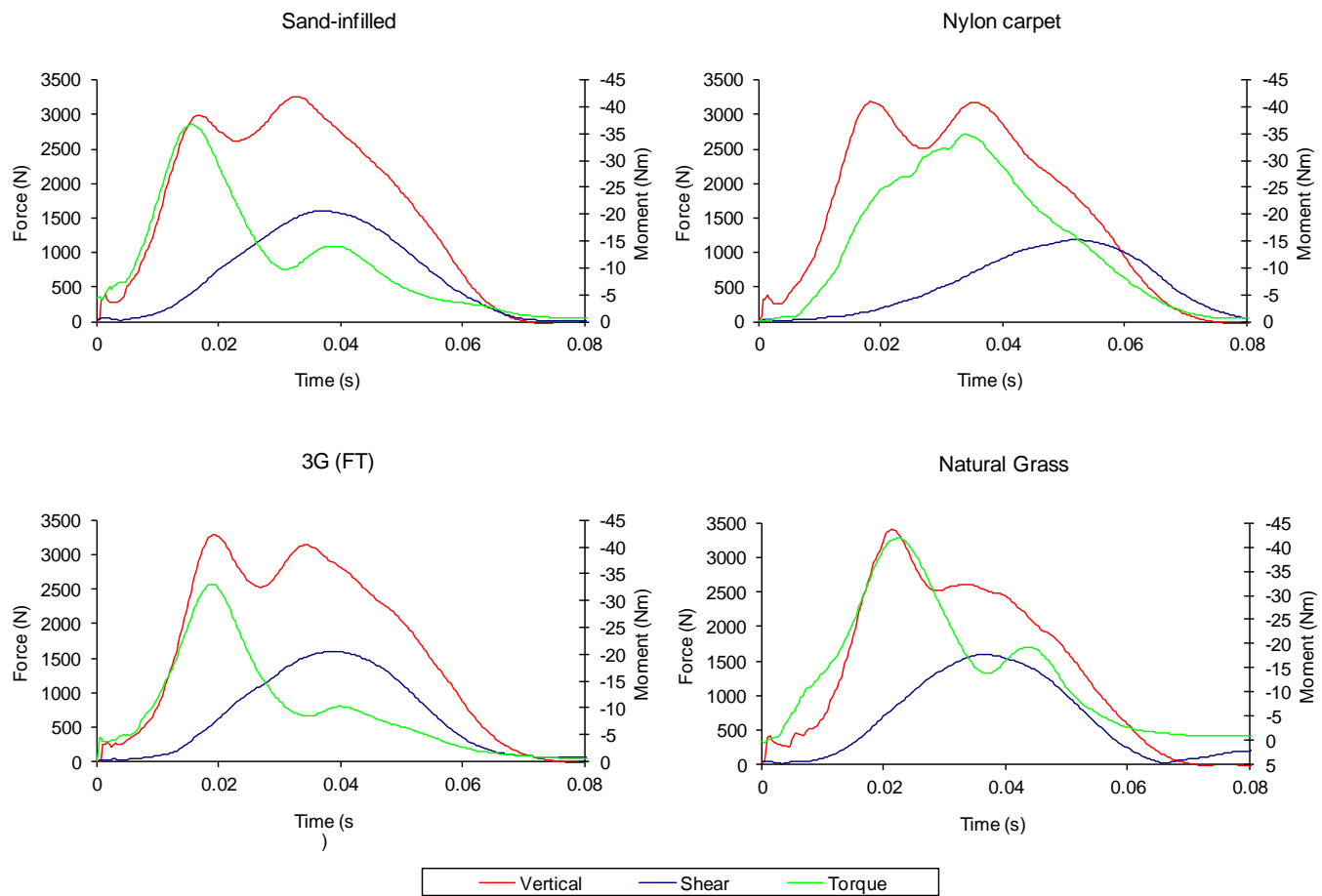


Figure 6.49 3D High Impact Test: Loading profiles on surfaces tested with pimped (top) and studded (bottom) test feet

Site	Test Foot	1st peak Vertical Force (N)			Peak Shear Force (N)			Peak Torque (Nm)		
		Mean	Min	Max	Mean	Min	Max	Mean	Min	Max
Sand-infilled	Pimpled	3030	2987	3109	1625	1575	1703	39	30	45
Nylon carpet*	Pimpled	3205	3158	3260	1414	1363	1492	42	41	44
3G (FT)	Studded	3365	3300	3399	1602	1552	1687	34	29	39
Natural Grass**	Studded	3408	3365	3450	1601	1557	1624	42	40	44

Site	Test Foot	Vertical Loading Rate (kNs ⁻¹)			Shear Loading Rate (kNs ⁻¹)			Torque Loading Rate (kNms ⁻¹)		
		Mean	Min	Max	Mean	Min	Max	Mean	Min	Max
Sand-infilled	Pimpled	342.4	309.4	398.2	91.6	83.3	108	5.0	3.7	6.0
Nylon carpet*	Pimpled	320.7	308.5	326.9	71.9	70.9	72.6	5.4	5.2	5.6
3G (FT)	Studded	394.6	375.8	420	87.7	77.7	104	3.6	3.2	4.4
Natural Grass**	Studded	353.8	353.3	354.4	92.7	86.3	99	3.5	3.1	4.0

Site	Test Foot	Peak Vertical Acceleration (g)			Peak Horizontal Acceleration (g)			Peak Angular Acceleration (rads ⁻²)		
		Mean	Min	Max	Mean	Min	Max	Mean	Min	Max
Sand-infilled	Pimpled	10.1	8.9	11.9	45.6	33.7	60.9	6909	5098	9216
Nylon carpet*	Pimpled	14.2	13.5	15.1	45.1	43.3	47.0	6821	6557	7109
3G (FT)	Studded	16.6	14.5	18.3	42.6	27.7	56.5	6448	4190	8550
Natural Grass**	Studded	13.3	10.0	16.6	29.6	26.8	32.4	4480	4050	4910

Site	Test Foot	Peak Vertical Displacement (mm)			Peak Horizontal Displacement (mm)			Peak Angular Displacement (rad)		
		Mean	Min	Max	Mean	Min	Max	Mean	Min	Max
Sand-infilled	Pimpled	5	3	7	46	27	79	0.71	0.41	1.23
Nylon carpet*	Pimpled	18	10	36	26	19	39	0.40	0.29	0.61
3G (FT)	Studded	11	7	14	47	37	60	0.73	0.57	0.92
Natural Grass**	Studded	7	6	9	37	35	38	0.57	0.54	0.59

Site	Test Foot	Linear Traction (μ_d)			Rotational Traction (λ_d)		
		Mean	Min	Max	Mean	Min	Max
Sand-infilled	Pimpled	0.62	0.56	0.66	0.017	0.014	0.019
Nylon carpet*	Pimpled	0.67	0.58	0.73	0.014	0.014	0.014
3G (FT)	Studded	0.62	0.55	0.70	0.021	0.014	0.028
Natural Grass**	Studded	0.67	0.59	0.74	0.024	0.018	0.029

* data from trials 2,3 & 5 **data from trials 3 & 4

Table 6.15 3D High Impact Test: results

Vertical loading rates ranged from 321kNs⁻¹ to 395kNs⁻¹, shear loading rates ranged from 72kNs⁻¹ to 93kNs⁻¹; and the torque loading rates ranged from 3.5kNms⁻¹ to 5.4kNms⁻¹. The nylon carpet surface produced lower vertical and shear loading rates but greater torque loading rates than the sand-infilled surface, whose test results were more varied. The 3G (FT) surface produced greater vertical loading rate,

lower shear loading rate and similar torque loading rate compared to the natural grass turf. However, the results for the natural grass surface were averaged from only two trials.

The accelerations of the test foot, or impact shock, are described as follows. For the four surfaces, the peak vertical acceleration ranged from 10g to 17g, the peak shear acceleration ranged from 30g to 48g, and the peak angular acceleration ranged from 4480 rads^{-2} to 6909 rads^{-2} . The nylon carpet surface produced greater vertical accelerations than the sand-infilled surface, but had similar peak acceleration results in the other directions. The natural grass surface had lower peak accelerations in all three directions, compared to the 3G (FT) surface.

As previously conducted with the other types of test, the acceleration data was double integrated to calculate a measurement of displacement. For all four surfaces examined in this test, the peak vertical displacement ranged from 5mm to 18mm, the peak shear displacement ranged from 26mm to 47mm, and the peak angular displacement ranged from 0.4 radians to 0.71 radians. The nylon carpet surface produced noticeably larger vertical displacements compared to the sand-infilled surface. However, the shear and angular displacement were lower on the nylon carpet surface. For the surfaces tested with the pimpled foot, the 3G (FT) produced higher displacements in all three directions compared to the natural grass surface.

Linear and rotational traction values were also calculated for this type of test. The linear traction coefficients ranged from 0.62 to 0.67 and the rotational traction coefficients ranged from 0.014 to 0.024. The nylon carpet surface produced a higher linear traction coefficient but lower rotational traction coefficient compared to the sand-infilled surface. The 3G (FT) surface produced both lower linear and rotational traction coefficients compared to the natural grass surface.

6.5.7 Comparison of the Multidirectional Test to the Unidirectional Tests

The response of a particular surface to impact under multidirectional loading may be different to when it is loaded in a single direction at a time. Due to the three dimensional nature of human impact during controlled sports movements, this may validate the use of the turf testing rig. The following section will compare the

results of the four surfaces examined in the 3D high impact test, with their corresponding results from the unidirectional tests in which the falling pendulum masses were the same. Therefore, the vertical impact test and the combined linear and rotational traction test were used for comparison. The data was analysed to look for consistent differences in the mean, minimum and maximum values between the multidirectional and unidirectional tests.

6.5.7.1 Vertical Direction

The response of the surfaces to the two different test procedures (3D high impact test and vertical impact test) varied between different surfaces, with respect to loads applied in the vertical direction (Table 6.16). A uniform increase or decrease in test parameters was not observed across the surfaces tested. For example, the peak vertical force and loading rate increased during the high impact test on the sand-infilled surface, whereas these values decreased for the nylon carpet surface for the same test. There was no consistent difference in peak forces between the two tests on the 3G surface and natural grass, although the loading rate was greater on the 3G surface during the high impact test. The largest difference in peak forces (+100N) and loading rate (+40kNs⁻²) represented a 3.4% increase of the peak load and a 12.3% increase of the peak loading rate measured during the vertical impact test, respectively.

The impact shocks on most of the surfaces increased only slightly (1g or 7%) during the high impact test. The vertical displacement of the test foot differed by -6mm to +4mm during the high impact test across the four surfaces. This represented a 55% decrease on the sand-infilled surface and a 25% increase on the nylon carpet surface.

Surface	Parameter			
	Peak Force (N)	Loading Rate (kNs ⁻²)	Impact Shock (g)	Displacement (mm)
Sand Infill	+100	+15	+1	-6
Nylon Carpet	-40	-12	+1	+2to4
3G (FT)	NC	+40	+1	+4
Natural grass	NC	NC	NC	-2

Table 6.16 Test results of the multidirectional 3d high impact test relative to unidirectional vertical impact test values (approximate values). NC= No consistent difference

6.5.7.2 Horizontal (Shear) direction

As can be seen from Table 6.17, the peak shear force, shear loading rate and horizontal impact shock were generally greater during the 3D high impact test compared to the combined linear and rotational test. Conversely, the horizontal displacement and the linear traction ratio decreased. The peak shear force increased by approximately 900N to 1000N (265-365%) during the 3D high impact test. The shear loading rate increased by approximately 35kNs^{-2} to 60kNs^{-2} (100 to 176%). The large increases in the peak loads and loading rates may be a consequence of the increased horizontal resistance to loading caused by the much greater vertical force applied during the 3D high impact test.

On the sand-infilled and nylon carpet, the impact shock increased by between 15g to 20g during the 3D high impact test. This represented a 52-80% increase. The horizontal displacement of the test foot was decreased by 30mm to 40mm (60-65%). Finally, the linear traction ratio decreased by 0.75 to 1.6 (55-72%) during the 3D high impact test.

Surface	Parameter				
	Peak Force (N)	Loading Rate ($\text{kN}\cdot\text{s}^{-2}$)	Impact Shock (g)	Displacement (mm)	Linear Traction Ratio
Sand Infill	+1000	+60	+20	-40	-0.75
Nylon Carpet	+900	+35	+15	-40	⁻ 1.1
3G (FT)	+900	+50	NC	-30	⁻ 1.6
Natural grass	+1000	+55	NC	-40	⁻ 1.45

Table 6.17 Approximate multidirectional test horizontal values relative to Combined Linear & Rotational Traction Test horizontal values. NC= No consistent difference

6.5.7.3 Rotational Direction

In general, the 3D high impact test produced greater peak torques and impact shocks, and decreased rotational displacement and rotational traction ratio than the combined linear and rotational traction test. The peak torques were increased by between 20Nm to 25Nm (138-190%). The angular acceleration of the test foot increased by 3000rads^{-2} (75%) on the sand-infilled and nylon carpet surfaces, but there was no

consistent difference between the two tests on the 3G and natural grass surfaces. The rotational displacement of the test foot decreased by between 0.4 radians to 1.0 radians (37-80%) and the rotational traction ratio decreased by between 0.022 to 0.037 (50-73%) during the 3D high impact test.

Surface	Parameter				
	Peak Torque (Nm)	Loading Rate (kNms ⁻²)	Impact Shock (rads ⁻²)	Displacement (rad)	Rotational Traction Ratio
Sand Infill	+26	NC	+3000	-0.6	-0.025
Nylon Carpet	+25	NC	+3000	-0.6	-0.037
3G (FT)	+20	NC	NC	-0.4	-0.022
Natural grass	+20to25	NC	NC	-0.4to ^{-1.0}	-0.03

Table 6.18 Approximate multidirectional test rotational values relative to Combined Linear & Rotational Traction Test rotational values. NC = no consistent difference.

6.6 Summary of the Design and Initial Testing of the Strathclyde Sports Turf Testing Rig

6.6.1 Design

The design of the Strathclyde Sports Turf Testing Rig (SSTTR) allowed different characteristics to be assessed *in situ* on various types of artificial and natural sports surfaces. Furthermore, the rig incorporated a degree of functional flexibility that permitted a variety of tests to be conducted. These included unidirectional and multidirectional tests.

Unidirectional tests allowed the characterisation of the standard mechanical properties of the sports surfaces, such as peak horizontal and vertical loading and loading rates; linear and rotational traction (under static and dynamic vertical loading); vertical loading/shock absorbancy; surface deformation under loading; and ‘foot’ sliding and twisting (horizontal and angular distance and acceleration).

The SSTTR’s multidirectional tests mimicked the complex and dynamic loading that occur in actual sporting movement. The combination of a vertical, shear and torque loading in one simultaneous impact action for *in situ* assessment is a breakthrough in the artificial turf testing arena. While the *TrakTester* device (Grund & Senner, 2010) and Villwock *et al*’s (2009) testing apparatus also provide combined vertical, loading and torque loading, the extent to which they mimic the biomechanical loading profiles observed in

actual sporting movements is unclear from published articles.

The importance of replicating the real-life playing conditions as closely as possible during the assessment of sports surfaces is widely recognised. In this sense, the use of a standard test foot material for all surfaces is inappropriate. While a standard test foot would allow for consistency in testing conditions across surfaces, the comparison of the characteristics of playing surfaces designed different uses and for different footwear is unrealistic and flawed. Therefore, the design of the SSTTR is flexible to allow the use of different types and design of test foot.

6.6.1.1 *Design limitations*

As with all prototypes, there are several limitations which identifies areas for future design enhancement and optimization. The limitations of the SSTTR are as follows:

1. *Anatomical validity of the test foot.* The design of the SSTTR's test foot does not represent the anatomical structure of the foot and the structure of a whole playing shoe. Therefore, it does not replicate the flattening of the foot arch and the pressure distribution over the sole which occurs in human movement. The *TrakTester* (Grund & Senner, 2010), for example, does include a sophisticated ankle-foot model which fits inside a proper sports shoe.
2. *A synchronicity problem between the vertical and shear pendulum impacts.* This issue was most clear in the low impact 3D test (section 6.5.5) when the interval between the vertical pendulum and shear pendulum impacting was greater than 10ms (the defined threshold for impact synchronicity). The two pendulums were designed to fall under gravity from the same height around frictionless radial bearings. While the pendulums impacted within 10ms of each for the majority of tests when the pendulums were used dynamically, it is not entirely obvious why this issue occurred sporadically or why this it was most prevalent in the low impact 3D test. However, there are four possible causes for the insynchronicity in the pendulums' impact:

a) *Use of a simplistic model of a pendulum during the design stage.* As discussed in section

6.3.3.1, the model used to calculate the masses of the pendulum and spring constants did not account for rotational inertia. This may have had a considerable effect on the pendulum mechanics.

- b) *Errors in the pendulums' design and construction.* Although quality controls checks were conducted throughout design and construction the test rig, small errors may have led to the two pendulums falling from slightly different heights
- c) *Different resistance levels in the pendulums' radial bearings.* This is unlikely as all four bearing (two for each pendulum) had the same specification and sourced from the same manufacturer. However, as the test rig was used outdoors on several occasions and the bearings were protected only by the polycarbonate fascia covering the upper section of the test rig, dirt may have got into a bearing(s) causing additional resistance.
- d) *Variable residual holding force of the electromagnets used to release the pendulums simultaneously.* As described in section 6.3.4, each magnet had a residual holding force of 70N with a 0mm air gap between the magnet and armature plate on the back of the pendulums. However, the magnet and armature plate would have to be perfectly aligned to achieve a 0mm air gap. It is likely that the use of the test rig *in situ*, on sometimes uneven ground, combined with the repeated releasing and raising of the pendulums, may have led to a misalignment of the magnets on the armature plate. This in effect may have altered the residual holding force after the magnets were electrically stimulated to release the pendulums. For example, if the residual holding force of pendulum A's magnet was greater than pendulum B's magnet, this may increase the resistance to motion of pendulum A, causing the two pendulums to impact at different times.

3. *Potential misalignment of the shear force load.* The alignment of the shear force load in tests when the vertical load was static (Test 1 and Test 3) sometimes tended to raise the test foot slightly off

ground on one edge in the resting position, therefore conversely push it slightly into the ground when the shear pendulum impacted. This sometimes resulted in an increase or decrease in the ‘static’ vertical load. This is likely to be a result of the alignment of the steel cable running from the L-crank lever to the test foot, and/or the degree the L-crank lever rotates around its axis when the shear pendulum impacts. A large rotation would cause the steel cable to become angled upwards relative to the horizontal. Furthermore, while attempts were made to keep the whole test rig level with the rig support feet (section 6.3.9), a very uneven test surface may have introduced alignment errors. This may account for the rise and fall in the ‘static’ vertical force observed on the less even natural and hybrid surfaces tested. Furthermore, when considering the traction results from Test 1, the variation in the static vertical loading needs to be taken into account.

4. *High loading rates.* The SSTTR tend to apply loads faster a greater rate than what was observed during the biomechanical analysis. This was possibly due to an inappropriate selection of the spring stiffness for the pendulum. Selecting spring with a lower spring constant or introducing additional damping into the pendulum head system will likely reduce the loading rates.
5. *Design and size of the test rig.* As with most prototypes, the main emphasis was to establish that the concept works and meets the initial design criteria. This first prototype of the SSTTR meets the requirements. However, the size and weight of the test rig caused some problems with manoeuvring it around sports pitches and transporting it to test sites. Furthermore, the SSTTR may be viewed as a little ugly and cumbersome. Future iterations should consider adapting its design and aesthetics to improve its manoeuvrability for *in situ* testing and marketability.

6.6.2 Biomechanical validity

Based on a drop-mass/spring/mass concept, the basic operation of the test rig was composed of two weighted pendulums and an L-crank lever system. This allowed the applications of loads to the surface via a test foot in vertical, horizontal and rotational directions in one impact, thus replicating the multidirectional and

dynamic loading which occurs in athletic sports movements.

As can be seen from the results of the high impact 3D test (Test 6) (section 6.5.6), the magnitudes of the vertical, shear and torque loads are broadly representative of the ground reaction forces and moments observed in the biomechanical testing of the human subjects (section Chapter 4).

To demonstrate this, Figure 6.50 shows a comparison of the upper quartile ground reaction force profiles (vertical, horizontal free moment) measured during the biomechanical testing of the five types of sports movements (*RUN*, *STOP*, 45° running ‘cut’ turn, 90° running ‘cross’ turn, 180° turn from a standing start) performed indoors on 3G artificial turf (T3) with the ground loadings (vertical, shear, torque) produced by the SSTTR during high impact 3D on similar 3G artificial turf *in situ*. It was suggested that the applied loads should reflect the ‘top end’ of ground loadings that may occur during a player surface interaction (Shorten, 2002). Therefore, the upper quartile of ground loadings measured during the biomechanical tests was used as the input for the test rig instead of the mean values.

The peak magnitude of the three loads produced by the SSTTR replicate the peak ground reaction for at least one of the types of moments. Therefore, it can be argued that the SSTTR produces load applications that are typical of a range of sports movement that are performed on artificial turf. For example, in the 3D High Impact Test, the SSTTR produced a peak vertical load of 3250N. This is comparable with the vertical GRF in the 45° running cut movement (*45L*) and stopping movement (*STOP*). Similarly, the SSTTR’s peak shear load (1400-1600N) is broadly representative of the ground reaction forces observed in the turning movements. Finally the peak torque produced by the SSTTR (34-42Nm) is equivalent to the free moments that occur in the tight angle turning movement (*90L*).

While the SSTTR generally replicates ground loading which occur in highly dynamic movements, it produces markedly higher loads than the ground reaction forces which occur in normal straight line running, including fast running. This may have implications for other types of testing procedures which may be based on the lower ground loadings that occur in running compared to other movements. By replicating a range of

highly dynamic movements, the SSTTR follows the recommendation of Walker (2003) and (Shorten, 2002) that applied loads must reflect the peak loads applied by athletes to the surface.

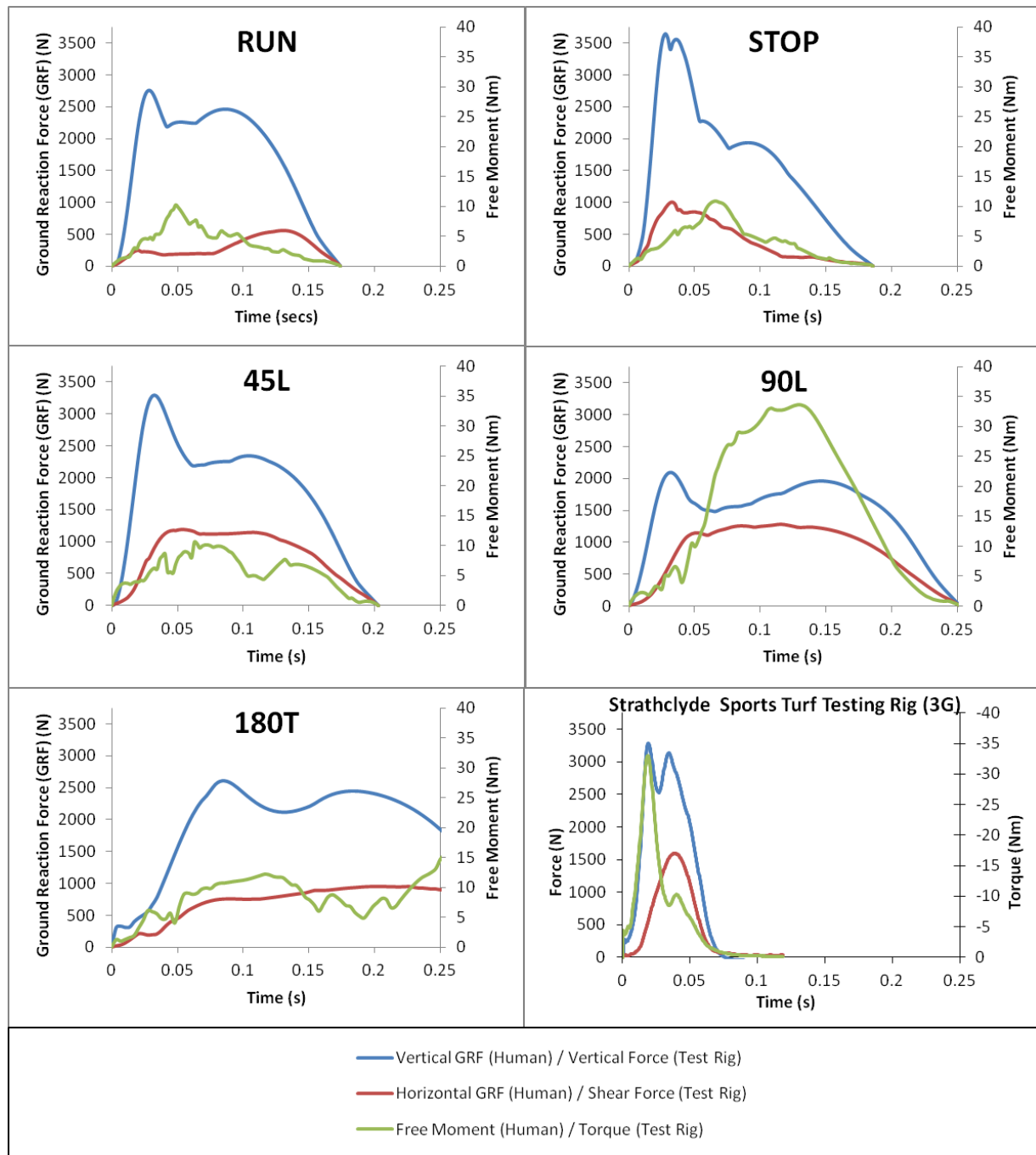


Figure 6.50 Comparison of the 3-dimensional loading profiles obtained during the biomechanical analysis of upper quartile ground reaction forces of five types of sports movements and from the SSTTR on similar 3G artificial turfs

Figure 6.50 also indicates that the loading rates of the SSTTR were typically greater than the impact phase vertical loading rates in the sports movements. Given that the magnitudes of the loads are generally representative of the vertical GRFs measured in athletic sports movements, the duration to the peak loads are too quick. For example, the SSTTR achieves a peak vertical force in approximately 15-20ms (equating to a

loading rate of 390kNs^{-1}), compared to approximately 40ms for the vertical GRF in the *45L* (equating to a loading rate of 90kNs^{-1}). In contrast, the duration to the peak shear and torque loads applied the SSTTR (35-50ms) tended to reflect the durations to the horizontal GRF and free moments impact peaks in the different types of movements (which tended to vary across movements). To resolve the issue with the SSTTR's vertical loading rate, a reduction in the duration to the peak vertical load may be achieved by incorporating additional damping into the vertical shaft system or use springs with a reduced spring constant.

It is customary to compare the results of an investigation with other published work; in this case to establish whether the biomechanical properties of surfaces are characterised consistently between different testing methods. Originally, this study had intended to run comparison trials of the SSTTR with the Berlin Athlete, the current standard testing procedure to testing shock absorbency. However, this was not done due to time and cost restraints. Nevertheless, a comparison of test results from different test procedures may be difficult and not meaningful due to the widely different loads that are applied to the surface by different test procedures and the non-linear response of surfaces to applied loads. However, with the recent introduction of other test procedures (Grund & Senner, 2010; Villwock *et al.*, 2009) that better replicate actual player-surface loading, a comparison of test procedures may be possible in the future.

Overall, the biomechanical validity of the Strathclyde Sports Turf Testing Rig has been broadly demonstrated in that it applies realistic biomechanical loads in a timely fashion.

CHAPTER 7. CONCLUSIONS

This study set out to understand the biomechanical interaction between sports players and artificial turf. The objective was to derive the critical biomechanical characteristics of this interaction in order to develop a biomechanically valid testing rig for the mechanical characterisation of artificial turf.

Given the widely reported limitations of current artificial turf mechanical testing methods, in that they do not generally replicate the actual multi-dimensional ground loadings generated during sports movements nor account for the non-linear response of these types of surfaces, there was a need for a new type of testing method.

To develop a new testing method that can overcome these limitations, an understanding of the biomechanical interaction of players and artificial turf was required as the input to the design. However, previous research regarding subject biomechanical loadings of artificial turf for a variety of different sporting movements was sparse and has generally been focussed on the vertical ground reaction force (GRF) during straight line running.

Through a biomechanical analysis of sports players performing a range of running and turning movements on three types of artificial turf, this study has generated new knowledge and a further understanding regarding the three-dimensional biomechanical interaction of players and artificial turf. In particular, the analysis of knee moments during typical sports movements on different types of artificial turf demonstrates original insight into this area. Similar tests were conducted on outdoor sites to collect data for accelerations and knee angles in order to validate the more extensive data collected in the biomechanics laboratory.

Firstly, this study found no significant difference in ground loadings between three artificial turfs, suggesting that ground reaction forces, as measured by force plates, are independent of the surface type. Moreover, performing movements on the different types of artificial turf did not typically impact knee moments. This suggests that a mechanical test rig applying a biomechanically valid force (or combination of

forces) could simulate the knee loading which occurs in typical sports movements on artificial turf and be applied to characterise different surfaces.

Secondly, the inclusion of a range of typical sports movements has led to a greater understanding of the ground loading profiles of different types of movements. Movements with fast approach velocities, such as sprinting and 45° turns, tended to produce higher vertical GRFs (and loading rates), up to 3.5 times bodyweight. Movements with slower approach velocities, such as the 90° cross turns, produced lower vertical GRF, up to twice bodyweight. Furthermore, movements with significant changes in momentum, such as the running stop and the 45° turn, tended to produce higher horizontal GRFs (up to 1.6 times bodyweight) and linear traction coefficients. Cutting-type turning movements produced the highest peak horizontal forces of approximately 1.6BW. Finally movements that require the player to turn while running tended to produce the highest free moments and rotational traction coefficients. While the rotational traction coefficient increased to 20mm in movements with a higher angle of turn, the free moments for all movements included in this study remained below an approximate limit of 30Nm, although some individual subjects achieved higher values.

Thirdly, the type of movements had an impact on the magnitude of knee kinematics and kinetics. Movements involving changes in momentum (e.g. running stop, 90° and 180° turns) tended to produce the highest peak knee flexion, whilst turning movements also tended to increase peak frontal plane knee angles. In terms of knee kinetics, running stop and 45° turning movements tended to produce the largest knee extensor moments while the slower 90° and 180° turns produced higher frontal and transverse plane moments.

The biomechanical data was incorporated into the design and construction of a test rig which mimicked the biomechanical interactions of sports movements performed on artificial turf. The new test rig was able to apply three dimensional loads simultaneously (vertical impact, horizontal shear and torque about the vertical axis) to outdoor sports surfaces. This testing procedure is unique in terms of the ability to

combine these three load actions in a variety of load magnitudes which are truly representative of the load actions which would be applied by the player during a number of typical sport actions. The test rig was used to measure the 3-dimensional compliance of artificial and natural turfs and generated initial data on the characteristics of these turfs in relation to a specifically selected range of sports manoeuvres, in terms of peak horizontal and vertical loading and loading rates; linear and rotational traction (under static and dynamic vertical loading), vertical loading/shock absorbancy, surface deformation under loading, 'foot' sliding and twisting (horizontal and angular distance and acceleration). Further refining and testing of the rig to confirm accuracy and reliability will allow turf characterisation parameters of greatest importance to be incorporated into new procedures for the testing of current and future artificial surfaces. This may lead to new validated testing procedures that manufacturers and installers of sports surfaces and the governing bodies of sports use to set the standard for quality, safety and performance of artificial turf surfaces in the future.

Original contributions to the research field:

- Added to the understanding of the biomechanical interaction with artificial turf during a variety of movements commonplace in field sports, such as football, hockey and rugby.
- The inclusion of a range of movement types in the same study has allowed a comparison of the resultant ground loadings and an understanding of knee moments during sports movements on artificial turf.
- No other studies could be identified that have examined the knee kinematics for a comparable STOP movement, 90° turns or 180 degree turn from a standing start performed on artificial turf.
- This is the first study of its kind to measure the biomechanical interactions of sports player movements on artificial turf and use this data as the input to the design and construction of a test rig, which mimicked these biomechanical interactions.

- Development and initial testing of a new 3-dimensional artificial turf testing rig that has been biomechanically validated to replicate the magnitude and timescales of ground loadings that occur during typical sports movements.

BIBLIOGRAPHY

- Alentorn-Geli, E., Myer, G.D., Silvers, H.J., Samitier, G., Romero, D., Lazaro-Haro, C., & Cugat, R. (2009) Prevention of non-contact anterior cruciate ligament injuries in soccer players. Part 1: Mechanisms of injury and underlying risk factors. *Knee.Surg.Sports Traumatol.Arthrosc.*; 17(7): 705-729
- American Society for Testing and Materials. (1994) ASTM F-355 Procedure A: Standard method of testing for shock absorbing properties of playing surface systems and materials. Available from: <http://www.astm.org/Standards/F355.htm>
- American Society for Testing and Materials (1997) F-1551-94: Standard test methods for the comprehensive characterisation of synthetic turf playing surface and materials. *ASTM Annual Book of Standards*; 15(7): 515-528
- AMI (2010) *The global artificial grass market 2009*, Applied Market Information Ltd.
- Andersson, H., Ekblom, B., & Krustup, P. (2008) Elite football on artificial turf versus natural grass: movement patterns, technical standards, and player impressions. *J Sports Sci.*; 26(2): 113-122
- Andreasson, G., Lindenberger, U., Renstrom, P., & Peterson, L. (1986) Torque developed at simulated sliding between sports shoes and an artificial turf. *Am.J.Sports Med.*; 14(3): 225-230
- Aoki, H., Kohno, T., Fujiya, H., Kato, H., Yatabe, K., Morikawa, T., & Seki, J. (2010) Incidence of injury among adolescent soccer players: a comparative study of artificial and natural grass turfs. *Clin.J Sport Med.*; 20(1): 1-7
- Baker, S.W. & Bell, M.J. (1986) The playing characteristics of natural turf and synthetic turf surfaces for association football. *J.Sports Turf Res.Inst.*; 62(1): 9-35
- Baker, S.W. & Woolacott, A.R. (2005) Comparison of the playing performance of "Third Generation" artificial grass with natural grass used for professional soccer. *International Turf Grass Society Research Journal*; 10(1): 15-25
- Bell, A.L., Pederson, D.R., & Brand, R.A. (1990) A comparison of the accuracy of several hip center location prediction methods. *J.Biomechanics*; 23(6): 617-621
- Bencke, J., Naesborg, H., Simonsen, E.B., & Klausen, K. (2000) Motor pattern of the knee joint muscles during side-step cutting in European team handball. Influence on muscular co-ordination after an intervention study. *Scand.J.Med.Sci.Sports.*; 10(2): 68-77.
- Benoit, D. L., Ramsey, D. K., Lamontagne, M., Xu, L., Wretenberg, P., & Renström, P. (2006) Effect of skin movement artifact on knee kinematics during gait and cutting motions measured in vivo. *Gait & Posture*; 24[2]: 152-164. Available from: <http://linkinghub.elsevier.com/retrieve/pii/S0966636205001700?showall=true>
- Bentley, J.A., Ramanathan, A.K., Arnold, G.P., Wang, W., & Abboud, R.J. (2011) Harmful cleats of football boots: A biomechanical evaluation. *Foot Ankle Surg*; 17(3): 140-144. Available from: <http://pubget.com/paper/21783074>
- Besier, T.F., Lloyd, D.G., Ackland, T.R., & Cochrane, J.L. (2001a) Anticipatory effects on knee joint loading during running and cutting maneuvers. *Medicine & Science in Sports & Exercise*; 33(7). Available from: http://journals.lww.com/acsm-msse/Fulltext/2001/07000/Anticipatory_effects_on_knee_joint_loading_during.15.aspx
- Besier, T.F., Lloyd, D.G., Cochrane, J.L., & Ackland, T.R. (2001b) External loading of the knee joint during running and cutting maneuvers. *Med.Sci.Sports Ex.*; 33(7): 1168-1175

- Bharti, K., Maman, P., & Jaspal, S. (2006) Effect of turf surfaces on the incidence of low back pain in field hockey. *Indian Journal of Sports Studies*; 6(2): 10-15
- Bloomfield, J., Polman, R., & O'Donoghue, P. (2007) Physical demands of different positions in FA Premier League Soccer. *Journal of Sports Science and Medicine*; 6(3): 63-70
- Bobbert, M.F., Schamhardt, H.C., & Nigg, B.M. (1992a) Calculation of ground reaction force estimates during running from positional data. *J.Biomech.*; 24(12): 1095-1105
- Bobbert, M.F., Yeadon, M.R., & Nigg, B.M. (1992b) Mechanical analysis of the landing phase in heel-toe running. *J.Biomech.*; 25(3): 223-34.
- Bonstingel, R.W., Morehouse, C.A., & Niebel, B.W. (1975) Torques developed by different types of shoes on various playing surfaces. *Med.Sci.Sports Ex.*; 7(2): 127-131
- Boyer, K.A., Boyer, K.A., F, Nigg, B.M., & Nigg, B.M. (2007) Changes in Muscle Activity in Response to Different Impact Forces Affect Soft Tissue Compartment Mechanical Properties. *J.Biomech.Eng.*; 129(4): 594-602
- Boyer, K. A. & Nigg, B. M. (2004) Muscle activity in the leg is tuned in response to impact force characteristics. *Journal of biomechanics*; 37[10]: 1583-1588. Available from: <http://linkinghub.elsevier.com/retrieve/pii/S0021929004000314?showall=true>
- Boyer, K. A. & Nigg, B. M. (2006) Soft tissue vibrations within one soft tissue compartment. *Journal of biomechanics*; 39[4]: 645-651. Available from: <http://linkinghub.elsevier.com/retrieve/pii/S0021929005000618?showall=true>
- Brachet, P. (2005). *An experimental/computational investigation between athletes and playing surfaces*. Ph.D. Thesis University of Strathclyde, Glasgow.
- British Standards Institute. (1990) BS 7044:1990 Artificial sports surfaces. Part 2: Methods of Tests. London, The British Standards Institute.
- British Standards Institute. (2005a) BS EN 14808:2005 Surfaces for sports areas - Determination of shock absorption.
- British Standards Institute. (2005b) BS EN 14809:2005 Surfaces for sports areas. Determination of vertical deformation.
- British Standards Institute. (2006) BS EN 14837:2006 Surfaces for sports areas. Determination of slip resistance.
- British Standards Institute. (2007a) BS EN 15301-1:2007 Surfaces for sports areas. Part 1: Determination of rotational resistance.
- British Standards Institute. (2007b) BS EN 15330-1:2007 Surfaces for sports areas - Synthetic turf and needle-punched surfaces primarily designed for outdoor use - Part 1: Specification for synthetic turf.
- British Standards Institute. (2008) BS EN 1177:2008 Impact attenuating playground surfacing. Determination of critical fall height.
- Brooks, J.H., Fuller, C.W., Kemp, S.P., & Reddin, D.B. (2005) Epidemiology of injuries in English professional rugby union: part 1 match injuries. *Br.J Sports Med.*; 39(10): 757-766
- Brooks, J.H., Fuller, C.W., Kemp, S.P., & Reddin, D.B. (2006) Incidence, risk, and prevention of hamstring muscle injuries in professional rugby union. *Am.J Sports Med.*; 34(8): 1297-1306
- Brosnan, J.T., McNitt, A., & Serentis, T.J. (2009) Effects of varying surface characteristics on the hardness and traction of baseball field playing surfaces. *International Turf Grass Society Research Journal*; 11(1): 1053-1065
- Cappozzo, A., Catani, F., Della Croce, U., & Leardini, A. (1995) Position and orientation in space of bones during movement: anatomical frame definition and determination. *Clin.Biomech.*; 10(4): 171-178
- Cappozzo, A., Catani, F., Leardini, A., Benedetti, M.G., & Della Croce, U. (1996) Position and orientation in space of bones

- during movement: Experimental artefacts. *Clinical Biomechanics*; 11(2): 90-100
- Cavanagh, P.R. (1990) *Biomechanics of distance running* Champaign, IL., Human Kinetics.
- Cavanagh, P.R. & Lafortune, M.A. (1980) Ground reaction forces in distance running. *J.Biomech.*; 13: 397-406
- Chateau, H., HOLDEN, L., Robin, D., Falala, S., Pourcelot, P., ESTOUP, P., Denoix, J.M., & Crevier-Denoix, N. (2010) Biomechanical analysis of hoof landing and stride parameters in harness trotter horses running on different tracks of a sand beach (from wet to dry) and on an asphalt road. *Equine Veterinary Journal*; 42(S38): 488-495
- Clarke, J. D., Carre, M. J., & Kirk, R. F. (2008) "A comparison of test methodologies to enable the improved understanding of soccer boot traction," *In The Engineering of Sport 7. Vol 2.*, M. Estivalet & P. Brisson, eds., Paris: Springer, pp. 607-610.
- Clarke, T. E., Frederick, E. C., & Cooper, L. B. (1983) "Biomechanical measurement of running shoe cushioning properties," *In Biomechanical aspects of sports shoes and playing surfaces*, B. M. Nigg & B. A. Kerr, eds., Calgary: University of Calgary, pp. 25-33.
- Cole, G.K., Nigg, B.M., Ronsky, J.L., & Yeadon, M.R. (1993) Application of the joint coordinate system to three dimensional joint attitude and movement representations: a standardisation proposal. *J.Biomechanical Eng.*; 115(4A): 344-349
- Creaby, M.W. & Dixon, S.J. (2008) External Frontal Plane Loads May Be Associated with Tibial Stress Fracture. *Medicine & Science in Sports & Exercise*; 40(9). Available from: http://journals.lww.com/acsm-msse/Fulltext/2008/09000/External_Frontal_Plane_Loads_May_Be_Associated.16.aspx
- De Wit, B., De Clercq, D., & Aerts, P. (2000) Biomechanical analysis of the stance during barefoot and shod running. *J.Biomech.*; 33(3): 269-278
- Dempster, W. T. (1955) "Space requirements of the seated operator," *In WADC-TR-55-159*, Ohio: Aerospace Medical Research Laboratories, pp. 55-159.
- Derrick, T.R. (2004) The effects of knee contact angle on impact forces and accelerations. *Med Sci.Sports Exerc.*; 36(5): 832-837
- Di Salvo, V., Gregson, W., Atkinson, G., Tordoff, P., & Drust, B. (2009) Analysis of High Intensity Activity in Premier League Soccer. *Int J Sports Med*; 30(03): 205-212
- Dick, R., Hootman, J.M., Agel, J., Vela, L., Marshall, S.W., & Messina, R. (2007) Descriptive epidemiology of collegiate women's field hockey injuries: National Collegiate Athletic Association Injury Surveillance System, 1988-1989 through 2002-2003. *J Athl.Train.*; 42(2): 211-220
- Dixon, S., Collop, A., & Batt, M. (2005) Compensatory adjustments in lower extremity kinematics in response to a reduced cushioning of the impact interface in heel-toe running. *Sports Engineering*; 8(1): 47-55
- Dixon, S.J. (2008) Use of pressure insoles to compare in-shoe loading for modern running shoes. *Ergonomics*; 51(10): 1503-1514. Available from: <http://dx.doi.org/10.1080/00140130802239562> [Last accessed 28 May 2012].
- Dixon, S.J., Batt, M.E., & Collop, A.C. (1999) Artificial playing surfaces research: a review of medical, engineering and biomechanical aspects. *Int.J.Sports Med.*; 20(4): 209-218
- Dixon, S.J., Collop, A.C., & Batt, M.E. (2000) Surface effects on ground reaction forces and lower extremity kinematics in running. *Med.Sci.Sports Exerc.*; 32(11): 1919-1926
- Dowling, A.V., Corazza, S., Chaudhari, A.M., & Andriacchi, T.P. (2010) Shoe-surface friction influences movement strategies during a sidestep cutting task: implications for anterior cruciate ligament injury risk. *Am.J Sports Med*; 38(3): 478-485. Available from: PM:20194954
- Dragoo, J.L. & Braun, H.J. (2010) The effect of playing surface on injury rate: a review of the current literature. *Sports medicine (Auckland, N.Z.)*; 40(11): 981-990. Available from: PM:20942512

- Drakos, M.C., Hillstrom, H., Voos, J.E., Miller, A.N., Kraszewski, A.P., Wickiewicz, T.L., Warren, R.F., Allen, A.A., & O'Brien, S.J. (2010) The effect of the shoe-surface interface in the development of anterior cruciate ligament strain. *Journal of biomechanical engineering*; 132(1): 011003
- Dunlop, J. (2002) Measurement of sports surface resilience. Available from: www.iss.de/artificial%20Athlete
- Durá, H. & Martinez, L. (1999) The influence of friction on sports surfaces in turning movements. *Sports Engineering*; 2(2): 97-102. Available from: <http://dx.doi.org/10.1046/j.1460-2687.1999.00024.x>
- Ekstrand, J. & Gillquist, J. (1983) The avoidability of soccer injuries. *Int.J.Sports Med.*; 4: 124-128
- Ekstrand, J. & Nigg, B.M. (1989) Surface-related injuries in soccer. *Sports Med.*; 8(1): 56-62
- Ekstrand, J., Timpka, T., & Hagglund, M. (2006) Risk of injury in elite football played on artificial turf versus natural grass: a prospective two-cohort study. *Br.J Sports Med.*; 40(12): 975-980
- Elmqvist, L. G. & Johnson, R. J. (1994) "Anterior cruciate ligament injuries," In *Orthopaedic sports medicine: principles and practice*, J. C. DeLee & D. Drez, eds., Philadelphia: WB Saunders Co, pp. 1313-1314.
- European Synthetic Turf Organisation. (2010) Synthetic turf. http://www.theesto.com/synthetic_turf/synthetic_turf.html; Available from: http://www.theesto.com/synthetic_turf/synthetic_turf.html
- Exeter Research. (2010) S2T2 - Shoe and Surface Traction Tester. Available from: <http://www.exeter-research.com/index.html>
- Farley, C.T., Houdijk, H.H.P., Van Strein, C., & Louie, M. (1998) Mechanism of leg stiffness adjustment for hopping on surfaces of different stiffnesses. *J.Applied Physiology*; 85(3): 1044-1055
- Fédération Internationale de Football Association. (2009a) FIFA Quality concept for football turf: Handbook of test methods. <http://www.fifa.com/aboutfifa/footballdevelopment/pitchequipment/footballfields/qualityconcept.html>; Available from: <http://www.fifa.com/aboutfifa/footballdevelopment/pitchequipment/footballfields/qualityconcept.html>
- Fédération Internationale de Football Association. (2009b) FIFA Quality concept for football turf: Handbook of test methods. <http://www.fifa.com/aboutfifa/footballdevelopment/pitchequipment/footballfields/qualityconcept.html>; Available from: <http://www.fifa.com/aboutfifa/footballdevelopment/pitchequipment/footballfields/qualityconcept.html>
- Federation Internationale de Hockey. (2008) Handbook of performance requirements for synthetic turf hockey pitches. Brussels, F.I.H. Available from: <http://www.worldhockey.org>
- Feehery, R.V. (1986) The biomechanics of running on different surfaces. *Clin.Podiatr.Med.Surg.*; 3(4): 649-59.
- Ferber, R., Davis, I.M., & Williams, D.S., III (2003) Gender differences in lower extremity mechanics during running. *Clin.Biomech (Bristol, Avon.)*; 18(4): 350-357. Available from: PM:12689785
- Ferris, D.P., Liang, K., & Farley, C.T. (1999) Runners adjust leg stiffness for their first step on a new running surface. *J.Biomech.*; 32: 787-794
- Ferris, D.P., Louie, M., & Farley, C.T. (1998) Running in the real world: adjusting leg stiffness for different surfaces. *Proc.R.Soc.Lond.B*; 265: 989-994
- FIFA. (2001) FIFA guide to artificial surfaces. Available from: www.fifa.com
- Fleming, P.R., Young, C., Roberts, J.R., Jones, R., & Dixon, N. (2005) Human perceptions of artificial surfaces for field hockey. *Sports Eng.*; 8: 121-136
- Fong, D.T., Hong, Y., Chan, L.K., Yung, P.S., & Chan, K.M. (2007) A systematic review on ankle injury and ankle sprain in sports. *Sports Med.*; 37(1): 73-94

- Frederick, E.C. (1986) Kinematically mediated effects of sport shoe design: a review. *J.Sports Sci.*; 4(3): 169-84.
- Frederick, E.C., Hagy, J.L., & Mann, R.A. (1981) The prediction of vertical impact force during running. *J.Biomech.*; 14: 495-500
- Fried, T. & Lloyd, G.J. (1992) An overview of common soccer injuries. Management and prevention. *Sports Med.*; 14(4): 269-275
- Friesenbichler, B., Stirling, L. M., Federolf, P., & Nigg, B. M. (2011) Tissue vibration in prolonged running. *Journal of biomechanics*; 44[1]: 116-120. Available from: <http://linkinghub.elsevier.com/retrieve/pii/S002192901000480X?showall=true>
- Fuller, C.W., Dick, R.W., Corlette, J., & Schmalz, R. (2007) Comparison of the incidence, nature and cause of injuries sustained on grass and new generation artificial turf by male and female football players. Part 2: training injuries. *Br.J Sports Med.*; 41 Suppl 1:i27-32.: i27-i32
- Garcilazo, R. (2007) Lower extremity mechanics during cutting tasks in different shoe-turf combinations. *McNair Scholars Research Journal*; 3(1): 35-44
- Gerritsen, K.G.M., Vandenbogert, A.J., & Nigg, B.M. (1995) Direct dynamics stimulation of the impact phase in heel-toe running. *J.Biomechanics*; 28(6): 661-668
- Griffin, L.Y., Agel, J., Albohm, M.J., Arendt, E.A., Dick, R.W., Garrett, W.E., Garrick, J.G., Hewett, T.E., Huston, L., Ireland, M.L., Johnson, R.J., Kibler, W.B., Lephart, S., Lewis, J.L., Lindenfeld, T.N., Mandelbaum, B.R., Marchak, P., Teitz, C.C., & Wojtys, E.M. (2000) Noncontact anterior cruciate ligament injuries: risk factors and prevention strategies. *J Am.Acad.Orthop.Surg.*; 8(3): 141-150
- Grood, E.S. & Suntay, W.J. (1983) A joint coordinate system for the clinical description of three-dimensional motions: application to the knee. *Trans.of ASME, J.Biomechanical Eng.*; 105: 136-144
- Grund, T. & Senner, V. (2010) Development, validation and enhancement of a new device for testing soccer shoes under game-relevant conditions, *Proceedings of 2nd SportSURF Conference: Science, Technology and Research into Sport Surfaces (STARSS)*, Loughbrough, U.K. 22th Apr.
- Grund, T., Senner, V., & Gruber, K. (2007) Development of a test device for testing soccer boots under game-relevant high-risk loading conditions. *Sports Eng.*; 10: 55-63
- Guisasola, I.N. (2008). *Human-natural sports surface interaction*. Cranfield University.
- Hamill, J. (1996) Evaluating sports shoes using ground reaction force data, Portugal: 24th Jun.
- Hardin, E. (2000). *Consequences of repeated impacts. Doctoral Dissertation*. University of Massachusetts Amherst, Dept. of Exercise Science, Amherst, Massachusetts.
- Hardin, E., Van Den Bogart, A.J., Antonie, J., & Hamill, J. (2004) Kinematic Adaptations during Running: Effects of Footwear, Surface, and Duration. *Medicine & Science in Sports & Exercise*; 36(5)
- Harrison, M. (1999) Factors affecting the results of the 'Berlin Artificial Athlete' shock absorption test. Available from: www.iss.de/artificial%20Athlete
- Harrison, M. & Harting, B. (2000) Artificial athletes - accuracy and round-robin results. Available from: www.iss.de/conferences
- Heidt, R.S., Dormer, S.G., cawley, P.W., Scranton, P.E., Losse, G., & Howard, M. (1996) Difference in friction and torsional resistance in athletic shoe-turf surface interfaces. *Am.J.Sports Med.*; 24(6): 834-842
- Hennig, E.M. (2011) The influence of soccer shoe design on player performance and injuries. *Res.Sports Med*; 19(3): 186-201. Available from: PM:21722006
- Herzog, W. (1978). *Einfluss der Laufgeschwindigkeit und des Sportplatzbelges auf die Belastung des menschlichen*

Bewegungsapparates (The influence of running velocity and playing surface on the load on the human locomotor system). ETH, Zurich.

Holden, J.P. & Cavanagh, P.R. (1991) The free moment of ground reaction in distance running and its changes with pronation. *J.Biomech.*; 10: 887-897

Hunter, J., Marshall, R.N., & McNair, P.J. (2005) Relationships between ground reaction force impulse and kinematics of sprint-running acceleration. *J.Applied Biomechanics*; 21(1): 31-43

Hussain, I., Mohammed, A., & Khan, A. (2011) Penalty stroke in field hockey: a biomechanical study. *Internation Journal of Sports Science and Engineering*; 5(1): 53-57

Inklaar, H. (1994) Soccer Injuries II: Aetiology and prevention. *Sports Med.*; 18(2): 81-93

International Association of Athletics Federations. (2003) Performance factors in sprinting. IAAF. Available from: <http://www.iaaf.org/theSport/whatisathletics/TrackandField/disc=200/index.newsId=4673.html>

International Football Associations Board. (2012) The Laws of the Game. Available from: <http://www.fifa.com/worldfootball/lawsofthegame/index.html>; <http://www.fifa.com/worldfootball/lawsofthegame/i/index.html>

International Rugby Board. (2010) IRB Regulation 22: Standard relating to the use of artificial playing surfaces. Available from: <http://www.irb.com/lawregulations/regulations/index.html>

International Society of Biomechanics (2002) ISB recommendation on the definition of joint coordinate system of various joints for the reporting of human joint motion - part I: ankle, hip and spine. *J.Biomechanics*; 35: 535-548

Ishai, G.A. (1975). *Whole body gait kinetics*. PhD Thesis University of Strathclyde.

Jones, P., Kerwin, D., Irwin, G., & Nokes, L. (2009) Three Dimensional Analysis of Knee Biomechanics when Landing on Natural Turf and Football Turf. *Journal of Medical and Biological Engineering*; 29(4): 184-188

Kaelin, X., Denoth, J., Stacoff, A., & Stussi, E. (1985) "Cushioning during running - material tests versus subject tests.," *In Biomechanics: principles and applications*, S. Perren, ed., London: Martinus Nijhoff Publishers, pp. 651-656.

Kaila, R. (2007) Influence of Modern Studded and Bladed Soccer Boots and Sidestep Cutting on Knee Loading During Match Play Conditions. *The American Journal of Sports Medicine*; 35(9): 1528-1536. Available from: <http://ajs.sagepub.com/content/35/9/1528.abstract>

Keenan, G.S., Franz, J.R., Dicharry, J., Croce, U.D., & Kerrigan, D.C. (2011) Lower limb joint kinetics in walking: The role of industry recommended footwear. *Gait & Posture*; 33(3): 350-355. Available from: <http://www.sciencedirect.com/science/article/pii/S0966636210002705>

Keller, T.S., Weisberger, A.M., Ray, J.L., Hasan, S.S., Shiavi, R.G., & Spengler, D.M. (1996) Relationship between vertical ground reaction force and speed during walking, slow jogging, and running. *Clinical Biomechanics*; 11(5): 253-259

Korhonen, M.T., Suominen, H., Viitasalo, J.T., Liikavainio, T., Alen, M., & Mero, A.A. (2010) Variability and symmetry of force platform variables in maximum-speed running in young and older athletes. *J Appl.Biomech*; 26(3): 357-366. Available from: PM:20841628

Kuhlman, S., Sabick, M., Pfeiffer, R., Cooper, B., & Forhan, J. (2010) Effect of loading condition on the traction coefficient between shoes and artificial turf surfaces. *Proceedings of the Institution of Mechanical Engineers, Part P: Journal of Sports Engineering and Technology*; 224(2): 155-165. Available from: <http://dx.doi.org/10.1243/17543371JSET56>

Lafortune, M.A., Henning, E., & Lake, M.J. (1996a) Dominant role of interface over knee angle for cushioning impact loading and regulating initial leg stiffness. *J.Biomech*.

- Lafortune, M.A., Lake, M.J., & Henning, E. (1996b) Differential shock transmission response of the human body to impact severity and lower limb posture. *J.Biomech.*; 29(12): 1531-1537
- Lee, S.J. & Hidler, J. (2008) Biomechanics of overground vs. treadmill walking in healthy individuals. *Journal of Applied Physiology*; 104(3): 747-755. Available from: <http://jap.physiology.org/content/104/3/747.abstract>
- Lees, A., Asai, T., Andersen, T.B., Nunome, H., & Sterzing, T. (2010) The biomechanics of kicking in soccer: a review. *J Sports Sci.*; 28(8): 805-817. Available from: PM:20509089
- Lees, A. & Nolan, L. (1998) The biomechanics of soccer: a review. *J.Sports Science*; 16: 211-234
- Livesay, G.A., Reda, D.R., & Nauman, E.A. (2006) Peak torque and rotational stiffness developed at the shoe-surface interface: the effect of shoe type and playing surface. *Am.J.Sports Med.*; 34(3): 415-422
- Lloyd, D.G. & Stevenson, M.G. (1990) Dynamic friction measurements on artificial sports surfaces. *J.Sports Turf Res.Inst.*; 66: 149-160
- Lopez de, S.C., Juarez, D., Mallo, J., & Navarro, E. (2010) Biomechanical analysis of the penalty-corner drag-flick of elite male and female hockey players. *Sports Biomech*; 9(2): 72-78. Available from: PM:20806843
- Low, D.C. (2010). *The Effect of Playing Surfaces and Footwear on the Biomechanical Response of Soccer Players*. PhD Thesis Thesis University of Exeter.
- McGhie, D. & Ettema, G. (2012) Biomechanical analysis of traction at the shoe-surface interface on third generation artificial turf. *Procedia Engineering*; 34(0): 873. Available from: <http://www.sciencedirect.com/science/article/pii/S1877705812017638>
- McLean, S.G., Neal R.J., Myers P.T., & Walters, M.R. (1999) Knee joint kinematics during the sidestep cutting maneuver: potential for injury in women. *Med.Sci.Sports Exerc.*; 31(7): 959-68.
- McLean, S.G., Neal, R.J., Myers, P.T., & Walters, M.R. (1999) Knee joint kinematics during the sidestep cutting maneuver: potential for injury in women. *Medicine & Science in Sports & Exercise*; 31(7). Available from: http://journals.lww.com/acsm-msse/Fulltext/1999/07000/Knee_joint_kinematics_during_the_sidestep_cutting.7.aspx
- McMahon, T.A., Valiant, G.A., & Frederick, E.C. (1987) Groucho running. *J.Applied Physiology*; 62: 2326-2337
- McNair, P.J. & Marshall, R.N. (1994) Kinematic and kinetic parameters associated with running in different shoes. *Br.J.Sports Med.*; 28(4): 256-260
- McNitt, A., Middour, R., & Waddington, D. (1997) Development and evaluation of a method to measure traction on turfgrass surfaces. *Journal of Testing and Evaluation*; 25(1): 99-107
- Meijer, K., Dethmers, J., Savelberg, H., Willems, P., & Wijers, B. (2006) "Biomechanical Analysis of Running on Third Generation Artificial Soccer Turf," *In The Engineering of Sport 6*, E. F. Moritz & S. Haake, eds., Springer New York, pp. 29-34.
- Mellalieu, S., Trewartha, G., & Stokes, K. (2008) Science and rugby union. *Journal of Sports Sciences*; 26(8): 791-794. Available from: <http://dx.doi.org/10.1080/02640410701819099> [Last accessed 4 June 2012].
- Meyers, M.C. (2010) Incidence, Mechanisms, and Severity of Game-Related College Football Injuries on FieldTurf Versus Natural Grass: A 3-Year Prospective Study. *Am.J Sports Med.*
- Milburn, P.D. (1993) Biomechanics of rugby union scrummaging. Technical and safety issues. *Sports medicine (Auckland, N.Z.)*; 16(3): 168-179. Available from: <http://ukpmc.ac.uk/abstract/MED/8235190>
- Milner, C.E., Davis, I.S., & Hamill, J. (2006) Free moment as a predictor of tibial stress fracture in distance runners. *Journal of biomechanics*; 39(15): 2819-2825. Available from: <http://www.sciencedirect.com/science/article/B6T82-4HHWWDB-1/2/593df012cdd977c645b545ea8ac9b6b4>

- Morag, E. & Johnson, D. A. (2001) Traction requirements of young soccer players, Zurich, Switzerland
- Murphy, D.F., Connolly, D.A., & Beynon, B.D. (2003) Risk factors for lower extremity injury: a review of the literature. *Br.J Sports Med.*; 37(1): 13-29
- Murtaugh, K. (2001) Injury patterns among female field hockey players. *Med.Sci.Sports Exerc.*; 33(2): 201-207. Available from: PM:11224806
- Murtaugh, K. (2009) Field hockey injuries. *Curr.Sports Med.Rep.*; 8(5): 267-272
- Myklebust, G., M+^hlum, S., Holm, I., & Bahr, R. (1998) A prospective cohort study of anterior cruciate ligament injuries in elite Norwegian team handball. *Scandinavian Journal of Medicine & Science in Sports*; 8(3): 149-153. Available from: <http://dx.doi.org/10.1111/j.1600-0838.1998.tb00185.x>
- Naunheim, R., Parrott, H., & Standeven, J. (2004) A comparison of artificial turf. *J Trauma.*; 57(6): 1311-1314
- Naunheim, R. S. (2008) "Impact attenuation, performance and injury related to artificial turf," *In Handbook of Biomechanics and Human Movement Science*, Y. Hong & R. Bartlett, eds., Abingdon, Oxon: Routledge, pp. 446-458.
- Nicholas, J.A., Rosenthal, P.P., & Gleim, G.W. (1988) A historical perspective of injuries in professional football: twenty-six years of game-related events. *JAMA*; 260(7): 939-944
- Nigg, B. M. (1983) "External force measurements with sports shoes and playing surfaces," *In Biomechanical aspects of sports shoes and playing surfaces*, B. M. Nigg & B. A. Kerr, eds., Calgary: University of Calgary Printing, pp. 11-24.
- Nigg, B.M. (1985) Biomechanics, load analysis and sports injuries in the lower extremities. *Sports Med.*; 2: 367-379
- Nigg, B.M. (1990) The validity and relevance of tests used for the assessment of sports surfaces. *Med.Sci.Sports Exerc.*; 22(1): 131-139
- Nigg, B.M. (1997) Impact forces in running. *Current Opinion in Orthopedics*; 8: 43-47
- Nigg, B.M. (2001) The role of impact forces and foot pronation: a new paradigm. *Clin.J.Sports Med.*; 11: 2-9
- Nigg, B. M., Denoth, J., Kerr, B. A., Luethi, S., Smith, D., & Stacoff, A. (1984) "Load sport shoes and playing surfaces," *In Sports shoes & playing surfaces*, E. C. Frederick, ed., Champaign: Human Kinetics Publ., pp. 1-23.
- Nigg, B.M. & Liu, W. (1999) The effect of muscle stiffness and damping on simulated impact force peaks during running. *J.Biomech.*; 32: 849-856
- Nigg, B.M. & Wakeling, J.M. (2001) Impact forces and muscle tuning: a new paradigm. *Exerc.Sports Sci.Rev.*; 29(1): 37-41
- Nigg, B.M. & Yeadon, M.R. (1987) Biomechanical aspects of sports surfaces. *J.Sports Sci.*; 5: 117-145
- Nordin, M. & Frankel, V.H. (2001) *Basic biomechanics of the musculoskeletal system*, 3rd ed. Baltimore, Lippincott Williams & Wilkins.
- Norris, C.M. (1998) *Sports injuries: diagnosis and management* Oxford, Butterworth Heinemann.
- Novacheck, T.F. (1998) The biomechanics of running. *Gait & Posture.*; 7(1): 77-95.
- Nunome, H., Ikegami, Y., Nishikawa, T., & Horio, T. (2007) A valid shock absorbency test for artificial turf. *Journal of biomechanics*; 40: S740.
- Nunome, H., Suito, H., Shinkai, H., & Ikegami, Y. (2008) A new valid shock absorbency test for third generation artificial turf, Seoul, Korea: 14th Jul.

- O'Hara, A. (2003) The Portable Biomechanical Artificial Surface Tester. *Unpublished report.Mech.Eng.University of Strathclyde*;
- Pain, M.T.G. & Challis, J.H. (2001) The role of the heel pad and shank soft tissue during impacts: a further resolution of a paradox. *J.Biomech.*; 34: 327-333
- Palastanga, N., Field, D., & Soames, R. (1994) *Anatomy and human movement*, 2ndth ed. Oxford, Butterworth-Heinemann.
- Patritti, B., Lake, M. J., & Lees, A. (2003) Adaptations in running kinematics associated with expected changes in cushioning at the foot-ground interface, Dunedin, N.Z.: International Society of Biomechanics XIXth Congress Proceedings,
- Petersen, J. & Holmich, P. (2005) Evidence based prevention of hamstring injuries in sport. *Br.J Sports Med.*; 39(6): 319-323
- Pine, D. (1991) Artificial vs. natural turf: injury perception fan the debate. *Phys.& Sports Med.*; 19(8): 125-128
- Pohl, M. B., Mullineaux, D. R., Milner, C. E., Hamill, J., & Davis, I. S. (2008) Biomechanical predictors of retrospective tibial stress fractures in runners. *Journal of biomechanics*; 41[6]: 1160-1165. Available from: <http://linkinghub.elsevier.com/retrieve/pii/S0021929008000456?showall=true>
- Pollard, C., McClay-Davis, I., & Hamill, J. (2003) Gender differences in knee joint kinematics and kinetics during an unanticipated cutting maneuver. Dunedin, N.Z., International Society of Biomechanics XIXth Congress Proceedings.
- Pollard, C. D., Davis, I. M., & Hamill, J. (2004) Influence of gender on hip and knee mechanics during a randomly cued cutting maneuver. *Clinical biomechanics (Bristol, Avon)*; 19[10]: 1022-1031. Available from: <http://linkinghub.elsevier.com/retrieve/pii/S0268003304001688?showall=true>
- Powell, J.W. & Schootman, M. (1992) A multivariate risk analysis of selected playing surfaces in the National Football League: 1980 to 1989. An epidemiologic study of knee injuries. *Am.J.Sports Med.*; 20(6): 686-694
- Queen, R.M., Charnock, B.L., Garrett, W.E., Jr., Hardaker, W.M., Sims, E.L., & Moorman, C.T., III (2008) A comparison of cleat types during two football-specific tasks on FieldTurf. *Br.J Sports Med*; 42(4): 278-284. Available from: PM:17717058
- Rand, M.K. & Ohtsuki, T. (2000) EMG analysis of lower limb muscles in humans during quick change in running directions. *Gait & Posture*; 12(2): 169-83.
- Reenalda, J., Freriks, B., & Buurke, J. (2011) A comparison of ground reaction force patterns of conventional running shoes and minimalistic footwear in habitually shod runners. *Footwear Science*; 3(sup1): S130-S131. Available from: <http://dx.doi.org/10.1080/19424280.2011.575388> [Last accessed 9 February 2012].
- Reid, D.C. (1992) *Sports injury assessment and rehabilitation* London, Churchill Livingstone.
- Reilly, T. & Howe, T. (1996) "Injury prevention and rehabilitation.," *In Science and Soccer*, T. Reilly, ed., London: E & FN Spon.,
- Reilly, T., Lees, A., Davids, K., & Murphy, W.J. (1988) *Science and football*. London, E & Fn Spon.
- Reilly, T. & Thomas, V. (1976) A motion analysis of work-rate in different positional roles in professional football match-play. *Journal of Human Movement Studies*; 2: 87-89
- Reinschmidt, C., Van Den Bogart, A.J., Murphy, N., Lundberg, A., & Nigg, B.M. (1997) Tibiocalcaneal motion during running - measured with external and bone markers. *J.Clin.Biomechanics*; 12(1): 8-16
- Renstrom, P., Peterson, L., & Edburg, B. (1977) *Valhalla aertificial pitchat, Gothenburg: 1975-1977: a two-year evaluation*. Sweden, Rapport Naturvardsverket.
- Rishiraj, N., Taunton, J.E., & Niven, B. (2009) Injury profile of elite under-21 age female field hockey players. *J Sports Med.Phys.Fitness.*; 49(1): 71-77

- Robin, D., Chateau, H., Pacquet, L., Falala, S., Valette, J.P., Pourcelot, P., Ravary, B., Denoix, J.M., & Crevier-Denoix, N. (2009) Use of a 3D dynamometric horseshoe to assess the effects of an all-weather waxed track and a crushed sand track at high speed trot: Preliminary study. *Equine Veterinary Journal*; 41(3): 253-256
- Rodeo, S.A., O'Brien, S., Warren, R.F., Barnes, R., Wickiewicz, T.L., & Dillingham, M.F. (1990) Turf-toe: an analysis of metatarsophalangeal joint sprains in professional football players. *Am.J.Sports Med.*; 18(3): 280-285
- Runciman, R.J. & Nicol, A.C. (1993) Strain Gauged Six-Component Load Transducer for use in Upper Limb Biomechanics. *Proceedings of the Institution of Mechanical Engineers, Part H: Journal of Engineering in Medicine*; 207(4): 231-237. Available from: <http://pih.sagepub.com/content/207/4/231.abstract>
- Sanchis, M., Rosa, D., Gamez, J., Alcantara, E., Gimeno, C., Such, M. J., Prat, J., & Dejoz, R. (2008) "Development of a new technique to evaluate abrasiveness of artificial turf," *In The Engineering of Sport 7. Vol 2.*, M. Estivalet & P. Brisson, eds., Paris: Spiringer, pp. 149-156.
- Schlaepfer, F., Unold, E., & Nigg, B. M. (1983) "The frictional characteristics of tennis shoes.," *In Biomechanical aspects of sports shoes and playing surfaces.*, B. M. Nigg & B. A. Kerr, eds., Calgary: University Printing, pp. 153-160.
- Schneiders, A.G., Takemura, M., & Wassinger, C.A. (2009) A prospective epidemiological study of injuries to New Zealand premier club rugby union players. *Phys.Ther.Sport.*; 10(3): 85-90
- Senter, C. & Hame, S.L. (2006) Biomechanical analysis of tibial torque and knee flexion angle: implications for understanding knee injury. *Sports Med.*; 36(8): 635-641
- Setterbo, J.J., Garcia, T.C., Campbell, I.P., Reese, J.L., Morgan, J.M., Kim, S.Y., Hubbard, M., & Stover, S.M. (2009) Hoof accelerations and ground reaction forces of Thoroughbred racehorses measured on dirt, synthetic, and turf track surfaces. *Am.J.Vet.Res.*; 70(10): 1220-1229
- Severn, K.A., Fleming, P.R., & Dixon, N. (2010) Science of synthetic turf surfaces: Player-GC surface interactions. *Sports Technology*; 3(1): 13-25
- Shorten, M. (2001) ASTM F08.51 on playing surfaces - notes on the alternative tests of sports surface shock absorption. Available from: www.biomechanica.com
- Shorten, M. (2002) The myth of running shoe cushioning. Kyoto, Japan, IVth International Conference on the Engineering of Sport.
- Shorten, M. & Himmelsbach, M. S. (2002) Traction of cleated shoes on natural and artificial turf football surfaces. *Biomechanica*. Available from: www.biomechanica.com
- Shorten, M., Hudson, B., & Himmelsbach, M. S. (2003) Shoe-surface traction of conventional and in-filled synthetic turf football surfaces, Dunedin, N.Z.
- Shorten, M. & Mientjes, M. (2003) The effects of shoe cushioning on impact force during running, *Proceedings of Proc.6th ISB Symp.Footwear Biomechanics*, University of Otago, New Zealand
- Shorten, M. & Winslow, D.S. (1992) Spectral analysis of impact shock during running. *Int.J.Sports Biomechanics*; 8: 288-304
- Shorten, M. & Mientjes, M.I.V. (2011) The heel impact force peak during running is neither heel nor impact and does not quantify shoe cushioning effects. *Footwear Science*; 3(1): 41-58. Available from: <http://dx.doi.org/10.1080/19424280.2010.542186> [Last accessed 10 February 2012].
- Sigward, S. M. & Powers, C. M. (2006) The influence of gender on knee kinematics, kinetics and muscle activation patterns during side-step cutting. *Clinical biomechanics (Bristol, Avon)*; 21[1]: 41-48. Available from: <http://linkinghub.elsevier.com/retrieve/pii/S0268003305001798?showall=true>
- Simonsen, E.B., Magnusson, S.P., Bencke, J., Naesborg, H., Havkrog, M., Ebstrup, J.F., & Sorensen, H. (2000) Can the hamstring

- muscles protect the anterior cruciate ligament during a side-cutting maneuver? *Scand.J.Med.Sci.Sports*; 10(2): 78-84.
- Skovron, M.L., Levy, M., & Agel, J. (1990) Living with artificial grass: a knowledge update. Part 2: epidemiology. *Am.J.Sports Med.*; 18(5): 510-513
- Stacoff, A., Steger, J., Stussi, E., & Reinschmidt, C. (1996) Lateral stability in sideward cutting movements. *Med.Sci.Sports Exerc.*; 28(3): 350-358
- Stansfield, B. (2000). *Hip joint forces: hip joint forces of 40 to 60 year old normal and total hip replacement subjects during walking and stair, ramp and camber negotiation*. Ph.D. Thesis University of Strathclyde.
- Stefanyshyn, D.J., Lee, J.S., & Park, S.K. (2010) The influence of soccer cleat design on resultant joint moments. *Footwear Science*; 2(1): 13-19. Available from: <http://dx.doi.org/10.1080/19424280903535454> [Last accessed 29 August 2011].
- Steffen, K., Andersen, T.E., & Bahr, R. (2007) Risk of injury on artificial turf and natural grass in young female football players. *Br.J Sports Med.*; 41 Suppl 1:i33-7. Epub;2007 Jun 5.: i33-i37
- Stephenson, S., Gissane, C., & Jennings, D. (1996) Injury in rugby league: a four year prospective survey. *British Journal of Sports Medicine*; 30(4): 331-334. Available from: <http://bjsm.bmj.com/content/30/4/331.abstract>
- Stergiou, P. & Bates, B.T. (1997) The relationship between subtalar and knee joint function as a possible mechanism for running injuries. *Gait & Posture*; 6: 177-185
- Stiles, V. H., Dixon, S. D., Guisasola, I. N., & James, I. T. (2008) "Kinematic Response to Variations in Natural Turf During Running," *In The Engineering of Sport 7. Volume 1*, M. Estivalet & P. Brisson, eds., Springer Paris, pp. 499-508.
- Stiles, V. H. & Dixon, S. J. (2003) The biomechanical assessment of tennis surface cushioning properties during a tennis-specific movement. Dunedin, N.Z., International Society of Biomechanics XIXth Congress Proceedings.
- Stiles, V.H. & Dixon, S.J. (2006) The influence of different playing surfaces on the biomechanics of a tennis running forehand foot plant. *J Appl.Biomech.*; 22(1): 14-24
- Stiles, V.H. & Dixon, S.J. (2007) Biomechanical response to systematic changes in impact interface cushioning properties while performing a tennis-specific movement. *J.Sports Science*; 25(11): 1129-1239
- Stiles, V. H., Dixon, S. J., Guisasola, I. N., & James, I. T. (2007) "Biomechanical response to variations in natural turf surfaces during running and turning," *In 'STARSS 2007', proceedings of the first international conference of the SportsSURF network*, P. R. Fleming, C. Young, & S. Dixon, eds., Loughborough, UK: Loughborough University,
- Stiles, V.H., James, I.T., Dixon, S.J., & Guisasola, I.N. (2009) Natural turf surfaces: the case for continued research. *Sports Med.*; 39(1): 65-84
- Strudwick, A., Reilly, T., & Doran, D. (2002) Anthropometric and fitness profiles of elite players in two football codes. *J Sports Med Phys.Fitness*; 42(2): 239-242
- Stucke, H., Baudzus, W., & Baumann, W. (1984) "On friction characteristics of playing surfaces," *In Sports shoes and playing surfaces*, E. C. Frederick, ed., Champaign, IL: Human Kinetics, pp. 87-97.
- The Sports Council (1984) *Specifications for artificial sports surfaces. Part 2: surfaces for general sports use* London, Sports Council.
- Thomason, J.J. & Peterson, M.L. (2008) Biomechanical and Mechanical Investigations of the Hoof-Track Interface in Racing Horses. *Veterinary Clinics of North America: Equine Practice*; 24(1): 53-77
- Trewartha, G., Casanova, R., & Wilson, C. (2008) A kinematic analysis of rugby lineout throwing. *J Sports Sci.*; 26(8): 845-854. Available from: PM:18569550

- UEFA. (2002) Artificial Turf Manual. Available from: www.uefa.com
- Valiant, G.A. (1987) Ground reaction forces developed on artificial turf. *Science & Football: Proc.1st World Congress of Science & Football*: 406-415
- Van Gheluwe, B., Deporte, E., & Hebbelinck, M. (1983) "Frictional forces and torques of soccer shoes on artificial turf.," *In Biomechanical aspects of sports shoes and playing surfaces.*, B. M. Nigg & B. A. Kerr, eds., Calgary: University Printing, pp. 161-168.
- Vaughan, C.L. (1984) Biomechanics of running gait. *Crit.Rev.Biomed.Eng.*; 12(1): 1-48. Review.
- Verlhest, R. (2007) A new slide tester, Sheffield, UK 3th Apr.
- Verlhest, R., Malcolm, P., Verleysen, P., Degriek, J., De Clercq, D., & Philippaerts, R. (2009) "Ground reaction force of a drop jump on different kinds of artificial turf," *In Science and Football VI: The Proceedings of the Sixth World Congress on Science and Football*, T. Reilly & F. Korkusuz, eds., London: Routledge, pp. 70-75.
- Villwock, M.R., Meyer, E.G., Powell, J.W., Fouty, A.J., & Haut, R.C. (2009) Football playing surface and shoe design affect rotational traction. *Am.J Sports Med.*; 37(3): 518-525
- Wakeling, J.M., Liphardt, A., & Nigg, B.M. (2003) Muscle activity reduces soft tissue resonance at heel-strike during walking. *J.Biomech.*; 36: 1761-1769
- Wakeling, J.M. & Nigg, B.M. (2001) Modification of soft tissue vibrations in the leg by muscular activity. *J.Applied Physiology*; 90: 412-420
- Wakeling, J.M., Tscherner, V.V., Nigg, B.M., & Stergiou, P. (2001) Muscle activity in the leg is tuned in response to ground reaction forces. *J.Applied Physiology*; 91: 1307-1317
- Walden, M., Hagglund, M., & Ekstrand, J. (2005) UEFA Champions League study: a prospective study of injuries in professional football during the 2001-2002 season. *Br.J Sports Med.*; 39(8): 542-546
- Walker, C. (2003) "The performance of sports surfaces," *In Materials in Sports Equipment*, M. Jenkins, ed., Abingdon, Cambridge: Woodhead Publishing, pp. 47-64.
- Wannop, J.W., Worobets, J.T., & Stefanyshyn, D.J. (2010) Footwear Traction and Lower Extremity Joint Loading. *The American Journal of Sports Medicine*; 38(6): 1221-1228
- Wassing GmbH. (2006) Securisport Sports Surface Tester. Available from: <http://www.wassing.com/>
- Werner, J., Hagglund, M., Walden, M., & Ekstrand, J. (2009) UEFA injury study: a prospective study of hip and groin injuries in professional football over seven consecutive seasons. *Br.J Sports Med.*; 43(13): 1036-1040
- Williams, S., Hume, P.A., & Kara, S. (2011) A review of football injuries on third and fourth generation artificial turfs compared with natural turf. *Sports medicine (Auckland, N.Z.)*; 41(11): 903-923. Available from: PM:21985213
- Winter, D.A. (1990) *Biomechanics of motor control of human control of human movement* Toronto, John Wiley Sons Inc.
- Winterbottom, W. (1985) Artificial grass surfaces for Association Football. *Sports Council, London*: 127
- Woods, C., Hawkins, R.D., Maltby, S., Hulse, M., Thomas, A., & Hodson, A. (2004) The Football Association Medical Research Programme: an audit of injuries in professional football--analysis of hamstring injuries. *Br.J Sports Med.*; 38(1): 36-41
- Young, C. C. (2009) Ankle Sprain. Available from: <http://emedicine.medscape.com/article/85393-overview>
- Zadpoor, A.A. & Nikooyan, A.A. (2010) Modeling muscle activity to study the effects of footwear on the impact forces and vibrations of the human body during running. *Journal of biomechanics*; 43(2): 186-193

Zanetti, E.M. (2009) Amateur football game on artificial turf: players' perceptions. *Appl.Ergon.*; 40(3): 485-490

Zernicke, R. F. & Whiting, W. C. (2000) "Mechanisms of musculoskeletal injury," *In Biomechanics in Sport*, V, V. M. Zatsiorsky, ed., London: Blackwell Scientific Ltd, pp. 507-522.

Zhang, S., Clowers, K., Kohstall, C., & Yu, Y.J. (2005) Effects of various midsole densities of basketball shoes on impact attenuation during landing activities. *J.Appl.Biomech.*; 21(1): 3-17

Zifchock, R.A., Davis, I., & Hamill, J. (2006) Kinetic asymmetry in female runners with and without retrospective tibial stress fractures. *Journal of biomechanics*; 39(15): 2792-2797. Available from: <http://www.sciencedirect.com/science/article/pii/S0021929005004471>

APPENDIX A: Force Platform Pilot Studies

See separate file on CD-ROM

APPENDIX B: Ground Loadings of Individual Subjects

See separate file on CD-ROM

APPENDIX C: Knee Angles of Individual Subjects

See separate file on CD-ROM

APPENDIX D: Knee Moments of Individual Subjects

See separate file on CD-ROM

APPENDIX E: SSTTR Initial Testing Results

See separate file on CD-ROM